New chemical tools for studying Endolysosomal Two-pore Channels

Yu Yuan

University College London

A thesis submitted for the degree of Doctor of Philosophy

October 2020

Declaration

I, Yu Yuan, confirm that the work presented in this thesis is my own. Where information has been derived from other sources. I confirm that this has been indicated in the thesis.

Yu Yuan

Abstract

Two-pore channels (TPCs) are endolysosomal ion channels of physiological and pathophysiological significance. However, fundamental properties concerning ion permeability and activation mechanisms are ambiguous. Also, as the likely targets for Ca^{2+}-mobilizing messenger NAADP, the role of TPCs in cell-wide Ca^{2+} signalling is ill-defined. Importantly, their pharmacology is limited to cell-impermeable activators and a few non-selective inhibitors, which brings challenges for characterizing TPCs. In this thesis, I address the above issues.

I began by examining the mechanism of action of the lysosomotropic agent, glycyl-L-phenylalanine 2-naphthylamide (GPN), which has long been appreciated for mediating Ca^{2+} signals from lysosomes and for probing TPC function. Its action on lysosomes has recently been questioned. However, using fibroblasts, here I show that GPN mobilises Ca^{2+} from acidic organelles.

I move on to characterise two cell-permeable and selective TPC2 activators (A1 and H07). Additionally, I confirm that approved drugs targeting estrogen and dopamine receptors are selective TPC2 inhibitors.

I go on to show that A1 and H07 activate TPC2 differentially. A1 induced larger and quicker Ca^{2+} signals than H07 but similar Na^{+} signals. A1 and H07 targeted distinct sites on TPC2. Besides, H07 but not A1-induced Ca^{2+} signals were regulated by external (luminal) pH. The implication is that TPC2 may be regulated in an agonist-specific manner.

Finally, by using GPN and inhibiting TPC activity with novel inhibitors or siRNA knockdown, I show that TPCs are required for histamine- but not bradykinin-induced Ca^{2+} signals. More specifically, histamine-mediated Ca^{2+} signals were reduced upon TPC2 but not TPC1 knockdown. Thus, TPCs are implicated in global Ca^{2+} signalling evoked by physiological stimuli likely in an isoform-dependent manner.

Collectively, this research has provided novel TPC modulators with which to further characterize fundamental properties and physiological roles of TPCs.

Impact statement

TPCs are in the spotlight in recent literature. TPCs have been associated with a growing number of diseases, including neurodegeneration (e.g. Parkinson's disease), fatty liver disease, cardiac dysfunction and viral infection (e.g. Ebola). It is worth noting that recent works have also suggested a likely role for TPCs in SARS-CoV2 infectivity. However, the lack of cell-permeable and selective TPC modulators is impeding characterization of TPCs in the above pathophysiological contexts. In fact, on the whole, our understanding of TPCs is limited. Even the basic attributes (i.e. gating mechanism and ion selectivity) are still debated.

In this thesis, the identification of A1 and H07 as cell-permeable and highly selective TPC2 activators is of major impact to the TPC field. Considering that NAADP and $PI(3,5)P_2$ are membrane-impermeable, A1 and H07 permit an easy route for characterization of TPCs. With these new compounds, one can expect that the physiological and pathophysiological of TPCs can now be studied in detail. My findings uncover agonist-specific TPC2 activity. This resolves the long-held controversy surrounding whether TPCs are NAADP-gated non-selective Ca^{2+}-permeable channels or are $PI(3,5)P_2$-gated Na^+-selective channels. Indeed, in the collaborative paper published this year (Gerndt et al., 2020), A1 and H07 were shown to mimic NAADP and $PI(3,5)P_2$, respectively. Importantly, A1 and H07 were associated with distinct lysosomal functions. This further broadens the impact of this study to researchers studying the lysosome.

In this thesis, I also confirm that a number of approved drugs targeting estrogen and dopamine receptors are TPC2 antagonists. These compounds were first introduced from a drug-repurposing approach designed by our (Patel) lab (Penny et al., 2019). This new set of tools have facilitated the recognition of the role of TPCs in global Ca^{2+} signals evoked by physiological agonists (e.g. histamine). This may have implications of how dysfunction in TPCs contribute to pathologies. Furthermore, the use of drug repurposing technique to pursue TPC inhibitors is cost-efficient for both research into pharmacology of TPCs and drug development into clinical use. This is because the clinical profiles of these approved compounds have already been well-established.

Overall, developing the pharmacology of TPCs, as I have done here, is essential, not only for research purposes, but for aiding treatment of TPC-related diseases. The findings in this thesis thus bring TPCs into a new research stage.

Acknowledgments

First and foremost, my deepest gratitude goes to Professor Sandip Patel for being the cornerstone of my research. He witnessed and accompanied my entire research journey, starting from an inexperienced Master student and gradually become an independent researcher. Without his scientific insight, professional guidance and continuous encouragement, my study would be fruitless and there would be no thesis. I also thank Dr Sean Davidson for being my secondary supervisor and providing support when I needed.

I have been lucky to collaborate with Professor Christian Grimm, Professor Franz Bracher and their teams from Ludwig Maximilian University of Munich Germany, with whom I characterized novel TPC activators. I thank them for generating HEK293 cell lines stably expressing plasma-membrane TPC2 and a number of GCaMP6s-tagged plasmids. A special thank you to Drs Susanne Gerndt and Yu-kai Chao who have dealt with the logistics patiently. Thanks should also go to Drs Christopher Penny, Taufiq Rahman and Professor Patel for identification of putative TPC inhibitors. Also, I would like to recognize my graduate tutor Professor Michael Duchen for his formative and simulating discussion on research progress, as well as to Dr William Andrews for valuable advice on site-directed mutagenesis.

A huge and wholehearted hug to everyone in the Patel lab, to Martina, Kristin, Becky and Steve for nurturing a pleasant and enjoyable laboratory where ideas, laughter and alcohol are shared. I extend my thank to previous lab members Drs Bethan Kilpatrick, Christopher Penny and Elizabeth Yates for their technical support. Special mention to Dr Bethan Kilpatrick for her tireless tutoring of the techniques presented in this thesis, without her the completion of my experiments would not have been possible.

Finally, I would like to express my deepest love and appreciation to my parents. Not only they generously support the 10-year study and life in the UK, but also their empathy, patience, attention and respect allowed me to freely pursue my goals. They gave me the courage to embrace every challenge with a positive attitude. I am forever indebted to Ning Ding, for being the most reliable and unique source of friendship. She never walks in front or behind me, as we always stand beside each other.

Table of Contents

List of Tables

List of Figures

Abbreviations

ALS	Amyotrophic lateral sclerosis
AM	Acetoxymethyl ester
ATP	Adenosine trisphosphate
AUC	Area under the Ca^{2+} curve
BAF	Bafilomycin A1
BAPTA	1,2-Bis(2-aminophenoxy)ethane-N,N,N′,N′-tetraacetic acid tetrakis
BBIQ	Bisbenzylisoquinoline alkaloids
cADPR	Cyclic adenosine 5′-diphosphate ribose
Cav	Voltage-operated Ca^{2+} channel
CAX	Ca^{2+}/H^{+} exchanger
CICR	Calcium-induced calcium release
DABCO	1,4 diazabicyclo[2,2,2]octane
DAG	diacylglycerol
DMEM	Dulbecco's Modified Eagle Medium
DMSO	Dimethyl sulfoxide
EBOV	Ebola virus
EGF	Epidermal growth factor
EGFR	Epidermal growth factor receptor
EGTA	Ethylene glycol-bis(β-aminoethyl ether)-N,N,N',N'-tetraacetic acid
ER	Endoplasmic reticulum
FBS	Fetal Bovine Serum
FDA	Food and Drug administration
GA	Golgi apparatus
GCaMP	Genetically encoded calcium indicator (GFP Calmodulin M13)
GECO	Genetically encoded calcium indicator for optimal imaging
GFP	Green fluorescent protein
GPCR	G-protein coupled receptor
GPN	Glycyl-L-phenylalanine 2-naphthylamide
HBS	HEPES-buffered saline
HEK	Human embryonic kidney-293
HIV	Human immunodeficiency virus
Hsa	Human
HVA	High voltage activated
IMM	Inner mitochondrial membrane
Iono	Ionomycin
IP_3	Inositol (1,4,5) trisphosphate
IP_3R	Inositol (1,4,5) trisphosphate receptor
JNK	C-Jun N-terminal kinase
KD	Knockdown
KO	Knockout
LAMP	Lysosome associated membrane protein

LDL	Low-density lipoprotein
Letm1	Leucine zipper-EF-hand containing transmembrane protein 1
LGCC	Ligand gated Ca^{2+} channels
LLOMe	L-leucyl-L-leucine methyl ester
LMP	Lysosomal membrane permeabilization
LRRK2	Leucine-rich repeat kinase 2
LTR	Lysotracker Red
LVA	Low voltage activated
MAPK	Microtubule associated protein kinase
MBS	MES-buffered saline
MCS	Membrane contact site
MCU	Mitochondrial Ca^{2+} uniporter
MICU1	Mitochondrial uptake 1 protein
ML-SA	Mucolipin synthetic agonist
ML-SI	Mucolipin synthetic inhibitor
MLIV	Mucolipidosis type IV
Mmu	Mus musculus (Mouse)
mRFP	Monomeric red fluorescent protein
mTOR	Mammalian target of rapamycin
NAADP	Nicotinic acid adenine dinucleotide phosphate
NAD	Nicotinamide adenine dinucleotide
NADP	Nicotinamide adenine dinucleotide phosphate
NAFLD	Non-alcoholic fatty liver disease
NaP	Sodium proprionate
Nav	Voltage-operated Na^+ channel
NCLX	Mitochondria-localized Na^+/Ca^{2+} exchanger
NCX	Na^+/Ca^{2+} exchanger
NMDAR	N-methyl-D-aspartate receptor
NMDG	N-methyl-D-glucamine
NPC	Niemann-Pick type C disease
OMM	Outer mitochondrial membrane
ORP1L	Oxysterol-binding protein-related protein 1L
P2X	Purinergic receptor
PBS	Phosphate buffered saline
PCR	Polymerase chain reaction
PD	Parkinson's disease
PDGF	Platelet-derived growth factor receptors
$PI(3,5)P_2$	Phosphatidylinositol (3,5)-bisphosphate
PI(3)P	Phosphatidylinositol 3-phosphate
$PI(4,5)P_2$	Phosphatidylinositol 4,5-bisphosphate
PIKfyve	Phosphoinositide Kinase, FYVE-Type Zinc Finger Containing
PKA	Protein kinase A
PLC	Phospholipase C
PM	Plasma membrane

PMCA	Plasma membrane Ca^{2+} ATPases
PPADS	pyridoxalphosphate-6-azophenyl-2',4'-disulfonic acid
PTP	Permeability transition pore
PTP1B	Protein-tyrosine phosphatase 1B
qPCR	Quantitative polymerase chain reaction
RNA	Ribonucleic acid
RTK	Tyrosine kinase receptor
RyR	Ryanodine receptor
SDM	Site-directed mutagenesis
SERCA	Sarco/endo-plasmic reticulum Ca^{2+} ATPase
SG	Secretory granule
shRNA	Small hairpin RNA
siRNA	Small interfering RNA
SNARE	Soluble N-ethylmaleimide-sensitive factor activating protein receptor
SOCE	Store-operated Ca^{2+} entry
SPCA	Secretory pathway Ca^{2+} ATPase
SPSS	Statistical Product and Service Solutions
SR	Sarcoplasmic reticulum
STARD3	StAR-related lipid transfer domain protein 3
STIM	Stromal interaction molecule
TCA	Tricyclic anti-depressants
TFEB	Transcription Factor EB
TPC	Two-pore channel
TRP	Transient receptor potential
TRPA	Transient receptor potential ankyrin
TRPC	Transient receptor potential canonical
TRPM	Transient receptor potential melastatin
TRPML	Transient receptor potential mucolipin
TRPP	Transient receptor potential polycystic
TRPV	Transient receptor potential vanilloid
UBC	Ubiquitin-conjugating enzyme
UV	Ultraviolet
v/v	Volume by volume
VAP	(Vesicle associated membrane protein)-associated protein
VDAC	Voltage-dependent anion channels
VEGF	Vascular endothelial growth factor
VGCC	Voltage gated Ca^{2+} channels
VGIC	Voltage-gated ion channel
VSD	Voltage sensor domain
w/v	Weight by volume
WT	Wild-type

Chapter 1: Introduction

1.1 Overview

Changes in cytosolic Ca^{2+} are important for the regulation of a wide array of physiological processes. Ca^{2+} signals can be derived from intracellular Ca^{2+} stores and/or the extracellular space. The ER is the most well-characterized Ca^{2+} store. However, in recent years, acidic organelles, such as lysosomes, have been appreciated to store and release Ca^{2+}. There are a handful of ion channels that localize to acidic Ca^{2+} stores and enable Ca^{2+} release. Two-pore channels (TPCs), belonging to the voltage-gated ion channel superfamily, are one class and have been recognized as the likely principle targets for NAADP, a Ca^{2+} mobilizing messenger that is central to Ca^{2+} signalling through acidic stores. TPCs regulate diverse physiological events. For example, TPCs increase Ca^{2+} around lysosomes to regulate endocytic trafficking. Localized lysosomal Ca^{2+} release can also be propagated into large and global signals by triggering Ca^{2+} release from the ER. TPCs are required for NAADP-induced global Ca^{2+} signals, but it is less clear as to whether TPCs are involved in physiological Ca^{2+} signals induced by extracellular stimuli. TPCs have also been linked to a growing number of pathophysiological events, such as Parkinson's disease and Ebola infection. However, compared to other voltage-gated ion channels, our understanding of TPCs is still superficial. In addition, the activation mechanism and ion selectivity of TPCs are debated. There is much evidence indicating that TPCs are NAADP-gated Ca^{2+} permeable channels, whereas other evidence indicates that TPCs are $PI(3,5)P_2$-gated Na^+ selective channels. Further and detailed characterization of the channel is crucial, but this has been impeded by the lack of selective and cell-permeable TPC activators and inhibitors. Pharmacology of TPCs has attracted enthusiastic attention in recent years, starting primarily from 2018. This thesis characterized novel TPC modulators and explored fundamental (e.g. ion selectivity) and functional properties of TPCs.

1.2 Ca^{2+} signalling

Ca^{2+} is a ubiquitous and abundant cation inside the body. It can impact numerous physiological processes from fertilization to cell death (Berridge et al., 2000). This versatility is ascribed to findings that Ca^{2+} signals can display complex patterns that vary in amplitude, frequency and location (i.e. there are various "Ca signatures"). The

Ca^{2+}-signalling toolkit forms the basis of the various "Ca^{2+} signatures" (Berridge et al., 2003). The toolkit contains components that permit elevation of cytosolic Ca^{2+} by mobilizing Ca^{2+} from intracellular stores and/or the external Ca^{2+} entry. Also, the toolkit contains a series of "Ca^{2+} clearance" components that can buffer, extrude or compartmentalize Ca^{2+}. Cells make use of these components to precisely regulate the spatial and temporal features of the Ca^{2+} signals, allowing specific outcomes (e.g. transients, waves or oscillations) to be generated upon stimulation. The Ca^{2+} signature is then "decoded" by Ca^{2+}-sensitive processes. Dysfunction in any of the components within the toolkit could remodel the signature, leading or contributing to pathologies (Karlstad et al., 2012).

At rest, the cytosolic Ca^{2+} concentration is low at about 100 nM (Berridge et al., 2000). Maintaining cytosolic Ca^{2+} is the prerequisite for cells to generate accurate Ca^{2+} signals in response to an external stimulus. Thus, the Ca^{2+} clearance components are vital as they elicit homeostatic function by maintaining cytosolic Ca^{2+} and ensure Ca^{2+} signals to be tightly controlled in time and space (Clapham, 2007; Karlstad et al., 2012). Among a number of endogenous Ca^{2+} binding proteins, some are known to serve as cytosolic Ca^{2+} buffers. The buffers can impose restrictions on the diffusion of Ca^{2+} within the cells and thus are essential for development of local Ca^{2+} signals. Prototypical Ca^{2+} buffers include parvalbumins, calbindin-D28k and calretinin (Schwaller, 2010). The latter two are fast acting buffers (Berridge et al., 2003; Nägerl et al., 2000), while parvalbumins slowly binds Ca^{2+} (Lee, schwaller et al., 2000). Functionally, fast and slow buffers differentially regulate Ca^{2+} signals. For example, in neurons, calbindin-D28k but not parvalbumins reduce the amplitude of the presynaptic Ca^{2+} transients (Schmidt et al., 2003). Parvalbumins instead accelerate Ca^{2+} decay (Collin et al., 2005; Schmidt et al., 2003). Cytosolic Ca^{2+} can also be extruded across the plasma membrane. This is achieved by plasma membrane Ca^{2+}-ATPase (PMCA) and Na^{+}/Ca^{2+} exchanger (NCX) (Brini & Carafoli, 2011). PMCA employs ATP for Ca^{2+} transport to the outside of the cells. PMCA is of high affinity and low capacity for Ca^{2+}. In contrast, NCX has low affinity and high capacity. NCX exchanges three Na^{+} for one Ca^{2+}. Notably, depending on the membrane potential and electrochemical gradient of Ca^{2+} and Na^{+}, NCX can also function in a reverse mode: transporting Na^{+} out for Ca^{2+} in (Blaustein & Lederer, 1999; Verkhratsky et al., 2018). Moreover, cytosolic Ca^{2+} can be sequestered into internal Ca^{2+} stores. This process,

for example, allows the ER Ca^{2+} store refilling (details are discussed in 1.2.2.1 ER Ca^{2+} signalling). Together, the Ca^{2+} clearance components permit cells to transport Ca^{2+} into the extracellular space or into the intracellular stores. This capacity of cells is essential for shaping and terminating Ca^{2+} signals. Importantly, it maintains low cytosolic Ca^{2+}, assuring high levels of Ca^{2+} of the stores and extracellular space, and thus preparing cells for generation of Ca^{2+} signals.

1.2.1 Ca^{2+} entry

In the extracellular milieu, Ca^{2+} concentration is about 10,000 times higher than that in the cytoplasm (Berridge et al., 2000). It is therefore unsurprising that one source for Ca^{2+} signals is Ca^{2+} entering from the external space. In excitable cells (e.g. neurons), voltage-gated Ca^{2+} channels (VGCCs) offer one important route of Ca^{2+} entry. VGCCs are gated by voltage and open after depolarization of the membrane. From a biophysical perspective, VGCCs can be divided into low-voltage activated (LVA) and high-voltage activated (HVA) channels (Schampel & Kuerten, 2017). T-type VGCCs are LVA channels that open by small voltage changes. In comparison, HVA channels, which include L, N, P/Q and R-type VGCCs, not only require strong depolarization for activation but also display prolonged opening. Functionally, for instance, L-type VGCCs regulate synaptic tones in neurons and excitation-contraction coupling in cardiac and skeletal muscle cells (Zamponi et al., 2015).

Ligand-gated ion channels (LGCCs) also mediate Ca^{2+} influx. One example is N-methyl-D-aspartate receptors (NMDARs) which are gated by the excitatory neurotransmitter glutamate in the central nervous system (Iacobucci & Popescu, 2017). Functionally, NMDARs are important for synaptic plasticity, learning, and memory (Hansen et al., 2018). Transient receptor potential (TRP) channels are another family of ion channels that facilitate Ca^{2+} entering across the plasma membrane. There are 28 different TRP channels, which can be classified into six subtypes: TRPC, TRPV, TRPM, TRPA, TRPP and TRPML (Venkatachalam & Montell, 2007). Most TRP channels are expressed in the plasma membrane, although some have lysosomal localizations (e.g. TRPML1-3 and TRPM2) (Patel & Cai, 2015). TRP channels are activated by a variety of stimuli. For example, TRPV channels are gated by change in temperature, and thus function as thermosensors (Islas, 2017). TRPC channel activation requires stimulation of phospholipase C (PLC) pathway, with some TRPC

isoforms specifically activated by diacylglycerol (DAG) (Harteneck & Gollasch, 2011; Hofmann et al., 1999; Riccio et al., 2002). Moreover, a functional requirement of TRPC channels in store-operated Ca^{2+} entry (SOCE) has been extensively reported albeit controversially (Lopez et al., 2020; Salido et al., 2009). SOCE is a ubiquitous Ca^{2+} entry pathway that is activated by ER Ca^{2+} depletion, serving as a mechanism for store refilling (details about SOCE are discussed in 1.2.2.1 ER Ca^{2+} signalling).

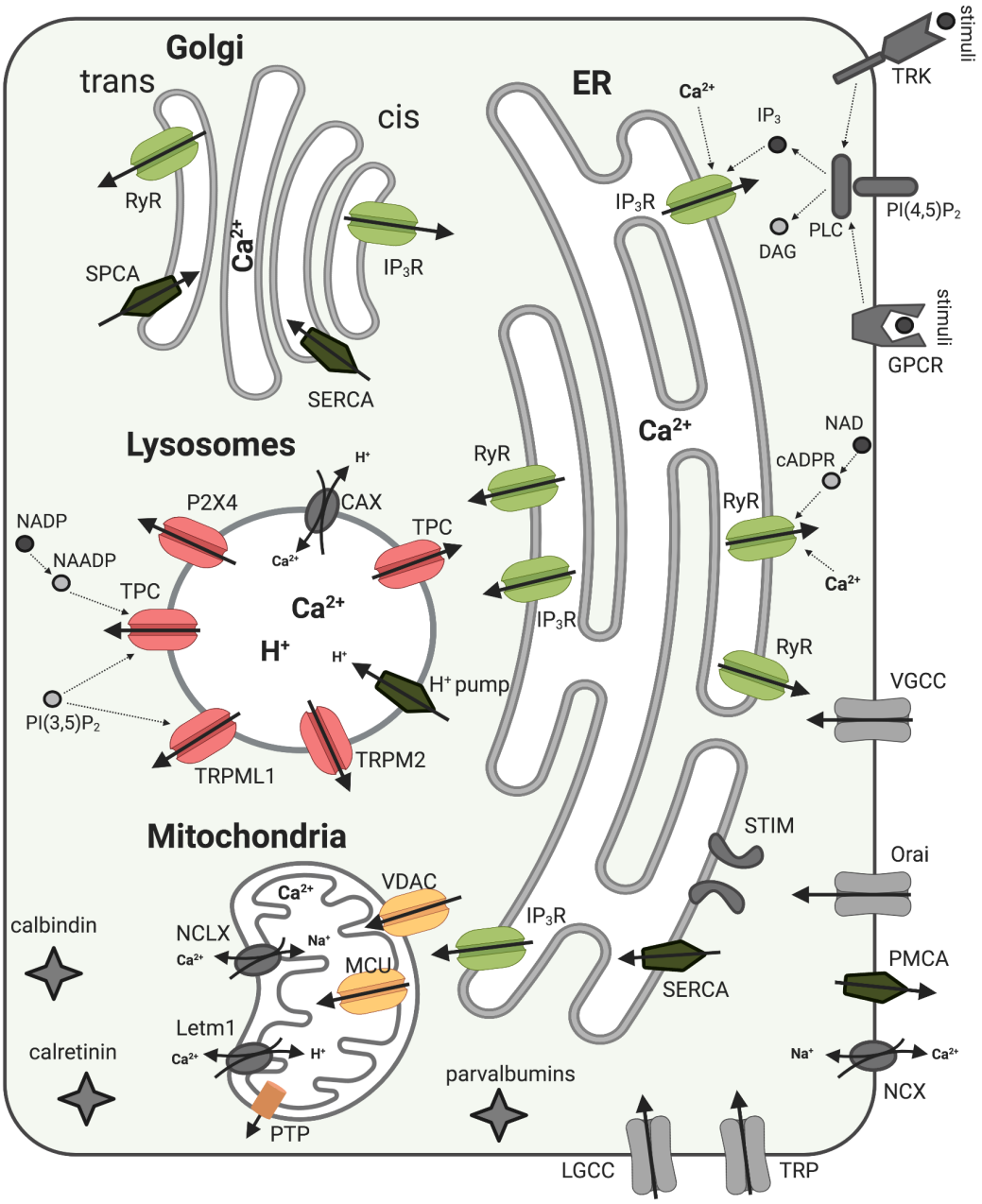

Figure 1.1 The Ca^{2+} signalling network

Ca^{2+} signals are generated from Ca^{2+} entering across the plasma membrane (through VGCC, LGCC, store-operated Orai channels and TRP channels) and Ca^{2+} release from intracellular

Ca^{2+} stores (the ER, Golgi and lysosomes). The latter is mediated by resident Ca^{2+} channels (such as IP_3Rs, RyRs, TRPML1 and TPCs) that open in response to Ca^{2+} messengers (including IP_3, cADPR and NAADP), some of which indirectly activate the channels by binding to an accessory protein. The phosphoinositide $PI(3,5)P_2$ activates lysosomal Ca^{2+} channels. Ca^{2+} enters the mitochondria via VDAC and MCU on the outer and inner membrane, respectively, and leaves via NCLX, Letm1 and PTP. Cytosolic Ca^{2+} buffers (parvalbumin, calbindin and calretinin), Ca^{2+} pumps (PMCA, SERCA and SPCA) and Ca^{2+} exchangers (NCX) maintain intracellular Ca^{2+} homeostasis and modulate Ca^{2+} signals. (Note: organelles are not to scale).

1.2.2 Ca^{2+} release

1.2.2.1 ER Ca^{2+} signalling

As the largest organelle in the cells, the endoplasmic reticulum (ER) represents a prominent intracellular Ca^{2+} pool (Berridge, 2002). The ER stores Ca^{2+} at a concentration of 100-800 μM. Inositol-1,4,5- trisphosphate receptors (IP_3Rs) and ryanodine receptors (RyRs) are responsible for releasing Ca^{2+} from the ER. IP_3Rs open in response to the second messenger IP_3 (Streb et al., 1983). IP_3 is a product of PLC pathway which can be activated upon stimulation of G-protein coupled receptors (GPCRs) or receptor tyrosine kinases (RTK), inducing cleavage of $PI(4,5)P_2$ into cytosolic IP_3 and DAG. In accord, a number of physiological agonists (e.g. histamine and bradykinin) that work through GPCRs induce ER-dependent global Ca^{2+} signals by activating IP_3Rs (Cruzblanca et al., 1998; Johnson et al., 1990). There are three IP_3R subtypes expressed in mammals. Although they differ in their affinity to IP_3 (Iwai et al., 2007), all IP_3Rs can be additionally regulated by cytosolic Ca^{2+} in a biphasic manner (Bezprozvanny et al., 1991; Foskett et al., 2007). Specifically, a modest increase in cytosolic Ca^{2+} activates the channel, mobilizing more Ca^{2+} from the ER (the so-called "calcium-induced calcium release (CICRs)" mechanism). Conversely, higher levels of Ca^{2+} abolish the channel activity and thus terminate Ca^{2+} release. IP_3 primes IP_3Rs to be regulated by cytosolic Ca^{2+}, although the exact mechanism is not very clear (Marchant & Taylor, 1997; Rossi & Taylor, 2018; Thillaiappan et al., 2019; Vais et al., 2012). RyRs are another important family of ion channels expressed on the ER to control Ca^{2+} release. RyRs are regulated by the second messenger, cADPR, which is produced from nicotinamide adenine dinucleotide (NAD) by a family of ADP-ribosyl cyclases, including CD38 and CD157 (Galione & Churchill, 2000).

Unlike IP_3, cADPR may indirectly activate the channel requiring initial binding to an accessory protein (Lee et al., 1994; Walseth et al., 1993). In addition to cADPR, like IP_3Rs, RyRs can also be activated by a small increase in cytosolic Ca^{2+} so function via the CICR mechanism (Bezprozvanny et al., 1991). At high Ca^{2+} levels (e.g. > ~10 μM), the channel is inhibited. There are three RyR isoforms (RyR1-3) that are found ubiquitously in mammals. RyR1 and RyR2 are primarily expressed in skeletal and cardiac muscle, respectively. RyR3 has a broader expression (Mackrill et al., 1997). Functionally, the L-type VGCCs on the PM communicate to RyRs via CICRs or direct physical interaction to regulate Ca^{2+}-sensitive muscle contraction. RyRs thus are implicated in excitation-contraction coupling (Chang et al., 2017; Franzini-Armstrong et al., 1999).

In addition to regulated Ca^{2+} release, there is also continuous Ca^{2+} leak from the ER (Camello et al., 2002), which is counteracted by sarcoendoplasmic reticulum Ca^{2+} ATPase (SERCA) that constantly pump Ca^{2+} back into the ER lumen. The SERCA functions to maintain the ER Ca^{2+} concentration. Like PMCA, the SERCA also uses ATP to effect Ca^{2+} transport. Uniquely, the SERCA can be inhibited by the lactone thapsigargin that irreversibly blocks the pump and thus eventually depletes ER Ca^{2+} through the leak pathway (Michelangeli & East, 2011; Thastrup et al., 1990). Maintaining ER Ca^{2+} is critical for the "classical" function of ER in protein folding and packaging (Berridge, 2002). In the case of IP_3/cADPR-induced Ca^{2+} release which could deplete the ER stores, a Ca^{2+}-entry mechanism is activated, known as store-operated Ca^{2+} entry (SOCE) (Putney, 2005). SOCE sustains the ER Ca^{2+} signals allowing refilling of the ER. SOCE is mediated by interaction between STIM (STIM1 and STIM2) proteins on the ER and Orai proteins on the PM. STIM is an ER Ca^{2+} sensing protein localized to the ER membrane. STIM monitors ER Ca^{2+} levels by its luminal EF-hands (Zhang et al., 2005). Upon ER depletion, Ca^{2+} dissociates from the EF hand, and consequently, STIM undergoes a conformational change. This drives its relocation to ER-plasma membrane junctions where it interacts with Orai-1, a plasma membrane Ca^{2+} channel. This interaction opens Orai and Ca^{2+} entry (Hogan & Rao, 2015). SOCE is thus achieved by ER-PM crosstalk. Indeed, the ER does not work alone and also exchanges Ca^{2+} information with organelles (e.g. mitochondria and lysosomes) (Burgoyne et al., 2015). Furthermore, dysfunction of ER Ca^{2+} has been

implicated in a number of diseases (e.g. neurodegeneration) (Mekahli et al., 2011; Popugaeva & Bezprozvanny, 2013). ER is a vital Ca^{2+} organelle.

1.2.2.2 Golgi Ca^{2+} signalling

The Golgi apparatus (GA) is known for its function in protein sorting and processing. Besides, the GA has emerged as a dynamic intracellular Ca^{2+} store, which is equipped with relatively similar Ca^{2+} homeostatic components as those of the ER. For example, the cis-Golgi subcompartment is endowed with functional IP_3Rs and SERCA (Behne et al., 2003; Pinton et al., 1998), while the trans-Golgi utilize RyRs for releasing Ca^{2+} and the secretory pathway Ca^{2+} ATPase (SPCA) for Ca^{2+} uptake (Lissandron et al., 2010; Baelen et al., 2003). Compared to SERCA, SPCA is less sensitive to thapsigargin (Tu et al., 2007). The GA stores a high level of Ca^{2+} like the ER, but it contributes a very small percentage of cellular Ca^{2+}. In line with this, upon cell stimulation (e.g. by ATP), compared to the ER, there is a small drop in GA Ca^{2+} and a rapid termination on GA Ca^{2+} release (Vanoevelen et al., 2004). Nonetheless, dysregulated GA Ca^{2+} has been linked to diseases, including Hailey-Hailey syndrome (a skin disease), neurodegenerative diseases and ischemia and reperfusion injury (a cardiac disease) (Li et al., 2013).

1.2.2.3 Mitochondrial Ca^{2+} signalling

Mitochondria were the first organelles linked to Ca^{2+} signalling (DeLuca & Engstrom, 1961). Mitochondria maintain low Ca^{2+} levels similar to that in the bulk cytoplasm (100 nM), but when cells engage in Ca^{2+}-dependent processes, mitochondria sequester Ca^{2+} from the cytosol. The Ca^{2+} buffering capacity of mitochondria endows the organelle with an important role in shaping Ca^{2+} signals (Rizzuto et al., 2012). For example, in neurons, mitochondria buffer Ca^{2+} resulting from VGCC-induced Ca^{2+} influx (Tang & Zucker, 1997). In addition, by a close apposition with the ER, mitochondria manage local Ca^{2+} release from the ER via IP_3Rs, and thus influencing the extent of subsequent global Ca^{2+} wave propagation (Jouaville et al., 1995; Tang & Zucker, 1997). Ca^{2+} has to cross two membranes, the outer mitochondrial membrane (OMM) and the inner mitochondrial membrane (IMM), to enter the mitochondrial matrix. Due to the abundant expression of voltage-dependent anion channels (VDACs), Ca^{2+} can easily pass through the OMM (Báthori et al., 2006). The IMM is impermeable but Ca^{2+} can be transported through the mitochondrial Ca^{2+} uniporter (MCU) that

utilizes the negative potential across the IMM (Baughman et al., 2011; Kirichok et al., 2004; Perocchi et al., 2010). Ca^{2+} accumulating inside the mitochondria is essential for the appropriate intrinsic functions of the organelles, including metabolite transport and ATP production (Tarasov et al., 2012). However, too much Ca^{2+} inside mitochondria can promote cell death. Indeed, mitochondrial Ca^{2+} overload has been linked to cardiomyocyte necrosis and neuronal excitotoxicity (Orrenius et al., 2003).

To balance Ca^{2+} entry, mitochondria can also release Ca^{2+}. This is primarily achieved by the mitochondria-localized Na^{+}/Ca^{2+} exchanger NCLX (Palty et al., 2010). Another Ca^{2+} extrusion component could be the Ca^{2+}/H^{+} antiporter Letm1 (Austin et al., 2017; Jiang et al., 2009). Moreover, the IMM-localized mitochondrial permeability transition pore (PTP) also permits Ca^{2+} efflux. Notably, long-lasting PTP opening is usually observed in pathological conditions where there is a mitochondrial Ca^{2+} overload. Such opening leads to disruption of membrane potential, cessation of ATP production, loss of pyridine nucleotides and cytochrome c, and consequent cell death (Petronilli et al., 2001; Rasola & Bernardi, 2011). In contrast, short-term opening may allow a physiological regulation on Ca^{2+} by likely providing a fast Ca^{2+} release mechanism (Barsukova et al., 2011; Bernardi & von Stockum, 2012).

1.2.2.4 Lysosomal Ca^{2+} signalling

Lysosomes form the degradation centre of the cell filled with various hydrolytic enzymes (Xu & Ren, 2015). To carry out their degradative function, lysosomes fuse with autophagosomes to allow exposure of unwanted intracellular materials (e.g. proteins, lipids and polysaccharides) to the hydrolases. Lysosomes are thus key for macroautophagy. Alternatively, cytosolic materials can be directly taken up by lysosomes during microautophagy or chaperone-mediated autophagy (Parzych & Klionsky, 2014). Besides, lysosomes are implicated in endocytosis and exocytosis via fusion with endosomes and the PM, respectively. In addition to aforementioned functions, lysosomes have also been appreciated as acidic Ca^{2+} stores that can store and release Ca^{2+} (Morgan et al., 2011; Patel & Docampo, 2010). Lysosomal Ca^{2+} release has been shown to be essential for endo-lysosomal membrane fusion and fission (Luzio et al., 2007) .

The extreme acidic and proteolytic environments bring difficulties in directly measuring lysosomal Ca^{2+}. Nevertheless, using dextran-based indicators, the luminal Ca^{2+} has been determined to be 400-700 μM (Christensen et al., 2002; Lloyd-Evans et al., 2008), similar to that of the ER. Consistent with a small size, the lysosome generates localized Ca^{2+} signals. However, such signals are not easy to be detected given their small and localized nature. Recent techniques therefore have developed organelle-targeted genetically-encoded Ca^{2+} indicators (e.g. GCaMP and GECO) which permit better resolution (Morgan et al., 2015; Shen et al., 2012). In this thesis, GCaMP6s has been applied to monitor and study lysosomal Ca^{2+} release. These local signals, can also be converted into global signals by triggering ER Ca^{2+} release via CICRs (Kilpatrick et al., 2013; Kilpatrick, Yates, et al., 2016; Penny et al., 2015). In accord, a number of physiological agonists (e.g. histamine and ATP) that are thought to be exclusively coupled to IP_3 production induce lysosome-dependent Ca^{2+} signals (Pandey et al., 2009; Soares et al., 2007).

To date, GPN is the most widely used tool in probing lysosomal Ca^{2+} signalling (Morgan et al., 2020). As a hydrophobic compound, GPN can easily diffuse into the lysosomes where it is cleaved by the hydrolase, cathepsin C (Jadot et al., 1984). The generated di-peptides disrupt the lysosomal membrane by inducing osmotic pressure, resulting in increased cytosolic Ca^{2+}. GPN-induced Ca^{2+} signals have been noted in various cell lines (Haller et al., 1996; Kilpatrick et al., 2013; Soares et al., 2007). GPN pre-treatment abolishes Ca^{2+} signals mediated by TPCs and TRPML1 (Calcraft et al., 2009; Kilpatrick, Yates, et al., 2016), which are lysosomal Ca^{2+} release channels (see subsequent paragraph and 1.3 Two-pore channels). The capacity of GPN in inducing lysosomal Ca^{2+} makes it popular in the lysosomal Ca^{2+} field, especially given there are very few cell-permeable lysosomal Ca^{2+} mobilizing tools. Indeed, GPN has been used in the context of lysosomal Ca^{2+} signalling (Faris et al., 2019; Haller et al., 1996; Kilpatrick et al., 2013), membrane repair (Skowyra et al., 2018) and exocytosis (Liu et al., 2018; Sivaramakrishnan et al., 2012). Moreover, GPN-mediated Ca^{2+} signals are reduced in neurodegenerative diseases (Coen et al., 2012; Kilpatrick, Magalhaes, et al., 2016; Lloyd-Evans et al., 2008; Visentin et al., 2013) pointing to impaired lysosomal Ca^{2+} homeostasis in those diseases. However, quite recently, GPN was proposed to release Ca^{2+} directly from the ER and not lysosomes (Atakpa et al., 2019). In chapter 2, I re-examined the mechanisms underlying GPN action.

Like other Ca^{2+} stores, lysosomes also sequester Ca^{2+}, but the mechanism is less clear. The prevailing view is that Ca^{2+}/H^+ exchanger (CAX) utilizes the H^+ gradient created by V-type ATPase H^+ pump to drive Ca^{2+} into the lumen (Morgan et al., 2011; Patel & Docampo, 2010). Favouring this, dissipation of the H^+ gradient by bafilomycin A1 that inhibits the V-type ATPase reduces lysosomal Ca^{2+} (Christensen et al., 2002). However, notably, CAX appears to be absent in humans (Melchionda et al., 2016). Therefore, other mechanisms include coupled Na^+/Ca^{2+} and Na^+/H^+ exchange or H^+-independent Ca^{2+} uptake via P-type ATPases (Patel & Docampo, 2010). Further research is required for understanding the mechanism underlying lysosomal Ca^{2+} uptake. Functionally, such uptake shapes ER Ca^{2+} signals (Atakpa et al., 2018; López-Sanjurjo et al., 2013).

To note, lysosomes are the chief acidic Ca^{2+} stores but others also include endosomes, secretory granules and lysosome-related organelles (Morgan et al., 2011). To release Ca^{2+}, acidic stores express several Ca^{2+}-permeable channels, such as TRP channels. TRP mucolipins (TRPMLs) are the best-characterized TRP channels on acidic stores. Like other TRP channels, TRPMLs are members of voltage-gated ion channel superfamily, and consists of six transmembrane domains and a pore region (Zhang et al., 2017). There are three TRPML isoforms (TRPML1-3) in humans (Venkatachalam & Montell, 2007). Mutation in TRPML1 causes Mucolipidosis IV (MLIV) (Dong et al., 2008) that is characterized by severe neurodegeneration. TRPML1 is primarily localized on lysosomes, which is confirmed in colocalization study where fluorescent-labelled TRPML1 overlaps with the lysosomal marker LAMP1 (Kiselyov et al., 2005; Zeevi et al., 2009). Although TRPML2 and TRPML3 have been shown to localize with lysosomes, they also have endosomal and the PM localization (Kim et al., 2009). The PM localization offers an easy route for electrophysiological characterization. Indeed, patch-clamp with whole cells uncovers that TRPML3 is permeable to Ca^{2+} (Kim et al., 2007). Alternatively, patch-clamp onto whole endolysosomes that are enlarged with vacuolin1 allows TRPML1 to be characterized. Compared to TRPML3 that is impermeable to Fe^{2+}, TRPML1 is a non-selective channel that permeable to Fe^{2+} as well as Ca^{2+} (Dong et al., 2008). How TRPML1 is endogenously activated has not been fully addressed. Nonetheless, the phosphoinositide, phosphatidylinositol 3,5-bisphosphate ($PI(3,5)P_2$) can induce

TRPML1 currents likely via binding to the N-terminus of the channel (Chen et al., 2017; Dong et al., 2010). $PI(3,5)P_2$ is a endolysosomal phosphoinositide (PIP). $PI(3,5)P_2$ uncovers a role of TRPML1 in membrane trafficking (Dong et al., 2010). This has subsequently been confirmed by the synthetic TRPML1 agonist, ML-SA1, as ML-SA1 corrected trafficking defects in MLIV (Chen et al., 2014) and Neiman-Pick disease type C (NPC, Shen et al. 2012) by increasing TRPML1-induced local Ca^{2+} release. In addition, Ml-SA1 reveals that TRPML1 can induce global Ca^{2+} signals by mobilizing Ca^{2+} from lysosomes (Garrity et al., 2016; Kilpatrick, Yates, et al., 2016). Other synthetic TRPML1 modulators include the agonist MK6-83 (Chen et al., 2014) and the antagonist ML-SI3 (Samie et al., 2013).

P2X receptors are important mediators of purinergic signalling at the PM (Khakh & North, 2012). They are ATP-gated channels that are permeable to both Ca^{2+} and Na^{+}. Among seven P2X receptor subtypes, P2X4 is the one that primarily localized to lysosomes (Qureshi et al., 2007). Notably, lysosomes store high levels of ATP. In lysosomes, P2X4 was shown to be activated by ATP from the luminal side not the cytosolic side in a lysosomal pH-dependent manner (Huang et al., 2014). P2X4 tends to be more active at less acidic pH. Functionally, lysosomal P2X4 Ca^{2+} signals regulate membrane fusion (Murrell-Lagnado & Frick, 2019). Finally, in addition to TRPML1, TRPM2 that belongs to another subfamily of TRP channels has been found on lysosomes in pancreatic beta cells and dendritic cells to effect Ca^{2+} release (Lange et al., 2009; Sumoza-Toledo & Penner, 2011). The primary agonist for TRPM2 is ADPR. ADPR is a breakdown product of cADPR which has also been reported to activate TRPM2 (Kolisek et al., 2005; Yu et al., 2019). Functionally, TRPM2 Ca^{2+} signals have been linked to apoptosis (Faouzi & Penner, 2014; Lange et al., 2009). TRPM2 is the least explored lysosomal ion channels, which warrants more investigations.

1.2.2.5 NAADP

Central to lysosomal Ca^{2+} signalling is the Ca^{2+} mobilising messenger NAADP. NAADP can be synthesised from NADP and nicotinic acid via a CD38 catalysed base-exchange reaction (Aarhus et al., 1995). However, it is unclear as to how CD38 with a catalytic domain facing outside can generate intracellular Ca^{2+} messengers (Lee, 2000). Recently, the proposal of the existence of Type III CD38 with cytosolic catalytic domain may offer a route to solve the issue (Lee & Zhao, 2019).

NAADP was first characterized in sea urchin egg homogenates. Here, NAADP Ca^{2+} signalling is different from that by IP_3 and cADPR. NAADP responses were insensitive to IP_3 or cADPR inhibition (Lee & Aarhus, 1995). Besides, cytosolic Ca^{2+} that is known to regulate IP_3 and cADPR in a biphasic manner had no effect on NAADP (Chini & Dousa, 1996). That is, NAADP does not function through a CICR mechanism. Importantly, thapsigargin which depletes the ER stores did not abolish NAADP activity (Lee & Aarhus, 1995). Subsequently, using subcellular fractionation of sea urchin egg homogenates, NAADP responses were shown to be abolished by perturbing lysosome-related reserve granules (Churchill et al., 2002). Together, it was thus concluded that NAADP acts on acidic Ca^{2+} stores, which are different from the ER. It was this original study which laid the foundations for lysosomal involvement in Ca^{2+} signalling. To date, NAADP has been extensively examined in mammalian cells. Interestingly, NAADP functions differently between species. In the sea urchin, low concentrations of NAADP (<1 nM) induce little Ca^{2+} signals but fully suppress subsequent NAADP responses (Aarhus et al., 1996; Genazzani et al., 1996, 1997). However, in mammals, NAADP induces bell-shaped concentration-response curves: low (sub-micromolar) concentrations are associated with activation while higher concentrations lead to inhibition (Cancela et al., 1999). Moreover, irrespective of species, in intact cells, the ER is required for NAADP-induced Ca^{2+} signals (Cancela et al., 1999; Churchill & Galione, 2000). This is in contrary to the findings that NAADP does not target at the ER in broken cell systems. To explain this paradox, a "trigger hypothesis" has been proposed. Namely, NAADP induces lysosomal Ca^{2+} release, which then trigger Ca^{2+} release from the ER via CICRs, together amplifying the signals (Patel et al., 2001).

A few ion channels have been proposed as the molecular targets of NAADP, including RyRs. This is evidenced by increased RyRs activity in the presence of NAADP and decreased NAADP Ca^{2+} signals when reducing RyRs activity (Dammermann & Guse, 2005; Hohenegger et al., 2002; Langhorst et al., 2004). However, this is also in line with NAADP "trigger hypothesis". In other words, RyRs are not NAADP targets but are required for amplifying NAADP-induced lysosomal Ca^{2+} signals. Notably, there are also studies that report insensitivity of RyRs to NAADP (Copello et al., 2001; Ogunbayo et al., 2011; Wagner et al., 2014). Another candidate is TRPML1 as Zhang

and colleagues have shown that NAADP induced TRPML1-dependent Ca^{2+} signals (Zhang et al., 2009, 2011). However, another study failed to link TRPML1 to NAADP action (Yamaguchi et al., 2011). TRPM2 has also been associated with NAADP action (Beck et al., 2006), but recent studies dissociate TRPM2 from NAADP signalling (Tóth et al., 2015; Turlova et al., 2018). In contrast, there is abundant evidence to support TPCs as likely NAADP targets.

1.3 Two-pore channels

TPCs are members of the voltage-gated ion channel (VGICs) superfamily. As their name implies, TPCs contain two homologous shaker-like domains (I and II). Each domain comprises six transmembrane helices (S1-S6) and a pore region formed by S5 and S6 connected by a re-entrant loop (Guo et al., 2016; Hooper et al., 2011; Kintzer & Stroud, 2016; She et al., 2018, 2019). TPC dimerises to form functional channels that allow ion fluxes (Churamani et al., 2013; Guo et al., 2016; Kintzer & Stroud, 2016; Rietdorf et al., 2011; She et al., 2018, 2019), and thus maintains the typical pseudo-tetramer structure of VGICs (Yu et al., 2005). TPCs are expressed in plant vacuoles (Peiter et al., 2005) and within the acidic compartments of the endo-lysosomal system (of animals) (Brailoiu et al., 2009; Calcraft et al., 2009; Zong et al., 2009). TPCs exist as three isoforms (TPC1-3) in animals. Plants possess TPC1 gene only (Furuichi et al., 2001). Genes encoding TPCs are absent in key protostomes (e.g. flies or worms) (Calcraft et al., 2009). Although deuterostomes, such as dogs and sea urchins possess all three TPC genes, in humans and mice, only TPC1 and TPC2 are expressed and TPC3 exists as a pseudogene (Brailoiu et al., 2009; Brailoiu, Hooper, et al., 2010; Calcraft et al., 2009; Zhu et al., 2010). Within the endo-lysosomal system, TPC2 specifically targets to lysosomes via its N-terminal di-leucine motif, while TPC1 has a wider distribution (Brailoiu et al., 2009; Brailoiu, Rahman, et al., 2010; Calcraft et al., 2009; Zong et al., 2009) biased to endosomal compartments (Castonguay et al., 2017).

1.3.1 NAADP and TPCs

In 2009, three independent research groups suggested that TPCs are molecular targets for NAADP (Brailoiu et al., 2009; Calcraft et al., 2009; Zong et al., 2009). In these studies, NAADP-induced Ca^{2+} signals were largely potentiated upon TPC

overexpression and were abolished upon knockdown of TPC with shRNA. To further support that TPCs are NAADP likely targets, Brailoiu et al., 2009 generated and overexpressed dominant-negative mutant TPC1 ($TPC1^{L273P}$) and subsequently observed reduced NAADP but not cADPR Ca^{2+} signals. In a follow-up study by Brailoiu and colleagues, similar effects was observed with an equivalent dominant-negative TPC2 mutant ($TPC2^{L265P}$) (Brailoiu, Rahman, et al., 2010). Later, other Ca^{2+}-imaging based cellular studies further related NAADP action to TPCs, once again, showing NAADP Ca^{2+} signals are modulated by molecular manipulations of TPC expression (Brailoiu, Rahman, et al., 2010; Brailoiu, Hooper, et al., 2010; Hooper et al., 2011; Ogunbayo et al., 2011; Ruas et al., 2010; Yamaguchi et al., 2011). Importantly, TPC expression displays hallmark characteristics of NAADP-induced Ca^{2+} signals. For example, Ca^{2+} signals can be fully blocked by bafilomycin A1, indicating lysosomal origins (Brailoiu et al., 2009; Calcraft et al., 2009; Ruas et al., 2010). Concentration-response curves of Ca^{2+} signals are bell-shaped in mammals (Calcraft et al., 2009; Zong et al., 2009). Ca^{2+} signals can be blocked by NAADP antagonist, Ned-19 (Brailoiu, Rahman, et al., 2010). Finally, Ca^{2+} signals are generated via trigger hypothesis, that is, lysosomal Ca^{2+} release through NAADP-gated TPCs can be amplified by further ER Ca^{2+} release (Brailoiu, Rahman, et al., 2010; Calcraft et al., 2009; Ogunbayo et al., 2011; Ruas et al., 2010). Electrophysiological characterizations of TPCs have been performed as well. Such characterization is not easy given the vesicular localization of TPCs. Several approaches have been utilized to solve this. Functional TPC2 can be re-directed to the PM upon N-terminus mutation, which offers one approach. Other approaches are directly patch-clamping onto vacuolin-enlarged TPC positive-endolysosomes and reconstituting TPC into planer lipid bilayers. These approaches were first performed in 2010 by Brailoiu, Schieder and Pitt's teams to study TPC2 (Brailoiu, Rahman, et al., 2010; Pitt et al., 2010; Schieder et al., 2010), and were later used for TPC1 (Pitt et al., 2014; Rybalchenko et al., 2012). Each approach uncovers that TPCs are Ca^{2+}-permeable channels that are gated by NAADP.

Although multiple lines of evidence points towards TPCs as NAADP receptors, the molecular basis for NAADP action is not very clear. To date, there has been no evidence suggesting a direct action of NAADP on TPCs. Instead, an indirect action has been revealed. Photoaffinity labelling studies in mammalian and sea urchins have

shown that radioligand [^{32}P-5N$_3$]-NAADP labelled proteins are much smaller (22/23 kDa) than TPCs (Lin-Moshier et al., 2012; Walseth et al., 2012). Such NAADP-protein interaction (i.e. NAADP binding) persists in single and double TPC knockout mice (Lin-Moshier et al., 2012; Ruas et al., 2015) and the NAADP binding protein co-immunoprecipitated with TPCs in sea urchin egg homogenates (Walseth et al., 2012). Together, the current idea about NAADP mechanism is that NAADP activates TPCs indirectly via binding small accessory proteins that form part of a TPC channel complex. The identity of such proteins is unknown. Nevertheless, TPC2 was found to co-immuniprecipitate with small GTPase (e.g. Rabs) (Lin-Moshier et al., 2014) and kinases (e.g. LRRK2 and mTOR) (Cang et al., 2013; Gómez-Suaga et al., 2012). These proteins regulate TPC2 channel activity. Perhaps, the identity of such NAADP binding protein lies somewhere within those identified TPC interactomes (Castonguay et al., 2017; Grimm et al., 2014; Lin-Moshier et al., 2014).

With the aid of NAADP, TPCs have also been shown to be regulated by other molecules. Both TPC isoforms can be activated by luminal Ca^{2+} (Pitt et al., 2010; Rybalchenko et al., 2012). Luminal H^+ also favours TPC activity (Rybalchenko et al., 2012; Schieder et al., 2010), but the pH effects are complicated (Pitt et al., 2010). Indeed, TPC1 is permeable to H^+ (Pitt et al., 2014). Consistent with this, NAADP was shown to alkalize the acidic stores (Morgan et al., 2007). High Mg^{2+} (e.g. 2 mM) can act both luminally or cytosolically to inhibit TPC2 opening (Jha et al., 2014). The Mg^{2+} effect on TPC1 has not yet been tested. In addition, MAPK kinases, P38 and JNK, inhibits TPC2 NAADP-induced Ca^{2+} release (Jha et al., 2014). TPC1 and TPC2 are N-glycosylated. Such N-glycosylation confers an inhibitory effect on TPC1 activity, as reflected by potentiated NAADP Ca^{2+} signals upon mutation of glycosylated residues (Hooper et al., 2011). Furthermore, aside from NAADP, the endolysosomal membrane lipid, PI(3,5)P_2, has been shown to activate TPC1 and TPC2 (see 1.3.4 PI(3,5)P_2 and controversy over activation mechanism and ion selectivity). TPC1 is additionally gated by membrane potential (Cang et al., 2014; Rybalchenko et al., 2012; She et al., 2018) and cytosolic Ca^{2+} (Pitt et al., 2014).

1.3.2 TPCs in health and disease

As molecular targets for NAADP, TPCs have been widely studied and have been associated with a range of physiological processes and also diseases. For example, cellular differentiation requires functional TPCs. This has been noted during differentation of neuronal and skeletal muscle cells (Aley et al., 2010; Zhang et al., 2013). TPC2 has also been linked to osteoclastogenesis (Notomi et al., 2017) and zebrafish myogenesis (Kelu et al., 2019). Moreover, NAADP Ca^{2+} signalling and TPC2 is vital for vascular endothelial growth factor (VEGF)-induced angiogenesis (Favia et al., 2014), a process essential for cancer progression. The role of TPCs in cancer has been uncovered in recent years (this will be discussed in subsequent paragraph of this section). Aside from creating blood vessels, NAADP has a dual regulatory role on vascular tone. Blood vessels are composed of endothelial cells and vascular smooth muscle cells. In endothelial cells, NAADP is implicated in acetylcholine and histamine-induced Ca^{2+} signals (Brailoiu, Gurzu, et al., 2010; Esposito et al., 2011). Such signals stimulates vasorelaxation in intact blood vessels. Conversely, in endothelium-denuded vessels, NAADP causes vasoconstriction (Brailoiu, Gurzu, et al., 2010). In accord, it has been demonstrated that NAADP induces vascular smooth muscle contractility (Boittin et al., 2002). In a very recent study, TPC1 was shown to be required for the contractile function of NAADP in rat aortic smooth muscle (Trufanov et al., 2019).

TPCs also play key roles in endo-lysosomal trafficking, a process that is known to be mediated by local Ca^{2+} release from lysosomes (Luzio et al., 2007). A consistent observation is that overexpression of TPC2 leads to enlarged vesicular structures (Kilpatrick et al., 2017; Lin-Moshier et al., 2014; Ruas et al., 2010; Wang et al., 2012). Human TPC1 overexpression has no such effects, but TPC1 knockdown has been associated with enlargement and clustering of late endosomes and lysosomes (Kilpatrick et al., 2017). TPC2 is thought to regulate fusion events underlying the transit of cholesterol and growth factors (e.g. EGF and PDGF) (Grimm et al., 2014; Ruas et al., 2014). TPC1 mediates retrograde trafficking of cholera toxin from endosomes to Golgi complex (Ruas et al., 2010, 2014). Moreover, TPCs are also required for exocytosis, such as secretion of cytolytic granules in cytotoxic T cells (Davis et al., 2012) and acrosome reaction in mammalian sperm (Arndt et al., 2014).

Local Ca^{2+} signals through TPCs are likely mediators of TPC-associated trafficking effects. Supporting this, for example, it has been found that TPC2 overexpression-induced pigmentation defects can be reversed by fast Ca^{2+} chelator BAPTA but not the slow chelator EGTA (Lin-Moshier et al., 2014). And TPC2 ablation-induced mis-trafficking of LDL-cholesterol can be selectively phenocopied by BAPTA (Grimm et al., 2014). Two independent proteomic screens have revealed a physical association of TPCs with Rab GTPases (membrane trafficking regulators) and SNAREs (membrane fusion mediators) (Grimm et al., 2014; Lin-Moshier et al., 2014). Perturbing Rab7 activity abolishes NAADP Ca^{2+} signals and TPC2 overexpression-induced trafficking defects (Lin-Moshier et al., 2014), whereas SNAREs-mediated fusion event is Ca^{2+} dependent (Atlas, 2014). Together, the interaction between TPCs and Rab GTPases/SNAREs could form the molecular basis for TPCs' role in membrane trafficking.

TPCs also regulate autophagy that involves fusion between autophagosomes and lysosomes for degradation. The nutrient-sensing kinase, mTOR, is a key regulator of autophagy and associates with TPCs on lysosomes. When cells are replete with energy (i.e. high level of ATP), mTOR phosphorylates TPCs to keep the channel closed, which can be reflected by reduced NAADP or $PI(3,5)P_2$-activated TPC activity (Cang et al., 2013; Ogunbayo et al., 2018). Conversely, upon energy deprivation, mTOR is inhibited and thus removes the "lock" on TPC activation. mTOR inhibition is known to drive TFEB nuclear translocation, restoring autophagy function (Martina et al., 2012). In this regard, TPC activation could be linked to autophagy initiation. However, whether TPCs affect TFEB subcellular translocation is not very clear, although there is one case where sphingosine 1 phosphate-induced Ca^{2+} release through TPC1 leads to nuclear translocation of TFEB (Höglinger et al., 2015). The role of NAADP/TPCs on autophagy has been uncovered in various cell lines. In several cell types, it was shown that functional TPCs are required for autophagy progression (e.g. starvation or glutamate-induced autophagy) (García-Rúa et al., 2016; Pereira et al., 2011, 2017). However, the exact role, in fact, could be complex. In skeletal muscle cells that are devoid of TPC2, increased autophagic flux was observed upon starvation (Lin et al., 2015). From the same study, TPC2 has been shown to be required for mTOR reactivation and autophagy termination. Furthermore, it has been shown that LRRK2, another autophagy regulator, interacts with TPC2. Upon overexpression, LRRK2

impairs autophagy and induces a persistent increase in autophagosome (Gómez-Suaga et al., 2012). Such effects have been shown to be caused by LRRK2-activated TPC2 Ca^{2+} release and subsequent recruitment of CaMKKβ/AMPK signalling. Like TPC2, LRRK2 is also involved in membrane trafficking by interacting with Rab7 (Gómez-Suaga et al., 2014). There could be an interplay between these three proteins (TPC2, LRRK2 and Rab7) in regulating membrane fusion at a late stage of the autophagic process, but this requires further investigation.

LRRK2 is known as a PD linked gene. G2019S mutation confers increased kinase activity to LRRK2. Such a mutation is a common genetic cause of PD (Martin et al., 2014). Impaired autophagy has been found in LRRK2-mediated PD (Manzoni, 2017; Manzoni et al., 2013; Plowey et al., 2008), implying a role of TPC2 in PD (see above paragraph). Indeed, in patients' fibroblasts with $LRRK2^{G2019S}$ PD, the aberrant endo-lysosomal morphology, including enlarged and clustered lysosomes, can be improved by molecular silencing of TPC2 (not TPC1), or inhibiting its regulators (NAADP, $PI(3,5)P_2$ or Rab7) (Hockey et al., 2015). This echoes other studies where TPC2 overexpression is associated with morphology defects (Lin-Moshier et al., 2014; Ruas et al., 2010). What is more, such phenotypes can be reversed by treatment with BAPTA and are associated with exaggerated NAADP global Ca^{2+} signals. Together, pathogenic LRRK2 may enhance TPC2 Ca^{2+} functionality to cause dysfunction. TPC2 could be potential druggable target for PD to correct defective autophagy and membrane trafficking.

TPCs have also been implicated in other diseases, such as non-alcoholic fatty liver disease (NAFLD). It has been shown that mice deficient in TPC2, which are under high-cholesterol dietary condition, have cholesterol overload and liver damage, compatible with NAFLD (Grimm et al., 2014). Mechanistically, this is likely due to impaired trafficking of LDL-cholesterol and EGF upon TPC2 KO. As mentioned earlier, there is a functional requirement of TPC2 in fusion between endosomes and lysosomes. Thus, boosting TPC2 activity could be a treatment for liver disorders.

TPCs are also implicated in infectious viral diseases. Ebola virus (EBOV) is known to cause haemorrhagic fever with a high mortality rate (Baize et al., 2014). EBOV invades host cells through macropinocytosis, trafficking through the endo-lysosomal

system where it binds to NPC1 (Carette et al., 2011), subsequently fusing with late lysosomes and releasing its viral RNA into the cytoplasm. The significance of TPCs in EBOV entry was discovered by Sakurai et al (2015). In this study, TPC knockout, knockdown or overexpression of a dominant-negative TPC2 all prevented EBOV escape into the cytoplasm. Similarly, Ned-19 (NAADP antagonist) and tetrandrine (TPC blocker) effectively attenuated EBOV infection. Thus, TPCs are essential for Ebola infectivity likely via facilitating the late fusion step. Moreover, recently, TPCs have also been linked to the infectious cycle of another virus, Middle East Respiratory Syndrome coronavirus (MERS-CoV) (Gunaratne, Johns, et al., 2018; Gunaratne, Yang, et al., 2018). It was found that TPC knockdown or overexpression reduces MERS-CoV pseudovirus translocation through the endo-lysosomal system (Gunaratne, Yang, et al., 2018). The same inhibitory effect can also be seen in the presence of tetrandrine or its analogues that block NAADP Ca^{2+} responses. In addition, it was found that NAADP-mediated Ca^{2+} signals through TPCs regulate the activity of proprotein convertases, such as furin, which are required for MERS-CoV fusion activity and cytoplasmic translocation (Gunaratne, Yang, et al., 2018). Furthermore, TPCs were found to participate in the life-cycle of HIV. Perturbing TPC activity inhibits the endo-lysosomal release of HIV Tat protein, and thus subsequent HIV gene replication and cell-to-cell infection (Khan et al., 2020). Together, TPCs appear to be common host factors that regulate a range of viral infections. Pharmacological modulators of TPC could be clinically beneficial for the treatment of infectivity.

Cancer is another disease that has been associated with TPCs. Expression of TPCs has been noted in various cancer cell lines (Brailoiu et al., 2009; Jahidin et al., 2016; Nguyen et al., 2017). Recent evidence have suggested that TPCs are required for angiogenesis and metastasis. Also, TPCs may play roles in tumorigenesis. This is because TPC2 is found on chromosome 11, region 13.2, whose amplification is known to be associated with cancer (Wilkerson & Reis-Filho, 2013). Also, this region has a cyclin gene, an established driver of oncogenesis. Of relevance, Huang et al (2006) observed increased TPC2 levels in oral squamous cell carcinoma cell lines (Huang et al., 2006). Regarding a role in angiogenesis, as mentioned above, VEGF-induced angiogenesis in endothelial cells relies on NAADP Ca^{2+} signalling through TPC2 (Favia et al., 2014). This has been demonstrated in both vitro and vivo. Angiogenesis is essential for tumour growth, and recently, it has been shown that cancer cell

proliferation requires functional TPCs (Faris et al., 2019). Cell adhesion and migration are two critical steps for metastatic formation, which were found to be reduced by perturbing TPC activity via either siRNA or Ned-19 (NAADP antagonist) (Nguyen et al., 2017). In accord, reduced metastatic tumour formation upon impaired TPC activity has been noted in an *in vivo* model. The reduced adhesion and migration are likely to be caused by defective trafficking of integrins (migration mediator) upon TPC knockdown (Nguyen et al., 2017). Together, TPCs could be drug targets for cancer treatment by interfering with tumorigenesis, angiogenesis and metastasis.

The significance of TPCs are not limited to above-mentioned diseases. TPCs are also mediators of cardiac dysfunction, such as ischemia-reperfusion injury (Davidson et al., 2015). Besides, TPCs have been linked to diabetes as NAADP/TPCs are required for glucose-induced Ca^{2+} signals that are essential for insulin secretion (Arredouani et al., 2015; Masgrau et al., 2003; Naylor et al., 2009). TPCs also possess roles in obesity (Lear et al., 2015) and Alzheimer's disease (Neely Kayala et al., 2012).

1.3.3 TPC pharmacology

As TPCs are important for health and disease, it is essential to find modulators of the channel to aid research and drug discovery. However, the work in this field is limited and relatively preliminary. Current TPC activators and inhibitors are summaried in Table1.1 and Table 1.2, respectively.

Aside from NAADP, another current known endogenous TPC activator is $PI(3,5)P_2$. This was reported by (Wang et al., 2012) first, and confirmed by other studies later (Boccaccio et al., 2014; Cang et al., 2013, 2014; Grimm et al., 2014; Ruas et al., 2015). The activity of NAADP and $PI(3,5)P_2$ is not limited to TPCs, as they have also been shown to activate TRPML1 (Dong et al., 2010; Zhang et al., 2009), although the action of NAADP on TRPML1 is not widely accepted (Yamaguchi et al., 2011). NAADP and $PI(3,5)P_2$ are anionic and thus membrane-impermeable. Complex techniques (e.g. microinjection or use of isolated lysosomes) have been used for allowing them to reach the endo-lysosomal targets. Cell-permeable NAADP has been developed and used in certain studies (Cang et al., 2014; Parkesh et al., 2008; Sakurai et al., 2015; Wang et al., 2012). However, this version of NAADP requires meticulous care as it is

notoriously unstable (Parkesh et al., 2008). Besides, synthesis of NAADP-AM requires diisopropylethylamine (DIEA) which cannot be completely removed in the final NAADP-AM product. It has been reported that DIEA can inhibit SERCA via a cytosolic alkalizing effect and thus inducing Ca^{2+} signals. Therefore, prior to using, NAADP-AM should be tested to ensure it can induce a bell-shape dose-response curve for Ca^{2+} signals which are sensitive to Ned-19 (NAADP antagonnist) (Galione et al., 2014; Zhang et al., 2013). The cell-permeable TPC activators have only recently been pursued through Ca^{2+}-imaging based drug screening assay (Zhang et al., 2019). The novel activators (i.e. tricyclic anti-depressants (TCAs)) have no visible effect on TRPML1. Structurally, they can be divided into two groups, LyNA-VA1.X and LyNA-VA2.X (named by the authors). They activate TPC2 at micromolar concentrations. They also modulate TPC1, but activation or inhibition appears to rely on TCAs' chemical structures. From the same study but a separate screen, another identified TPC modulator is riluzole which is known as an effective drug treatment for ALS (Liu & Wang, 2018). Riluzole is a activator for TPC2 but a inhibitor for TPC1. In chapter 3, I further identify cell-permeable TPC activators.

Table 1.1 Summary of TPC activators

Name	**(Original/other) Identity**	**Method (s)**	**Potency (e.g. EC_{50})**	**Paper (s)**
NAADP	Ca^{2+} mobilizing messenger	Ca^{2+} measurements in sea urchin egg homogenate	EC_{50}= 20-30 nM. Self-inactivation if concentration ≤1 nM	i) Genazzani et al., 1996 ii) Aarhus et al., 1996
		Ca^{2+} measurements in mammalian cells	Bell-shape concentration-response curve: maximal response at 100 nM, no response > 1 μM	i) Cancela et al., 1999 ii) Galione, 2011
$PI(3,5)P_2$	Endolysosomal membrane lipid	Patch-clamp recording in enlarged endolysosomes transfected with TPC1 or TPC2	EC_{50}= 0.39μM	Wang et al., 2012
LyNA-VA1.X 1.1 Amitriptyline	Tricyclic antidepressants		i) EC_{50}= 43-112 μM for TPC2	Zhang et al., 2019

1.2 Clomipramine 1.3 Desipramine 1.4 Imipramine 1.5 Nortriptyline		i) Ca^{2+} measurements in cells transfected with TPC2 ii) Patch-clamp recording in enlarged endolysosomes transfected with TPC1 or TPC2 iii) Patch-clamp recording in whole-cells transfected with PM TPC2 ($TPC2^{LL/AA}$)	ii) EC_{50}= 10-27 μM for TPC1	
LyNA-VA2.X 2.1 Chlorpromazine 2.2 Triflupromazine			i) EC_{50}= ~60 μM for TPC2 ii) Block of TPC1 activity at ~70 μM	
Riluzole	Glutamate receptor antagonist		i) EC_{50}= ~180 μM for TPC2 ii) Block of TPC1 activity at ~150 μM	

NAADP mobilizes Ca^{2+} through TPCs (Patel, 2015). Early studies centered around NAADP signalling have resulted in identification of a few NAADP antagonists. The most classical and widely-used one is Ned-19, which is identified from NAADP-based virtual screening (Naylor et al., 2009). Ned-19 exhibits high degree of similarity to NAADP in terms of its three-dimensional shape and electrostatic properties. Since its discovery, Ned-19 has been widely used and has facilitated our understanding on the role of NAADP/TPCs in a number of physiological and pathophysiological events (Ali et al., 2016; Favia et al., 2014; Hockey et al., 2015; Rah et al., 2017; Sakurai et al., 2015; Suárez-Cortés et al., 2017). PPADS and BZ194 were identified as NAADP antagonists around the same time as Ned-19 (Billington & Genazzani, 2007; Dammermann et al., 2009). PPADS is a competitive P2 receptor antagonist. PPADS blocked NAADP-induced Ca^{2+} signals in both sea urchin eggs and mammalian cells but requiring 100 μM (Billington & Genazzani, 2007; Singaravelu & Deitmer, 2006). BZ194 is a N-alkalyted nicotinic acid derivative. Like PPADS, BZ194 also required high micromolar concentrations to affect NAADP signalling (Dammermann et al., 2009). In comparison, Ned-19 appears to be more potent as functional studies in sea urchin egg homogenate revealed its IC_{50} within nanomolar range (Naylor et al., 2009; Rosen et al., 2009). Regarding their mechanism of action, given that NAADP activates TPCs via binding to an accessory protein (Lin-Moshier et al., 2012; Walseth et al., 2012), the NAADP analogue, Ned-19, is likely to act via similar indirect and complex mechanism. BZ194 might be the same as it also has some structural similarity of

NAADP. For PPADS, it reversibly competes with [^{32}P]-NAADP binding which means it could also function indirectly on TPCs (Billington & Genazzani, 2007). Such indirect action on TPCs could raise concern given that NAADP also appears to target other receptors (e.g. TRPML1 and RyRs) (Dammermann et al., 2009; Hohenegger et al., 2002; Langhorst et al., 2004; Zhang et al., 2009) although this is still contested (Ogunbayo et al., 2011; Wagner et al., 2014; Yamaguchi et al., 2011). BZ194 was shown to block NAADP-activated RyR activity (Dammermann et al., 2009).

Aside from the above-mentioned antagonists, in another early study, a number of L-type voltage-gated Ca^{2+} channel antagonists (e.g. nifedipine, diltiazem and verapamil) were shown to selectively block NAADP-induced Ca^{2+} signals in sea urchin egg homogenates at low micromolar concentrations (Genazzani et al., 1997). None of these compounds affected NAADP binding. Therefore, it is possible that they work at the level of TPCs. In 2014, through molecular docking against a structural model of sea urchin TPC1, Cav antagonists as well as Nav antagonists were found to target the pore-region of TPCs (Rahman et al., 2014). This similarity in drug binding sites between TPCs and Cav/Nav channels is likely due to a common ancestry shared between these channels. As suggested by Rahman and colleagues, the binding site could have been formed before a duplication event that was required for the formation of both Cav and Nav. After molecular docking, functional studies followed. Rahman and colleagues noted that there is a positive correlation between Cav and Nav antagonists' docking capacity and their capacity in inhibiting NAADP-induced Ca^{2+} signals. Rahman's team therefore identified a number of Cav and Nav antagonists as TPC pore blockers (Rahman et al., 2014). The pore-region could be the target for other TPC blockers.

In 2015, along with studying the role of TPCs on Ebola infectivity, tetrandrine was yielded as a potent TPC blocker (Sakurai et al., 2015). Tetrandrine is a bisbenzylisoquinoline alkaloid (BBIQ) isolated from the plant *Stephania tetrandra* (Bhagya & Chandrashekar, 2016). In the study, tetrandrine effectively inhibited Ebola release by blocking TPC activity (Sakurai et al., 2015). Tetrandrine is very potent in terms of its action on TPCs. At 500 nM, it blocked NAADP and $PI(3,5)P_2$-induced TPC currents. And at 2 μM, it blocked NAADP-AM induced Ca^{2+} release. Although potent, tetrandrine has multiple targets, including Rasip-cAMP-PKA pathway (Zhao et al., 2013) and Ca^{2+}-activated K^+ channels (King et al., 1988; Wang & Lemos, 1994).

Importantly, tetrandrine is also a well-defined Cav antagonist (King et al., 1988; Liu et al., 1991; Wang & Lemos, 1994). There has been no study looking into the molecular basis of tetrandrine inhibition. Given its identity as a Cav antagonist, tetrandrine is predicted to target the pore-region of TPCs like it did to the evolutionarly-linked Cav (King et al., 1988; Rahman et al., 2014). Two years later, another TPC antagonist, naringenin, was published (Pafumi et al., 2017). Naringenin is a flavonoid that can be found in fruits and herbs. Naringenin blocked $PI(3,5)P_2$-induced TPC channel activity and NAADP-induced Ca^{2+} release but requiring concentrations up to 1 mM. In addition to that, like tetrandrine, naringenin also has targets other than TPCs, such as TRPM3 (Straub et al., 2013), TRPP2 (Waheed et al., 2014), N-type Cav channels (Zhou et al., 2019) and Ca^{2+}-activated K^+ channels (Saponara et al., 2006; Yang et al., 2014). In a later study, through molecular docking, a direct action of naringenin on TPCs has been predicted, likely by interacting with the hydrophobic residues that constitute the gate of the pore (Benkerrou et al., 2019).

In 2018/2019, research into pursuing inhibitors of TPC continued given there are few selective TPC inhibitors and some indirectly affect TPCs (e.g. BZ194, PPADS and Ned-19). Using sea urchin egg homogenate as a screening platform, Guanratne and colleagues identified 18 compounds as selective NAADP inhibitors (Gunaratne, Johns, et al., 2018). Some of the compounds were further characterized. At low micromolar concentration, they inhibited NAADP Ca^{2+} signals in mammalian cells as well as TPC-dependent MERS-CoV infectivity. SKF96365, PF-543 and racecadotril have been highlighted as they are the most effective ones in all three testing systems. Notably, this is not the first paper to link SKF96365 to NAADP, in fact, in Moccia et al., 2004, it has been shown that SKF96365 blocks NAADP-dependent starfish oocyte activation at fertilization at low micromolar concentration (Moccia et al., 2004). Moreover, SKF96365 is also a T-type voltage-gated Cav channel blocker (Singh et al., 2010). PF-543 is a sphingosine kinase inhibitor (Schnute et al., 2012), and racecadotril is a neutral endopeptidase inhibitor used to treat diarrhea (Matheson & Noble, 2000; Schwartz, 2000). The mechanism of action of these novel inhibitors are unclear, but given that they have no effect on NAADP binding, perhaps they directly act on TPCs, warrenting further investigation. In a companion paper, tetrandrine analogues (e.g. fangchinoline) were also identified as inhibitors of NAADP Ca^{2+} signalling and MERS translocation (a step required for virus entry into the cells) (Gunaratne, Yang, et al., 2018).

To expand the pharmacology of TPCs in the context of clinically used drugs, our lab screened a library of FDA-approved drugs against a model of the human TPC2 pore (Penny et al., 2019). The model was generated based on the mouse TPC1 structure published in 2018 (She et al., 2018). The results were then cross-referenced with data from two previous high-throughput Ebola screens. Use of the latter was because if TPCs are required for Ebola infection, then anti-Ebola drugs may be inhibitors of TPCs. Such a screening strategy yielded a number of novel TPC blockers, including dopamine receptor antagonists (e.g. fluphenazine) and estrogen receptor modulators (e.g. raloxifene). They blocked NAADP- and $PI(3,5)P_2$-induced TPC2 channel activity at low micromolar concentrations. Single channel analysis uncovered that they act via the TPC2 pore. In chapter 3, I further characterize these novel inhibitors.

To summarise, the study on pharmacology of TPCs is far from mature, although in recent years, efforts have been made to identify novel TPC activators and inhibitors.

Table 1.2 Summary of TPC inhibitors

Name	**(Original/other) Identity**	**Method (s)**	**Potency (e.g. IC_{50})**	**Paper (s)**
Ned-19	N/A (identified from NAADP-based virtual screen)	i) Test on NAADP Ca^{2+} responses in sea urchin egg homogenate ii) Test on NAADP Ca^{2+} responses in mammalian cells	i) IC_{50}= 65 nM in homogenate ii) Complete suppression of NAADP responses at 100 μM in mammalian cells	i) Naylor et al., 2009 ii) Rosen et al., 2009
PPADS	P2 receptor antagonist		Partial suppression of NAADP responses at 100 μM	i) Billington & Genazzani, 2007 ii) Singaravelu & Deitmer, 2006
BZ194	N-alkylated nicotinic acid derivative	Test on NAADP Ca^{2+} responses in mammalian cells	Partial suppression of NAADP responses at 100 μM	Dammermann et al., 2009

(Table 1.2 continued in next page**)**

Nifedipine; Diltiazem; Verapamil; Isradipine	Cav antagonists	Test on NAADP Ca^{2+} responses in sea urchin egg homogenate (Note: nifedipine, lidocaine and veratridine were also tested on NAADP-induced Ca^{2+} signals in mammalian cells expressing TPC1)	i) IC_{50}= 8-20 μM in homogenate ii) IC_{50} = 4 μM (Nif. in TPC1-expressing cells)	i) Genazzani et al., 1997 ii) Rahman et al., 2014
BayK 8644	Cav agonist		IC_{50}= 30 μM in homogenate	Genazzani et al., 1997
Lidocaine; Bupivacaine	Nav antagonists		i) IC_{50}= 100 μM (Lido.) or 1 mM (Bupi.) in homogenate ii) Complete suppression of NAADP responses at 100 μM (Lido. in TPC1-expressing cells)	Rahman et al., 2014
Veratridine	Nav agonist		i) IC_{50}= 52 μM in homogenate ii) Complete suppression of NAADP responses at 100 μM (Vera. in TPC1-expressing cells)	
Tetrandrine	i) Bisbenzylisoquin-oline (BBIQ) cyclic alkaloid ii) Cav antagonist	i) Test on $PI(3,5)P_2$ currents in cells transfected with TPCs ii) Test on NAADP Ca^{2+} release in mammalian cells	Effective at 0.5-2 μM	Sakurai et al., 2015
Naringenin	Plant flavonoid	Test on $PI(3,5)P_2$ currents in cells transfected with TPCs	Effective at 1 mM	Pafumi et al., 2017
SKF96365	T-type Cav antagonist	i) Test on NAADP Ca^{2+} responses in sea urchin egg homogenate ii) Test on NAADP Ca^{2+} responses in mammalian cells	i) IC_{50}= 2-16 μM (in homogenate) ii) Effective at 10 μM (in cells)	Gunaratne, Johns, et al., 2018
PF-543	Sphingosine kinase inhibitor			
Racecadotril	Endopeptidase inhibitor			

(Table 1.2 continued in next page**)**

Fangchinoline; Thaligine	Bisbenzylisoquinoline (BBIQ) cyclic alkaloids	Test on NAADP Ca^{2+} responses in mammalian cells	Effective at 10 μM	Gunaratne, Yang, et al., 2018
Fluphenazine; Pimozide; Thioridazine; Trifluoperazine	Dopamine receptor antagonists	Test on NAADP Ca^{2+} responses in sea urchin egg homogenate (Note: fluphenazine and raloxifene were also tested on NAADP-mediated channel activity of TPC2 re-directed to the PM or on $PI(3,5)P_2$ currents in cells transfected with TPC2)	i) IC_{50}= 28-94 μM (in homogenate) ii) Effective at 100 μM to block TPC2 channel activity mediated by NAADP (Ralo. and Flu.) iii) IC_{50}= 0.63 μM (Ralo. on $PI(3,5)P_2$ currents) iiii) IC_{50}= 8.2 μM (Flu. on $PI(3,5)P_2$ currents)	Penny et al. 2019
Raloxifene; Clomiphene; Tamoxifen; Toremifene; Bazedoxifene	Selective estrogen receptor modulators			
Amodiaquine	Antimalarial reagent			

1.3.4 $PI(3,5)P_2$ and controversy over activation mechanism and ion selectivity

The endolysosome-specific phosphoinositide $PI(3,5)P_2$ is synthesized from PI(3)P through a PI5 kinase, PIKfyve, which is localized on the endolysosomes (McCartney et al., 2014). In mammals, PIKfyve is the sole lipid kinase that phosphorylates PI(3)P to generate $PI(3,5)P_2$ (Zolov et al., 2012). PIKfyve regulates $PI(3,5)P_2$ levels through association with proteins Fig4 and Vac14 (Hasegawa et al., 2017). $PI(3,5)P_2$ deficiencies caused by mutations in PIKfyve and its associated proteins have been linked to neurodegenerative diseases, such as amyotrophic lateral sclerosis (ALS) and Charcot-Marie-Tooth disease (Chow et al., 2007, 2009). Physiologically, insulin, growth factors and hyperosmotic shock have been shown to induce a transient increase in $PI(3,5)P_2$ level (Sbrissa et al., 1999; Sbrissa & Shisheva, 2005; Zolov et al., 2012), suggesting that $PI(3,5)P_2$ is required for cellular homeostasis and adaption. Moreover, $PI(3,5)P_2$-deficient cells exhibit enlarged endolysosomes. $PI(3,5)P_2$ thus plays a role in membrane trafficking (Dong et al., 2010; Dove et al., 2009; Zhang et al., 2007). Such aberrant morphology can be reversed by TRPML1 overexpression, consistent with that TRPML1 as a likely target for $PI(3,5)P_2$ (Chen et al., 2017; Dong et al., 2010).

As briefly mentioned above, TPCs have also been reported to be the molecular targets for $PI(3,5)P_2$. In the study by Wang and colleagues (Wang et al., 2012), $PI(3,5)P_2$ induced inward-rectifying currents from vacuolin-enlarged lysosomes overexpressing WT TPC2 but not the inactive pore-mutant ($TPC2^{D273K}$). $PI(3,5)P_2$ also activated currents from lysosomes overexpressing TPC1 or in cells overexpressing TPC2 re-directed to the PM. Importantly, $PI(3,5)P_2$-induced TPC currents were abolished in pancreatic ß-cells from TPC double knockout mice. However, what was suprising was that in parallel tests, there was no sensitivity of TPCs to NAADP, and NAADP-induced Ca^{2+} signals were not affected upon TPC double KO. In addition to that, when examining the relative ion permeability, Wang and colleagues noted that TPC2 is highly Na^+ selective with little Ca^{2+} permeability. This therefore was in contrast with early electrophysiological analysis, where TPCs were demonstrated to act as NAADP-gated channels that are permeable to Ca^{2+} (Na^+ was not tested) (Brailoiu, Rahman, et al., 2010; Pitt et al., 2010, 2014; Rybalchenko et al., 2012; Schieder et al., 2010).

Wang's study is not isolated. In fact, since the initial controversy, certain studies agreed with Wang et al., 2012. For example, through directly patch-clamping onto TPC1-positive lysosomes, Cang's team observed TPC1 currents activated by $PI(3,5)P_2$ but not NAADP (Cang et al., 2014). Furthermore, they noted that TPC1 is highly Na^+ selective with PNa/PCa of 232. In another study by Cang's team, TPC has been shown to function as a nutrient sensor linked to mTOR. ATP regulates TPC-mediated Na^+ currents via mTOR. ATP action is dependent on $PI(3,5)P_2$ levels. In the same study, in contrast to $PI(3,5)P_2$, NAADP does not activate TPC2 (Cang et al., 2013). In the study of Boccaccio et al., 2014 and Guo et al., 2017, $PI(3,5)P_2$ but not NAADP elicited currents in human TPC2 expressing plant and yeast vacuoles and in cells expressing PM TPC2. In addition, both studies noted the channel is highly Na^+ selective with little Ca^{2+} permeability when activated by $PI(3,5)P_2$ (Boccaccio et al., 2014; Guo et al., 2017). Data from the aforementioned labs thus consistently link $PI(3,5)P_2$ and Na^+ selectivity but not NAADP and Ca^{2+} permeability to TPC activation. In a recent study exploring the structure of mouse TPC1, the channel was once again shown to be highly selective to Na^+ in the presence of $PI(3,5)P_2$ (She et al., 2018).

However, since the initial controversy, there have also been a number of studies supporting that NAADP-dependent activation of TPCs. Also, these studies confirmed

the action of $PI(3,5)P_2$ on TPCs. (Grimm et al., 2014; Hockey et al., 2015; Jha et al., 2014; Lee et al., 2016; Penny et al., 2019; Ruas et al., 2015; Sakurai et al., 2015). In several of these studies, the Na^+ currents through TPCs have also been assessed along with Ca^{2+} currents. For example, Jha's team used the same enlarged lysosomal technique as (Cang et al., 2014; Wang et al., 2012), and found that both NAADP and $PI(3,5)P_2$ activated TPC Na^+ currents (Jha et al., 2014). In comparison, the current magnitude for NAADP was smaller than that of $PI(3,5)P_2$. Grimm et al (2014) used cells from TPC2 KO mice and confirmed that NAADP and $PI(3,5)P_2$ activate endogenous TPC2, and also indicated that NAADP-activated TPC2 is not selective between Na^+ and Ca^{2+} with PCa/PNa close to unity (Grimm et al., 2014). In 2015, Ruas's team generated an independent TPC double KO mice in which both NAADP and $PI(3,5)P_2$ currents were lost (Ruas et al., 2015). Ruas's team subsequently performed rescue experiments, showing that NAADP regained its activity in the KO cells when TPC1 or TPC2 were re-expressed, but not TPCs with mutated pore or TRPML1. Additonally, Ruas's team found that NAADP currents are non-selective and thus TPCs have relative equal permeability to Ca^{2+} and Na^+. Quite recently (2019), through single channel recording on TPC2 targeted to the PM or directly patch-clamping onto TPC2-positive enlarged lysosomes, our lab's work has further confirmed that NAADP and $PI(3,5)P_2$ activate TPCs (Penny et al., 2019). Using Na^+ as the major permeant ion, the single channel analysis indicates that TPC2 Na^+ conductance is 87pS. Comparing this with the Ca^{2+} conductance of TPC2 (40pS) (Brailoiu, Rahman, et al., 2010), which was obtained previously in the presence of NAADP, firmly points out that TPC2 is a non-selective Ca^{2+}-permeable channel. Together, the aforementioned studies, this body of work supports the notion that both NAADP and $PI(3,5)P_2$ are TPC activators, and that the channel is permeable to both Ca^{2+} and Na^+.

For those that failed to report TPC sensitivity to NAADP, several possible explanations have been proposed. It has been reported that N-terminally GFP-tagged TPC1 is insensitive to NAADP (Churamani et al., 2013) and Wang et al., 2012 used such a TPC1 construct (Wang et al., 2012). NAADP has been shown to activate the channel via putative small binding proteins which might have been accidentally removed when isolating lysosomes from the cells for patch-clamp recording. Regarding the maintained NAADP activity upon TPC double KO, this could be due

to the concentration of the cell-permeable NAADP-AM used being too high, and its DIEA contaminats causing undesired effects on Ca^{2+} and pH homeostasis (Zhang et al., 2013). Additonally, the KO might have been incomplete. The KO involved the deletion of the first 69 amino acids of TPC1. Such deletion was shown to lead to the generation of a variant TPC1 isoform, TPC1B (Ruas et al., 2014). In Ruas et al., 2015, TPC1B was found to be sensitive to NAADP (Ruas et al., 2015). However, it is hard to explain why in some cases, TPCs are highly Na^+ selective (little Ca^{2+} permeability), while in the others, TPCs are non-selective between Ca^{2+} and Na^+.

A co-regulation TPC model has been proposed (Patel, 2015), but there is only a limited amount of evidence directly supporting this. For example, $PI(3,5)P_2$ levels have been shown to associate with NAADP-induced TPC-dependent Ca^{2+} signals (Jha et al., 2014). Increasing $PI(3,5)P_2$ by expression of PIKfyve potentiated NAADP-induced Ca^{2+} signals, and inhibiting $PI(3,5)P_2$ synthesis by YM201636 (an inhibitor of PIKfyve) abolished NAADP responses. In another study, $PI(3,5)P_2$ was found to alter the ion selectivity of NAADP-activated TPC1, such that the channel was more Na^+- and H^+-permeable (Pitt et al., 2014).

To summarise, both NAADP and $PI(3,5)P_2$ have received abundant and independent electrophysiological evidence as TPC activators. Nevertheless, the gating mechanism of TPCs remain equivocal. Furthermore, the ion selectivity of TPCs remain controversial. In chapter 4, I address the above issues using novel activators from chapter 3.

1.4 TPC structure and mutagenesis

As with other VGICs, TPCs also possess a pseudo-tetrameric structure where four domains come together to form a central pore allowing ion fluxes. Specifically, the assembled TPC channel is a dimer of two-domain subunits (Churamani et al., 2013; Guo et al., 2016; Kintzer & Stroud, 2016; Rietdorf et al., 2011; She et al., 2018, 2019). Accordingly, TPCs are considered to hold an intermediate position in the evolution of VGICs. The gene encoding one-domain channels (e.g. Kv and TRP) underwent one round of duplication to form TPCs, the TPC gene then underwent another round of duplication to evolve into four-domain channels (e.g. Cav and Nav). Phylogenetic analyse confirmed this by showing that each domain of TPCs is closely related to the respective domain of Cav and Nav (Rahman et al., 2014). The physical structure of TPCs was first resolved in 2016. In that year, using X-ray crystallography, the structure of TPC1 from *Arabidopsis thaliana* (AtTPC1) was determined at 3.3 Å and 2.87 Å resolution (Guo et al., 2016; Kintzer & Stroud, 2016). Recently, using electron cryo-microscopy, the 3D structures of mouse TPC1 (MmuTPC1) and human TPC2 (HsaTPC2) were determined as well (She et al., 2018, 2019). Although there is low sequence similarity between plant and mammalian TPCs, the overall architecture is maintained (see Figure 1.2). Each subunit has two six-transmembrane domains, 6-TM1 (IS1-IS6) and 6-TM2 (IIS1-IIS6), connected by a cytosolic linker. Two termini (N/C-terminus) face the cytosolic side. The first four helices (S1-S4) form voltage sensor domain (VSD), and S5-S6 forms the pore region (Guo et al., 2016; Kintzer & Stroud, 2016; She et al., 2018, 2019). The ion selectivity filter motif is situated within the re-entrant pore loop between S5 and S6, which determines the identity of the permeating ions (Guo et al., 2017; She et al., 2018, 2019). When two subunits assembled into a functional TPCs, the pore-regions form a central pore that permit ion fluxes, and the VSD sits peripheral via S4-S5 linker (Penny & Patel, 2015). Interestingly, MmuTPC1 has a β-Hairpin structure at the pore-region formed between IIS5 and IIS6 and a longer C-terminus compared to HsaTPC2 (She et al., 2018, 2019).

These recent resolved TPC structures together with the previous mutagenesis studies have provided a molecular basis for understanding the channel. These are discussed (below) and illustrated (in Figure 1.3).

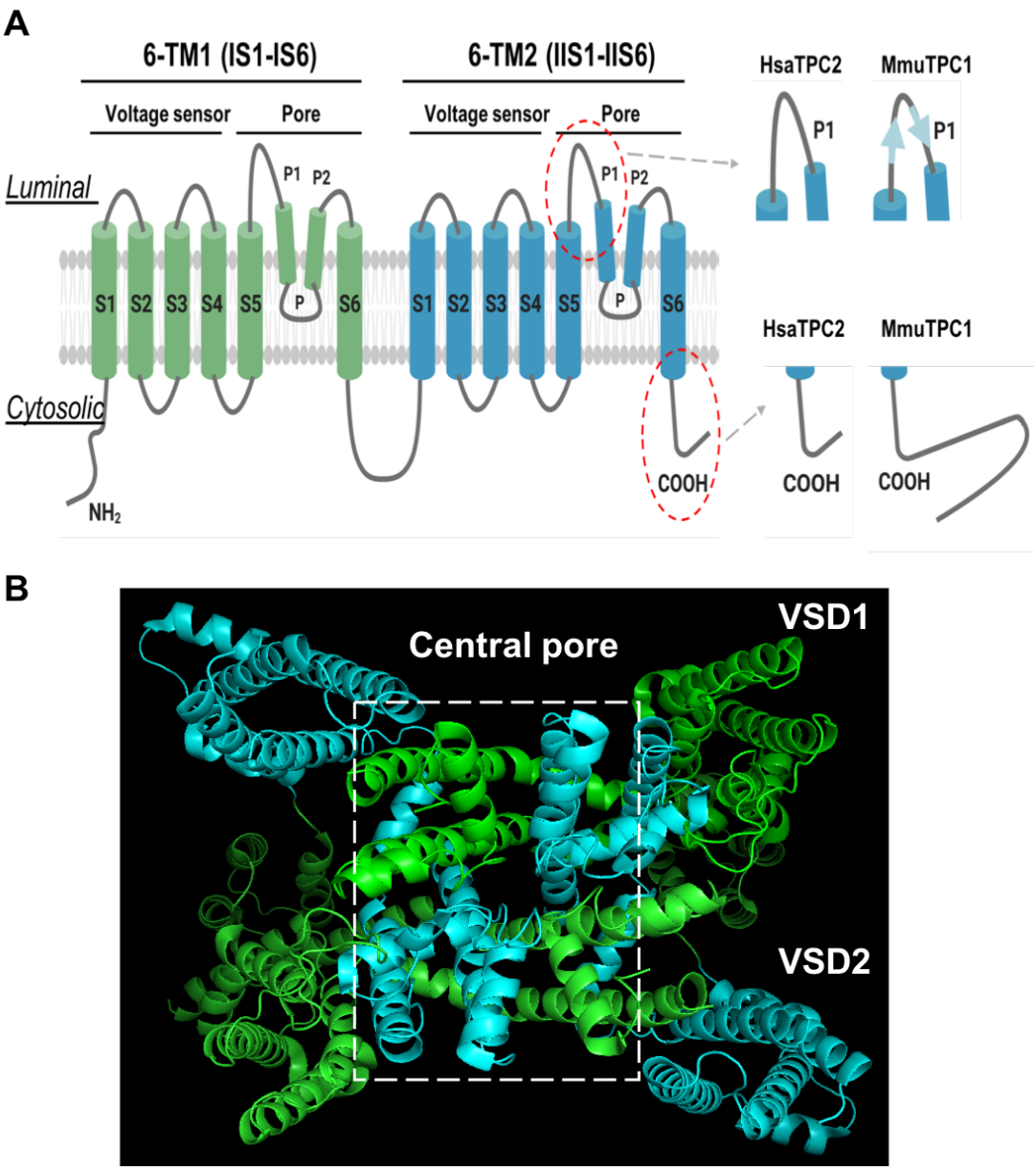

Figure 1.2 Topology and assembly of TPCs

(A) Topology and domain arrangement of an individual subunit of TPCs. The differences in structures between mouse TPC1 (MmuTPC1) and human TPC2 (HsaTPC2) are labelled with dashed circles and are compared on the right (arrow). Compared to TPC2, TPC1 has a β-Hairpin structure at the pore-region formed between IIS5 and IIS6 (top panel) and a longer C-terminus (bottom panel).

(B) Cartoon representation of an assembled TPC, from a luminal view (Protein Data Bank (PDB) ID: 6NQ1 (She et al., 2019)). The central TPC pore is labelled with a white square. VSD refers to voltage sensor domain.

1.4.1 Targeting

The N-terminus of TPCs is required for channel trafficking to the endo-lysosomal system. The N-terminus contains a di-leucine (LL) motif, mutation of which (L11A/L12A) can re-direct TPC2 to the plasma membrane (Brailoiu, Rahman, et al., 2010) without affecting the channel's gating mechanism and ion selectivity (Wang et al., 2012). As mentioned earlier, this PM TPC2 offers one route for electrophysiological characterization on the channel. At the PM, NAADP-induced Ca^{2+} signals were unaltered by the inhibition on the ER Ca^{2+} release (Brailoiu, Rahman, et al., 2010), supporting the trigger hypothesis and indicating that a close physical association between lysosomes and the ER are essential for Ca^{2+} coupling. TPC1's endo-lysosomal localization is independent of such motif (Brailoiu, Rahman, et al., 2010). Indeed, TPC1 isoform, TPC1B, which has an N-terminal truncation of the first 69 amino acid residues, also has endo-lysosomal localizations (Ruas et al., 2014, 2015). However, in Churamani et al. 2013, TPC1 was found on the ER upon full truncation of its N-terminus (Churamani et al., 2013). This thus suggests that TPC1 may require a segment of N-terminus for targeting, but this segment is unlikely to be within the first 69 residues.

1.4.2 PI(3,5)P_2-gating

The recent cryo-EM MmuTPC1 structure revealed that PI(3,5)P_2 binds to the channel via residues from 6-TM1 (Fig.1.2A). The most important residues are a cluster of arginines (R220, R221 and R224) on the IS4–IS5 linker (She et al., 2018). Mutating any arginines into alanine (A) largely abolished PI(3,5)P_2-induced channel currents. Interestingly, the three arginines have also been shown to be required for NAADP-induced TPC1-dependent Ca^{2+} signals (Patel et al., 2017). However, given NAADP activates the channel through interaction with an accessory binding protein (Lin-Moshier et al., 2012; Walseth et al., 2012), the study pointed that NAADP is unlikely to directly bind to the linker (Patel et al., 2017). PI(3,5)P_2 binds to the same region in TPC2, but notably the binding residues on IS4-IS5 linker are three lysines (K203, K204 and K207) instead of arginines (She et al., 2019). Mutation of any lysines largely reduced PI(3,5)P_2 activity. The IS4-IS5 linker region thus provides a binding pocket for PI(3,5)P_2 activation. Moreover, certain IS6 residues were found to be critical for PI(3,5)P_2 activity as well, such as the K331 on TPC1 (She et al., 2018). Mutation of

K331 completely abolished $PI(3,5)P_2$ activity. IS6 and IIS6 contain gating residues that control the opening and closing of the pore. The interaction between K331 and $PI(3,5)P_2$ causes a conformational change in IS6 helix leading to rotation of the gating residues to "expose" the pore, a similar motion of IIS6 helix concurrently occurs, and together triggering the pore (channel) open (She et al., 2018). On TPC2, such residues are S322 and R329 (She et al., 2019). R329 interacts with $PI(3,5)P_2$ to stimulate conformational change of IS6 helix, while S322 interacts with $PI(3,5)P_2$ to maintain such a change. Together, compared to NAADP, $PI(3,5)P_2$ has a direct action on TPCs via interaction with residues from IS4-IS5 linker and IS6.

1.4.3 Voltage-gating

TPC1 is both ligand- and voltage-gated (Cang et al., 2014; She et al., 2018), although NAADP activates the channel at all voltages (Rybalchenko et al., 2012). There are two VSDs (VSD1 and VSD2), both contain a set of positively charged arginine residues in the S4 helix. However, only the arginine residues at position R3 and R5 on IIS4 of VSD2 have been reported to be functionally relevant (She et al., 2018). Mutation of R3 arginine into glutamate (E) or isoleucine (I) has been shown to result in a voltage-independent channel (Cang et al., 2014; She et al., 2018). Mutation of R5 arginine into glutamate also abolished voltage-gating alongside the channels sensitivity to $PI(3,5)P_2$ (She et al., 2018). These two arginine residues might confer TPC1 voltage-gating via different mechanisms. In contrast to TPC1, TPC2 has been shown to have a voltage-independent activation (Pitt et al., 2010; Rybalchenko et al., 2012; Schieder et al., 2010; She et al., 2019). One consideration is that in TPC2, the residue that is equivalent to R3 arginine of TPC1 is isoleucine (I554). Indeed, replacing isoleucine with arginine yields a voltage-dependent TPC2 channel that requires both $PI(3,5)P_2$ and a positive membrane potential for activation (She et al., 2019). This isoform-specific voltage-dependence has allowed TPC1, but not TPC2, to confer endo-lysosomes with electrical excitability (Cang et al., 2014). Like mammalian TPC1, plant TPC1 is also voltage-gated, but it does not respond to NAADP/$PI(3,5)P_2$. The sensitivity of plant TPC1 to voltage also relies on arginine residues of VSD2 while VSD1 is voltage insensitive (Guo et al., 2016).

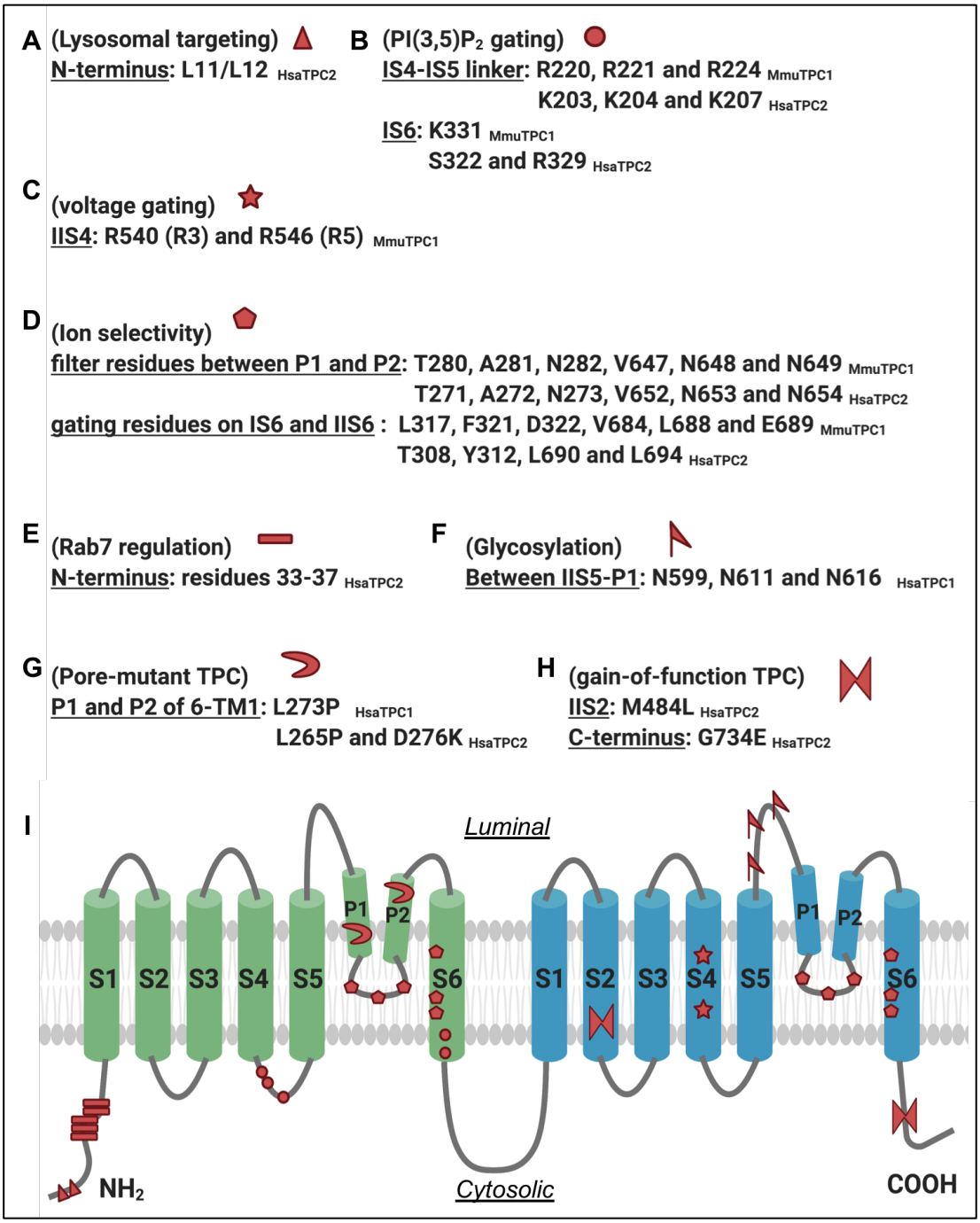

Figure 1.3 Molecular basis of TPC functionality

(A-H) Functional residues of TPCs associated with lysosomal targeting (A), PI(3,5)P_2 gating (B), voltage-gating (C), ion selectivity (D), protein regulation (E) and glycosylation (F). TPCs with L273P/L265P or D273K are pore-mutant TPCs (G). TPCs with M484L and/or G734E are naturally occurring gain-of-function TPCs (H).

(I) A topology diagram of TPC subunit with residues from (A-H). Residues of different functions are annotated with their respective symbols.

1.4.4 Ion selectivity

The pore region of TPCs consists of S5, S6 and a re-entrant pore loop (i.e. two pore helices: P1 and P2). Between P1 and P2, there are a number of conserved residues that form the filter (filter 1 and filter 2). In assembled channels, the filter residues embrace the central ion conducting pathway to impart ion selectivity (Guo et al., 2017; She et al., 2018, 2019). In addition to the filter residues, the gating residues on S6 helix also contributes to the ion selectivity. They are in charge of pore open and close while also restrain the size of permeating ions (She et al., 2018, 2019). As discussed earlier, the ion selectivity of TPCs is hotly debated. In some studies, TPCs are highly Na^+ selective and poorly Ca^{2+} permeable (Boccaccio et al., 2014; Cang et al., 2014; Guo et al., 2017; Wang et al., 2012), while in others, TPCs possess equal permeability to both Ca^{2+} and Na^+ (Grimm et al., 2014; Jha et al., 2014; Ruas et al., 2015). Consistent with the latter notion, structurally, TPCs have asparagine (N) residues within filter 2 (Rahman et al., 2014; She et al., 2018, 2019), similar to N-methyl-D-aspartate (NMDA) receptors that are known to be both Ca^{2+} and Na^+ permeable. Nonetheless, notably, it has been shown that exchanging residues in filter 2 of plant TPC1 (methionine (M629) and glycine (G630)) for mammalian TPC2 (valine (V652) and asparagine (N653)) increases plant TPC1 Na^+ permeability (PNa/PCa changes from 0.2 to 2.5) (Guo et al., 2017). The residues from filter 2 of TPCs have been proposed as determinants of channel Na^+ selectivity (Guo et al., 2016; She et al., 2018, 2019).

1.4.5 Pharmacology

As discussed above, the pharmacology of TPCs is limited. There is a very limited amount of research exploring the mechanism responsible for the effects of TPC blockers. Nevertheless, the pore-region of the channel has emerged as a potential action site. The majority of current available TPC blockers have been found to work through the pore (e.g. Cav channel blockers). In the recent study by Penny et al., 2019, the pore structure has successfully facilitated the identification of novel direct TPC blockers. This is not surprising given that TPCs are pore-forming channels and mutation of a conserved leucine residue within the pore can abrogate TPC functionality (Brailoiu et al., 2009; Brailoiu, Rahman, et al., 2010). However, what remains unclear is how the pore-region and the blockers interact structurally to render a functional inhibition on TPCs. The answer perhaps can be found from the

evolutionally linked Cav and Nav channels. As mentioned earlier, there is a pharmacological overlap between TPCs and Cav/Nav channels. The antagonists for either Cav or Nav block TPC activity via binding to the cytosolic end of TPC pore (Rahman et al., 2014). This is also the action site for the antagonists on their respective Cav or Nav channels. The interacting residues on TPC1 for these antagonists has been identified as L315 and V318 of IS6 and V675 of IIS6 (Rahman et al. 2014), but whether these residues are functionally involved in the effects of antagonists at TPCs require further investigations. Nonetheless, these residues are equivalent to the residues on Cav and Nav channels that are required for the effects of phenylalkamines and local anaesthetics on Cav and Nav channels, respectively (Hockerman et al., 1997; Yarov-Yarovoy et al., 2001). However, it is also important to note that certain Cav or Nav agonists (e.g. BayK 8644 and Veratridine) also blocked TPC activity with relatively similar potency as Cav/Nav antagonists (Rahman et al., 2014), the pore-region, presumably the pharmacological site of TPCs, therefore is not entirely similar to Cav/Nav channels.

1.4.6 Channel regulation by proteins

TPCs are known to be regulated by a number of proteins, which associate with TPCs. Rab7 is one of those proteins. Molecularly, the regulation of Rab7 on TPC2 is via binding to the N-terminus of the channel that contains a Rab GTPase binding motif (Lin-Moshier et al., 2014). Mutation of the motif (i.e. residues 33-37) was shown to abolish TPC2-Rab7 physical association, reduce NAADP-induced Ca^{2+} signals and reverse TPC2 overexpression-induced pigmentation defects. Other TPC regulators include a number of kinases (e.g. PKA, mTOR and LRRK2). It has been found that there is a Protein kinase A (PKA) phosphorylation site on the pore-region of 6-TM2 of TPC2, (Lee et al., 2016). Mutation of S666 into phosphomimic glutamate (S666E) was shown to potentiate TPC2 open probability, whereas a non-phosphorylating alanine mutation (S666A) reduced channel open probability. However, notably, S666 is on the luminal side. This brings into questions as to how cytosolic PKA affect TPC2 via this residue. mTOR has been shown to negatively regulate TPCs via phosphorylation (Cang et al., 2013; Ogunbayo et al., 2018), however, the molecular basis for this process is unclear. LRRK2 can activate TPC2 Ca^{2+} signals to regulate

autophagy (Gómez-Suaga et al., 2012), but again, the underlying mechanism remains unexplored.

1.4.7 Other loss-of-function and gain-of-function mutations

The pore-region of TPCs contains a conserved leucine residue that is critical for maintaining the normal function of the channel. This leucine residue (i.e. L273 in TPC1 and L265 in TPC2) maps to the re-entrant pore loop of 6-TM1. Substitution of the leucine into proline (P) can block NAADP Ca^{2+} signals and channel activity, turning the channel into a dominant-negative version (Brailoiu et al., 2009; Brailoiu, Rahman, et al., 2010; Rybalchenko et al., 2012). These pore-mutant TPCs are useful in that they facilitate the identification of a role of TPCs in EBOV infectivity (Sakurai et al., 2015). Wang et al., 2012 identified another pore-dead TPC2 by replacing a negatively charged aspartate (D) for a positively charged lysine (K). TPC2 with the D276K mutation abolishes $PI(3,5)P_2$-activated channel currents. Besides, it was shown that overexpression of wild-type but not $TPC2^{D273K}$ enlarges the structures of lysosomes, reflecting the role of TPC2 in membrane trafficking (Wang et al., 2012). Regarding gain-of-function mutation, both TPC1 and TPC2 can be N-glycosylated (Hooper et al., 2011; Zong et al., 2009). This is through several luminal-faced asparagine residues within the pore domain of 6-TM2. In TPC1, they are N599, N611 and N616 (Hooper et al., 2011). Mutation of these residues potentiates NAADP-induced Ca^{2+} signals through TPC1 (Hooper et al., 2011). Deglycosylation therefore enhances channel activity. Furthermore, in a genome-wide association study, two hair colour-related TPC2 variants, M484L and G734E, have been identified (Sulem et al., 2008). The role of TPC2 in pigmentation has subsequently been confirmed. For example, in *Xenopus* oocytes, overexpression of TPC2 (not TPC1) induces pigmentation defect (Lin-Moshier et al., 2014). Another two studies have noted that TPC2 regulates melanosomal pH and size, and thus in control of melanin production (i.e. pigmentation) (Ambrosio et al., 2016; Bellono et al., 2016). Chao et al., 2017 has specifically examined M484L and G734E mutation in relation to TPC2 channel activity and function. The results indicate that these mutations confer a gain-of-function activity to TPC2 (Chao et al., 2017). In M484L (found in IIS2) channel, there is an increased sensitivity to $PI(3,5)P_2$ activation. In the presence of G734E (found in

C-terminus) mutation, TPC2 displays a reduced sensitivity to inhibition by ATP and an increased responsiveness upon mTOR inhibition.

In summary, our molecular understanding on TPCs is broadening. In addition, mutagenesis studies provide research tools. In chapter 3, for example, I employed pore-mutant TPCs for characterisation of putative TPC agonists.

1.5 Ca^{2+} coupling between stores

1.5.1 Membrane contact sites

Membrane contact sites (MCSs) are regions of close membrane apposition (< 30 nm) that are stabilized by tethering complexes (Prinz, 2014). They are central for inter-organelle communications. Through MCSs, the ER interacts with the PM and other organelles to regulate a range of cellular processes, including cellular survival, membrane trafficking and lipid exchange (Prinz et al., 2020). Importantly, the contact sites between the ER and multiple organelles are also platforms for Ca^{2+} exchange, facilitating the regulation of Ca^{2+} signalling events and associated downstream Ca^{2+}-dependent pathways. For example, in cardiac muscle cells, the SR-PM junctions allows Ca^{2+} influx through L-type Cav to be amplified by RyRs via CICRs, and thus to initiate contraction (Chang et al., 2017; Franzini-Armstrong et al., 1999). In non-excitable cells, the ER-PM junctions underpins SOCE, a process required to refill the ER store following Ca^{2+} depletion (Chang et al., 2017). ER-mitochondria MCSs, which are also known as mitochondria-associated membranes (MAMs), facilitates mitochondria Ca^{2+} uniporter to sequester Ca^{2+} released from the ER (typically through IP_3 receptors), allowing regulation on both IP_3 Ca^{2+} signalling and energy supply (Csordás et al., 2006; Rizzuto, 1998). The ER also forms MCSs with endo-lysosomal organelles. The role of these MSCs on Ca^{2+} signalling is unfolding (see 1.5.2 ER-lysosomes).

1.5.2 ER-lysosomes

The ER and lysosomes are functionally connected. NAADP signalling serves a good example. In intact cells, NAADP Ca^{2+} signals are not only sensitive to bafilomycin A1, but can also be largely reduced by inhibition of ER Ca^{2+} release. The latter observation has been noted in a number of studies (Brailoiu, Rahman, et al., 2010; Cancela et al.,

1999; Kim et al., 2010; Kinnear et al., 2004). This was initially surprising given that NAADP action in homogenized sea urchin egg relies on acidic stores only (Genazzani et al., 1997). Soon after, the "trigger hypothesis" was defined to explain this (Patel et al., 2001; Patel & Brailoiu, 2012). That is, NAADP induces a "trigger" release of Ca^{2+} from lysosomes (local and small), which is then amplified by ER Ca^{2+} channels via CICRs to generate global signals. To note, the crosstalk between lysosomes and the ER is bi-directional. Aside from lysosomes-to-ER Ca^{2+} coupling, ER Ca^{2+} release by IP_3 and cADPR can also evoke lysosomal Ca^{2+} release as reflected by an increase in lysosomal pH (a feature of NAADP activation) (Morgan et al., 2013). Alternatively, lysosomes have been shown to take up Ca^{2+} released from the ER, likely via CAX, to function as Ca^{2+} buffers (Atakpa et al., 2018; López-Sanjurjo et al., 2013). The lysosome-ER Ca^{2+} coupling has been illustrated in Figure1.4.

The realization of above-mentioned functional connections is conditional. In broken cell preparations (e.g. homogenised sea urchin egg), NAADP signals were maintained upon ER inhibition (Lee & Aarhus, 1995). In mammalian cells, this can also be observed when re-directing TPC2 to the PM by mutating its N-terminal di-leucine motif (Brailoiu, Rahman, et al., 2010). Thus, for "channel chatter" to occur, TPC/lysosomes must be placed in a region that is close to the ER (Fig.1.4). Electron microscopy identified MCSs between lysosomes and the ER in fibroblasts (Kilpatrick et al., 2013). This region is < 20 nm. 80%-100% of lysosomes are estimated to have ER contacts. Echoing such extensive contacts, in fibroblasts, direct mobilization of lysosomal Ca^{2+} by osmotic permeabilization (i.e. use of GPN) initiated ER/IP_3-sensitive Ca^{2+} signals (Kilpatrick et al., 2013). Subsequent computational modelling, where lysosomes and the ER leak models were assembled, recaptured GPN responses (Penny et al., 2014). Through adapting this model to NAADP signalling, the lysosome-ER contact sites have been proposed to be responsible for driving local (lysosomes) to global (ER) transition (Penny et al., 2014, 2015). In addition, the MCSs also appear to play roles in reverse Ca^{2+} coupling. Recently, through proximity ligation assays, Taylor's team noted a close association between lysosomes and IP3 receptors from the ER in HEK cells (Atakpa et al., 2018). This close physical association is maintained by low lysosomal pH. Increasing lysosomal pH disrupts the contacts and potentiates IP_3-forming agonist-induced Ca^{2+} signals (indicative of failure in Ca^{2+} uptake). The lysosome-ER MCSs therefore have been proposed to be the platform for ER Ca^{2+}

sequestration by lysosomes (Atakpa et al., 2018). Favouring this, lysosomes take up Ca^{2+} released from the ER but not those from the PM SOCCs (Atakpa et al., 2018). Lysosomes have also been found to form MCSs with the sarcoplasmic reticulum (SR) in smooth muscle and cardiac muscle (Capel et al., 2015; Fameli et al., 2014).

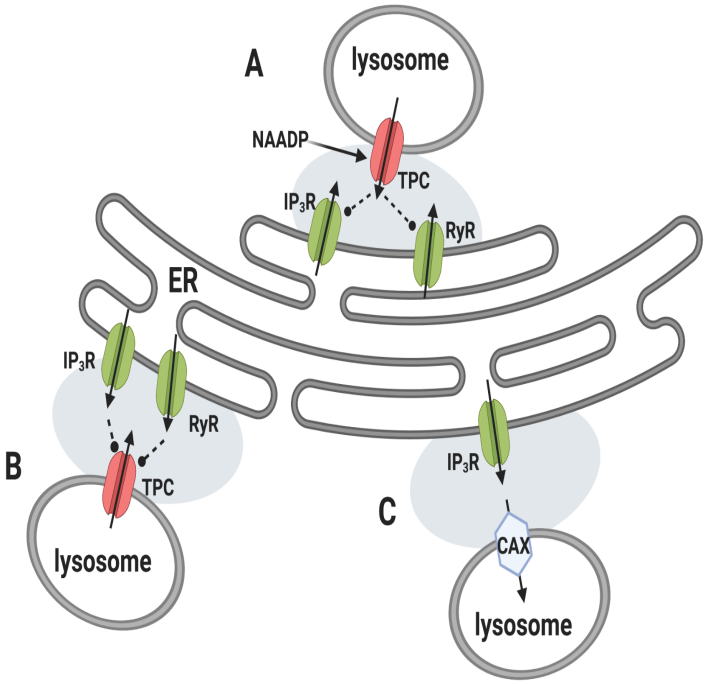

Figure 1.4 Ca^{2+} communication between lysosomes and ER

(A) Lysosome-to-ER Ca^{2+} signalling. NAADP induces local lysosomal Ca^{2+} release through TPCs, which is then amplified by ER Ca^{2+} channels IP_3Rs/RyRs via CICRs.

(B and C) ER-to-lysosome Ca^{2+} signalling. ER Ca^{2+} release induces further lysosomal Ca^{2+} release (B) or is sequestered by lysosomes (C).

The molecular compositions of these junctions, however, are ill-characterized. Nevertheless, VAP could be a potential candidate. VAP is an ER-localized protein and functions as a tether at MCSs formed between the ER and other organelles (e.g. the PM, mitochondria and endosomes) (Alpy et al., 2013; De Vos et al., 2012; Gomez-Suaga et al., 2017; Manford et al., 2012; Rocha et al., 2009). In one recent study, knocking down VAP reduced lysosome-ER contacts (Eden et al., 2016). Moreover, consistent with the idea that ER Ca^{2+} release through IP_3Rs is sequestered by lysosomes, Taylor's lab recently found that IP_3Rs are present at lysosome-ER MCSs. Notably, however, functionally, IP_3Rs are not required for the assembly of the contacts (Atakpa et al., 2018). Similarly, given that TPCs are implicated in local signals from lysosomes to the ER, TPCs may also be present at the contact sites. But whether TPCs function as tethers is hard to predict. In one recent study, this may have been answered given that molecularly silencing of TPC2 (but not TPC1) modestly reduced lysosome-ER MCSs (Kilpatrick et al., 2017). NAADP-mediated Ca^{2+} signals however were not characterized (Kilpatrick et al., 2017).

In comparison, more has been revealed regarding the molecular compositions of late endosomes-ER MCSs. For example, the contacts have been found to be mediated by the interaction between VAP (ER-localized protein) and sterol-binding proteins of endosomes, including ORP1L and STARD3 (Alpy et al., 2013; Rocha et al., 2009). To note, the VAP-ORP1L interaction is cholesterol sensitive and only occurs at low cholesterol levels to promote MCSs formation (Rocha et al., 2009). At high cholesterol levels, ORP1L dissociates from VAP, and instead binds to a Rab7 complex on the endosomes. As a result, late endosomes are trafficked away from the ER where presumably fusion between endosomes and lysosomes is promoted (Rocha et al., 2009). Moreover, the endosomes-ER contact sites have been shown to be stabilized by interaction between internalized EGF receptors and ER-localised phosphatase, PTP1B (Eden et al., 2010). PTP1B dephosphorylates EGFRs at the MCSs, leading to downregulated EGFR signalling which is known to play roles in a number of key cellular functions (e.g. migration) (Eden et al., 2012). Like lysosomes-ER MCSs, the endosomes-ER MCSs may also facilitate Ca^{2+} exchange. However, little is known about this at the moment. Nevertheless, TPC1 and NAADP Ca^{2+} signalling have been shown to be required for the formation of the contacts between endosomes and the ER (Kilpatrick et al., 2017).

1.5.3 Global TPC Ca^{2+} signalling

In accord with the Ca^{2+} coupling between lysosomes and the ER, it has long been appreciated that NAADP and lysosomes are required for physiological Ca^{2+} signals evoked by a large number of extracellular stimuli (e.g. histamine, carbachol, glucose and angiotensin II) (Aley et al., 2013; Favia et al., 2014; Pandey et al., 2009; Soares et al., 2007; Wang et al., 2012). In these studies, NAADP involvement was reflected by a reduced Ca^{2+} signal in the presence of self-inactivating concentrations of NAADP and/or Ned-19 (NAADP antagonist). Lysosome involvement was reflected by a reduced Ca^{2+} signal when lysosomal store is perturbed by GPN and/or bafilomycin A1. Extracellular stimuli that require NAADP/lysosomes for Ca^{2+} signalling has been summarised in dissertation by (Yates, 2017).

Given the above, it is likely that TPCs are physiologically employed to communicate with IP_3R and/or RyRs, and thus allow regulations on Ca^{2+}-sensitive cellular processes.

These could include fertilization (Churchill et al., 2003), cardiac (Macgregor et al., 2007) and vascular smooth muscle contraction (Boittin et al., 2002; Brailoiu, Gurzu et al., 2010; Trufanov et al., 2019) , insulin secretion (Arredouani et al., 2015; Masgrau et al., 2003), autophagy (Pereira et al., 2017), neurite outgrowth (Brailoiu et al., 2005), angiogenesis (Favia et al., 2014), von Willebrand factor secretion (Esposito et al., 2011) and nitric oxide release (Brailoiu, Gurzu et al., 2010; Zuccolo et al., 2019). However, direct evidence implicating the involvement of TPCs in global Ca^{2+} signals evoked by physiological stimuli is limited. Thus far, very few stimuli have been tested in TPC KD/KO cells (see Table1.3). Notably, although glucose was shown to induce TPC-dependent Ca^{2+} signals (see Table1.3, (Arredouani et al., 2015)), this has been questioned (Wang et al., 2012). In chapter 5, I explore the contribution of TPCs to physiological agonist-evoked Ca^{2+} signalling.

Table 1.3 Inferred Involvement of TPCs in physiological stimuli-induced Ca^{2+} signals

Stimulus	Concentration	Cell type	Method(s)	Paper(s)
VEGF	100 μg/L	Umbilical vein endothelial cells	TPC2 shRNA knockdown	Favia et al., 2014
Glucose	100 mM	Pancreatic β cells	TPC1/TPC2 knockout	Arredouani et al., 2015
RANKL	1 nM	Mouse bone marrow macrophage	TPC2 miRNA knockdown	Notomi et al., 2012
Fetal calf serum	20% (v/w)	Metastatic colorectal cancer cells	TPC1 siRNA knockdown	Faris et al., 2019

Norepinephrine	100 μM	Rat aortic smooth muscle cells	TPC1 siRNA knockdown	Trufanov et al., 2019

1.6 Aims

TPCs are important endo-lysosomal ion channels that have been linked to a growing number of physiological and pathophysiological events. However, our understanding of the channels is limited. Importantly, there are few effective pharmacological tools that can manipulate the channels to aid research and drug discovery. In this thesis, I identify and characterize novel TPC modulators with which I explore the basic attributes and the physiological functions of TPCs. My aims are as follows:

1. GPN is a cathepsin C substrate that can disrupt acidic stores by inducing osmotic pressure, and thus deplete Ca^{2+}. For this reason, GPN has been used for decades for probing lysosome Ca^{2+} signaling (i.e. indirect probing of TPCs). However, a recent paper has questioned GPN in regard to its mechanism of action. To confidently use GPN for functional studies in this thesis, I therefore re-examined the mode of action of GPN using fibroblasts where GPN induces robust Ca^{2+} signals.
2. The pharmacology of TPCs is limited. Through high throughput screening, our collaborator Christian Grimm's team identified two candidate TPC2 activators, A1 and H07. In addition, our recent published data in Penny et al., 2019 identified a number of putative TPC2 pore inhibitors. I therefore validated and characterized these compounds.
3. Thus far, the ion selectivity and gating mechanism of TPCs are hotly debated. Through characterizing the effects of A1 and H07 on TPC2, I addressed these shortcomings.
4. A number of physiological agonist-induced global Ca^{2+} signals are NAADP-dependent. However, there is little direct evidence that TPCs are involved in such signalling. Using GPN, novel TPC pore inhibitors and TPC siRNA, I explored the importance of TPCs in physiological Ca^{2+} signals evoked by extracellular stimuli.

Chapter 2: GPN mobilizes Ca^{2+} from acidic organelles - a re-examination.

2.1 Introduction

Acidic organelles, including lysosomes, are intracellular Ca^{2+} stores that regulate a number of physiological and disease-related events. Pharmacological tools for probing Ca^{2+} signalling through acidic stores are available, but rather limited. They can be grouped into two types: those that mobilize Ca^{2+} (e.g. TRPML and TPC activators) and those that disrupt acidic stores via dissipation of the pH gradient (e.g. bafilomycin A1) or permeabilization of the membrane (e.g. cathepsin C substrates). The lysosomotropic agent, GPN, is an example of the latter. GPN is thought to freely diffuse into acidic organelles where it is then cleaved by cathepsin C. Upon cleavage, it stimulates osmotic lysis of acidic compartments and subsequent leakage of small molecules and ions, including Ca^{2+} (Haller et al., 1996; Jadot et al., 1984). GPN is rather unique in that it ruptures acidic stores and mediates significant Ca^{2+} signals. For this reason, GPN has been extensively used for probing lysosome Ca^{2+} signalling for decades. Physiologically, for example, GPN revealed a role of lysosome Ca^{2+} in exocytosis (Liu et al., 2018; Sivaramakrishnan et al., 2012), also, it revealed that lysosomal Ca^{2+} can communicate with the ER Ca^{2+} to generate global Ca^{2+} signals (Kilpatrick et al., 2013; Penny et al., 2014, 2015). Patho-physiologically, it's uses suggested that Parkinson's disease and Niemann-Pick disease type C1 are accompnied with dysregulated lysosomal Ca^{2+} content (Kilpatrick, Magalhaes, et al., 2016; Lloyd-Evans et al., 2008). In addition, evidence that the TRPML1 synthetic activator, MLSA1, and the TPC activator, NAADP, mediate lysosome-dependent Ca^{2+} signals stem from the use of GPN (Churchill et al., 2002; Kilpatrick, Yates, et al., 2016; Shen et al., 2012). All in all, GPN is a valuable tool for acidic compartments. However, a recent study has challenged the long-held understanding of how GPN mediates changes in cytosolic Ca^{2+} (Atakpa et al., 2019). The study first showed that GPN is unable to permeabilize the lysosomal membrane, a characteristic of cathepsin C substrate, such as l-leucyl-l-leucine methyl ester (LLOMe) (Repnik et al., 2017; Thiele & Lipsky, 1990). Following this, it provided evidence that GPN-induced Ca^{2+} signals were independent of cathepsin C. Having questioned the role of lysosomes in GPN-

evoked Ca^{2+} signalling, the study pointed out that GPN is a weak base and provided evidence that GPN actually induces Ca^{2+} release from the ER via alkalizing the cytosol.

To confidently utilize GPN to probe lysosome Ca^{2+} and thus to facilitate functional studies, I re-examined the effects of GPN in human dermal fibroblasts where GPN mediates robust Ca^{2+} signals (Kilpatrick et al., 2013).

2.2 Methods

2.2.1 Cell culture

Human dermal Fibroblasts were maintained in Dulbecco's Modified Eagle Medium (DMEM), supplemented with 10% (v/v) Fetal Bovine Serum (FBS), 100 µg/mL streptomycin and 100 units/mL penicillin (all from invitrogen). They were kept at 37ºC in a humidified atmosphere with 5% CO_2. Cells were fed with fresh media every 4-5 days. Cells were passaged by scraping at 1 in 3 ratio (about 50,000 cells/ml) and plated onto coverslips in a 24 well-plate (0.5 ml/well). Cells were used for imaging when they were 80-90% confluent.

2.2.2 Live-cell imaging

Live-cell imaging experiments were performed at room temperature in HEPES-buffered saline (HBS) containing 10 mM HEPES, 1.25 mM KH_2PO_4, 2 mM $MgSO_4$, 3 mM KCl, 156 mM NaCl, 2 mM $CaCl_2$ and 10 mM glucose (modified pH to 7.4 with HCl). Where indicated (in figures), some experiments were performed in nominally Ca^{2+}-free HBS which had the same compositions as HBS except for the addition of $CaCl_2$.

To measure cytosolic Ca^{2+}, cells were incubated with 2.5 µM Fura-2 AM and 0.005% pluronic acid (Invitrogen) for 1 hour in HBS at room temperature. To measure lysosomal pH (i.e. acidity), cells were incubated with 100 nM Lysotracker red (Invitrogen) for 15 minutes in HBS at room temperature. To measure cytosolic pH, cells were incubated with 5 µM BCECF AM and 0.005% pluronic acid (Invitrogen) for 30 minutes in HBS at room temperature. After loading, cells were washed three times in HBS and then were mounted into an imaging chamber (i.e. coverslip holder)

with HBS for imaging. For experiments conducted in Ca^{2+}-free HBS, Ca^{2+}-free HBS replaced HBS 60 seconds after imaging/recording started.

2.2.3 Epifluorescence microscopy

Epifluorescence images were captured every 3 seconds with a cooled coupled device camera (TILL photonics) attached to an Olympus IX71 inverted fluorescence microscope, fitted with a 20x objective and a monochromatic light source. The Ca^{2+} probe, Fura-2, was excited at 340/380 nm and emitted fluorescence was captured using a 440 nm long pass filter. The pH probes, Lysotracker red and BCECF, were excited at 568 nm and 490/440 nm, respectively. Emitted fluorescence was captured with a 590 nm filter (Lysotracker red) and a 515 nm long pass filter (BCECF). Cells were stimulated with 0.1 % (v/v) DMSO (stock solution from Sigma), 1 mM LLOMe (Santa Cruz Biotechnology), 200 µM GPN (Santa Cruz Biotechnology), 5 mM NH_4Cl (Sigma), 1 µM thapsigargin (Santa Cruz Biotechnology) or 1 µM bafilomycin A1 (Cell Signalling). All compounds were prepared in DMSO except NH_4Cl which was prepared in H_2O.

2.2.4 Bafilomycin A1 treatment

Cells were either acutely treated with 1 µM bafilomycin A1 during recording or pre-treated for a period of time. In the case of the latter, for Fura-2 measurements, the treatment with bafilomycin A1 was maximally 2 hours at room temperature or 4 hours in culture followed by another 1 hour at room temperature. Cells were loaded with Fura-2 in the final 1 hour of bafilomycin A1 treatment at room temperature. For Lysotracker red measurements, the treatment with bafilomycin A1 was maximally 2 hours at room temperature or 5 hours in culture. After that, cells were loaded with Lysotracker red for 15 minutes at room temperature in the presence of bafilomycin A1.

2.2.5 Analysis

To quantify change in fluorescence, regions of interest (ROIs) were drawn around each cell and an area without cells for background subtraction. The ratio of Fura-2 (ex: 340 nm/380 nm) and BCECF (ex: 490 nm/440 nm) was calculated using TILLvisION software. Prior to stimulation, the basal ratio was established by averaging fluorescence from a 90 second recording. In the case of performing experiments in

Ca^{2+}-free medium, the basal ratio was acquired after cells were immersed in Ca^{2+}-free HBS. In rare cases where the baseline drifted (i.e. spontaneous increase in fluorescence) upon immersing cells into Ca^{2+}-free HBS, the basal ratio was acquired before Ca^{2+} removal. The magnitude of response (ΔCa^{2+} or Δcytosolic pH) was calculated by subtracting basal ratio from the peak ratio. For Lysotracker, after background subtraction, the fluorescence was normalised to basal (F/F_0) that obtained before stimulus addition.

2.2.6. Data presentation

Data are presented as representative results from single experiments or as mean +/- S.E.M. from several experiments. One coverslip was used per experiment. There were about 20-40 cells analysed per coverslip. Statistical analysis was performed using Prism 9 on datasets where there were three or more experiments per group/condition (i.e. n >=3, n refers to number of coverslips). Independent-Samples T-tests and one-way ANOVA were applied to test significance (as indicated in figures). $P<0.05$ was regarded as statistically significant.

2.3 Results

2.3.1 The cathepsin C substrates, GPN and LLOMe, reduce LTR staining

GPN is thought to work via proteolysis by cathepsin C (Jadot et al., 1984). I began by comparing the activity of GPN with that of LLOMe, another cathepsin C substrate, to investigate whether the two work in a similar way. Previous work using fibroblasts has shown that GPN increases lysosomal pH and mediates complex Ca^{2+} signals (Kilpatrick et al., 2013; Penny et al., 2014). Does LLOMe possess similar properties? In the first set of experiments, I examined the effects of GPN and LLOMe on lysotracker red (LTR). LTR is a fluorescent dye that is "trapped" within lysosomes through acidic pH-mediated protonation. This property allows LTR to label lysosomes and monitor their acidity (Kilpatrick et al., 2015). As shown in Fig.2.3.1A-C, GPN (200 μM) and LLOMe (1 mM) reduced LTR fluorescence compared to the vehicle DMSO control, indicative of their effects on lysosomes. In comparison, the reductions were at distinct rates; GPN mediated a rapid loss of LTR fluorescence, while LLOMe

reduced its fluorescence more slowly. These data are quantified in Fig.2.3.1D by calculating LTR fluorescence after 15 minutes of addition of DMSO, GPN or LLOMe.

2.3.2 GPN and LLOMe mediate cytosolic Ca^{2+} signals

Cathepsin C substrates induce lysosomal membrane permeabilization (LMP), a process characterized by damage to the membrane and leads to the release of luminal contents (e.g. Ca^{2+} and hydrolases). Consistent with this, LLOMe induces release of molecules with molecular weight of 4.4K from lysosomes (Repnik et al., 2017). However, in contrast to GPN, it is unclear as to whether LLOMe mediates Ca^{2+} signals. I therefore tested GPN and LLOMe on cytosolic Ca^{2+} levels of fibroblasts loaded with Fura-2, a cytosolic ratio-metric fluorescent Ca^{2+} indicator. Compared to the DMSO control, GPN mediated complex Ca^{2+} signals (Fig.2.3.2A and B). LLOMe also mediated complex Ca^{2+} signals (Fig.2.3.2C), although they were smaller in magnitude than those evoked by GPN. These data are quantified in Fig.2.3.2D where I calculated the magnitude of Ca^{2+} signals in response to DMSO, GPN or LLOMe by subtracting basal Ca^{2+} ratio from peak Ca^{2+} ratio.

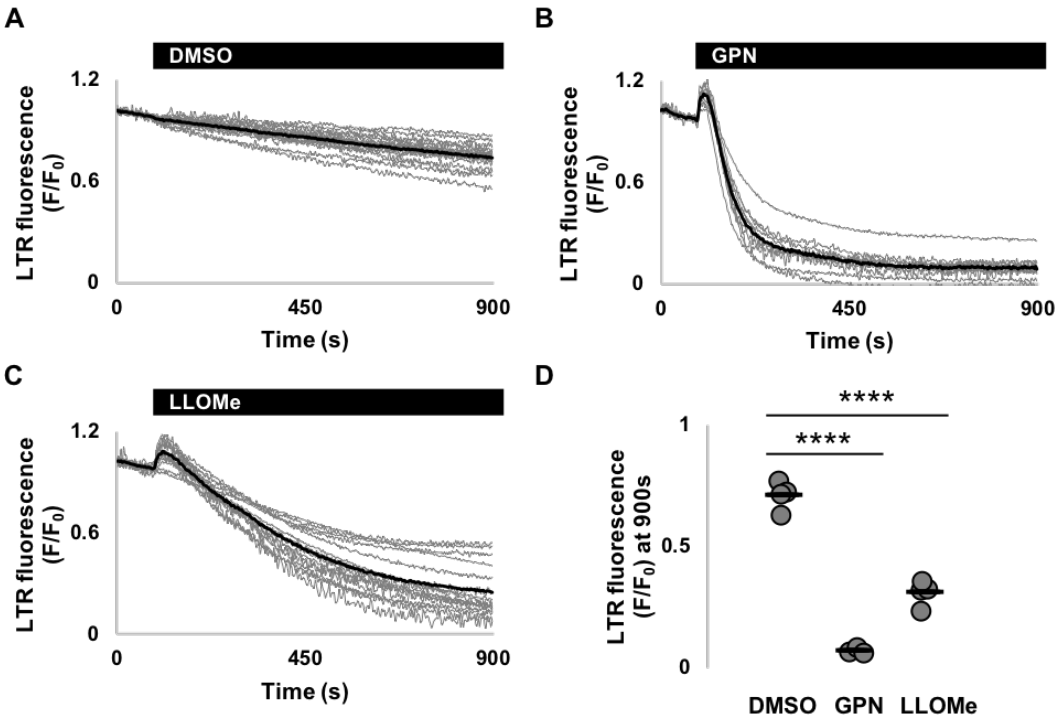

Figure 2.3.1 The cathepsin C substrates, GPN and LLOMe, reduce LTR staining
(A-C) Changes in lysotracker red fluorescence of individual fibroblasts stimulated with the vehicle DMSO control (A), 200 μM GPN (B) or 1 mM LLOMe (C). Lysotracker fluorescence

values have been normalized to basal levels (i.e. F/F_0). The bars above graphs indicate the time of addition of compounds, which was at 90s. Gray traces represent recordings of all individual cells and black traces represent the population average from a typical experiment.

(D) Summary data quantifying fluorescence of lysotracker 15 minutes following acute treatment with DMSO, GPN or LLOMe. Each plot point represents average results from an individual experiment such as the example shown in (A-C) (n=3-4); **** P<0.0001 was determined by one-way ANOVA.

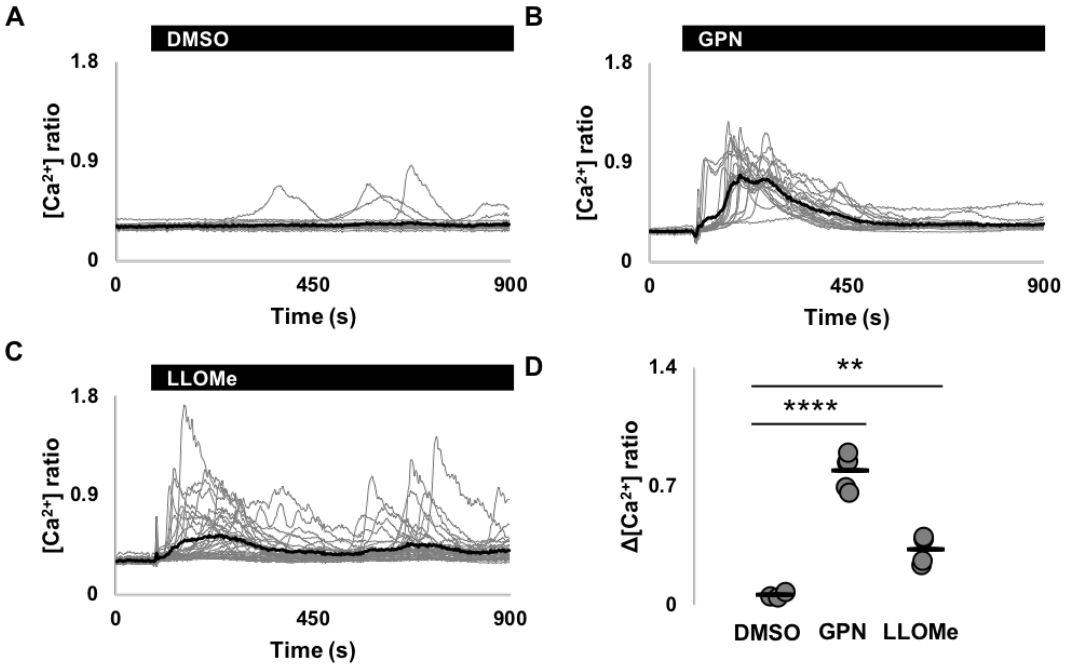

Figure 2.3.2 GPN and LLOMe mediate cytosolic Ca^{2+} signals

(A-C) Cytosolic Ca^{2+} levels of individual fibroblasts stimulated with DMSO (A), 200 μM GPN (B) or 1 mM LLOMe (C). The bars above graphs indicate the time of addition of compounds, which was at 90s. Gray traces represent recordings of all individual cells and black traces represent the population average from a typical experiment.

(D) Summary data quantifying magnitudes of Ca^{2+} responses to DMSO, GPN or LLOMe. Each plot point represents average results from an individual experiment such as the example shown in (A-C) (n=3-4); ** P<0.01 and **** P<0.0001 were determined by one-way ANOVA.

2.3.3 GPN but not LLOMe mediates Ca^{2+} signals in the absence of extracellular Ca^{2+}

Ca^{2+} signals are generated in two ways: extracellular Ca^{2+} influx and intracellular Ca^{2+} release. To investigate the contribution of each component to GPN- and LLOMe-mediated Ca^{2+} signals, I examined their Ca^{2+} signals in the absence of extracellular Ca^{2+}. As shown in Fig.2.3.3A and B, GPN mediated complex Ca^{2+} signals upon removal of extracellular Ca^{2+}, showing GPN mediates Ca^{2+} release. In contrast, LLOMe mediated few Ca^{2+} signals under the same cellular environment (Fig.2.3.3C); the magnitude of Ca^{2+} signals in the presence of LLOMe was not different from that in the presence of DMSO (Fig.2.3.3D). The Ca^{2+} signals by LLOMe therefore arise predominantly from Ca^{2+} influx.

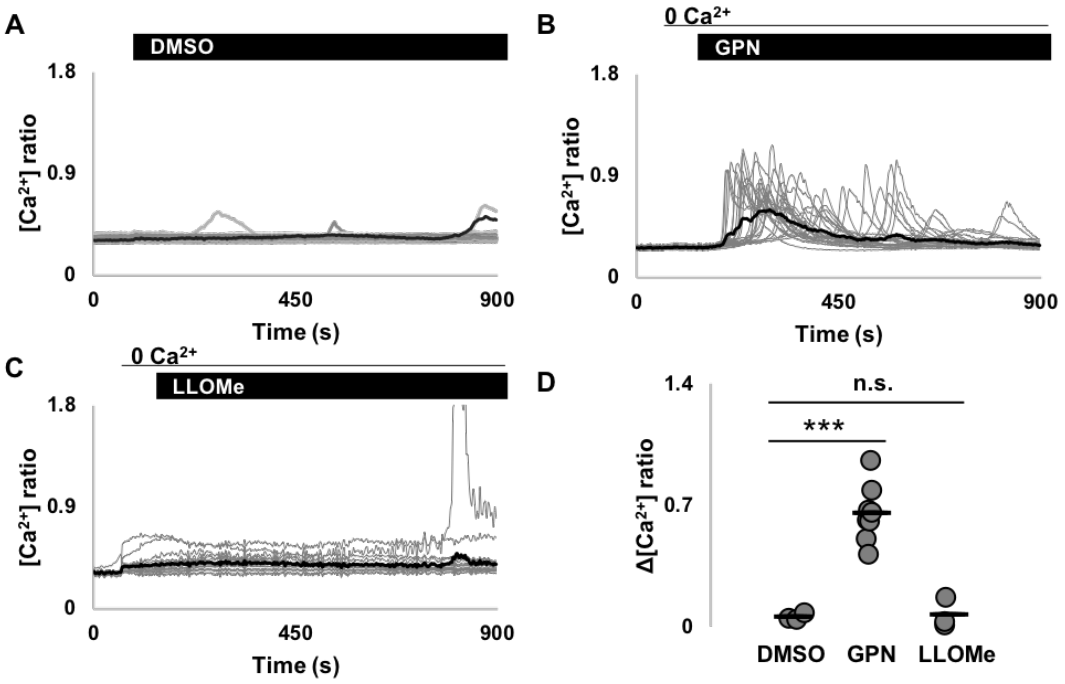

Figure 2.3.3 GPN but not LLOMe mediates Ca^{2+} signals in the absence of extracellular Ca^{2+}

(A-C) Cytosolic Ca^{2+} levels of individual fibroblasts stimulated with DMSO (A), 200 μM GPN (B) or 1 mM LLOMe (C). Cells were immersed into Ca^{2+}-free HBS at 60s (B and C). The bars above graphs indicate the time of addition of compounds, which was at 90s (A) or 150s (B and C). Gray traces represent recordings of all individual cells and black traces represent the population average from a typical experiment.

(D) Summary data quantifying magnitudes of Ca^{2+} responses to DMSO, GPN or LLOMe without extracellular Ca^{2+}. Each plot point represents average results from an individual experiment such as the example shown in (A-C) (n=3-8); n.s. not statistically significant *** P<0.001 were determined by one-way ANOVA.

2.3.4 GPN and NH_4Cl have similar effects on cytosolic pH but dissimilar effects on cytosolic Ca^{2+}

There is no doubt that GPN mediates Ca^{2+} signals, but the question is what the underlying mechanism is. The recent study by Atakpa has suggested that such Ca^{2+} signals are caused by GPN-mediated changes in cytosolic pH (Atakpa et al., 2019). To explore this possibility, I first studied whether GPN altered cytosolic pH in fibroblasts loaded with a cytosolic ratio-metric pH indicator, BCECF. As shown in Fig.2.3.4A, immediately after GPN addition, the cytosolic pH promptly increased. In the same recording period, GPN also increased lysosomal pH and cytosolic Ca^{2+}, as measured by LTR and Fura-2, respectively (Fig.2.3.4C and E). Next, I explored the relationship between pH and Ca^{2+}. Comparison of the kinetics of the Ca^{2+} and pH responses to GPN reveals that the increase in cytosolic pH occurred and peaked faster than the increase in cytosolic Ca^{2+} and lysosomal pH (Fig.2.3.4G). In comparison, the increase in cytosolic Ca^{2+} and the increase in lysosomal pH proceeded at a similar pace (Fig.2.3.4H).

To further explore the relationship between pH and Ca^{2+}. I utilized NH_4Cl. Like GPN, NH_4Cl is also a weak base. In fibroblasts, I observed that NH_4Cl increased cytosolic pH (Fig.2.3.4B). Also, it increased lysosomal pH as reflected by a gradual reduction in LTR fluorescence (Fig.2.3.4D). However, NH_4Cl induced negligible Ca^{2+} signals (Fig.2.3.4F). Comparison of the kinetics of the Ca^{2+} and pH responses to NH_4Cl is shown in Fig.2.3.4I and J.

Finally, the responses induced by GPN and those by NH_4Cl were quantified and compared. As shown in Fig.2.3.4K-M, NH_4Cl and GPN alkalized cytosolic pH to the same level, but compared to GPN, NH_4Cl has a smaller effect on lysosomal pH and little effect on cytosolic Ca^{2+}.

Collectively, these data indicate that changes in cytosolic Ca^{2+} are unlikely to be a result of changes in cytosolic pH as there are discrepancies in kinetics and pharmacology.

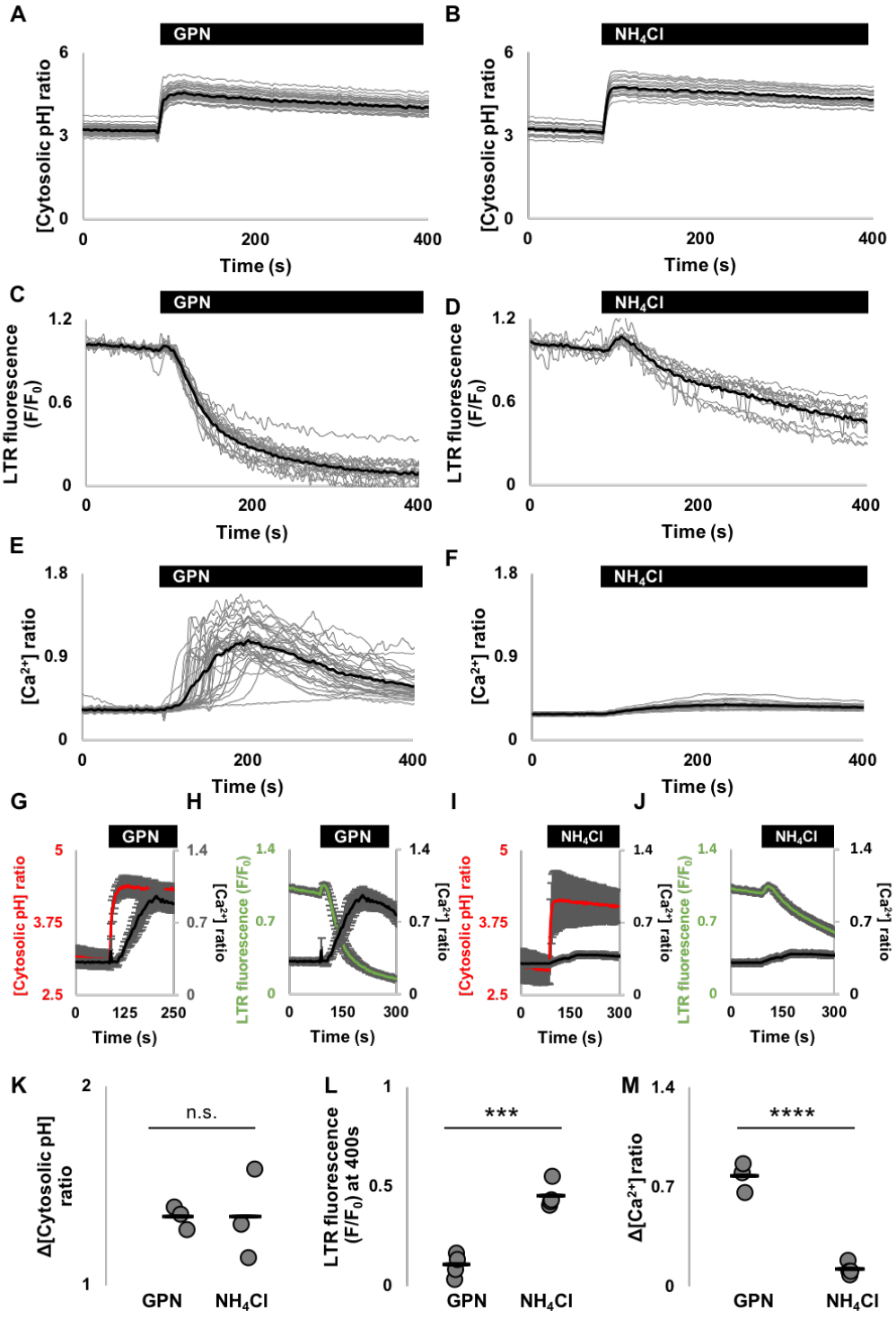

Figure 2.3.4 GPN and NH_4Cl have similar effects on cytosolic pH but dissimilar effects on cytosolic Ca^{2+}

(A, C and E) Changes in cytosolic pH (A), lysotracker fluorescence (a proxy for lysosomal pH) (B) and cytosolic Ca^{2+} (C) of individual fibroblasts stimulated with 200 μM GPN. The bars above graphs indicate the time of addition of compounds, which was at 90s. Gray traces represent recordings of all individual cells and black traces represent the population average from a typical experiment.

(B, D and F) Similar to A, C and E but cells were stimulated with 5 mM NH_4Cl.

(G and H) Comparison of various responses to GPN. Cytosolic pH changes versus cytosolic Ca^{2+} changes (G). Lysosomal pH changes versus cytosolic Ca^{2+} changes (H). Data are expressed as mean ± S.E.M (n=3-4).

(I and J) Similar to G and H but comparison of various responses to NH_4Cl.

(K-M) Summary data quantifying the changes in cytosolic pH (K), lysosomal pH (L) and cytosolic Ca^{2+} (M) by GPN or NH_4Cl. Each plot point represents average results from an individual experiment such as the example shown in (A-F) (n=3-4); n.s. not statistically significant *** P<0.001 **** P<0.0001 were determined by independent-samples t-tests.

2.3.5 Bafilomycin A1 tends to reduce LTR staining in a time-dependent manner

Bafilomycin A1 is one of the limited pharmacological tools for disrupting lysosomes. It is a V-ATPase inhibitor, which dissipates the proton gradient which is likely crucial for Ca^{2+} uptake (Christensen et al., 2002). In this context, bafilomycin A1 is thought to indirectly deplete lysosomal Ca^{2+}. However, Atapka has shown that bafilomycin A1 potentiated GPN-mediated Ca^{2+} signals, as it did to thapsigargin-mediated Ca^{2+} signals (Atakpa et al., 2018; López-Sanjurjo et al., 2013). I therefore examined the effects of bafilomycin A1 on GPN Ca^{2+} signals in fibroblasts. To start, I characterized the effects of bafilomycin A1 on lysosomal pH.

As shown in Fig.2.3.5A and B, acute addition of 1 μM bafilomycin A1 (up to 15 minutes) appeared to have little effect on LTR fluorescence, similar to the DMSO control. Considering that inhibition of V-ATPase by bafilomycin A1 might slowly affect lysosomal pH, the cells therefore were pre-treated with DMSO or bafilomycin A1 for 1-2 hours before LTR loading. As shown in Fig.2.3.5C and D, compared to DMSO control, a 1 hour treatment tended to reduce LTR fluorescence by about 50%, and a 2 hour treatment tended to reduce LTR fluorescence by about 70-80%. Thus, bafilomycin A1 appeared to affect lysosomal pH upon prolonged treatment. However, the LTR staining was still detectable.

To obtain a complete loss of LTR staining, the cells therefore might need to be exposed to bafilomycin A1 for an even longer time (>2 hours). The above treatments were implemented in HEPES buffered saline at room temperature (RT) that might have an impact on cell viability under longer treatment. Thus, I performed experiments where cells were pre-incubated with DMSO or bafilomcyin A1 for 1 to 5 hours in cultured media, prior to LTR loading. As shown in Fig.2.3.5E and F, interestingly, both 1 hour and 2 hour treatment in culture appeared to eliminate almost all LTR staining. This implies that bafilomycin A1 could be more active in culture conditions than at RT. Finally, LTR staining appeared to be completely eliminated upon 3 hour, 4 hour and 5 hour treatments with bafilomycin A1 in culture (Fig.2.3.5G-I). In Fig.2.3.5J, I quantified LTR fluorescence in bafilomycin A1-treated cells as a percentage (%) of

that in DMSO-treated cells. Collectively, these results suggest that bafilomycin A1 gradually increase lysosomal pH, which is likely to be promoted by culture conditions.

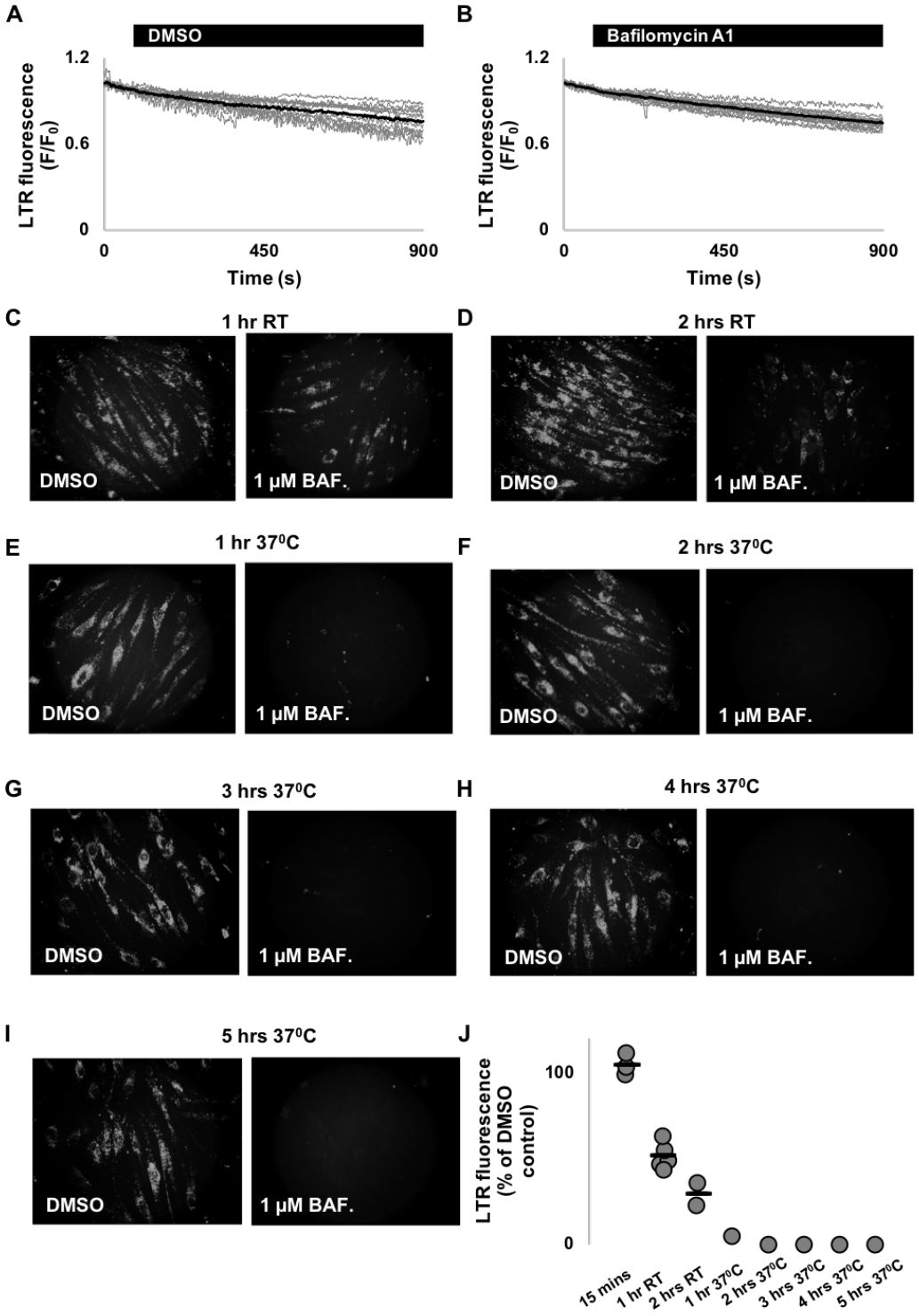

Figure 2.3.5 Bafilomycin A1 tends to reduce LTR staining in a time-dependent manner

(A and B) Changes in lysotracker red fluorescence of individual fibroblasts stimulated with the vehicle DMSO control (A) or 1 μM Bafilomycin A1 (B). The bars above graphs indicate the time of addition of compounds, which was at 90s. Gray traces represent recordings of all individual cells and black traces represent the population average from a typical experiment.
(C-I) Representative images of lysotracker red fluorescence of fibroblasts pre-treated with DMSO or 1 μM Bafilomycin A1 (BAF.) for the indicated time. Treatments were performed at room temperature in HBS (C and D) or at 37°C under culture conditions (E-I).
(J) Summary data quantifying fluorescence of lysotracker following Bafilomycin A1 as percentage (%) of that following DMSO. Each point represents a dataset (i.e. one DMSO test to control for one bafilomycin A1 test) (n=1-5).

2.3.6 Acute treatment with Bafilomycin A1 appears to potentiate GPN- and thapsigargin-mediated Ca^{2+} release

Having defined the effect of bafilomycin A1 on lysosomes via LTR, I went on to examine its effect on GPN-mediated Ca^{2+} signals. In parallel, I examined thapsigargin Ca^{2+} signals after bafilomycin A1 treatment. Thapsigargin is a well-defined SERCA blocker that induces ER Ca^{2+} release.

All Ca^{2+} tests with bafilomycin A1 were conducted without extracellular Ca^{2+} to ensure recording of Ca^{2+} release only. I first examined the effects of acute treatment with bafilomycin A1 (for about 15 minutes) on GPN-mediated Ca^{2+} signals. As shown in Fig.2.3.6A and B, compared to the DMSO control, bafilomycin A1 potentiated GPN-mediated complex Ca^{2+} signals. It is noteworthy that the magnitude of Ca^{2+} responses were unchanged (Fig.2.3.6C). Rather, bafilomycin A1 increased the area under the Ca^{2+} curve (AUC) (Fig.2.3.6D). Next, I assayed thapsigargin under the same condition and noticed that following DMSO, thapsigargin mediated small and transient Ca^{2+} signals in the absence of extracellular Ca^{2+}, consistent with its action on the ER (Fig.2.3.6E). While following bafilomycin A1, such Ca^{2+} signals tended to be larger (Fig.2.3.6F). Similar to GPN, this apparent potentiation was reflected by a tendency for the AUC to increase whereas the magnitude of responses appeared similar (Fig.2.3.6G and H). Upon acute treatment, although bafilomycin A1 enhanced GPN-mediated Ca^{2+} signals and tended to enhance thapsigargin- mediated Ca^{2+} signals, it had no apparent effect on LTR staining (Fig.2.3.5A, B and J). Therefore, this

potentiation in Ca^{2+} responses by bafilomycin A1 is not likely due to its lysosomal alkalizing effect.

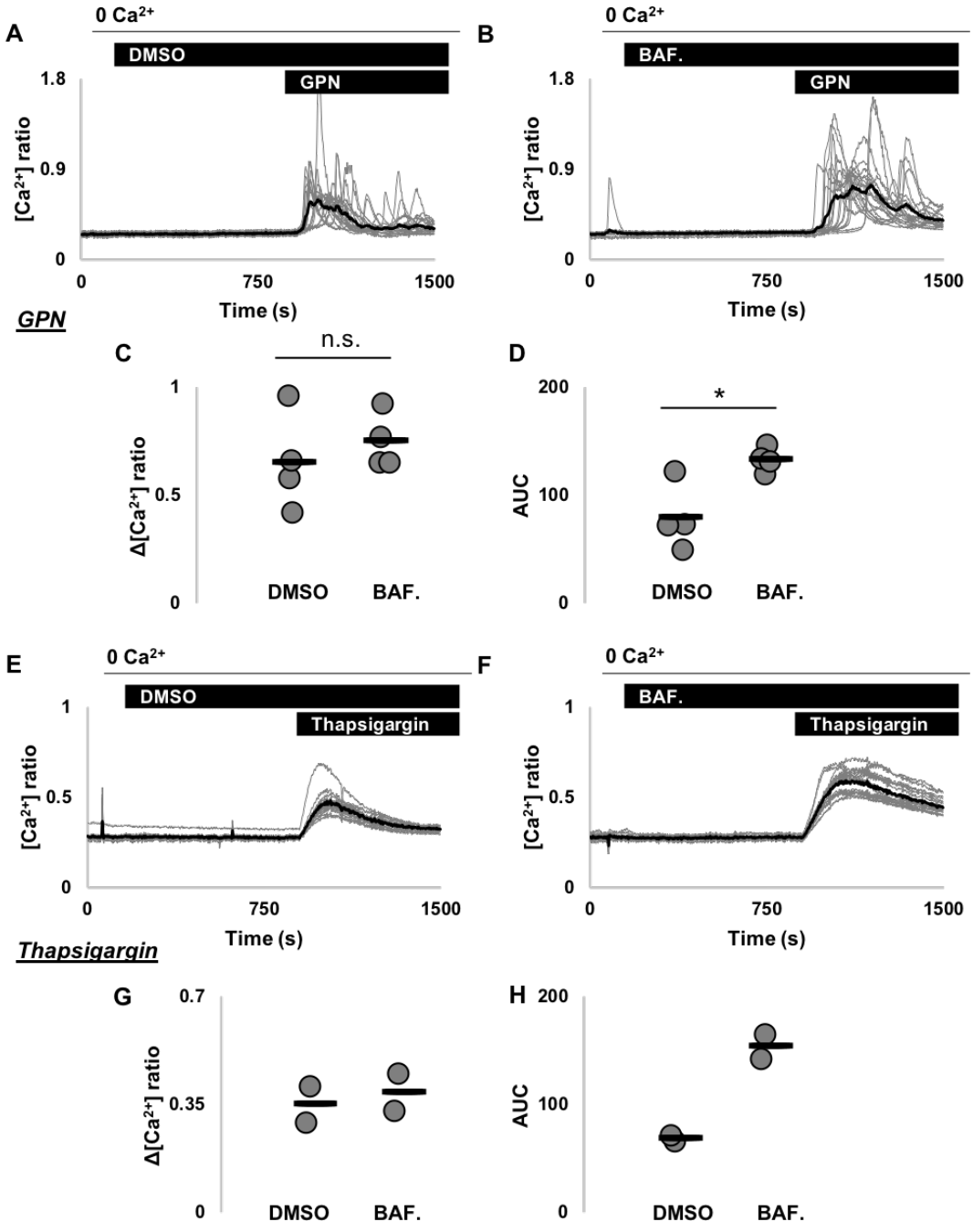

Figure 2.3.6 Acute treatment with Bafilomycin A1 appears to potentiate GPN- and thapsigargin-mediated Ca^{2+} release.

(A and B) Cytosolic Ca^{2+} responses to 200 μM GPN, following DMSO (A) or 1 μM Bafilomycin A1 (B), in the absence of extracellular Ca^{2+} in individual fibroblasts. Cells were immersed into Ca^{2+}-free HBS at 60s. The bars above graphs indicate the time of addition of

compounds, DMSO or bafilomycin A1 (BAF.) was added at 150s, thapsigargin or GPN was added at 900s. Gray traces represent recordings of all individual cells and black traces represent the population average from a typical experiment.
(C and D) Pooled data quantifying magnitudes of Ca^{2+} responses (C) and AUC (D) after GPN stimulation (between 900s and 1500s) in the presence of DMSO or Bafilomycin A1. Each plot point represents average results from an individual experiment such as the example shown in A and B (n=4); n.s. not statistically significant * $P<0.05$ were determined by independent-samples t-tests.
(E-H) Similar to A-D but cells were stimulated with 1 μM thapsigargin, replacing GPN (n=2).

2.3.7 Prolonged treatment with Bafilomycin A1 appears to potentiate GPN- and thapsigargin-mediated Ca^{2+} release

Previous data indicated an apparent potentiating effect of bafilomycin A1 on GPN- and thapsigargin-mediated Ca^{2+} signals that appeared to be independent of lysosomes as this occurred when there was no obvious change in lysosomal pH by bafilomycin A1. To investigate the effects of lysosomal pH on GPN-mediated Ca^{2+} signals, I therefore examined the effects of prolonged bafilomycin A1 treatment, such as 1 hour at RT, which tended to induce a moderate alkalization of lysosomal pH (Fig.2.3.5C and J). As shown in Fig.2.3.7A, GPN-mediated Ca^{2+} signals appeared to be potentiated in cells pre-treated with bafilomycin A1 for 1 hour at RT relative to cells treated with DMSO. This was reflected by a tendency for the AUC to increase (Fig.2.3.7B). To note, however, this did not reach statistical significance given that there was one case where bafilomycin A1 reduced GPN-mediated Ca^{2+} signals. Similarly, the 1 hour treatment enhanced thapsigargin-mediated Ca^{2+} signals (Fig.2.3.7C) as there was a significant increase in AUC (Fig.2.3.7D), while the magnitude remained unchanged (Fig.2.3.7B and D) like GPN. The 1 hour treatment hence tended to affect both GPN and thapsigargin-mediated Ca^{2+} signals in a similar way as the acute treatment did (Fig.2.3.6).

Next, I assayed GPN and thapsigargin in cells pre-treated with bafilomycin A1 for 2 hours at RT as this treatment appeared to have a greater alkalizing effect on lysosomal pH than the 1 hour treatment (Fig.2.3.5C, D and J). As shown in Fig.2.3.7 (E-H), the 2 hour treatment tended to enhance both GPN and thapsigargin-mediated Ca^{2+} signals

through an increase in AUC. The results of the 2 hour treatment hence appeared to be no different from those of the 1 hour treatment.

Taken together, the apparent potentiation effects of bafilomycin A1 on Ca^{2+} responses to GPN and thapsigargin are likely to be independent of lysosomal pH.

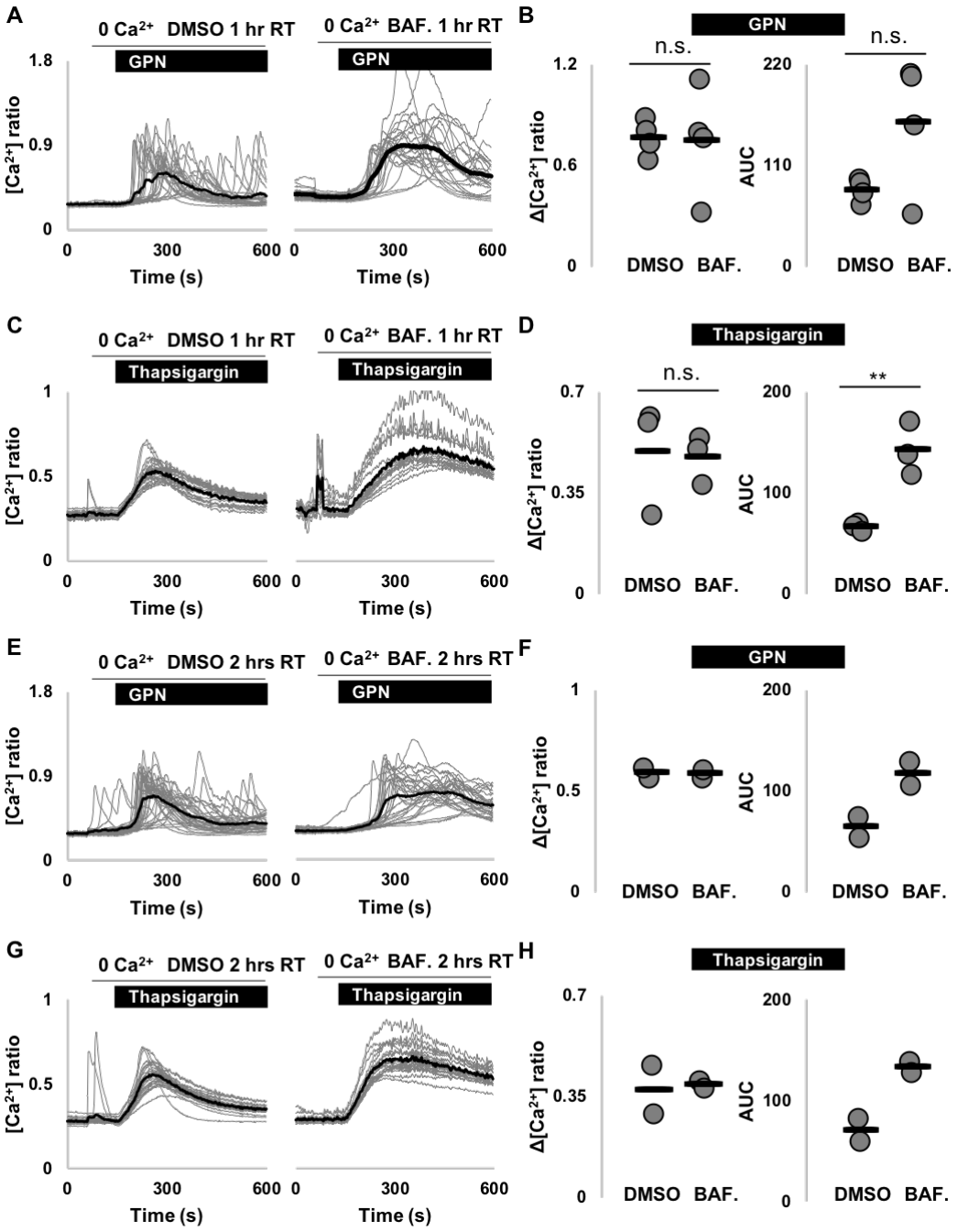

Figure 2.3.7 Prolonged treatment with Bafilomycin A1 appears to potentiate GPN- and thapsigargin-mediated Ca^{2+} release

(A) Cytosolic Ca^{2+} responses to 200 μM GPN, following 1 hour treatment at room temperature with DMSO or 1 μM Bafilomycin A1 (BAF.), in the absence of extracellular Ca^{2+} in individual fibroblasts. Cells were immersed into Ca^{2+}-free HBS at 60s. The bars above graphs indicate the time of addition of compounds, which was at 150s. Gray traces represent recordings of all individual cells and black traces represent the population average from a typical experiment.
(B) Pooled data quantifying magnitudes of Ca^{2+} responses and AUC after GPN stimulation in the presence DMSO or Bafilomycin A1 (for 1 hour). Each plot point represents average results from an individual experiment such as the example shown in A (n=4); n.s. not statistically significant was determined by independent-samples t-tests.
(C and D) Similar to A and B but cells were stimulated with 1 μM thapsigargin, replacing GPN (n=3); n.s. not statistically significant ** $P<0.01$ were determined by independent-samples t-tests.
(E and F) Similar to A and B but cells were pre-treated with DMSO or Bafilomycin A1 for 2 hours (rather than 1 hour) at room temperature before GPN stimulation (n=2).
(G and H) Similar to E and F but cells were stimulated with 1 μM thapsigargin, replacing GPN (n=2).

2.3.8 Chronic treatment with Bafilomycin A1 appears to inhibit GPN- but potentiate thapsigargin- mediated Ca^{2+} release

To further investigate the effects of lysosomal pH on GPN-mediated Ca^{2+} signals, I next assayed GPN and thapsigargin under conditions where bafilomycin A1 caused a demonstrable increase in lysosomal pH (Fig.2.3.5).

To achieve, the cells were pre-incubated with bafilomycin A1 for 1-4 hours in culture, followed by another 1 hour during Fura-2 loading at RT. As shown in Fig.2.3.8A, the 2 hour (1+1) treatment with bafilomycin A1 appeared to reduce GPN-mediated Ca^{2+} signals relative to DMSO pre-treated cells. To be precise, there was a tendency for the magnitude of responses to reduce, and AUC appeared to be unaltered (Fig.2.3.8B). In contrast, thapsigargin-mediated Ca^{2+} signals were potentiated following bafilomycin A1 treatment (Fig.2.3.8C) as reflected by an increase in the AUC (Fig.2.3.8D). The magnitude also tended to be larger (Fig.2.3.8D), but statistically, this was not significant as in one experiment bafilomycin A1 had no visible effect on thapsigargin

responses. Similar to the 2 hour treatment, following the 3 hour (2+1) treatment, there was a trend for GPN-mediated Ca^{2+} signals to be reduced (Fig.2.3.8E and F) and a significant increase in thapsigargin-mediated Ca^{2+} signals (Fig.2.3.8G and H). Finally, the 5 hour (4+1) treatment with bafilomycin A1 also appeared to reduce GPN-mediated Ca^{2+} signals (Fig.2.3.8I and J). This did not reach statistical significance, but in all experiments GPN responses were reduced upon bafilomycin A1 treatment. In comparison, there was a trend for thapsigargin-mediated Ca^{2+} signals to increase upon a 5 hour treatment (Fig.2.3.8K and L)

Collectively, pronounced alkalization of lysosomal pH appeared to selectively inhibit GPN-evoked Ca^{2+} signals.

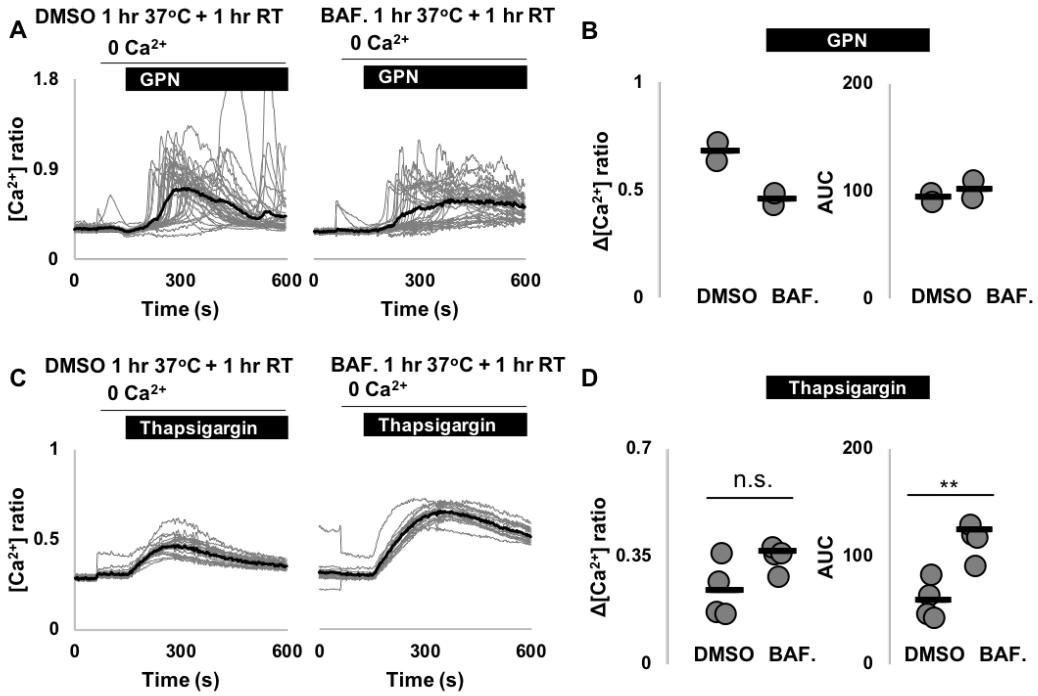

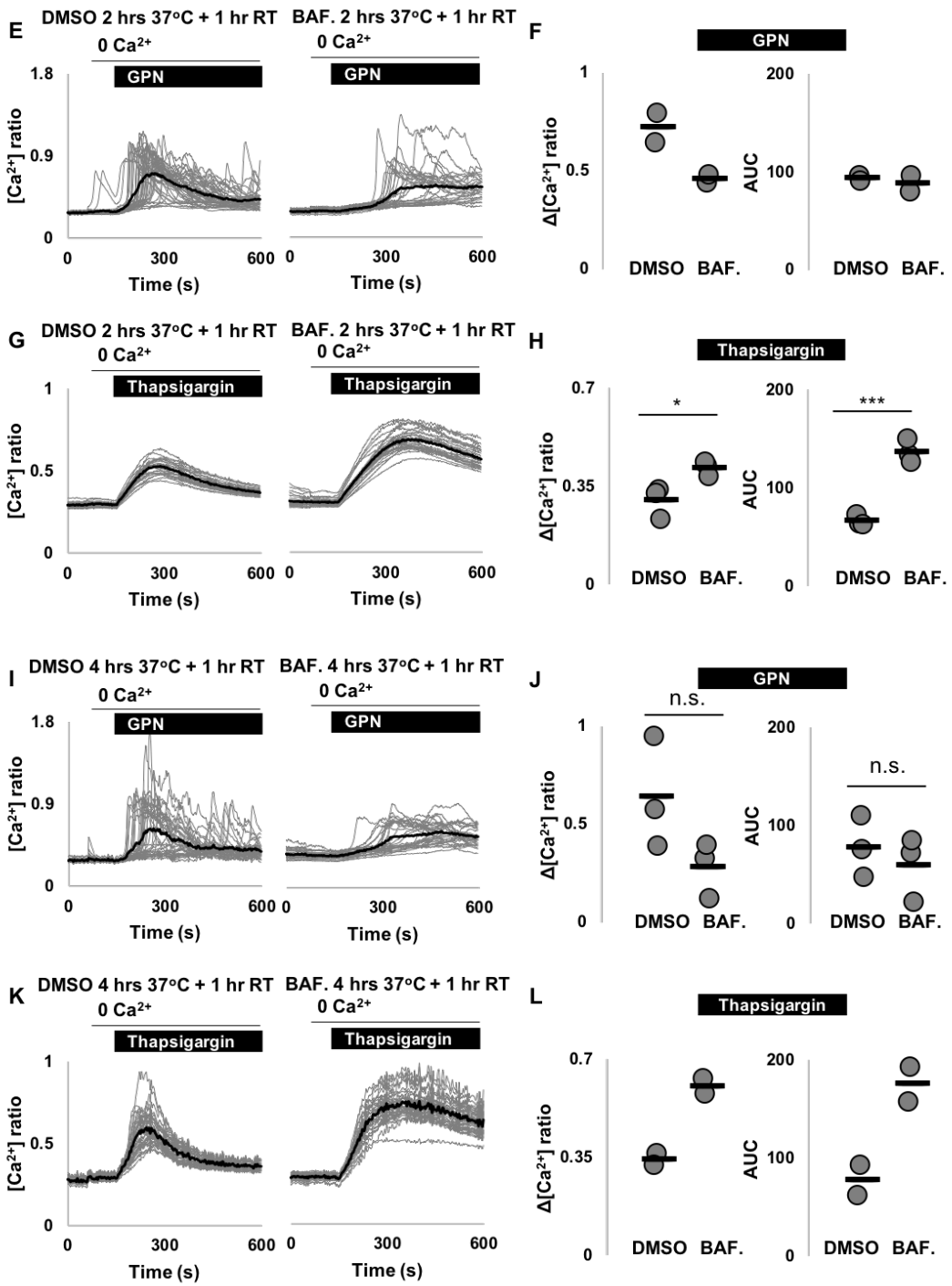

Figure 2.3.8 Chronic treatment with Bafilomycin A1 appears to inhibit GPN- but potentiate thapsigargin-mediated Ca^{2+} release

(A and C) Cytosolic Ca^{2+} responses to 200 μM GPN (A) or 1 μM thapsigargin (C), following 2 hour treatment with DMSO or 1 μM Bafilomycin A1, in the absence of extracellular Ca^{2+} in individual fibroblasts. Cells were immersed into Ca^{2+}-free HBS at 60s. The bars above graphs indicate the time of addition of compounds, which was at 150s. The 2 hour treatment refers to 1 hour under culture conditions followed by 1 hour at room temperature with Fura-2.

(B and D) Pooled data quantifying magnitudes of Ca^{2+} responses and AUC after GPN (B) or thapsigargin (D) stimulation in the presence of DMSO or Bafilomycin A1 (for 2 hours). Each plot point represents average results from an individual experiment such as the example shown in A and C (n=2, (B)) (n=4, (D)); n.s. not statistically significant, **P<0.01 were determined by independent-samples t-tests.
(E-H) Similar to A-D but cells were pre-treated with DMSO or Bafilomycin A1 for 3 hours rather than 2 hours before GPN (E and F) or thapsigargin (G and H) stimulation (n=2, (F) (n=3, (H)); * P<0.05 *** P<0.001 were determined by independent-samples t-tests.
(I-L) Similar to A-D but cells were pre-treated with DMSO or Bafilomycin A1 for 5 hours rather than 2 hours before GPN (I and J) or thapsigargin (K and L) stimulation (n=3, (J)) (n=2, (L)); n.s. not statistically significant was determined by independent-samples t-tests.

2.4 Discussion

GPN is thought to mediate Ca^{2+} signals from lysosomes upon its cleavage by cathepsin C followed by rupture of the lysosomal membrane. However, this view has recently been challenged in the study by Atakpa (Atakpa et al., 2019). Based on a series of observations, the study suggested that GPN mediates Ca^{2+} signals from the ER through its cytosolic alkalizing effects (Atakpa et al., 2019). In this chapter, using fibroblasts, I investigated how GPN mediates Ca^{2+} signals. My data dissociated GPN-evoked cytosolic pH changes from its Ca^{2+} responses and are consistent with the original assumption that GPN targets acidic organelles to mediate Ca^{2+} signals.

GPN is a cell-permeable substrate for cathepsin C (Jadot et al., 1984). Upon hydrolysis by cathepsin C, GPN is thought to evoke lysosomal membrane permeabilization (LMP) through generating osmotic stress. GPN-mediated increases in lysosomal pH and cytosolic Ca^{2+} therefore have been ascribed to leakage of H^+ and Ca^{2+} out of lysosomes. However, the study by Atakpa reveals that cathepsin C is not required for GPN-induced pH change and Ca^{2+} signals with compelling evidence (Atakpa et al., 2019). First, GPN responses persisted in cathepsin C knockout cells. Second, GPN's isomer, D-GPN, a non-cathepsin C substrate, was also able to increase cytosolic Ca^{2+}. Even so, it is still possible that GPN ruptures lysosomal membranes to induce Ca^{2+} and H^+ leak independently of cathepsin C. Generally, loss of endocytosed fluorophores, such as sulforhodamine B and Lucifer yellow, is regarded as a sign of LMP. In the study by

Atakpa, GPN was unable to cause loss of Lucifer yellow (Atakpa et al., 2019). However, in other studies, GPN was capable of releasing Lucifer yellow and also sulforhodamine B (Bright et al., 2016; Haller et al., 1996; Steinberg et al., 2010). Irrespective of this "inconsistency" between studies, it is possible that GPN-induced permeabilization is "mild" only permitting small ions to pass, while current assays (e.g. luminal dye loss or ESCRT-induced membrane repair (Skowyra et al., 2018)) can only detect moderate to severe degree of LMP. More importantly, although the non-cathepsin C substrate, D-GPN, can induce Ca^{2+} signals (Atakpa et al., 2019), it also reportedly mediates LMP (Jadot et al., 1990). Overall, while it is clear that the effects of GPN do not require cathepsin C, the study by Atakpa cannot firmly rule out a permeabilising effect of GPN on lysosomes. In this chapter, I only examined GPN's effects on LTR staining of lysosomes. Considering LTR staining more serves as a proxy of pH change rather membrane permeabilization, it is therefore crucial to apply appropriate test to study the effects of GPN on lysosomal integrity in fibroblasts, for example, by assaying the effect of GPN on endocytosed fluorophores.

LLOMe is another cathespin C substrate and mediates LMP (Repnik et al., 2017; Thiele & Lipsky, 1990). This was confirmed by Atakpa (Atakpa et al., 2019). Using fibroblasts, I therefore compared activity of GPN with that of LLOMe. Similar to GPN, LLOMe induced an increase in cytosolic Ca^{2+} in the presence of extracellular Ca^{2+} (Fig.2.3.2B and C). Upon removal of extracellular Ca^{2+}, GPN Ca^{2+} responses were still detectable (Fig.2.3.3B), in agreement with previous research (Kilpatrick et al., 2013; Penny et al., 2014). In stark contrast, however, there was little Ca^{2+} signalling induced by LLOMe by such modification of the external environment (Fig.2.3.3C). Atakpa and colleagues only assayed LLOMe in the absence of extracellular Ca^{2+}, similarly, they observed only very small Ca^{2+} response. (Atakpa et al., 2019). GPN and LLOMe therefore behave differently in increasing cytosolic Ca^{2+} with GPN-mediated Ca^{2+} signals deriving predominantly from Ca^{2+} release, whereas the Ca^{2+} signals induced by LLOMe relies on Ca^{2+} influx only. GPN-evoked Ca^{2+} signals were accompanied by an increase in lysosomal pH as reflected by a reduction in LTR staining (Fig.2.3.1B), which has been noted in previous researches as well (Kilpatrick et al., 2013). LLOMe-mediated Ca^{2+} signals were also accompanied with an increase in lysosomal pH (Fig.2.3.1C), although the effect on lysosomal pH was less pronounced compared to GPN (Fig.2.3.1D). This implies that lysosomes could be implicated in GPN and

LLOMe Ca^{2+} responses, but also raises a question of how lysosomes contribute to LLOMe-induced Ca^{2+} influx. In cells, lysosomes are widely distributed throughout the cytoplasm. A majority of them have perinuclear localizations, but there are also peripheral lysosomes that are in close proximity to the plasma membrane (Johnson et al., 2016; Jongsma et al., 2016; Pu et al., 2016). In light of this, LLOMe-induced Ca^{2+} influx might be a result of the crosstalk between lysosomes and the plasma membrane. Indeed, recently, the PM-lysosome crosstalk has been noted in hippocampal pyramidal neurons where back-propagating action potential-induced Ca^{2+} influx through VGCCs triggered lysosomal Ca^{2+} release (Padamsey et al., 2017). But on the other hand, the Ca^{2+} influx might be mediated via some of LLOMe's lysosome-independent activities. The mechanism by which LLOMe mediates Ca^{2+} signals is worth further investigation.

With evidence showing that the effects of GPN on Ca^{2+} were independent of cathespin C, Atapka et al. 2019 pursued other possible mechanisms. They found that GPN was capable of increasing cytosolic pH in a cathepsin C-independent manner. And strikingly, that inhibition of such increases reduced GPN-mediated Ca^{2+} signals (Atakpa et al., 2019). This thus led to a reasonable assumption that GPN mediated Ca^{2+} signals via its effect on cytosolic pH. In fibroblasts, I observed the increase in cytosolic pH by GPN (Fig.2.3.4A). However, this alkalization happened very rapidly compared to GPN-mediated Ca^{2+} signals (Fig.2.3.4G). This led me to question the causal relationship between changes in cytosolic pH and Ca^{2+}. I therefore examined NH_4Cl, another weak base. In the study by Atakpa using HEK cells, NH_4Cl resembled GPN in changing cytosolic pH and Ca^{2+} level (Atakpa et al., 2019). In fibroblasts, again, NH_4Cl increased cytosolic pH to a similar level as GPN (Fig.2.3.4A, B and K), however, it mediated weak Ca^{2+} signals which were not comparable to those evoked by GPN (Fig.2.3.4E, F and M). NH_4Cl could induce Ca^{2+} signals in a cell-type dependent manner. Favouring this, NH_4Cl induced small Ca^{2+} responses in PC12 cells (Fasolato et al., 1991) but large Ca^{2+} responses in endothelial cells (Danthuluri et al., 1990). The lack of correlation between changes in cytosolic pH and Ca^{2+}, both kinetically and pharmacologically, therefore suggests that GPN-mediated Ca^{2+} signals are unlikely to be a result of its cytosolic alkalizing effect.

As weak bases, aside from increasing cytosolic pH, in fibroblasts, GPN and NH_4Cl also increased lysosomal pH (Fig.2.3.4C and D). GPN-mediated Ca^{2+} signals

somewhat correlated with the lysosomal pH change, these two activities appeared to occur simultaneously and at a similar rate (Fig.2.3.4H). This is consistent with our lab's previous study where cytosolic Ca^{2+} and lysosomal pH were measured in the same cell (Kilpatrick et al., 2013). Moreover, GPN had a stronger alkalizing effect on lysosomal pH than NH_4Cl (Fig.2.3.4L), and correspondingly, GPN mediated greater Ca^{2+} responses than NH_4Cl (Fig.2.3.4M). These analyses therefore raise the possibility that GPN mediated Ca^{2+} signals are a result of its lysosomal alkalizing effect. It is worth noting, however, in the study by Atakpa, GPN-mediated Ca^{2+} signals were largely reduced by NaP (Atakpa et al., 2019). As a weak acid, NaP prevented GPN-induced cytosolic pH change leaving lysosomal pH untouched. According to this, alkalization of the cytosol but not lysosomes is essential for GPN Ca^{2+} responses, quite the opposite of the results in fibroblasts. Nevertheless, the use of weak acid is a clever way of exploring the relationship between changes in pH and Ca^{2+}. Therefore, it is worth considering examining the effects of NaP or NaP-like compound on GPN Ca^{2+} responses in fibroblasts. On the whole, the cytosolic pH mechanism is not tenable in my opinion, especially given that there is a weak correlation between cytosolic alkalization and cytosolic Ca^{2+} increase.

Although GPN appears to work independently of cathepsin C (Atakpa et al., 2019), there are empirical evidences that lysosomes are the sources of GPN Ca^{2+} signals. For example, there is a concomitant increase in lysosomal pH and cytosolic Ca^{2+} by GPN (Kilpatrick et al., 2013), as discussed above. GPN blocked Ca^{2+} responses to NAADP but not those to IP3 and cADPR (Churchill et al., 2002; Pandey et al., 2009; Soares et al., 2007). In addition, GPN Ca^{2+} signals were reduced in diseases associated with lysosomal Ca^{2+} defect or lysosomal morphology defect (Kilpatrick, Magalhaes, et al., 2016; Lloyd-Evans et al., 2008). However, Atakpa's team suggested that the ER but not lysosomes are the predominant target for GPN. Supporting a primary action on the ER, Atakpa and colleagues found that thapsigargin completely blocked GPN-mediated Ca^{2+} signals. It is not new that thapsigargin reduces GPN-mediated Ca^{2+} signals, and this has been indicated in a number of studies (Garrity et al., 2016; Haller et al., 1996; Kilpatrick et al., 2013; Liu et al., 2018), although there are also cases where GPN responses were insensitive to thapsigargin (Srinivas et al., 2002; Yagodin et al., 1999). In some cell types, it is therefore clear that GPN releases ER Ca^{2+}. However, as to how this occurs, prior researches have suggested that GPN mobilizes ER Ca^{2+} via a

lysosome-dependent mechanism. It has been reported that Lysosomes form functional contacts with the ER via MCSs. In brief, local Ca^{2+} release from lysosomes can "trigger" Ca^{2+} release from the ER to generate global Ca^{2+} signalling (Kilpatrick et al., 2013; Patel & Brailoiu, 2012; Penny et al., 2014, 2015). NAADP has been reported to utilize this form of coupling in sea urchins (Churchill & Galione, 2001) and also mammals (Cancela et al., 1999; Kinnear et al., 2004; Morgan, 2016). Prior to the study by Atakpa, a general accepted idea is that the ER Ca^{2+} release by GPN was secondary to initial Ca^{2+} release from lysosomes. Thus, lysosomes are origins for GPN Ca^{2+} signalling.

The effect of thapsigargin on GPN can reveal the involvement of the ER but cannot inform the exact mechanism by which GPN recruits the ER for signalling. Therefore, the use of thapsigargin cannot rule out the possibility that lysosomes are primary targets for GPN and it is required for GPN to recruit ER Ca^{2+}. Indeed, to suggest that the ER but not lysosomes are required by GPN for signalling, Atakpa and colleagues have relied more on other observations. For example, they found that bafilomycin A1 did not abolish but rather potentiated GPN-mediated Ca^{2+} signals (Atakpa et al., 2019), which is similar to an action of bafilomycn A1 on thapsigargin-mediated Ca^{2+} release (Atakpa et al., 2018; López-Sanjurjo et al., 2013). It may seem surprising but before the study by Atakpa, there were only a few studies that assayed GPN in the presence of bafilomycin A1. Contrary to what Atakpa and colleagues have observed, these studies observed an inhibitory effect of bafilomycin A1 on GPN-mediated Ca^{2+} signals (Gunaratne, Johns, et al., 2018; Zhang et al., 2014). Here, using fibroblasts, I tested the effect of bafilomycin A1 on GPN responses and I showed that bafilomycin A1 inhibited GPN- but not thapsigargin- mediated Ca^{2+} signals (Fig.2.3.8). Although in some cases my data are not statistically significant or repeated only twice, additional experiments by an independent member of the laboratory confirmed my findings (data not shown). Collectively, the trends I report here are indeed statistically significant. My data thus favours the notion that lysosomes are essential for GPN-mediated Ca^{2+} signalling. However, it is noteworthy that this selective inhibition was only apparent after a long incubation with bafilomycin A1. Lysosomes have a high luminal Ca^{2+}, similar to the ER (Christensen et al., 2002; Lloyd-Evans et al., 2008). Dissipation of lysosomal pH gradient, by inhibition of V-ATPase by bafilomycin A1, reduced lysosomal Ca^{2+}, as reflected by a reduction in luminal Ca^{2+} or an increase in cytosolic

Ca^{2+}, while re-acidification of lysosomal pH replenished lysosomes with Ca^{2+} (Christensen et al., 2002; Lloyd-Evans et al., 2008; López et al., 2005). Since the lysosomal pH gradient is thought to be essential for lysosomal Ca^{2+} uptake and maintenance, for depletion of lysosomal Ca^{2+}, bafilomycin A1 therefore relies on two events, a leakage of H^+ for pH gradient dissipation and a subsequent leakage of Ca^{2+} driven by prevention of Ca^{2+} uptake (Morgan et al., 2015). Regarding H^+ leak by bafilomcyin A1, this occurred slowly in fibroblasts. A 1 hour treatment with bafilomcyin A1 at RT only appeared to reduce 50% of LTR fluorescence (Fig.2.3.5C and J). In comparison, under culture conditions, the effect of bafilomycin A1 on H^+ leak appeared to be enhanced. A 1 hour treatment eliminated almost all LTR fluorescence (Fig.2.3.5E and J), although it should be noted that this experiment was performed once. Regarding Ca^{2+} leak, it is expected that this event occurs after prevention of Ca^{2+} uptake (Morgan et al., 2015), however, the information about how Ca^{2+} leaks out of lysosomes is almost non-existent. It may occur immediately after leakage of H^+ or more slowly. Considering the uncertainty, it could be possible that like the leakage of H^+, the leakage of Ca^{2+} progressed slowly as well. Given the above situations, one can easily explain why it took a long time for bafilomycin A1 to inhibit GPN-mediated Ca^{2+} signals. Also, a slow Ca^{2+} leak may explain why Ca^{2+} signals by acute bafilomycin A1 treatment were not detected by measurement of Ca^{2+} in the cytosol.

Favouring the slow Ca^{2+} leak upon elevation of lysosomal pH, an early study by Churchill and colleagues showed that bafilomycin A1 prevented Ca^{2+} uptake into lysosomes but only inhibited NAADP-mediated Ca^{2+} signals in sea urchin eggs when the eggs were first challenged with both bafilomycin A1 and NAADP (Churchill et al., 2002). This was interpreted as the lysosomal Ca^{2+} store being non-leaky to Ca^{2+} requiring prior opening of resident Ca^{2+}-permeable channels to effect Ca^{2+} depletion i.e. NAADP was used to speed the Ca^{2+} leak process. Alternatively, perhaps Ca^{2+} leak is not necessary. It is noteworthy that although Ca^{2+} uptake is thought to be regulated by lysosomal pH gradient possibly via CAXs (Christensen et al., 2002; Churchill et al., 2002; Morgan et al., 2011; Patel & Muallem, 2011). Garrity and colleagues have proposed pH-independent Ca^{2+} uptake (Garrity et al., 2016). It is worth considering that the increase in lysosomal pH might not equate to depletion of lysosomal Ca^{2+}. Dickson and colleagues have found that in secretory granules (SGs), increasing

luminal pH caused a dramatic reduction in luminal Ca^{2+} but a negligible increase in cytosolic Ca^{2+} (Dickson et al., 2012). Given that SGs' lumen has plenty of Ca^{2+} buffers which are active in binding and reducing free Ca^{2+} at alkaline pH, Dickson and colleagues hypothesized that the reduction in luminal Ca^{2+} caused by increased luminal pH is not due to Ca^{2+} leak out of SGs but due to increased Ca^{2+} buffering (Dickson et al., 2012). Microprobe analysis indicate that lysosomes store a total of 5-14 mM Ca^{2+} (James-Kracke et al. 1979; LeFurgey et al. 1991; Yagodin et al. 1999; reviewed in Morgan et al. 2011). Since the free Ca^{2+} is orders of magnitude lower (400-600 μM) (Christensen et al., 2002; Lloyd-Evans et al., 2008), like SGs, lysosomes likely also contain a large proportion of Ca^{2+} buffers. Therefore, it is possible that bafilomycin A1 inhibits GPN-mediated Ca^{2+} signals via an increase in lysosomal Ca^{2+} buffering capacity. However, this is not to say that I rule out that bafilomycin A1 inhibits GPN-mediated Ca^{2+} signals by preventing Ca^{2+} uptake and thus depleting lysosomal Ca^{2+}. Actually, it is probable that bafilomycin A1, or more specifically, lysosomal pH elevation has more than one mechanism to affect lysosomal Ca^{2+}.

It is interesting to note, upon shorter incubation times, I observed that bafilomycin A1 potentiated GPN-mediated Ca^{2+} signals (Fig.2.3.6-2.3.7). This finding was confirmed by an independent member of the laboratory (data not shown). This is in line with the recent findings by Atakpa (Atakpa et al., 2019). Based on this, the effects of GPN on lysosomes was ruled out (Atakpa et al., 2019). But in my parallel experiments, bafilomycin A1 also appeared to potentiate thapsigargin-mediated Ca^{2+} signals (Fig.2.3.6-2.3.7). Previous studies by the same lab also observed this potentiation and interpreted the results as a failure of lysosome in tempering ER Ca^{2+} release following disruption of the lysosomal pH gradient by bafilomycin A1 (Atakpa et al., 2018; López-Sanjurjo et al., 2013). However, here, in fibroblasts, the potentiation effect by bafilomycin A1 on GPN and thapsigargin is unlikely to be a result of inhibition of V-ATPase as they did not appear to correlate with the slow increase in lysosomal pH. More importantly, the potentiation was even observed when bafilomycin A1 hardly affected lysosomal pH (Fig. 2.3.5A and B and Fig. 2.3.6), indicating the mechanism for the effect is likely lysosome independent. Thus, in fibroblasts, the enhanced GPN signals after bafilomycin A1 treatment cannot argue against an action of GPN on acidic compartments. The exact mechanism for the potentiation effect is worthy of future investigations.

In conclusion, my data indicate that in fibroblasts, bafilomycin A1-sensitive acidic Ca^{2+} stores, such as lysosomes, are required for GPN-mediated complex Ca^{2+} signals. This finding is in contrast to the recent study by Atakpa but is consistent with the original assumption that GPN targets acidic organelles to mediate Ca^{2+} responses. However, the underlying mechanism is still unclear. Therefore, further work defining the exact mechanism is required.

Chapter 3: Characterization of novel small molecule probes for TPC2

3.1 Introduction

TPCs have been linked to health and disease (Grimm et al., 2017; Patel & Kilpatrick, 2018). To better understand the physiological and pathophysiological roles of TPCs, it is essential to have chemicals that can manipulate TPC activity.

Current known TPC activators are NAADP and $PI(3,5)P_2$ albeit controversial. However, these two ligands are cell-impermeable requiring microinjection to access TPCs, which is technically demanding. In addition, NAADP is proposed to activate TPCs by interacting with putative small binding proteins (Lin-Moshier et al., 2012; Walseth et al., 2012) which could be accidentally lost in broken cell preparations. A cell-permeable NAADP derivative (NAADP-AM) is available but it is fairly unstable (Galione et al., 2014; Parkesh et al., 2008; Zhang et al., 2013). Compared to TPCs, there are cell-permeable small-molecule synthetic activators for TRPML1 (e.g. ML-SAs and MK6-83) (Chen et al., 2014; Shen et al., 2012). Such activators offer an easy route for functional characterization of TRPML1 and have been very helpful in aiding our understanding of the channel. For example, ML-SAs have revealed the role of TRPML1 in lysosomal biogenesis and autophagy (Cao et al., 2017; Zhang et al., 2016). Also, it has uncovered that TRPML1 induces global Ca^{2+} signals via additionally mobilizing ER Ca^{2+} release and stimulating Ca^{2+} influx (Kilpatrick, Yates, et al., 2016). Moreover, the synthetic agonists established TRPML1 as a potential drug target for a number of diseases (Chen et al., 2014; Shen et al., 2012; Tedeschi et al., 2019). For better characterizations of TPCs, similar agonists are urgently required. Importantly, given that TPC2 knockout induces fatty liver diseases (Grimm et al., 2014), such agonists might be clinically beneficial in the long-term. In 2019/2020, studies on pursuing cell-permeable TPC activators have been extremely active. For example, using drug re-purposing approach, Zhang et al., identified tricyclic antidepressants (TCAs) as TPC activators (Zhang et al., 2019).

Regarding TPC inhibitors, although cell-permeable inhibitors are available, they are rather limited and few of them are selective for TPCs. As summarised in Table1.2, the

majority of the inhibitors are modifiers of voltage-gated Ca^{2+} (Ca_V) or Na^+ (Na_V) channels, including the most potent one, tetrandrine (Rahman et al., 2014; Sakurai et al., 2015). Naringenin has also been shown to block TPCs, but like tetrandrine, it has multiple targets (Straub et al., 2013; Waheed et al., 2014; Yang et al., 2014; Zhou et al., 2019). Aside from being non-selective, certain inhibitors might have an indirect action on TPCs, such as PPADS, BZ194 (a N-alkylated nicotinic acid derivative) and Ned-19 (Billington & Genazzani, 2007; Dammermann et al., 2009; Naylor et al., 2009; Rosen et al., 2009). These chemicals were identified specifically in regard to their action on NAADP binding and Ca^{2+} signalling, and NAADP has been shown to indirectly activate TPCs (Lin-Moshier et al., 2012; Walseth et al., 2012). Therefore, use of these chemicals complicates research on TPCs. Pursuing selective inhibitors that directly affect TPCs is critical not only for research purposes, but also, over the long term, for treatment of diseases, including PD, Ebola infection and cancer. PD is associated with upregulated TPC2 activity (Hockey et al., 2015). Ebola infection and metastatic tumour formation can be reduced upon TPC silencing (Nguyen et al., 2017; Sakurai et al., 2015). In 2018/2019, two independent groups searched for novel TPC blockers (Gunaratne, Johns, et al., 2018; Penny et al., 2019). To achieve this, both labs have taken advantage of the fact that TPCs are required for viral entry, that is, some antiviral drugs could be TPC inhibitors. Specifically, Gunaratne et al., utilized sea urchin egg homogenates to conduct a screening campaign and identified a number of inhibitors that selectively block NAADP-mediated Ca^{2+} signalling. The inhibitors for NAADP also blocked TPC-dependent MERS-CoV pseudovirus translocation with similar potency (Gunaratne, Johns, et al., 2018). Our lab performed a TPC2-structure based screen (Penny et al., 2019), the results from which were compared with two previously published high-throughput screening for Ebola antivirals (Johansen et al., 2015; Kouznetsova et al., 2014). This yielded a number of common hits that effectively blocked NAADP responses in sea urchin egg homogenate. Certain hits were tested in human cells and were found to block NAADP- and $PI(3,5)P_2$-activated TPC2 channel activity.

In this chapter, my aim was to validate and characterize novel putative TPC activators and to further characterize new TPC inhibitors.

3.2 Methods

3.2.1 Cell culture

Both HeLa cells (Kilpatrick, Yates, et al., 2016) and HEK293 cells stably expressing $TPC2^{LL/AA}$ (Gerndt et al., 2020) were maintained in Dulbecco's Modified Eagle Medium (DMEM), supplemented with 10% (v/v) Fetal Bovine Serum (FBS), 100 µg/mL streptomycin and 100 units/mL penicillin (all from Invitrogen). They were kept at 37°C in a humidified atmosphere with 5% CO_2. Cells were fed with fresh media every 3-4 days. Cells were passaged with trypsin (from Invitrogen) followed by plating onto poly-L-lysine (20 µg/ml, Sigma) coated coverslips in a 24 well-plate (HeLa: at 300,000 cells/ml; HEK293 stably expressing $TPC2^{LL/AA}$: at 150,000 cells/ml; 0.5 ml/well), 2 days before imaging.

3.2.2 Transfection

HeLa cells were transfected with plasmids the day after plating onto coverslips and before imaging/fixing, using lipofectamine 2000 according to the manufacturer's instructions.

Plasmids used are listed below:

Table 3.1 Plasmids

Name	Tag	Reference
PM TPC2 ($TPC2^{LL/AA}$)	mRFP or GFP	(Brailoiu, Rahman, et al., 2010)
L265P PM TPC2 ($TPC2^{LL/AA, L265P}$)	mRFP	(Gerndt et al., 2020)
TPC2 WT	GFP	(Brailoiu et al., 2009)
L265P TPC2 ($TPC2^{L265P}$)	GFP	(Brailoiu, Rahman, et al., 2010)
TPC2 WT	GCaMP6s	(Gerndt et al., 2020)
L265P TPC2 ($TPC2^{L265P}$)	GCaMP6s	(Gerndt et al., 2020)
TPC1 WT	GCaMP6s	Unpublished [1]
PM TRPML1 ($TRPML1^{\Delta NC}$)	GFP	(Yamaguchi et al., 2011)
TRPML1 WT	GFP	(Yamaguchi et al., 2011)
TRPML1 WT	GCaMP6s	(Gerndt et al., 2020)
LAMP1	GFP	(Falcón-Pérez et al., 2005)

[1] This clone was made by Dr. William Andrews and Prof. Sandip Patel by replacing the mRFP tag in TPC1 mRFP (Brailoiu et al., 2009) with GCaMP6s from TPC2 GCaMP6s (Gerndt et al., 2020).

3.2.3 Epifluorescence microscopy

3.2.3.1 Fura-2 Ca^{2+} measurements

Prior to the start of imaging, cells transfected with GFP or mRFP were identified via taking snapshots of their fluorescence upon excitation at 488 nm and 568 nm, respectively. Emitted fluorescence was captured using a 515 nm long pass filter (GFP) and a 590 nm filter (mRFP). Cytosolic Ca^{2+} was measured by Fura-2 and analysed as described in chapter 2. Cells were stimulated with A1 (5 µM, 10 µM, 20 µM, 30 µM and 60 µM), H07 (10 µM, 20 µM, 30 µM and 60 µM), ML-SA1 (1 µM, 3.16 µM 10 µM and 20 µM) (Merck), tetrandrine (10 µM) (Santa Cruz Biotechnology), cepharanthine (10 µM) (Cayman Chemical), fluphenazine (10 µM) (Sigma), pimozide (10 µM) (Santa Cruz Biotechnology), raloxifene (10 µM) (Cayman Chemical), clomiphene (10 µM) (Sigma), tamoxifen (10 µM) (Sigma), simvastatin (10 µM) (Sigma), lovastatin (10 µM) (Cayman Chemical), cerivastatin (10 µM) (Santa Cruz Biotechnology) and ionomycin (2 µM) (Cayman Chemical). All compounds were prepared in DMSO (0.1% (v/v) DMSO used as a control when required). Some Fura-2 measurements were performed in Ca^{2+}-free HBS, which has been indicated in figures.

A1 and H07 were gifts from laboratories of Prof. Christian Grimm and Prof. Franz Bracher based in Ludwig Maximilian University of Munich Germany. In Gerndt et al., 2020, A1 and H07 are referred to as TPC2-A1-N and TPC2-A1-P, respectively.

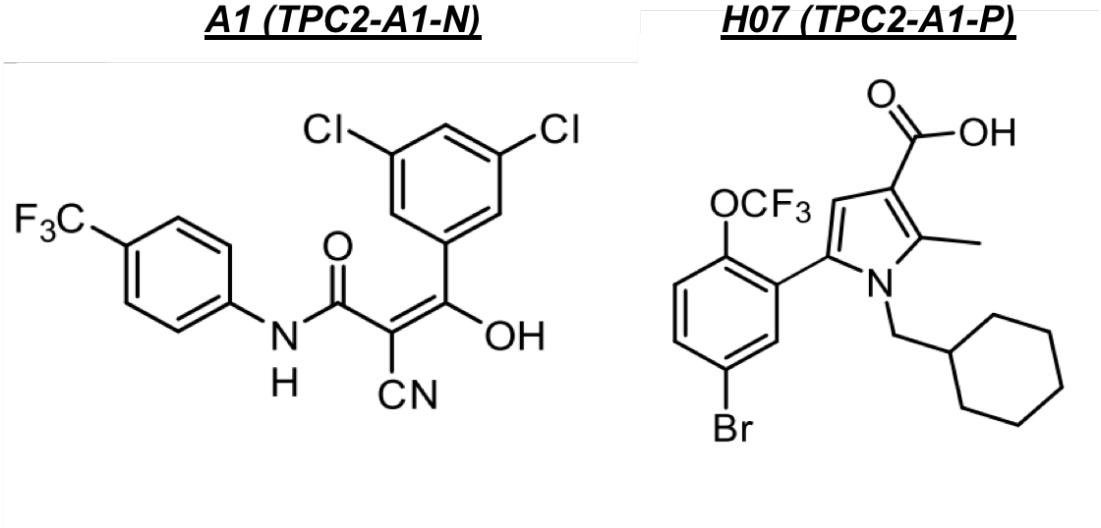

Figure 3.2.1 Chemical structures of A1 (TPC2-A1-N) and H07 (TPC2-A1-P) (Gerndt et al., 2020)

3.2.3.2 GCaMP6s Ca^{2+} measurements

GCaMP6s was excited at 470 nm and emitted fluorescence was captured with a 515 nm long pass filter. Images were acquired every 3s with 40x objective. All GCaMP6s experiments were conducted in Ca^{2+}-free HBS. Ca^{2+}-free HBS replaced HBS 30 seconds after imaging/recording started. Cells were challenged with A1 (30 μM), H07 (60 μM), ML-SA1 (20 μM), GPN (200 μM), thapsigargin (1 μM) and ionomycin (2 μM).

To quantify the change in Ca^{2+} as indicated by GCaMP6s fluorescence, ROIs were drawn around each cell and an area without cells for background subtraction. Fluorescence was calculated using TILLvisION software. The basal ratio (F_0) was acquired by averaging fluorescence from a 90 second recording before cell stimulation and after cells were immersed in Ca^{2+}-free HBS. Change in GCaMP6s fluorescence (ΔF) was normalised to basal ($\Delta F/F_0$) for the data presentation.

3.2.4 Cell fixation

For localization experiments, transfected cells were fixed with 4% (w/v) paraformaldehyde (VWR) in phosphate buffered saline (PBS) (Sigma) for 15 minutes at room temperature. After fixation, cells were washed three times in PBS and were then mounted onto microscope slides with 1,4 diazabicyclo [2,2,2] octane (DABCO) (Sigma) and sealed with colourless nail polish for confocal microscopy.

3.2.5 Spinning disk confocal microscopy

Confocal images were captured using an inverted Axio Observer.Z1 microscope attached to a VivaTome scanner (Zeiss) fitted with a 63x Plan Apochromat water-immersion objective. GFP and GCaMP6s were excited using a 432-482 nm band-pass (BP) filter and emitted fluorescence was captured using a 546-566 nm BP filter. mRFP was excited with a 546-566 nm BP filter and emitted fluorescence was captured with a 580-653 nm BP filter. Confocal images were processed using Image J (Rasband, W.S., ImageJ, U. S. National Institutes of Health, Bethesda, Maryland, USA, https://imagej.nih.gov/ij/, 1997-2018).

3.2.6 Data analysis

Data are presented as representative results from single experiments or as mean +/- S.E.M. from several experiments. For HEK293 cells stably expressing $TPC2^{LL/AA}$, ~90 cells were analysed per coverslip/experiment. For untransfected HeLa cells, ~70 cells were analysed per coverslip/experiment. For transfected HeLa cells, about 5-15 cells (GCaMP6s) or about 20-40 cells (GFP or mRFP) were analysed per coverslip/experiment. Statistical analysis was performed using Prism 9. Independent-Samples T-tests were applied to test significance of data from two groups/conditions having normal distributions. One-way ANOVA were applied to test significance of data from three or more groups/conditions having normal distributions. Where normal distributions and/or equal variances were not met, a Mann-Whitney U test was employed for data from two groups/conditions, and a Kruskal-Wallis H test was employed for data from more than two groups. $P<0.05$ was regarded as statistically significant. The half-maximal excitatory concentration (EC_{50}) was determined by nonlinear regression analysis using Prism 9.

3.3 Results

3.3.1 Putative TPC2 agonists, A1 and H07, evoke Ca^{2+} signals in cells stably expressing plasma membrane targeted TPC2

The lysosomal localization of TPC2 requires its N-terminal di-leucine motif (Brailoiu, Rahman, et al., 2010). Mutation of the motif targets TPC2 to the plasma membrane (PM). To identify TPC2 agonists, Grimm and colleagues generated a HEK293 cell line that stably expresses TPC2 in the plasma membrane ($TPC2^{LL/AA}$) (Gerndt et al., 2020) and used it in a FLIPR-based Ca^{2+} assay, to screen a library of 80,000 natural and synthetic compounds (Gerndt et al., 2020). Consequently, two putative TPC2 agonists were identified and were named A1 and H07. I began my analysis on A1 and H07 using the same cell line. Confocal imaging revealed expression of $TPC2^{LL/AA}$ at the PM (Fig. 3.3.1A). I tested the effects of A1 and H07 on cytosolic Ca^{2+}, which was recorded using Fura-2. As shown in Fig. 3.3.1B, following addition of 30 μM or 60 μM A1, cytosolic Ca^{2+} increased, then it plateaued. H07 at the same concentration caused a similar but delayed Ca^{2+} increase (Fig.3.3.1C). My results are consistent with A1 and H07 as TPC2 activators.

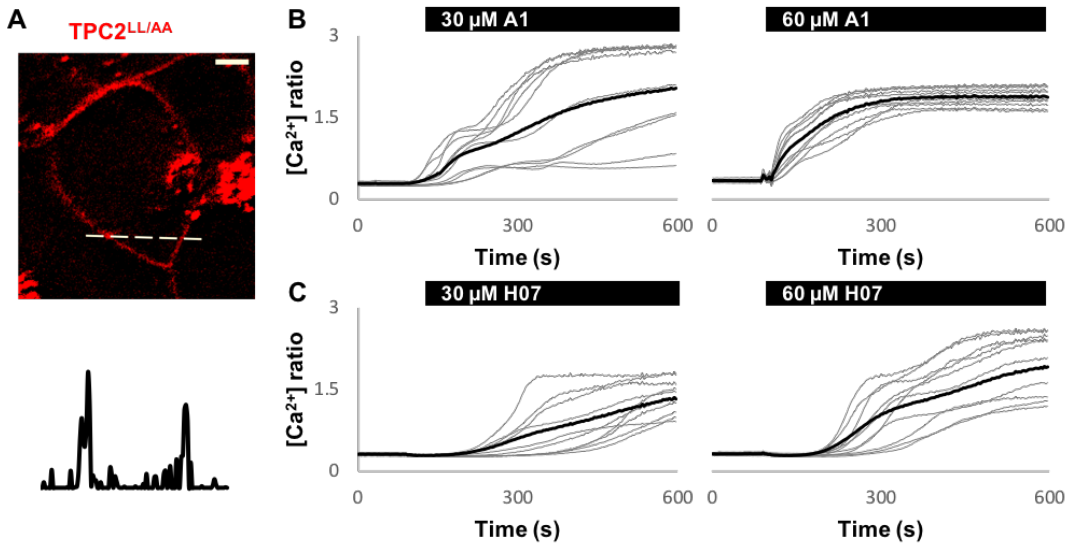

Figure 3.3.1 Putative TPC2 agonists, A1 and H07, evoke Ca^{2+} signals in cells stably expressing plasma membrane targeted TPC2

(A) Confocal images of HEK293 cells stably expressing mRFP-tagged $TPC2^{LL/AA}$ (red). Scale bar = 5 μm. The fluorescence intensity plot below corresponds to the dashed line.

(B and C) Cytosolic Ca^{2+} responses to A1 (30 μM or 60 μM) (B) or H07 (30 μM or 60 μM) (C) in individual HEK293 cells stably expressing $TPC2^{LL/AA}$. The bars above graphs indicate the time of addition of the compound, which was at 90s. Gray traces represent recordings of individual cells (10 cells were selected from a representative experiment) and black traces represent the average from all cells in the experiment.

3.3.2 A1 and H07 evoke Ca^{2+} signals in a concentration-dependent manner

The effects of A1 and H07 on cytosolic Ca^{2+} in cells stably expressing $TPC2^{LL/AA}$ were further characterized using a range of concentrations. Both A1- and H07-induced Ca^{2+} responses were concentration dependent (Fig. 3.3.2A). The magnitude of the Ca^{2+} signals for each concentration was calculated. Examination of the concentration-response curves revealed that the EC_{50} for A1 was 21.75 μM (Fig. 3.3.2B). As the responses to H07 did not saturate, I was unable to determine the EC_{50} for H07. Nevertheless, H07 is likely to have a higher EC_{50} than A1 given that the curve for H07 was shifted to the right of the curve for A1(Fig. 3.3.2B). In addition, notably, at 10 μM and 30 μM, respectively, A1-induced larger Ca^{2+} signals than H07 (Fig. 3.3.2B). Furthermore, as shown in Fig. 3.3.2C and D, the 30 μM A1-induced increase in

cytosolic Ca^{2+} occurred almost straight after agonist addition. In contrast, there was an apparent delay in the 30 µM H07-induced Ca^{2+} responses (Fig.3.3.2C). Increasing the H07 concentration to 60 µM failed to eliminate the delay (Fig.3.3.2D). The delay was quantified by calculating the magnitude of Ca^{2+} responses after around 2 minutes stimulation with A1 or H07 (Fig.3.3.2E). Taken together, these data indicate that A1- and H07-induced Ca^{2+} signals are kinetically different.

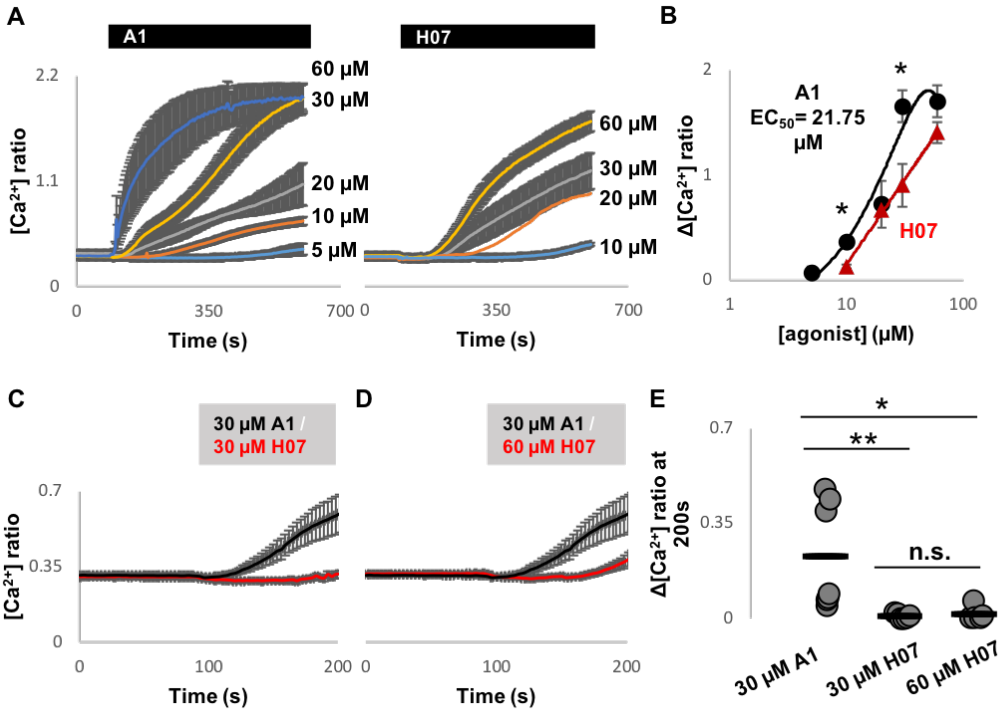

Figure 3.3.2 A1 and H07 evoke Ca^{2+} signals in a concentration-dependent manner

(A) Average cytosolic Ca^{2+} responses (mean or mean ± S.E.M, from 2-13 independent experiments (i.e. n=2-13)) to A1 or H07 at a range of concentrations in HEK293 cells stably expressing $TPC2^{LL/AA}$. The bars above graphs indicate the time of addition of the compound, which was at 90s.

(B) Concentration-response curves showing magnitudes of A1- or H07-induced Ca^{2+} responses in A. * $P<0.05$ was determined by independent-samples t-tests.

(C and D) Kinetic comparison of Ca^{2+} responses by A1 at 30 µM with that by H07 at 30 µM (C) or 60 µM (D) (mean ± S.E.M, from 5-6 independent experiments). X- and y-axes were expanded showing the first 2 minutes of imaging after stimulation with A1/H07. The full imaging time course can be found in A.

(E) Data quantifying magnitudes of Ca^{2+} responses after stimulation with A1 or H07 for about 2 minutes in C and D. Each plot point represents one experiment (n=5-6); n.s. not statistically significant * P<0.05 ** P<0.01 were determined by Kruskal-Wallis H test.

3.3.3 A1 and H07 evoke Ca^{2+} signals in cells transiently expressing plasma membrane targeted TPC2

To further validate A1 and H07, I examined their effects on cytosolic Ca^{2+} in HeLa cells transiently transfected with $TPC2^{LL/AA}$. When examined by confocal microscopy, $TPC2^{LL/AA}$ displayed PM localization (Fig.3.3.3A). As shown in Fig.3.3.3B, both A1 (30 μM) and H07 (30 μM) induced Ca^{2+} signals in cells expressing $TPC2^{LL/AA}$. The magnitudes of their respective Ca^{2+} signals were variable (Fig.3.3.3C). Never-the-less, compared to A1, H07-induced Ca^{2+} signals were smaller and delayed (Fig.3.3.3C and D), consistent with the results obtained in cells stably expressing $TPC2^{LL/AA}$ (see previous Fig.3.3.2).

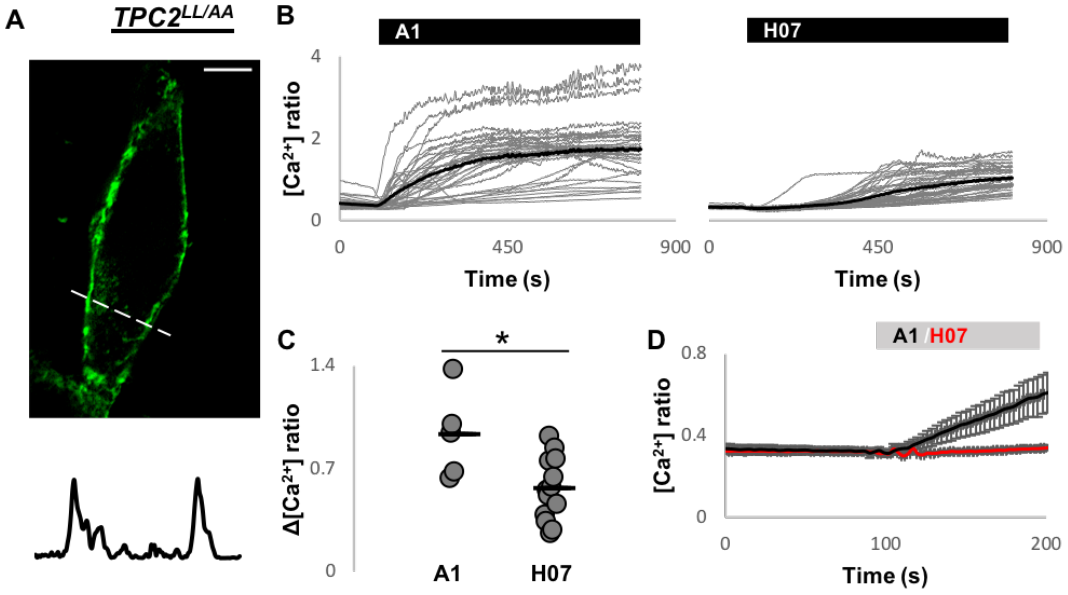

Figure 3.3.3 A1 and H07 evoke Ca^{2+} signals in cells transiently expressing plasma membrane targeted TPC2

(A) Representative confocal image of HeLa cells transiently expressing GFP-labelled $TPC2^{LL/AA}$ (green). Scale bar = 10 μm. The fluorescence intensity plot below the image corresponds to the dashed line.

(B) Cytosolic Ca^{2+} responses to A1 (30 μM) or H07 (30 μM) in individual HeLa cells transiently expressing $TPC2^{LL/AA}$. The bars above graphs indicate the time of addition of the compound, which was at 90s. Gray traces represent recordings of all individual cells and black traces represent the population average.
(C) Data quantifying magnitudes of Ca^{2+} responses to A1 or H07. Each plot points represents one experiment (n=5-12); * $P<0.05$ was determined by independent-samples t-tests.
(D) Kinetic comparison of Ca^{2+} responses by A1 at 30 μM with that by H07 at 30 μM (mean ± S.E.M, from 5-12 independent experiments). X- and y-axes were expanded showing the first 2-minute imaging results after stimulation with A1/H07.

3.3.4 Agonist-evoked Ca^{2+} signals are abolished upon mutation of the TPC2 pore or removal of extracellular Ca^{2+}

Having ascertained that A1 and H07 were capable of inducing Ca^{2+} signals in cells transiently expressing $TPC2^{LL/AA}$, I next tested A1 in cells transiently expressing $TPC2^{LL/AA, L265P}$. Leucine 265 (L265) maps to the pore loop of domain I of TPC2. Its mutation to proline (P) blocked NAADP-evoked Ca^{2+} signals and TPC2 channel activity (Brailoiu, Rahman, et al., 2010; Lin-Moshier et al., 2014; Sakurai et al., 2015). L265 therefore is required for normal functionality of TPC2, and TPC2 with L265P mutation is regarded as a "pore-dead" TPC2. Confocal imaging revealed that $TPC2^{LL/AA, L265P}$ was expressed at the PM (Fig. 3.3.4A). As shown in Fig.3.3.4B and C, A1 induced Ca^{2+} signals in cells expressing $TPC2^{LL/AA}$ but not in cells expressing $TPC2^{LL/AA, L265P}$. To determine whether the Ca^{2+} signals were due to intracellular Ca^{2+} release or extracellular Ca^{2+} influx, I examined the effect of removing extracellular Ca^{2+}. As shown in Fig.3.3.4B and D, A1-induced Ca^{2+} signals in cells expressing $TPC2^{LL/AA}$ were abolished in the absence of extracellular Ca^{2+}, indicating such Ca^{2+} signals were a result of Ca^{2+} influx. This is consistent with the PM localization of $TPC2^{LL/AA}$. These data were quantified in Fig.3.3.4E, where I calculated the magnitudes of A1-induced Ca^{2+} signals under the different conditions. Similar experiments were performed for H07. As shown in Fig. 3.3.4F-H and quantified in Fig. 3.3.4I, H07 was able to induce Ca^{2+} signals in cells expressing $TPC2^{LL/AA}$ but not in cells expressing $TPC2^{LL/AA, L265P}$. In the absence of extracellular Ca^{2+}, H07 failed to induce Ca^{2+} signals in cells expressing $TPC2^{LL/AA}$. Again, this is consistent with the

PM localization of TPC2$^{LL/AA}$. Collectively, these data indicate that A1 and H07 activate TPC2$^{LL/AA}$ to induce Ca^{2+} influx via the pore.

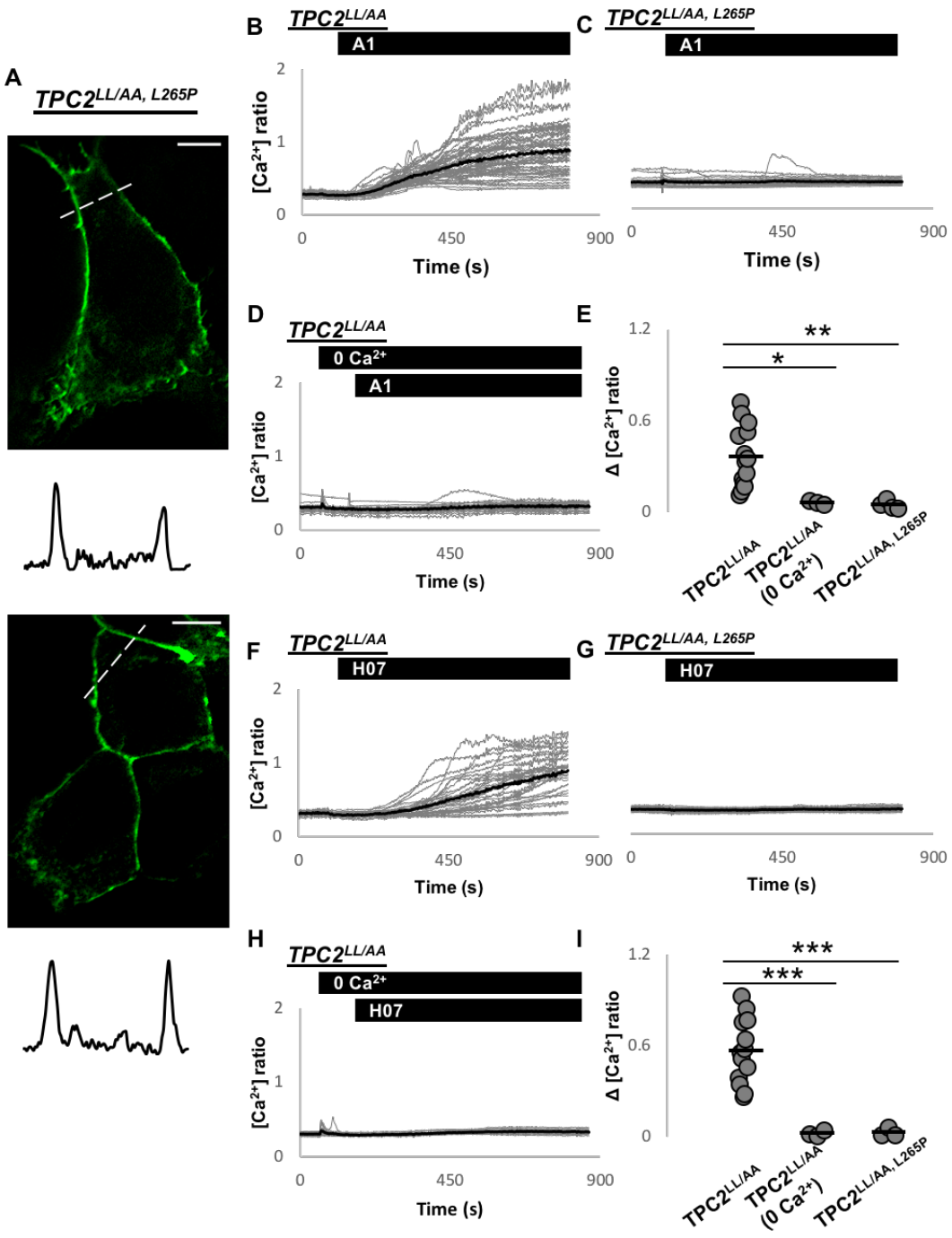

Figure 3.3.4 Agonist-evoked Ca^{2+} signals are abolished upon mutation of the TPC2 pore or removal of extracellular Ca^{2+}

(A) Confocal images of HeLa cells transiently expressing GFP-tagged TPC2$^{LL/AA, L265P}$(green). Scale bar = 10 µm. The fluorescence intensity plot below the image corresponds to the dashed line.

(B and C) Cytosolic Ca^{2+} responses to A1 (10 μM) in individual HeLa cells transiently expressing $TPC2^{LL/AA}$ (B) or $TPC2^{LL/AA, L265P}$ (C). The bars above graphs indicate the time of addition of the compound, which was at 90s. Gray traces represent recordings of all individual cells and black traces represent the population average.

(D) Cytosolic Ca^{2+} responses to A1 (10 μM) in individual HeLa cells transiently expressing $TPC2^{LL/AA}$ in the absence of extracellular Ca^{2+}. Cells were immersed into Ca^{2+}-free HBS at 60s, and A1 was added at 150s as indicated by the bar.

(E) Data quantifying magnitudes of Ca^{2+} responses to A1 under indicated conditions. Each plot points represents one experiment (n=3-13); * $P<0.05$ ** $P<0.01$ were determined by one-way ANOVA.

(F-I) Similar to B-E but cells were stimulated with H07 (30 μM) (n=3-12); *** $P<0.001$ was determined by one-way ANOVA.

3.3.5 A1 and H07 fail to evoke Ca^{2+} signals in cells expressing plasma membrane targeted TRPML1

I next examined the selectivity of A1 and H07 for TPC2 by testing them in cells transiently transfected with a PM version of TRPML1 ($TRPML1^{\Delta NC}$). Like TPC2, TRPML1 is targeted to lysosomes through di-leucine motifs and it can be directed to the PM upon deletion of the motifs (Falardeau et al., 2002; Zeevi et al., 2009). Confocal imaging revealed that $TRPML1^{\Delta NC}$ has a PM localization (Fig.3.3.5A). As shown in Fig.3.3.5B and D and quantified in Fig.3.3.5C and E, cells expressing $TRPML1^{\Delta NC}$ did not respond to A1 (10 μM) or H07 (30 μM) which were shown to induce robust Ca^{2+} signals in cells expressing $TPC2^{LL/AA}$. However, the synthetic TRPML1 agonist, MLSA1, evoked robust Ca^{2+} signals when added after A1 or H07 (Fig. 3.3.5B and D) in cells expressing $TRPML1^{\Delta NC}$, confirming that TRPML1 is functional at the PM. Taken together, there appears to be a selective action of A1 and H07 on TPC2 over TRPML1.

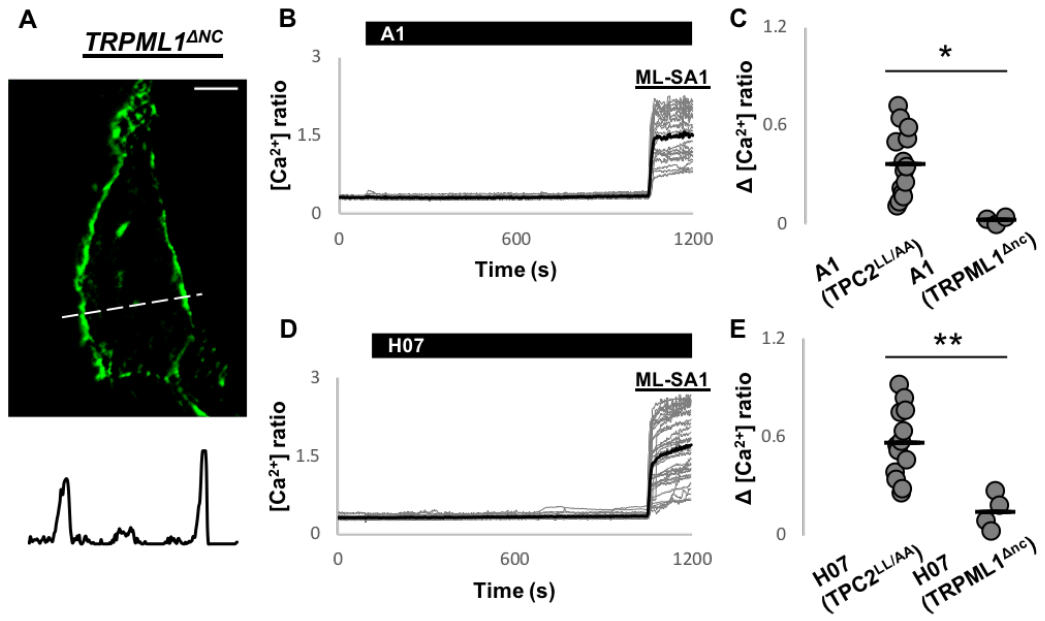

Figure 3.3.5 A1 and H07 fail to evoke Ca^{2+} signals in cells transiently expressing plasma membrane targeted TRPML1

(A) Representative confocal image of HeLa cells transiently expressing GFP-tagged $TRPML1^{\Delta NC}$ (green). Scale bar = 10 µm. The fluorescence intensity plot below the image corresponds to the dashed line.

(B and D) Cytosolic Ca^{2+} responses to A1 (10 µM) (B) or H07 (30 µM) (D) followed by ML-SA1 (20 µM) in individual HeLa cells transiently expressing $TRPML1^{\Delta NC}$. The bars above graphs indicate the time of addition of the compound, which was at 90s. Gray traces represent recordings of all individual cells and black traces represent the population average.

(C and E) Data quantifying magnitudes of Ca^{2+} responses to A1 (C) or H07 (E) in cells transiently expressing $TRPML1^{\Delta NC}$ or $TPC2^{LL/AA}$. Each plot points represents one experiment (n=3-13); * P<0.05 ** P<0.01 were determined by independent-samples t tests.

3.3.6 Tetrandrine and cepharanthine inhibit A1-mediated Ca^{2+} signals

In addition to using molecular approaches, I also applied pharmacological interventions to examine whether A1 activates TPC2. The bisbenzylisoquinoline (BBIQ) cyclic alkaloid, tetrandrine, is currently the most potent TPC blocker (Sakurai et al., 2015). Here, I tested the effect of tetrandrine and the tetrandrine analogue, cepharanthine, (Fig. 3.3.6A) on A1-induced Ca^{2+} signals in cells expressing $TPC2^{LL/AA}$ (Bailly, 2019). In the course of imaging, DMSO (vehicle) or tetrandrine or

cepharanthine were added to the cells 5 minutes prior to addition of A1. As shown in Fig. 3.3.6B, following DMSO, A1 induced clear Ca^{2+} signals in cells expressing $TPC2^{LL/AA}$. This response was blocked by pre-treatment with either 10 μM tetrandrine or 10 μM cepharanthine (Fig. 3.3.6C and D). These data were quantified in Fig. 3.3.6E by calculating magnitudes of the Ca^{2+} signals by A1 under different treatment conditions. These data indicate that A1-induced Ca^{2+} signals in cells expressing $TPC2^{LL/AA}$ were sensitive to tetrandrine and cepharanthine, thus, from the pharmacological perspective, A1 activates TPC2.

3.3.7 Estrogen receptor modulators inhibit A1-mediated Ca^{2+} signals

Recent work from my lab identified novel TPC blockers using a drug repurposing approach (Penny et al., 2019). That is, cross-referencing results from TPC2 structure-based virtual screen with data from two independent lab-based Ebola screens. This approach identified drugs targeting estrogen or dopamine receptors as candidate TPC2 pore blockers. However, due to cell-impermeable property of NAADP and $PI(3,5)P_2$, none of the drugs have been tested in intact cells. To validate these drugs in intact cells and also to strengthen pharmacological evidence that A1 activates TPC2, I investigated their effects on A1-induced Ca^{2+} signals in cells expressing $TPC2^{LL/AA}$. I first focused on the estrogen receptor modulators (SERMs). I started with raloxifene, the one that has been extensively studied in Penny et al., 2019. As shown in Fig. 3.3.7A and B, in the presence of DMSO, A1 induced Ca^{2+} signals in cells expressing $TPC2^{LL/AA}$, while in the presence of 10 μM raloxifene, the Ca^{2+} signals were abolished. I also tested other SERMs, such as clomifene and tamoxifen. As shown in Fig. 3.3.7C and D, both clomifene and tamoxifen appeared to abolish A1-induced Ca^{2+} signals like raloxifene did. The magnitudes of the responses to A1 in the presence of DMSO or SERMs were quantified in Fig. 3.3.7E. Taken together, these data indicate that SERMs inhibit A1-induced Ca^{2+} signals, but notably clomifene and tamoxifen testing was limited. Thus, SERMs are likely TPC2 blockers and additional pharmacological evidence was provided to suggest that A1 activates TPC2.

3.3.8 Dopamine receptor modulators inhibit A1-mediated Ca^{2+} signals

Another group of compounds identified as putative TPC2 pore blockers are dopamine receptor modulators, such as fluphenazine and pimozide (Penny et al., 2019). As

shown in Fig. 3.3.8(A-C), in cells expressing $TPC2^{LL/AA}$, following DMSO, A1 induced the expected Ca^{2+} signals. However, following 10 µM fluphenazine or 10 µM pimozide treatment, A1 responses were largely reduced. These data were quantified in Fig. 3.3.8D. Therefore, fluphenazine and pimozide inhibit A1-induced Ca^{2+} signals, providing evidence that they are TPC2 blockers and providing further evidence that A1 activates TPC2.

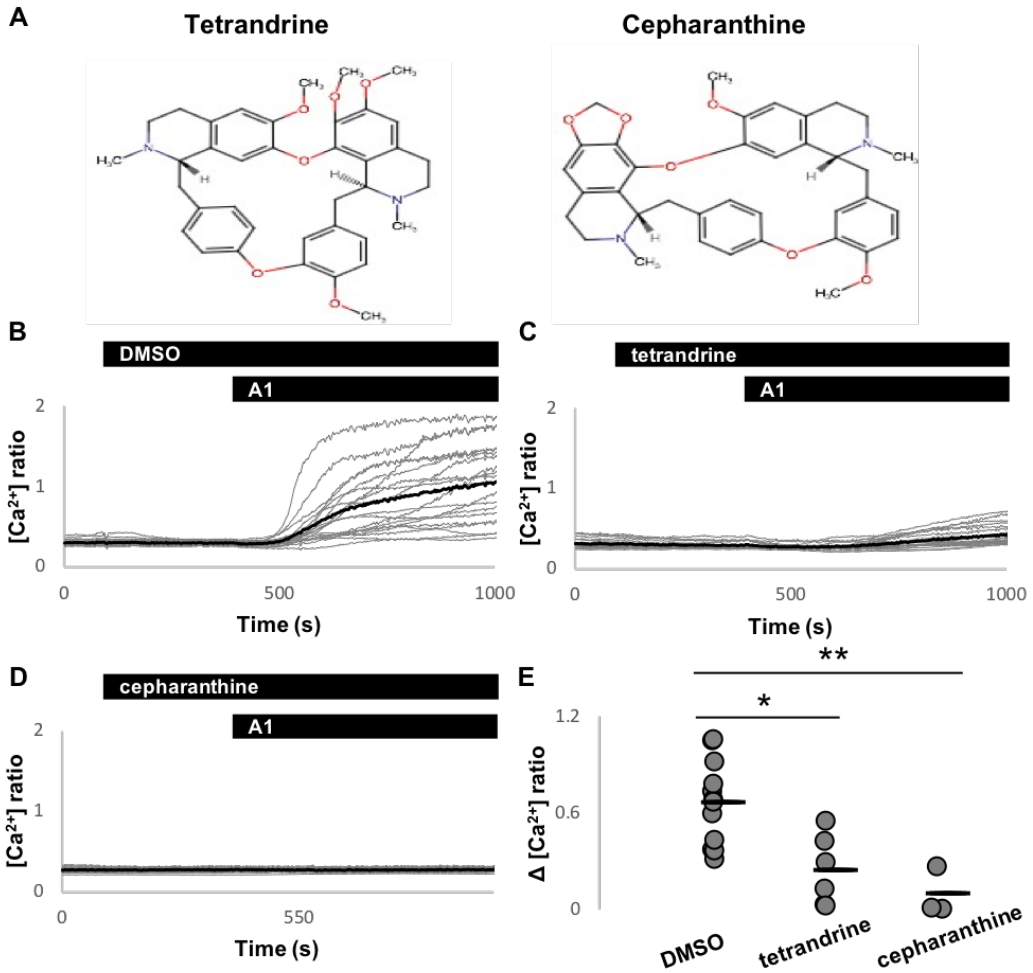

Figure 3.3.6 Tetrandrine and cepharanthine inhibit A1-mediated Ca^{2+} signals

(A) Chemical structures of tetrandrine and cepharanthine (http://www.ebi.ac.uk/chembldb) (B-D) Cytosolic Ca^{2+} responses to A1 (10 µM) following DMSO (B), tetrandrine (10 µM) (C) or cepharanthine (10 µM) (D) in individual HeLa cells transiently expressing $TPC2^{LL/AA}$. The bars above graphs indicate the time of addition of the compound, DMSO or tetrandrine or cepharanthine was added at 90s, A1 was added at 390s. Gray traces represent recordings of all individual cells and black traces represent the population average.

(E) Data quantifying magnitudes of Ca^{2+} responses to A1 following the indicated treatment. Each plot point represents one experiment (n=3-12); * P<0.05 ** P<0.01 were determined by Kruskal-Wallis H test.

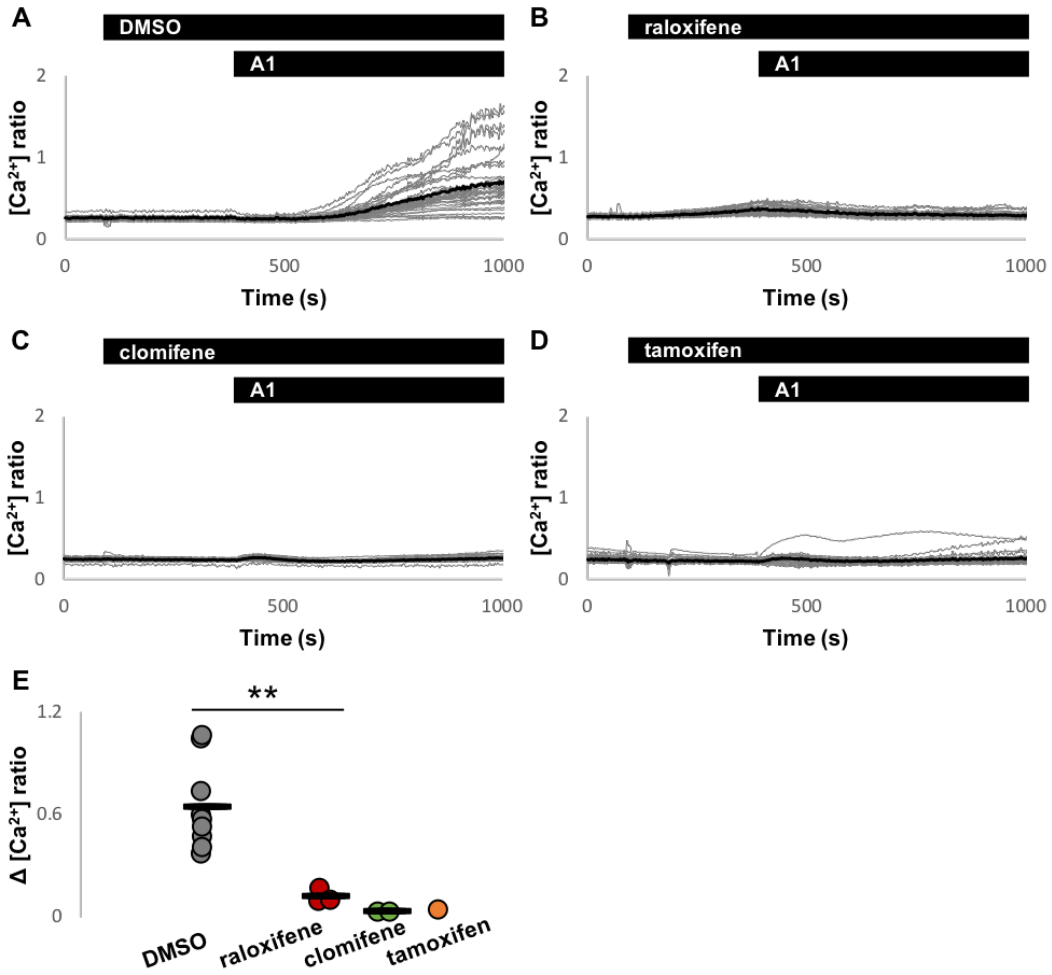

Figure 3.3.7 Estrogen receptor modulators inhibit A1-mediated Ca^{2+} signals

(A-D) Cytosolic Ca^{2+} responses to A1(10 μM) following DMSO (A), raloxifene (10 μM) (B), clomifene (10 μM) (C) or tamoxifen (10 μM) (D) in individual HeLa cells transiently expressing $TPC2^{LL/AA}$. The bars above graphs indicate the time of addition of the compound, DMSO or raloxifene or clomifene or tamoxifen was added at 90s, A1 was added at 390s. Gray traces represent recordings of all individual cells and black traces represent the population average.

(E) Data quantifying magnitudes of Ca^{2+} responses to A1 following the indicated treatment. Each plot point represents one experiment (n=1-9); ** P<0.01 was determined by independent-samples t-tests.

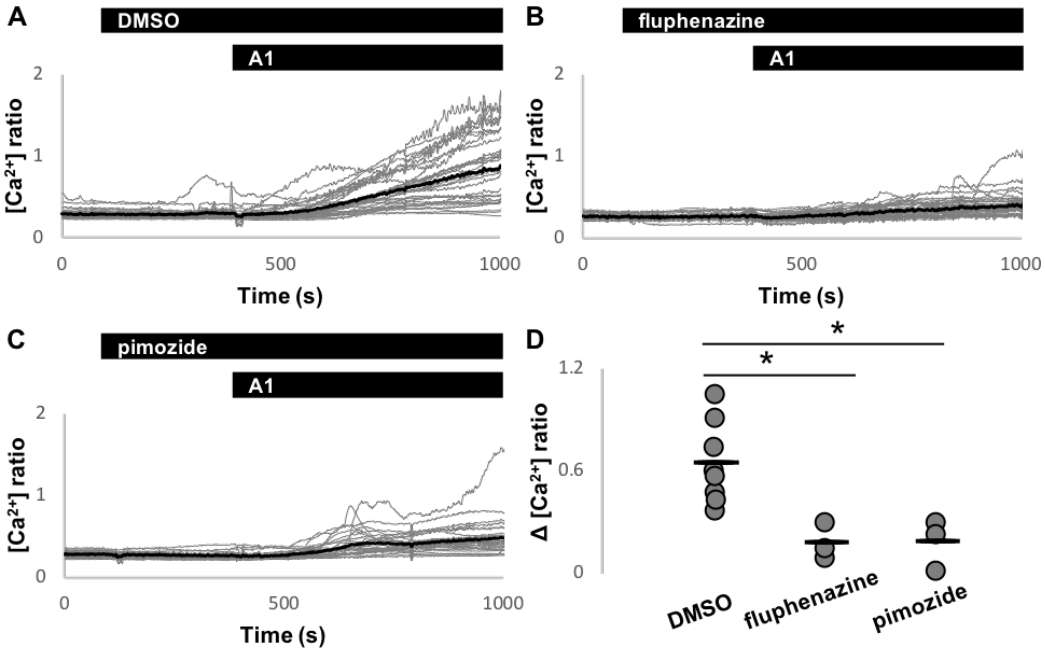

Figure 3.3.8 Dopamine receptor modulators inhibit A1-mediated Ca^{2+} signals

(A-C) Cytosolic Ca^{2+} responses to A1 (10 μM) following DMSO (A), fluphenazine (10 μM) (B) or pimozide (10 μM) (C) in individual HeLa cells transiently expressing $TPC2^{LL/AA}$. The bars above graphs indicate the time of addition of the compound, DMSO or fluphenazine or pimozide was added at 90s, A1 was added at 390s. Gray traces represent recordings of all individual cells and black traces represent the population average.

(D) Data quantifying magnitudes of Ca^{2+} responses to A1 following the indicated treatment. Each plot point represents one experiment (n=3-8); * $P<0.05$ was determined by one-way ANOVA.

3.3.9 Statins do not inhibit A1-mediated Ca^{2+} signals

To further interrogate A1 action, I sought essential negative controls. The screening strategy, which combined the data from the TPC2 virtual screen and Ebola screens, not only identified SERMs and dopamine receptor modulators as candidate TPC2 blockers, but also hinted that some drugs are unlikely to be TPC2 blockers (Penny et al., 2019). These included statins which are a class of HMG-CoA reductase inhibitors. As shown in Fig. 3.3.9A, statins rank relatively high in the TPC2 structure-based screen with 80% of statins from the library of FDA-approved drugs ranked within the

top 200. However, given that they were not very effective in blocking Ebola infection, they were not identified as candidate TPC2 blockers. Statins therefore might serve as potential negative controls for the study on A1. I tested a number of statins against A1-induced Ca^{2+} signals in cells expressing $TPC2^{LL/AA}$, including simvastatin, cerivastatin and lovastatin. As shown in Fig. 3.3.9B, A1 induced Ca^{2+} signals in DMSO treated cells. Comparable Ca^{2+} signals by A1 were detected in cells treated with any of the statins (Fig. 3.3.9C-E) when incubated at 10 μM for 5 minutes. Statins did not affect the magnitude of A1-induced Ca^{2+} signals (Fig.3.3.9F). Taken together, statins may not be TPC2 blockers.

A

Statins	TPC VS (Rank)	Ebola HTS (IC_{50}, μM)	Max response (% I)
M SIMVASTATIN	2	-	-
M LOVASTATIN	5	-	-
FLUVASTATIN	6	2.07	0.59
PRAVASTATIN	9	**no effect**	-
PITAVASTATIN	21	-	-
ROSUVASTATIN	93	**no effect**	-
CERIVASTATIN	118	0.07	0.62
SIMVASTATIN	119	44.6	0.69
LOVASTATIN	161	**no effect**	-
ATORVASTATIN	520	**no effect**	-
CILASTATIN	576	**no effect**	-
PENTOSTATIN	1246	-	-

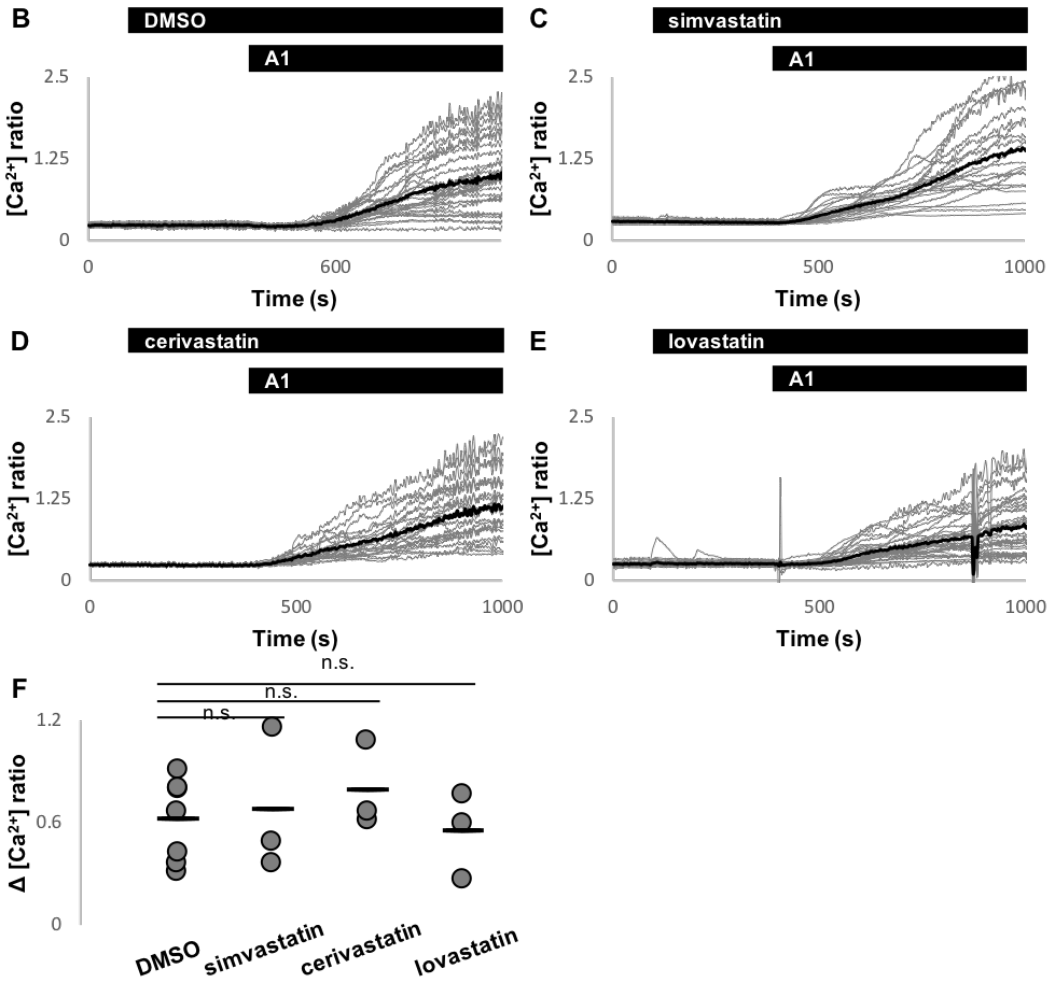

Figure 3.3.9 Statins do not inhibit A1-mediated Ca^{2+} signals

(A) Summary of statins' rank in the TPC2 virtual screen (Penny et al., 2019) and effects on Ebola infectivity (Johansen et al., 2015; Kouznetsova et al., 2014)

(B-E) Cytosolic Ca^{2+} responses to A1 (10 μM) following DMSO (B), simvastatin (10 μM) (C), cerivastatin (10 μM) (D) or lovastatin (10 μM) (E) in individual HeLa cells transiently expressing $TPC2^{LL/AA}$. The bars above graphs indicate the time of addition of the compound, DMSO or simvastatin or cerivastatin or lovastatin was added at 90s, A1 was added at 390s. Gray traces represent recordings of all individual cells and black traces represent the population average.

(F) Data quantifying magnitudes of Ca^{2+} responses to A1 following the indicated treatment. Each plot point represents one experiment (n=3-7); n.s. not statistically significant was determined by one-way ANOVA.

3.3.10 Tetrandrine, raloxifene and fluphenazine at 10 µM do not inhibit TRPML1-mediated Ca^{2+} signals upon acute treatment

Having observed that tetrandrine and the recently identified TPC2 pore blockers, raloxifene and fluphenazine, blocked A1-induced Ca^{2+} signals, I went on to study their selectivity for TPC2. To do this, the effects of tetrandrine, raloxifene and fluphenazine on TRPML1$^{\Delta NC}$-mediated Ca^{2+} signals were examined. To activate TRPML1$^{\Delta NC}$, I utilized ML-SA1. As shown in Fig. 3.3.10A and B, ML-SA1 responses were concentration dependent. I chose a sub-maximal concentration (3.16 µM) of ML-SA1 to study the effects of the drugs on TRPML1 signalling. As shown in Fig. 3.3.10 (C-E), following DMSO, ML-SA1 induced Ca^{2+} signals in cells expressing TRPML1$^{\Delta NC}$. The signals were also detected after the cells were exposed to 10 µM tetrandrine, raloxifene or fluphenazine for 5 minutes. Quantification revealed that the magnitude of response to ML-SA1 following treatment with these drugs were not statistically different from that following DMSO. In comparison, A1-induced Ca^{2+} signals in cells expressing TPC2$^{LL/AA}$ were largely reduced under the same drug treatment conditions (i.e. 10 µM for 5 minutes) (Fig. 3.3.10C-E). Taken together, these data indicate that tetrandrine, raloxifene and fluphenazine have a selective action on TPC2 over TRPML1.

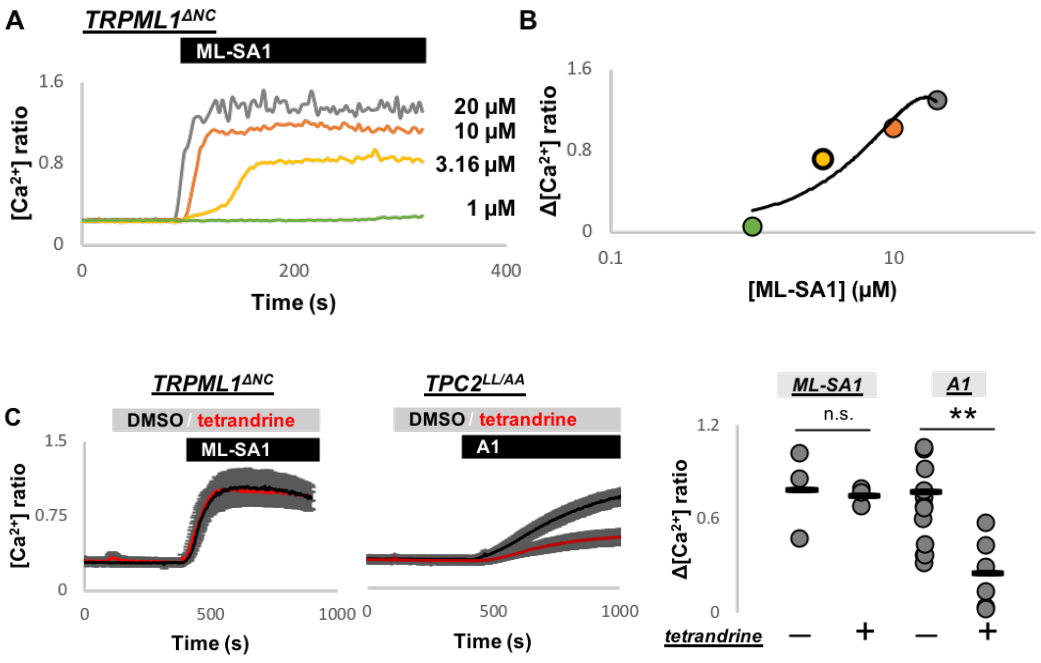

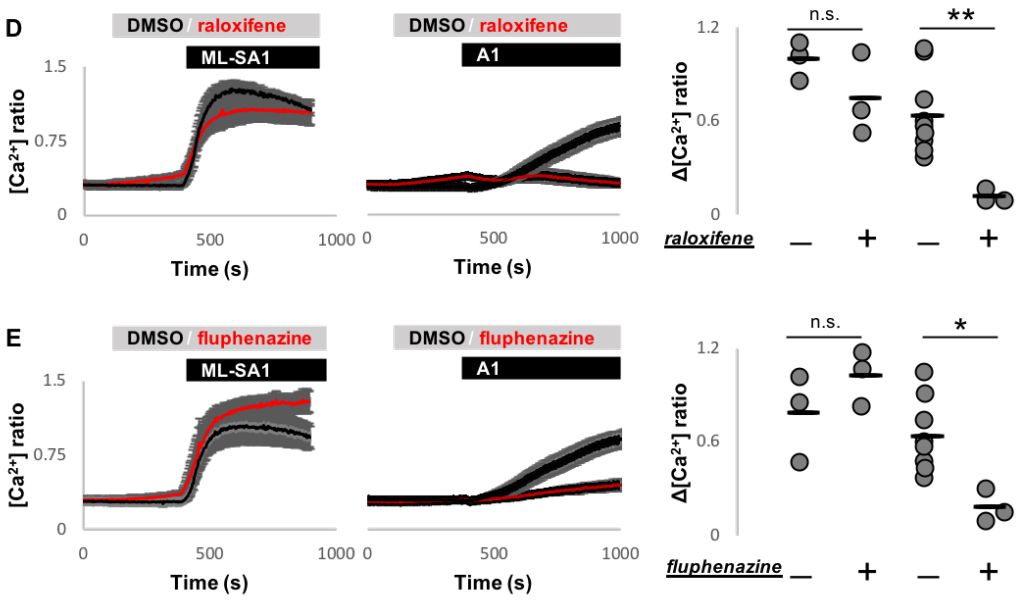

Figure 3.3.10 Tetrandrine, raloxifene and fluphenazine at 10 μM do not inhibit TRPML1-mediated Ca^{2+} signals upon acute treatment

(A) Average cytosolic Ca^{2+} responses (mean of individual cells in one experiment) to ML-SA1 of a range of concentrations in HeLa cells transiently expressing $TRPML1^{\Delta NC}$. The bar above graph indicates the time of addition of the compound, which was at 90s.

(B) Concentration-response curve showing magnitude of ML-SA1-induced Ca^{2+} responses in A.

(C-E) Left panel: the effect of tetrandrine (10 μM) (C), raloxifene (10 μM) (D) and fluphenazine (10 μM) (E) on cytosolic Ca^{2+} responses to ML-SA1 (3.16 μM) in cells transiently expressing $TRPML1^{\Delta NC}$ compared to the DMSO control. Data presented as mean ± S.E.M, from 3 independent experiments.

(C-E) Middle panel: the effect of tetrandrine (10 μM) (C), raloxifene (10 μM) (D) or fluphenazine (10 μM) (E) on cytosolic Ca^{2+} responses to A1 (10 μM) in cells transiently expressing $TPC2^{LL/AA}$ compared to the DMSO control. Data are same as those in Fig. 3.3.6-3.3.8 but presented as mean ± S.E.M, from 3-12 independent experiments.

(C-E) Right panel: pooled data quantifying magnitude of Ca^{2+} responses to ML-SA1 or A1 in the absence and presence of tetrandrine (C), raloxifene (D) or fluphenazine (E). * $P<0.05$ ** $P<0.01$ were determined by independent-samples t-tests.

3.3.11 A1 and H07 mediate Ca^{2+} release in cells transiently expressing lysosomal TPC2 but not in cells expressing pore-mutant lysosomal TPC2

Through using PM TPC2, A1 and H07 have been identified as TPC2 activators. Given that lysosomes but not the PM are TPC2 native localization, one crucial test is to test whether A1 and H07 can activate lysosomal TPC2 to induce Ca^{2+} release. To study this, I transfected cells with TPC2 or pore-mutant TPC2 ($TPC2^{L265P}$) with their endo-lysosomal targeting sequences intact. TPCs were fused with the genetically encoded Ca^{2+} indicator, GCaMP6s, at their cytosolic C-termini. GCaMP6s is expected to measure Ca^{2+} levels near surface of the Ca^{2+} stores. All experiments with GCaMP6s were performed in the absence of extracellular Ca^{2+} to ensure signals were derived from Ca^{2+} stores only. When examined by confocal imaging, TPC2 GCaMP6s displayed some degree of punctate distribution (Fig. 3.3.11A). Similar to TPC2 GCaMP6s, a proportion of $TPC2^{L265P}$ GCaMP6s also has punctate distribution (Fig.3.3.11B). As shown in Fig. 3.3.11C, A1 and H07 induced Ca^{2+} signals in cells expressing TPC2 GCaMP6s. The responses to A1 (30 μM) were larger than the responses to H07 (60 μM). In comparison, neither A1 nor H07 induced Ca^{2+} signals in cells expressing $TPC2^{L265P}$ GCaMP6s (Fig.3.3.11D), but subsequent addition of ionomycin induced robust responses. Quantification of A1 and H07 responses in cells expressing control or pore-mutant TPC2 GCaMP6s are shown in Fig.3.3.11E. Taken together, these data indicate that A1 and H07 activate lysosomal TPC2 to induce pore-dependent Ca^{2+} release and are therefore cell-permeable.

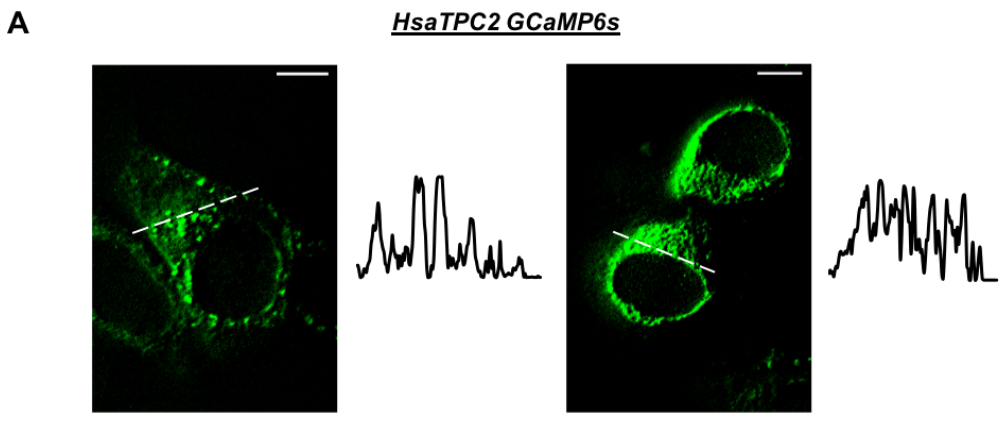

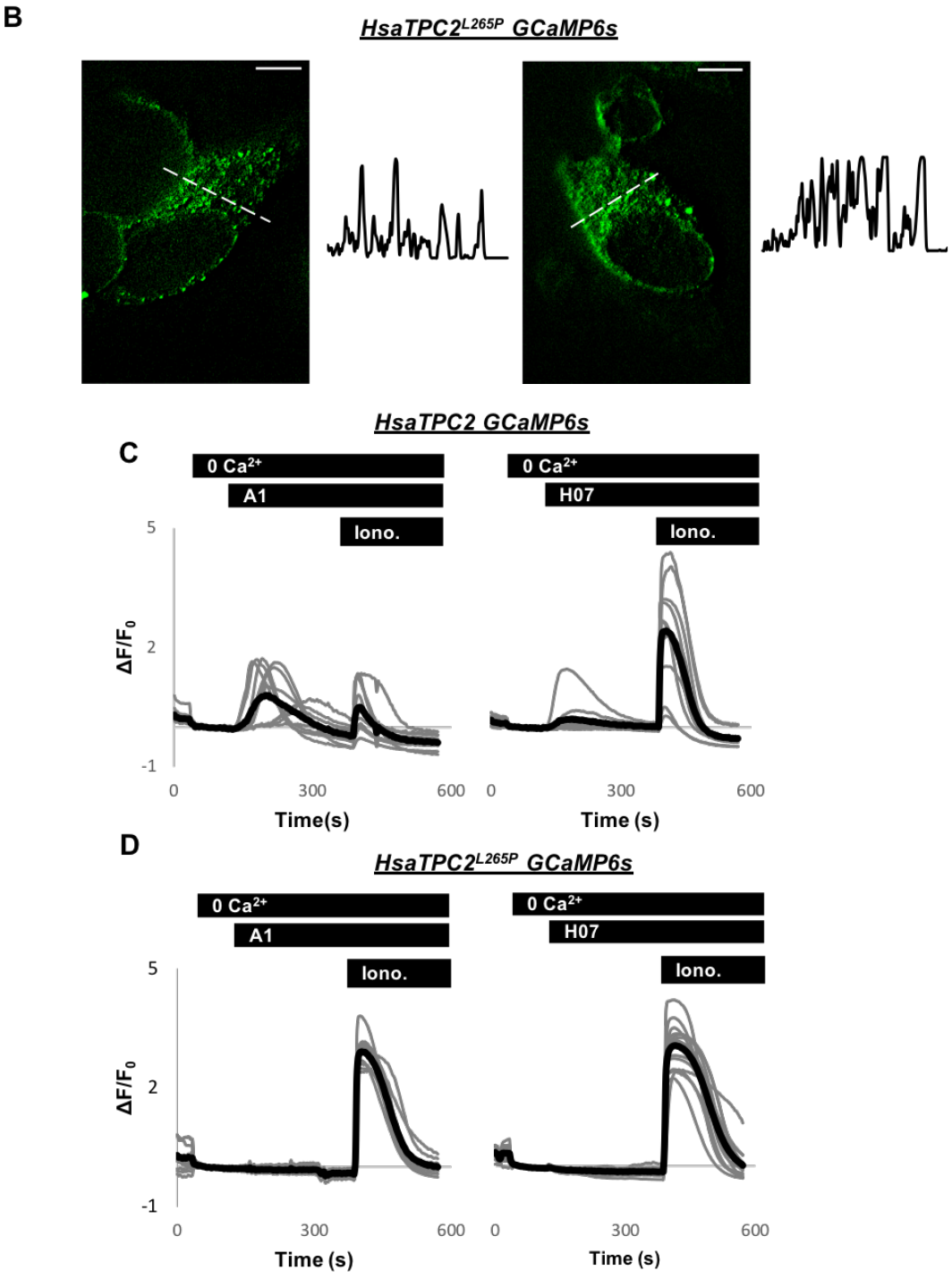
B
HsaTPC2L265P GCaMP6s
HsaTPC2 GCaMP6s
C
0 Ca2+
A1
Iono.
0 Ca2+
H07
Iono.
5
2
-1
ΔF/F0
0
300
600
Time(s)
Time (s)
D
HsaTPC2L265P GCaMP6s
0 Ca2+
A1
Iono.
0 Ca2+
H07
Iono.
5
2
-1
ΔF/F0
0
300
600
Time (s)

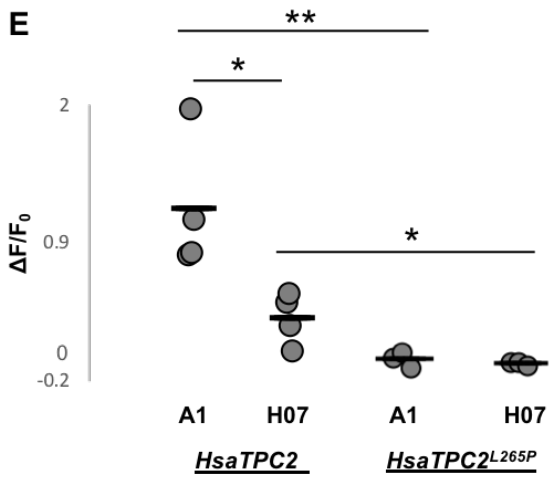

Figure 3.3.11 A1 and H07 mediate Ca^{2+} release in cells expressing lysosomal TPC2 but not in cells transiently expressing pore-mutant lysosomal TPC2

(A and B) Confocal images of HeLa cells transiently expressing TPC2 GCaMP6s (A) or $TPC2^{L265P}$ GCaMP6s (B). Scale bar = 10 μm. The fluorescence intensity plot on the right hand corresponds to the dashed line.

(C) Cytosolic Ca^{2+} responses to A1 (30 μM) or H07 (60 μM), and then to ionomycin (Iono.) (2 μM) in individual HeLa cells transiently expressing TPC2 GCaMP6s, in the absence of extracellular Ca^{2+}. Cells were immersed into Ca^{2+}-free HBS at 30s. The bars above graphs indicate the time of addition of the compound, A1 or H07 was added at 120s, Iono. was added at 390s. Gray traces represent recordings of all individual cells and black traces represent the population average.

(D) Cytosolic Ca^{2+} responses to A1 (30 μM) or H07 (60 μM), and then to Iono. (2 μM) in individual HeLa cells transiently expressing $TPC2^{L265P}$ GCaMP6s, in the absence of extracellular Ca^{2+}.

(E) Data quantifying magnitude of Ca^{2+} responses to A1 or H07 in cells expressing TPC2 GCaMP6s with or without L265P. Each plot point represents one experiment (n=3-4);

* $P<0.05$ ** $P<0.01$ was determined by one-way ANOVA.

3.3.12 A1 and H07 fail to mediate Ca^{2+} release in cells transiently expressing lysosomal TRPML1

To examine whether A1 and H07 are selective to activate TPC2 to induce Ca^{2+} release, I tested A1 and H07 in cells expressing TRPML1 GCaMP6s. Confocal imaging revealed that TRPML1 GCaMP6s displayed reticular but not punctate distribution (Fig.3.3.12A). As shown in Fig. 3.3.12B and D, cells expressing TRPML1 GCaMP6s did not respond to A1 (30 μM) or H07 (60 μM). However, the cells did respond to ML-SA1 as robust Ca^{2+} signals were detected after addition of ML-SA1, confirming TRPML1 GCaMP6s was functional. As quantified in Fig. 3.3.12C and E, cells expressing TPC2 GCaMP6s but not TRPML1 GCaMP6s responded to A1 (30 μM) and H07 (60 μM). Collectively, these data suggest that there is a selective action of A1 and H07 on TPC2 over TRPML1.

3.3.13 A1 and H07 fail to mediate Ca^{2+} release in cells transiently expressing lysosomal TPC1

In humans, there are two TPC isoforms, TPC1 and TPC2, which share similar structures. To further investigate the selectivity of A1 and H07 for TPC2, I examined their effects on TPC1. To do this, I employed cells transfected with TPC1 GCaMP6s. TPC1 GCaMP6s displayed some degree of punctate distribution as revealed by confocal imaging (Fig.3.3.13A). As shown in Fig. 3.3.13B and D, A1 (30 μM) and H07 (60 μM) failed to induce Ca^{2+} signals in cells expressing TPC1 GCaMP6s. Subsequent addition of ionomycin however induced robust Ca^{2+} signals. As quantified in Fig. 3.3.13C and E, the responses to A1 (30 μM) or H07 (60 μM) in cells expressing TPC1 GCaMP6s were negligible compared to cells expressing TPC2 GCaMP6s. Taken together, A1 and H07 exhibit selectivity for TPC2 over TPC1.

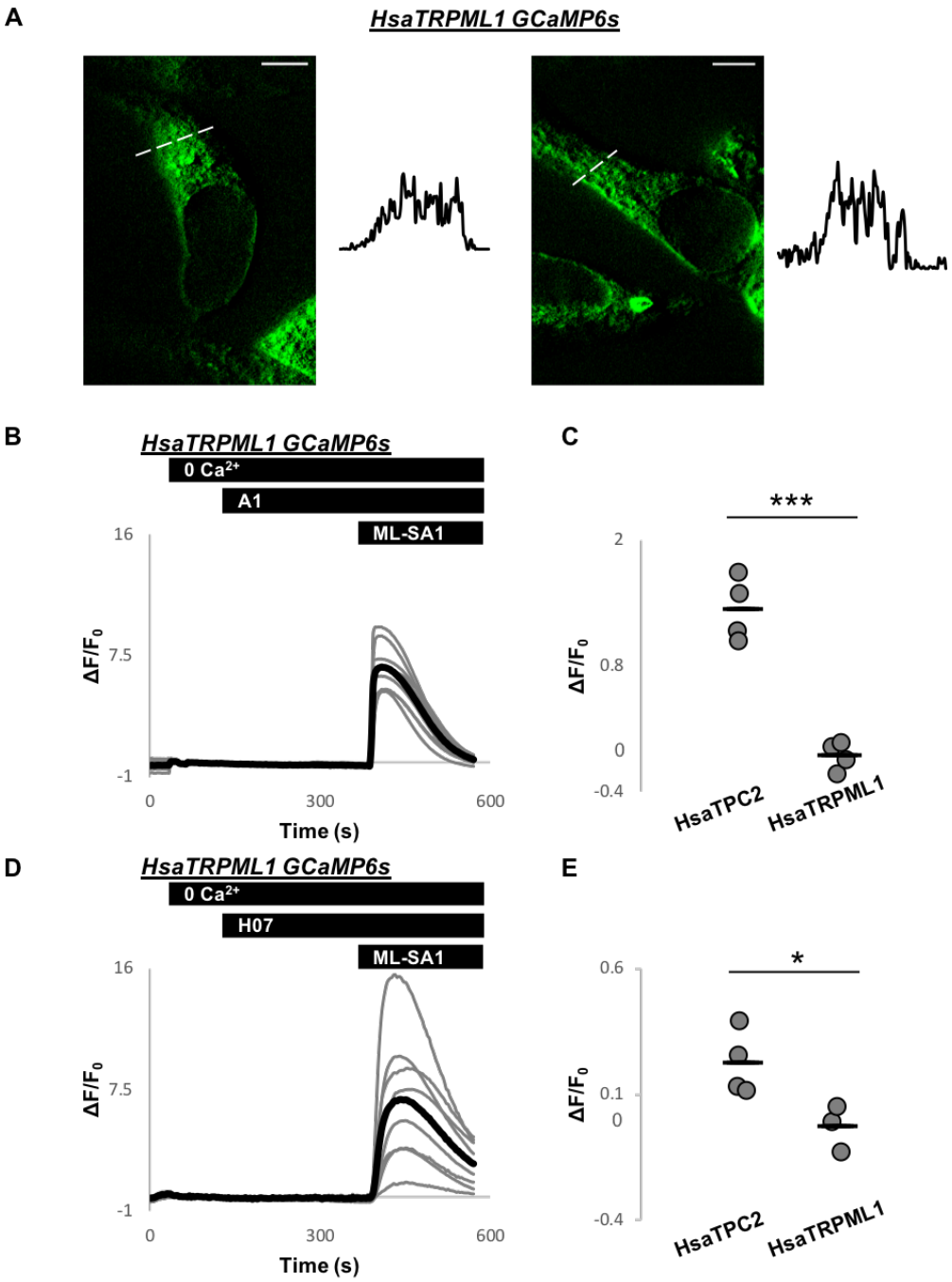

Figure 3.3.12 A1 and H07 fail to mediate Ca^{2+} release in cells transiently expressing lysosomal TRPML1

(A) Confocal images of HeLa cells transiently expressing TRPML1 GCaMP6s. Scale bar = 10 μm. The fluorescence intensity plot on the right hand corresponds to the dashed line.

(B and D) Cytosolic Ca^{2+} responses to A1 (30 μM) (B) or H07 (60 μM) (D), and then to ML-SA1 (20 μM) in individual HeLa cells transiently expressing TRPML1 GCaMP6s, in the absence of extracellular Ca^{2+}. Cells were immersed into Ca^{2+}-free HBS at 30s. The bars above graphs indicate the time of addition of the compound, A1 or H07 was added at 120s, ML-SA1

was added at 390s. Gray traces represent recordings of all individual cells and black traces represent the population average.

C and E) Data quantifying magnitudes of Ca^{2+} responses to A1 (C) or H07 (E) in cells expressing TRPML1 GCaMP6s or TPC2 GCaMP6s. Each plot point represents one experiments (n=3-4); * P<0.05 *** P<0.001 were determined by independent-samples t-tests.

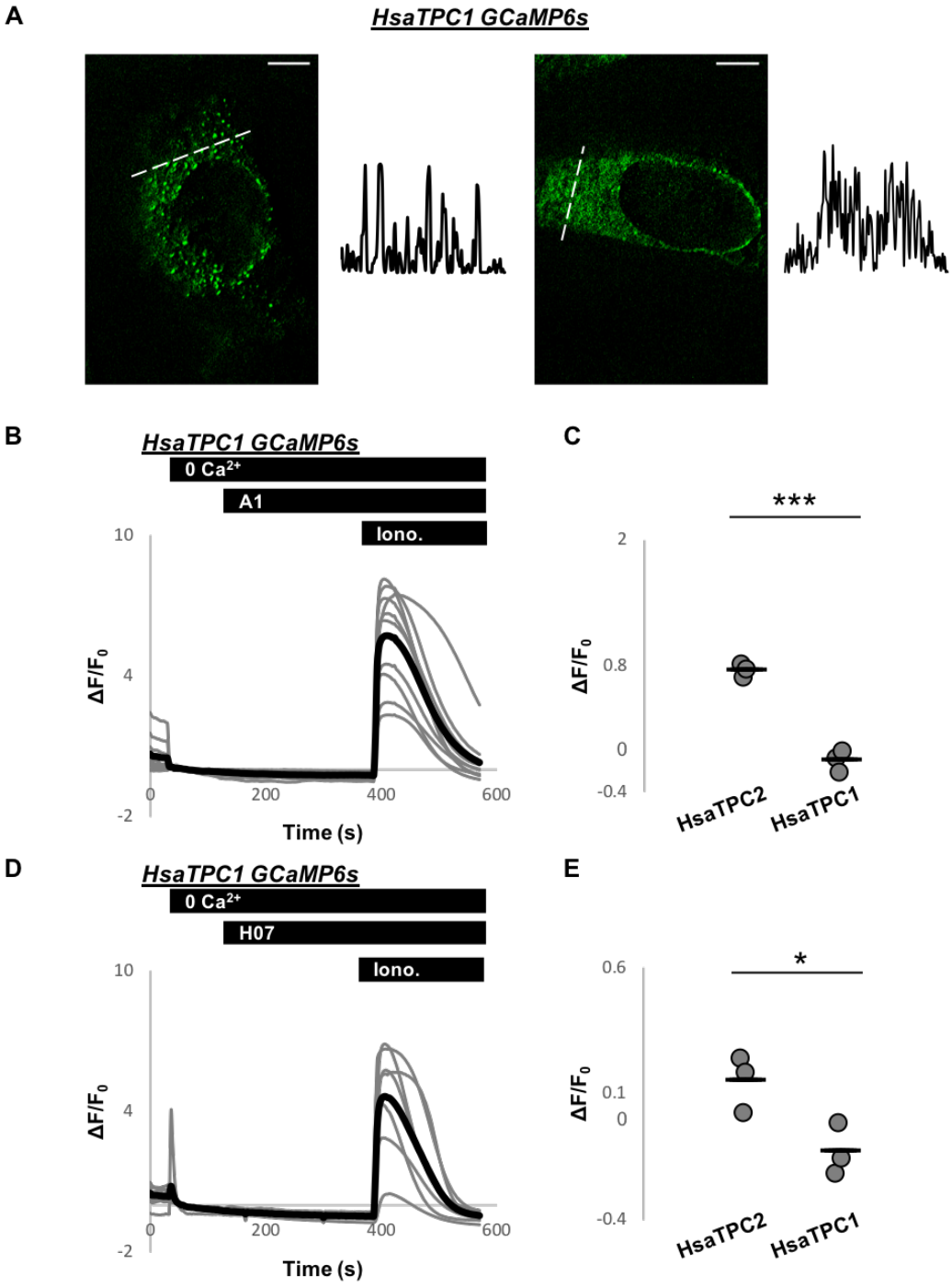

Figure 3.3.13 A1 and H07 fail to mediate Ca^{2+} release in cells transiently expressing lysosomal TPC1

(A) Confocal images of HeLa cells transiently expressing TPC1 GCaMP6s. Scale bar = 10 μm. The fluorescence intensity plot on the right hand corresponds to the dashed line.

(B and D) Cytosolic Ca^{2+} responses to A1 (30 μM) (B) or H07 (60 μM) (D), and then to ionomycin (Iono.) (2 μM) in individual HeLa cells transiently expressing TPC1 GCaMP6s, in the absence of extracellular Ca^{2+}. Cells were immersed into Ca^{2+}-free HBS at 30s. The bars above graphs indicate the time of addition of the compound, A1 or H07 was added at 120s, Iono. was added at 390s. Gray traces represent recordings of all individual cells and black traces represent the population average.

(C and E) Data quantifying magnitudes of Ca^{2+} responses to A1 (C) or H07 (E) in cells expressing TPC1 GCaMP6s or TPC2 GCaMP6s. Each plot point represents one experiments (n=3); * $P<0.05$ *** $P<0.001$ were determined by independent-samples t-tests.

3.3.14 A1-mediated Ca^{2+} release is abolished by GPN and partially reduced by thapsigargin

My data shown above indicate that A1 and H07 can activate TPC2 to induce Ca^{2+} release. To explore the source of the Ca^{2+}, I investigated the contributions of lysosomes and the ER. I first studied A1. To assess the contributions of lysosomes, cells expressing TPC2 GCaMP6s were treated with GPN which is thought to deplete lysosomal Ca^{2+} as discussed in Chapter 2. As shown in Fig. 3.3.14 B, GPN induced small and sustained Ca^{2+} signals. Following GPN, A1-induced Ca^{2+} signals were almost fully blocked (Fig. A, B and D). These data were quantified in Fig. 3.3.14E by calculating the magnitude of the A1 response after DMSO or GPN treatment. To assess the contributions of the ER, I used thapsigargin to inhibit SERCA. Thapsigargin induced transient Ca^{2+} signals that were larger than those evoked by GPN (Fig. 3.3.14B and C). Following thapsigargin, A1-induced Ca^{2+} signals were partially reduced (Fig. 3.3.14A, C and F). The magnitudes of the A1 responses in the presence of DMSO or thapsigargin were quantified in Fig. 3.3.14G. Taken together, these data indicate that both lysosomes and the ER contribute to A1-induced Ca^{2+} signals.

3.3.15 H07-mediated Ca^{2+} release is abolished by GPN but potentiated by thapsigargin

To investigate the contributions of lysosomes and the ER to H07-induced Ca^{2+} signals in cells expressing TPC2 GCaMP6s, I again used GPN and thapsigargin. As shown in Fig. 3.3.15 A, B and D and quantified in Fig. 3.3.15E, H07-induced Ca^{2+} signals were almost fully blocked upon GPN incubation, indicating involvement of lysosomes. Strikingly, thapsigargin incubation potentiated H07-induced Ca^{2+} signals (Fig. 3.3.15A, C, F and G). These data therefore indicate that lysosomes contribute to H07-induced Ca^{2+} signals, and that the ER appears to have a negative impact on H07 Ca^{2+} signalling.

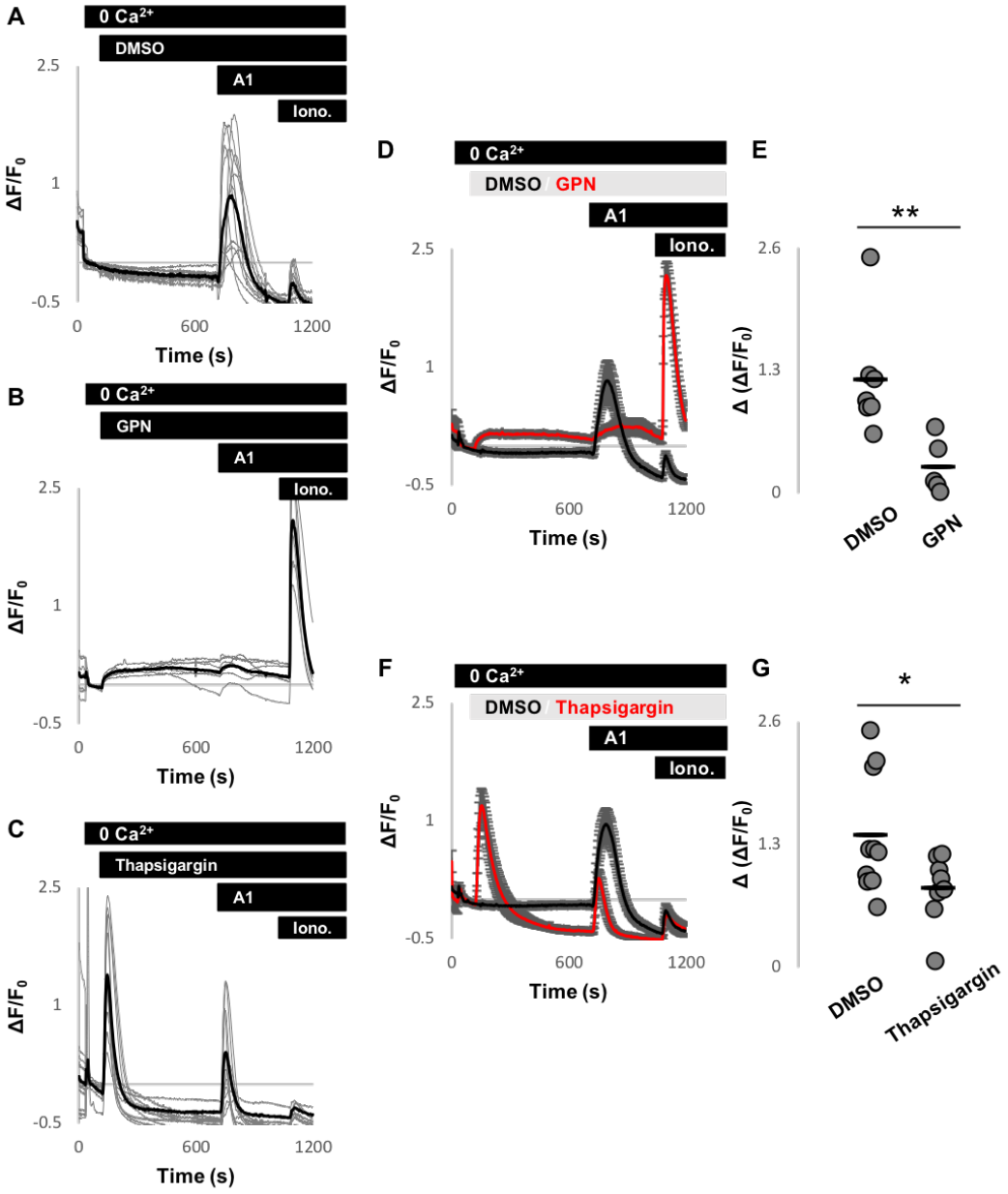

Figure 3.3.14 A1-mediated Ca^{2+} release is abolished by GPN and partially reduced by thapsigargin

(A-C) Cytosolic Ca^{2+} responses to A1 (30 μM), and then to ionomycin (Iono. 2 μM) in the presence of DMSO (A) or GPN (200 μM) (B) or thapsigargin (1 μM) (C) in individual HeLa cells transiently expressing TPC2 GCaMP6s. Experiments were performed in the absence of extracellular Ca^{2+}. Cells were immersed into Ca^{2+}-free HBS at 30s. The bars above graphs indicate the time of addition of the compound, DMSO or GPN or thapsigargin was added at 120s, A1 was added at 720s, Iono. was added at 1080s. Gray traces represent recordings of all individual cells and black traces represent the population average.

(D) Average cytosolic Ca^{2+} responses (mean ± S.E.M, from 5-7 independent experiments) to A1 (30 μM), and then to Iono. (2 μM) in the presence of DMSO or GPN (200 μM).

(E) Data quantifying A1 responses in D. ** P<0.01 was determined by Mann-Whitney U test. (F) Average cytosolic Ca^{2+} responses (mean ± S.E.M, from 8-10 independent experiments) to A1 (30 μM), and then to Iono. (2 μM) in the presence of DMSO or thapsigargin (1 μM). (G) Data quantifying A1 responses in F. * P<0.05 was determined by independent-samples t-tests.

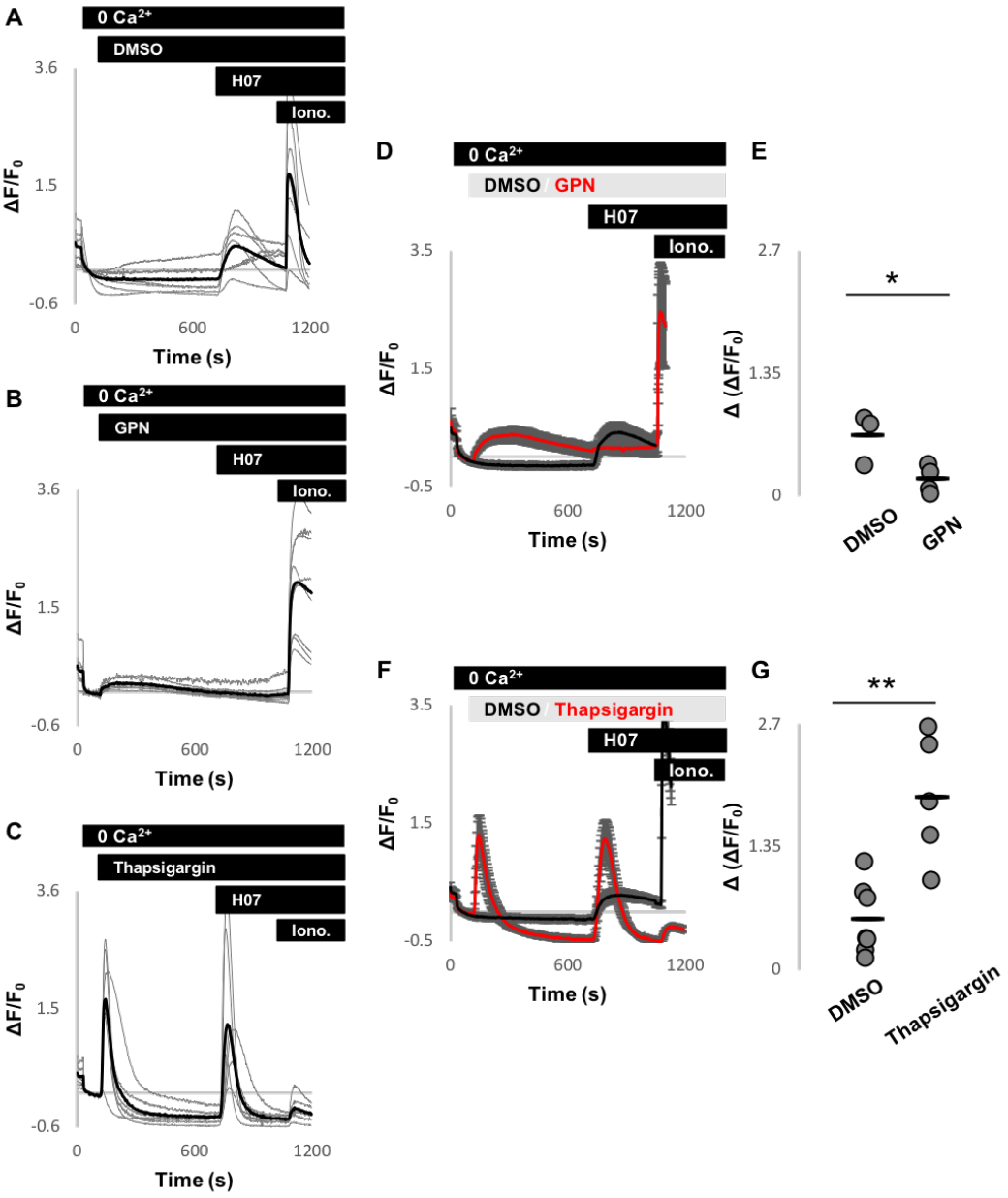

Figure 3.3.15 H07-mediated Ca^{2+} release is abolished by GPN but potentiated by thapsigargin

(A-C) Cytosolic Ca^{2+} responses to H07 (60 μM), and then to ionomycin (Iono. 2 μM) in the presence of DMSO (A) or GPN (200 μM) (B) or thapsigargin (1 μM) (C) in individual HeLa cells transiently expressing TPC2 GCaMP6s. Experiments were performed in the absence of extracellular Ca^{2+}. Cells were immersed into Ca^{2+}-free HBS at 30s. The bars above graphs indicate the time of addition of the compound, DMSO or GPN or thapsigargin was added at 120s, H07 was added at 720s, Iono. was added at 1080s. Gray traces represent recordings of all individual cells and black traces represent the population average.

(D) Average cytosolic Ca^{2+} responses (mean ± S.E.M, from 3-4 independent experiments) to H07 (60 μM), and then to Iono. (2 μM) in the presence of DMSO or GPN (200 μM).

(E) Data quantifying A1 responses in D. * $P<0.05$ was determined by independent-samples t-tests.

(F) Average cytosolic Ca^{2+} responses (mean ± S.E.M, from 5-7 independent experiments) to H07 (60 μM), and then to Iono. (2 μM) in the presence of DMSO or thapsigargin (1 μM).

(G) Data quantifying A1 responses in F. ** $P<0.01$ was determined by independent-samples t-tests.

3.3.16 A1 and H07 mediate Ca^{2+} release in non-transfected cells

Investigations on A1 and H07 so far have relied on TPC2 overexpression. To study whether A1 and H07 act on endogenous TPC2, I examined their effects on cytosolic Ca^{2+} in untransfected HeLa cells labelled with Fura-2. As shown in Fig. 3.3.16A, 10 μM A1 appeared to induce modest Ca^{2+} signals. The response to A1 tended to increase as concentration increased. 30 μM A1 was able to induce conspicuous Ca^{2+} signals. Similarly, H07 induced Ca^{2+} signals as well (Fig. 3.3.16B). However, the response to H07 was not readily detected until 60 μM. By comparison, 60 μM H07-induced Ca^{2+} signals were much smaller than those induced by 30 μM A1 (Fig. 3.3.16C), similar to the results obtained in cells expressing TPC2 GCaMP6s. The experiments in untransfected HeLa cells were performed in the absence of extracellular Ca^{2+}. Notably, in certain cases, there were spontaneous Ca^{2+} signals upon removal of extracellular Ca^{2+} (Fig. 3.3.16 A and B). However, such signals did not appear to have an impact on subsequent agonist responses (Fig.3.3.16A, B and D). Taken together, A1 and H07 induce endogenous Ca^{2+} release.

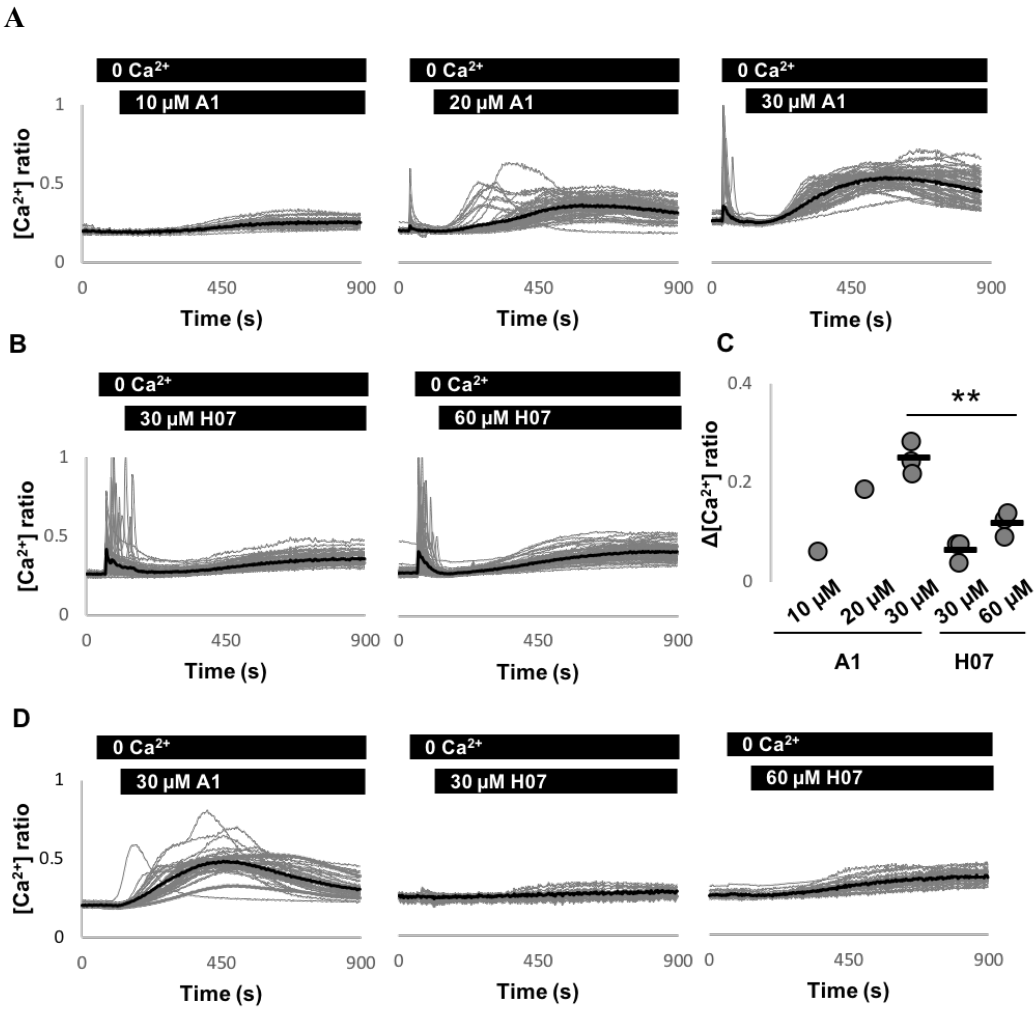

Figure 3.3.16 A1 and H07 mediate Ca^{2+} release in non-transfected cells

(A) Cytosolic Ca^{2+} responses to A1 of a range of concentrations in individual HeLa cells in the absence of extracellular Ca^{2+}. Cells were immersed into Ca^{2+}-free HBS at 60s. The bars above graphs indicate the time of addition of the compound, which was at 150s. Gray traces represent recordings of all individual cells and black traces represent the population average.

(B) Cytosolic Ca^{2+} responses to H07 of 30 μM (left panel) or 60 μM (right panel) in individual HeLa cells in the absence of extracellular Ca^{2+}.

(C) Data quantifying magnitudes of Ca^{2+} responses to A1 or H07 of indicated concentrations. Each plot point represents one experiment (n=1-3); ** $P<0.01$ was determined by independent-samples t-tests.

(D) Cytosolic Ca^{2+} responses to A1 of 30 μM (left panel) or H07 of 30 μM (middle panel) or H07 of 60 μM (right panel) in individual HeLa cells in the absence of extracellular Ca^{2+}.

3.3.17 Endogenous A1-mediated Ca^{2+} release is inhibited by mutation of the TPC2 pore and is potentiated in cells transiently expressing TPC2

In the final set of experiments, I examined whether endogenous TPC2 contribute to A1-induced Ca^{2+} signals in non-transfected cells. The modest Ca^{2+} signals induced by H07 in non-transfected cells made it difficult to dissect the underlying mechanism for such Ca^{2+} signals. I therefore focused on A1. To do this, I tested A1 in cells transfected with LAMP1 (to serve as a control) or the TPC2 pore-mutant ($TPC2^{L265P}$) which can function in a dominant-negative manner (Brailoiu, Rahman, et al., 2010; Sakurai et al., 2015). As shown in Fig. 3.3.17A, 30 μM A1 induced Ca^{2+} signals in cells expressing LAMP1, similar to its activity in untransfected cells (Fig.3.3.16). In cells expressing $TPC2^{L265P}$, A1 Ca^{2+} signals were largely reduced compared to LAMP1 control cells (Fig.3.3.17A and B). Thus, endogenous TPC2 is likely to be required for A1 action. In addition, I also tested A1 in cells overexpressing TPC2 or TRPML1. As shown in Fig. 3.3.17A and C, cells overexpressing TPC2 responded quicker to A1 than cells expressing LAMP1. Cells overexpressing TRPML1 responded to A1 in a manner akin to cells expressing LAMP1 (Fig.3.3.17 A and D).

All data were quantified by calculating magnitude and also the time to peak (Fig. 3.3.17E and F). I segregated the data into transfected (GFP-positive) cells and non-transfected (GFP-negative) cells. As shown in Fig. 3.3.17E, compared to LAMP1-positive cells, there was a smaller magnitude of the responses in cells overexpressing $TPC2^{L265P}$ but not TPC2 or TRPML1. There was no difference in the GFP-negative cells in all of the conditions. The time taken for the A1 signal to peak was quantified in Fig. 3.3.17F. Compared to LAMP1- positive cells, there was a reduced time to peak in cells overexpressing TPC2 but not TRPML1 or $TPC2^{L265P}$. Again, there was no difference between LAMP1-negative cells with other negative cells in time taken for the signal to peak.

Collectively, these data indicate that A1 likely activates endogenous TPC2.

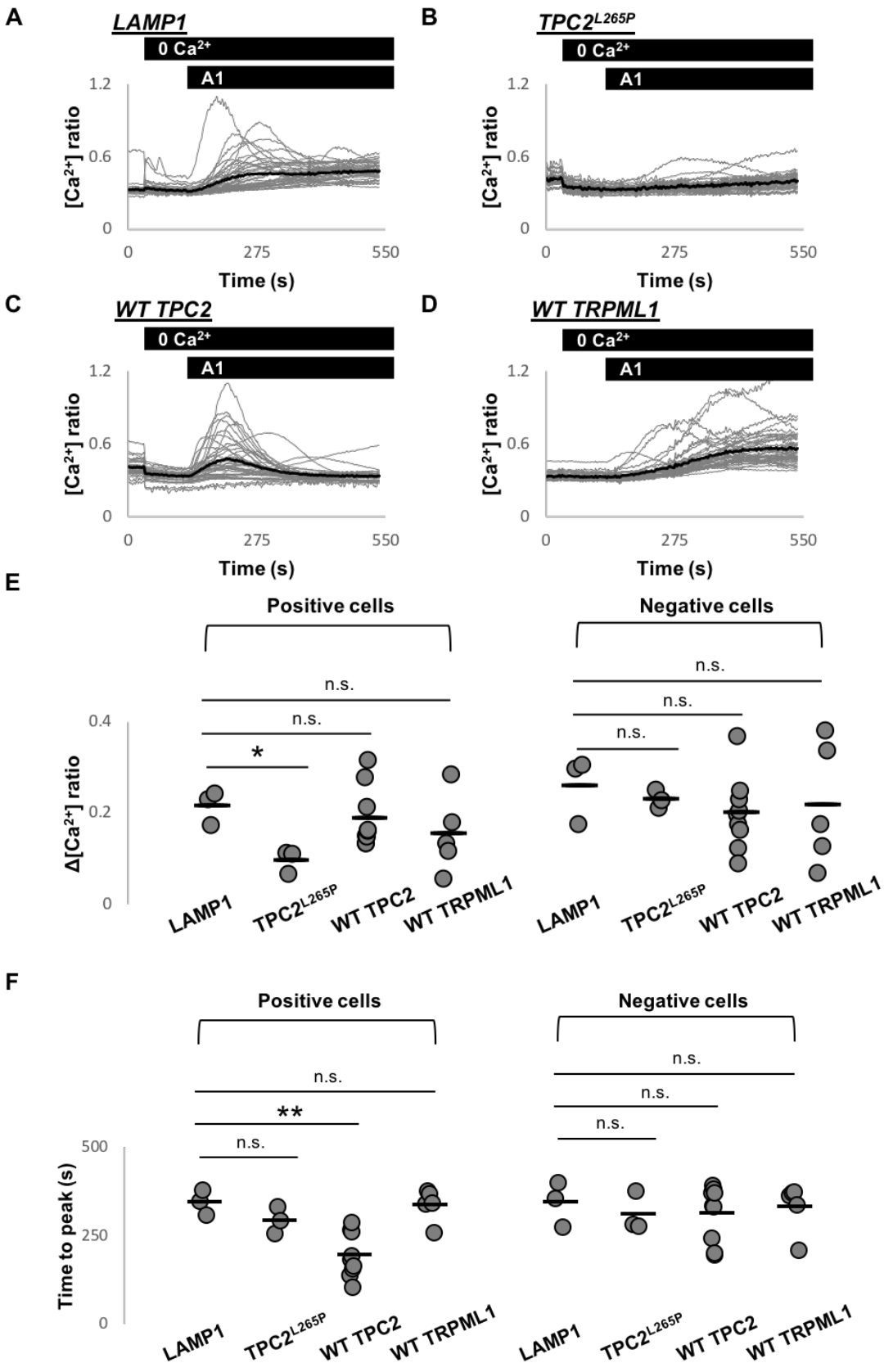

Figure 3.3.17 Endogenous A1-mediated Ca^{2+} release is inhibited by mutation of the TPC2 pore and is potentiated in cells transiently expressing TPC2

(A-D) Cytosolic Ca^{2+} responses to A1 (30 μM) in individual HeLa cells transiently expressing LAMP1 (A), $TPC2^{L265P}$ (B), WT TPC2 (C) or WT TRPML1 (D) in the absence of extracellular Ca^{2+}. Cells were immersed into Ca^{2+}-free HBS at 30s. The bars above graphs indicate the time of addition of the compound, which was at 120s. Gray traces represent recordings of all individual cells and black traces represent the population average.
(E and F) Summary data quantifying magnitudes of Ca^{2+} responses (E) and time taken to reach signal peak (F) after A1 stimulation following the indicated conditions. Each plot point represents average results from all GFP-positive or GFP-negative cells in one experiment (n=3-9); n.s. not statistically significant * $P<0.05$ ** $P<0.01$ were determined by one-way ANOVA.

3.4 Discussion

TPCs are ion channels of physiological and pathophysiological importance (Davis et al., 2012; Gómez-Suaga et al., 2012; Grimm et al., 2014; Hockey et al., 2015; Sakurai et al., 2015). It is therefore important to have chemicals that modulate TPCs. They can be used as research tools for characterization of TPCs and in the long term, they may have the potential to be developed into therapeutics for diseases. However, the pharmacology of TPCs is limited. To fill this gap, efforts have been made to search for novel TPC modulators. In this chapter, I have validated and characterized novel TPC2 agonists and inhibitors. Work related to this analysis has been published recently (Gerndt et al., 2020; Penny et al., 2019).

Due to the endo-lysosomal localization of TPCs and the impermeability of NAADP and $PI(3,5)P_2$, characterization on TPCs is not easy to perform, requiring complex techniques (e.g. microinjection). To tackle the problem, Grimm and colleagues have pursued cell-permeable TPC activators (Gerndt et al., 2020). Targeting of TPC2 to the PM, achieved by mutation of the N-terminal di-leucine motif, supports robust Ca^{2+} entry in response to NAADP (Brailoiu, Rahman, et al., 2010). By screening 80,000 natural and synthetic compounds against cells stably expressing PM TPC2, Grimm and colleagues identified A1 and H07 as likely TPC2 activators as they induced Ca^{2+} signals (Gerndt et al., 2020). In agreement, using the same cell line, I observed dose-dependent Ca^{2+} signals (Fig.3.3.2A and B). Driven by this, I performed further validation tests. TPC2 with the L265P mutation is known to be a “pore-dead” channel as it no longer supports NAADP Ca^{2+} signalling and channel activity (Brailoiu,

Rahman, et al., 2010; Lin-Moshier et al., 2014; Sakurai et al., 2015). A lack of action of A1 or H07 upon L265P mutation (Fig.3.3.4C and G) thus indicates that their Ca^{2+} activities require a functional TPC2 pore. At the PM, the luminal side of TPC2 faces the extracellular medium. Accordingly, Ca^{2+} signals through NAADP-activated PM TPC2 are a result of Ca^{2+} influx (Brailoiu, Rahman, et al., 2010). Similarly, A1 and H07 also induced Ca^{2+} influx with PM TPC2 (Fig.3.3.4D and H). Taken together, my first set of experiments using PM TPC2 uncover a pore-dependent action of A1 and H07 on TPC2.

Endogenous expression of TPC2 at the PM has not yet been reported. As lysosomes are the native environment for TPC2 (Brailoiu, Rahman, et al., 2010; Calcraft et al., 2009; Zong et al., 2009), I designed experiments to examine whether A1 and H07 can activate lysosomal TPC2 to induce Ca^{2+} release. I utilized the genetically encoded Ca^{2+} indicator, GCaMP6s, which has a large dynamic range and a similar or slightly higher Ca^{2+} affinity (Kd=144 nM) (Chen et al., 2013) than Fura-2 (Kd=135-224 nM) (Baylor & Hollingworth, 1988; Grynkiewicz et al., 1985). GCaMP6s was fused to the cytosolic C-terminus of TPC2 or the pore-mutant TPC2 ($TPC2^{L265P}$), and thus accumulates around lysosomes. However, GCaMP6s is unlikely to exclusively record Ca^{2+} release from lysosomes given its high Ca^{2+} affinity. To note, tagging was performed at the C-terminus because the N-terminus contains residues required for lysosomal targeting of TPC2 (Brailoiu, Rahman, et al., 2010) and Rab7 interaction (Lin-Moshier et al., 2014). A transient increase in GCaMP6s fluorescence by A1 or H07 was observed in cells expressing TPC2 GCaMP6s but not TPC2 GCaMP6s with a “broken” pore (Fig.3.3.11). Thus, A1 and H07 can activate TPC2 to induce pore-dependent Ca^{2+} signals, similar to their actions on PM TPC2. In addition, more importantly, these results reveal that A1 and H07 are cell-permeable. Consistent with this, they are highly lipophilic with logP values of around 5 (Gerndt et al., 2020). Therefore, compared to cell-impermeable NAADP and $PI(3,5)P_2$, A1 and H07 can readily access TPC2 in intact cells. This is of major significance as this can largely reduce the difficulty in characterizations on TPCs. In addition, use of A1 or H07 in intact cells also minimises the risk of losing essential proteins that might be required for TPC2 activation (Lin-Moshier et al., 2012; Walseth et al., 2012). In sum, I demonstrate that A1 and H07 are cell-permeable TPC2 activators.

Aside from being cell-impermeable, $PI(3,5)P_2$ has been shown to bind TRPML1 and induce TRPML1 currents (Chen et al., 2017; Dong et al., 2010). NAADP may also act on TRPML1 as NAADP responses were abolished in TRPML1 knockout cells (Zhang et al., 2009, 2011), although the view is not supported elsewhere (Lloyd-Evans et al., 2014; Yamaguchi et al., 2011). Considering that TPC activators might also act through TRPML1, I therefore examined the effects of A1 and H07 on TRPML1. TRPML1 can also be redirected to the PM upon mutation or deletion of its di-leucine motifs which are located at both termini (Falardeau et al., 2002; Vergarajauregui & Puertollano, 2006; Yamaguchi et al., 2011; Zeevi et al., 2009) or through increasing constitutive activity of the channels (i.e. V432P mutation) (Dong et al., 2008, 2009). Here, I used TRPML1 with deleted di-leucine motifs ($TRPML1^{\Delta NC}$). PM TRPML1 was functional as it allowed robust Ca^{2+} entry when activated by ML-SA1 (Fig.3.3.5). However, it remained silent in the presence of A1 or H07. Given that TRPML1 primarily localizes to lysosomes, A1 and H07 were also tested against cells expressing TRPML1 GCaMP6s. Again, although the expressing cells responded well to ML-SA1, they did not respond to A1 or H07 (Fig.3.3.12B-E). TRPML1 therefore may not be a target for A1 or H07. However, it should be noted that A1 was only tested with 10 μM and 30 μM and H07 was only tested with 30 μM and 60 μM, the effects of higher concentrations of A1/H07 (e.g. 100 μM) on TRPML1 should be studied.

I also examined the effect of the compounds on TPC1 which utilize NAADP and/or $PI(3,5)P_2$ for activation (Cang et al., 2013, 2014; Pitt et al., 2014; Rybalchenko et al., 2012). In contrast to TPC2, the endo-lysosomal localization of human TPC1 does not require its di-leucine motifs (Brailoiu, Rahman, et al., 2010). There is no evidence that human TPC1 can be re-directed to the PM upon mutation, although a proportion of mouse TPC1 expressed in the PM when transfected into cells (She et al., 2018). Given A1 and H07 were identified from the screen using human TPC2, I focused my efforts on human TPC1 fused to GCaMP6s. TPC1 GCaMP6s detected Ca^{2+} release by ionomycin, but not A1 or H07 (Fig. 3.3.13B-E). Based on this, A1 and H07 seem to not activate TPC1, although again it should be noted that A1 was only tested with 30 μM and H07 was only tested with 60 μM.

When transfected into the cells, a proportion of GCaMP6s-tagged TPC2, pore-mutant TPC2 ($TPC2^{L265P}$) or TPC1 have punctate appearance, consistent with localisation to lysosomes (Bandyopadhyay et al., 2014; Kilpatrick, Yates, et al., 2016). However, there were also reticulum structures, suggesting some are likely mis-targeted to other organelles such as the ER. TRPML1 GCaMP6s appeared to be exclusively localized to the ER. The reason behind the mis-targeting is unclear requiring further investigations. Lysosomes and the ER have very different luminal pH environments for their resident ion channels. Lysosomes have luminal pH of 4.5-5 whereas the ER is neutral. Given that TPC2 and TRPML1 are active when re-directed to the PM where has a neutral environment (Fig. 3.3.10 and (Brailoiu, Rahman, et al., 2010; Dong et al., 2008, 2009; Wang et al., 2012; Yamaguchi et al., 2011)), the ER-mis-targeting is unlikely to interfere with their activation by agonists. For TPC1, although in one study, TPC1 induced currents at both acidic and neutral pH when activated by $PI(3,5)P_2$ (Wang et al., 2012), while in the other, in the presence of NAADP, TPC1 was active at acidic but not neutral pH (Rybalchenko et al., 2012). If TPC1 activity is pH-sensitive perhaps, here, the lack of action of A1 and H07 for TPC1 is due to that TPC1 is inactive at neutral pH. However, in patch-clamp recording directly onto whole endolysosomes, compared to $PI(3,5)P_2$, again, A1 and H07 cannot activate TPC1 currents (Gerndt et al., 2020). Therefore, here, the insensitivity of TPC1 to A1/H07 is unlikely to be caused by pH, rather, TPC1 may not be a target for the two compounds. Nonetheless, future works need to establish the luminal pH effects on endo-lysosomal ion channels. Besides, the localization of GCaMP6s-tagged clones requires to be characterized in more detail. To achieve this, colocalization analysis should be performed to assess the percentage of GCaMP6s-tagged clones that overlap with LTR, LAMP1 or EEA1 (an endosomal marker).

Very recently, through a screening approach followed by electrophysiology analyses, Zhang and colleagues have also identified a number of novel TPC2 activators, including tricyclic anti-depressants (TCAs) and riluzole (named as Ly-NA1 by authors) (Zhang et al., 2019). These compounds require EC_{50} of 43-112 μM (TCAs) or 180 μM (riluzole) for activation and thus less potent than A1 and H07 (Gerndt et al., 2020, Fig.3.3.2A and B). Neither TCAs nor riluzole affect TRPML1 activity. However, they act through TPC1. For example, some TCAs can activate TPC1 in a voltage-dependent manner with EC_{50} of 10-27 μM, including clomipramine and desipramine. The other

TCAs, such as chlorpramine, and riluzole have been shown to inhibit TPC1. It is interesting to note, structurally, clomipramine and desipramine (activate TPC1) are similar but slightly different from chlorpramine (inhibit TPC1). Structure-activity relationships are warranted to understanding agonism versus antagonism of these compounds. Together, TCAs and riluzole are non-selective TPC modulators with complex effects on channel activity (Zhang et al., 2019), while A1 and H07 seems to be highly selective TPC2 activators.

The ability of A1 and H07 to activate recombinant TPC2 to induce Ca^{2+} signals led me to hypothesize that they activate native (endogenous) TPC2. In non-transfected HeLa cells that likely express TPC2 (Sakurai et al., 2015), in the absence of extracellular Ca^{2+}, A1 and H07 induced dose-dependent Ca^{2+} release albeit small (Fig.3.3.16). This indicates that they possess endogenous Ca^{2+} activity. To determine the underlying mechanism, A1 was studied in cells expressing GFP-tagged pore-mutant TPC2 ($TPC2^{L265P}$) that is also known to behave in a dominant-negative manner (Brailoiu, Rahman, et al., 2010; Penny & Patel, 2015; Sakurai et al., 2015). Additionally, A1 was also tested in cells overexpressing TPC2 or TRPML1. In control experiments, cells were transfected with LAMP1, an inert protein. Compared to A1 signals in the presence of LAMP1, the signals in the presence of mutant TPC2 were largely reduced (Fig.3.3.17A, B and E). Conversely, the signals were promoted by overexpression of TPC2 but not TRPML1 (Fig. 3.3.17A-F), further supporting a selective action of A1 on TPC2 over TRPML1. Importantly, this set of data reveals that A1 is likely to action through endogenous TPC2. Such an ability of A1 is important as this could propel TPC2 research. For example, A1 could be applied to investigate the physiological and pathological roles of TPC2, just like ML-SA1 which has been used for probing TRPML1 signalling (Kilpatrick, Yates, et al., 2016; Shen et al., 2012). Furthermore, ML-SA1-induced endogenous Ca^{2+} signals are highly variable (Kilpatrick, Yates, et al., 2016), this may indicate why overexpression is required to investigate the physiological or disease relevance of TRPML1 Ca^{2+} responses. In comparison, A1-induced endogenous Ca^{2+} signals are relatively consistent, so for similar investigations on TPC2, overexpression could be omitted. In this regard, A1 seems to be a better probe. To further validate that A1 activates endogenous TPC2, future works could assay A1 in TPC2 KO cells (Grimm et al., 2014; Ruas et al., 2015) or in cells depleted of TPC2 by siRNA (Hockey et al., 2015). For H07, its modest

endogenous Ca^{2+} signal is challenging. To facilitate investigations on underlying mechanism, future works should consider using cells expressing the M484L gain-of-function variant of TPC2 (Chao et al., 2017).

TPCs were initially recognized as NAADP-gated Ca^{2+} permeable channels (Brailoiu et al., 2009; Calcraft et al., 2009; Zong et al., 2009). But other studies showed that TPCs were Na^{+} channels activated by $PI(3,5)P_2$ not NAADP (Cang et al., 2013; Wang et al., 2012). There are also studies that link TPCs to both NAADP and $PI(3,5)P_2$ activity (Grimm et al., 2014; Jha et al., 2014; Ruas et al., 2015), raising a co-regulation idea (reviewed in (Patel, 2015)). The ion selectivity of TPCs, however, is still hotly debated. Based on certain electrophysiology studies, TPCs are non-selective Ca^{2+}-permeable channels (Grimm et al., 2014; Pitt et al., 2014; Ruas et al., 2015), while others indicate that TPCs are highly selective for Na^{+} with little Ca^{2+} permeability (Cang et al., 2014; Guo et al., 2017; She et al., 2019; Wang et al., 2012). In this chapter, regardless of TPC2's localization (at the PM or on the membrane of intracellular compartments), A1 or H07 induced consistent increases in cytosolic Ca^{2+} level. Thus, this confirms the Ca^{2+} permeability of TPC2 in a cellular environment.

It is notable that, although both A1 and H07 activate TPC2 to induce Ca^{2+} signals, their effects on mobilizing Ca^{2+} appear to be different. First, in cells expressing PM TPC2, there was a greater Ca^{2+} responses to A1 than to H07 at 10 μM and 30 μM, respectively (Fig3.3.2A and B). In addition to that, strikingly, there was an apparent delay in H07- but not A1-induced Ca^{2+} signals - a delay that persisted even at the relatively high concentration of H07 (Fig.3.3.2C-E). The reason for the delay is unclear, but this indicates a kinetic difference between the Ca^{2+} signals by A1 and H07. Secondly, in cells expressing TPC2 GCaMP6s, A1 at 30 μM induced larger Ca^{2+} signals than H07 at 60 μM (Fig.3.3.11 C and E). Consistent with this was the far smaller ionomycin Ca^{2+} signals after A1 compared to that after H07. A1 therefore mobilized a greater fraction of the stores mobilized by ionomycin. Finally, in native (non-transfected) cells, A1, again, induced greater Ca^{2+} signals than H07 (Fig.3.3.16). Therefore, in all three contexts, A1 tends to mobilize more Ca^{2+} than H07. But what could be the causes? Through patch-clamp technique, interestingly, Gerndt et al., 2020 have observed that H07 induced bigger Na^{+} currents than A1 in endo-lysosomes derived from cells overexpressing TPC2. Accordingly, the cause is unlikely to be that

H07 has a low efficacy for TPC2 than A1. Also, H07 is more lipophilic than A1 with a logP value of 5.35 (H07) vs. 4.56 (A1) (Gerndt et al., 2020). Therefore reduced activity is not due to H07 being less cell-permeable and unable to reach the same intracellular concentrations as A1. Since there is no evidence that the ability of H07 to "access" TPC2 is worse than A1, rather it could be better, it is reasonable to consider that TPC2 itself might be the cause for the differential effects of the agonists on mobilizing Ca^{2+}. Therefore, one hypothesis is that TPC2 is more permeable to Ca^{2+} when activated by A1 than by H07, that is, ion selectivity through TPC2 is agonist-dependent. This hypothesis will be studied and discussed in detail in chapter 4.

Ca^{2+} release from lysosomes is known to "trigger" further Ca^{2+} release from the ER likely through MCSs (Kilpatrick et al., 2013; Patel & Brailoiu, 2012; Penny et al., 2014). A key feature of NAADP is that it utilizes the "trigger" hypothesis for Ca^{2+} signalling (Cancela et al., 1999; Kinnear et al., 2004; Morgan, 2016). In cells expressing TPC2 GCaMP6s, A1-induced Ca^{2+} release was inhibited by both GPN and thapsigargin (Fig.3.3.14). A1 therefore recruits both lysosomes and the ER stores for signalling. GPN has recently been questioned for its action on lysosomes (Atakpa et al., 2019). In previous chapter, I showed that lysosomes are GPN primary targets. Given that GPN's effect on A1 is more pronounced than thapsigargin, lysosomes therefore might be the origin of the A1 signals. H07 signals were eliminated by GPN as well (Fig.3.3.15), indicating that H07 recruits lysosomal stores to induce Ca^{2+} release. However, strikingly, such signals were potentiated by thapsigargin (fig.3.3.15). Although this meant the ER is not the Ca^{2+} source for H07 signals, what could be the reason behind such potentiation? It has been reported that lysosomes sequester Ca^{2+} released from the ER (Atakpa et al., 2018; López-Sanjurjo et al., 2013). Namely, after thasigargin treatment, lysosomes should store more Ca^{2+}. Thus, for H07, following thapsigargin, more Ca^{2+} can be mobilized from lysosomes. As A1 also requires ER Ca^{2+} for signalling, thapsigargin therefore did not potentiate A1 signals. The findings that A1 but not H07 mobilize ER Ca^{2+} is not unexpected, given that A1 signals resembled the larger thapsigargin signals while H07 signals resembled the smaller GPN signals. The larger Ca^{2+} release by A1 than H07 therefore might be partially due to selective coupling to the ER. To note, the reason to say "partially" is because the "ER coupling" cannot explain the differential Ca^{2+} responses by A1 and H07 in cells expressing PM TPC2 that is functionally isolated from the ER (Brailoiu, Rahman, et

al., 2010). Therefore, the larger Ca^{2+} release by A1 than H07 might also be caused by A1 mobilizing more lysosomal Ca^{2+} than H07. To investigate this, GCaMP6s is not ideal as it also detects Ca^{2+} from the ER (evidence by thapsigargin responses), consistent with its high Ca^{2+} binding affinity (Chen et al., 2013; Lock et al., 2015). Therefore, a low Ca^{2+} binding affinity probe would be better, such as GECO1.2 (Davis et al., 2020). Finally, it is worth to mention that given that GPN functions differently from thapsigargin and it largely abolished A1 and H07 signals, here, the action of GPN on lysosomes has been further supported.

Regarding TPC inhibitors, among a limited number of inhibitors, tetrandrine is the most potent one (Sakurai et al., 2015). Here, tetrandrine inhibited A1-induced Ca^{2+} signals in cells expressing PM TPC2, providing the first pharmacological evidence that A1 activates TPC2 (Fig.3.3.6B, C and E). Conversely, the results indicate that A1 signalling can be used as a platform for identification of potential TPC2 blockers. With the help of A1, tetrandrine's analogue, cepharanthine has been recognized as a TPC2 blocker (Fig.3.3.6). Given that cepharanthine and tetrandrine belong to a large family of structurally close bisbenzylisoquinoline (BBIQ) alkaloids (Bailly, 2019), perhaps, other BBIQ alkaloids also function as TPC blockers. Favouring this, in 2018, Gunaratne's team found BBIQ alkaloids (e.g. tetrandrine and fangchinoline) can effectively inhibit TPC-dependent MERS pseudovirus translocation, and this correlated well with their inhibitory effects on NAADP signalling (Gunaratne, Yang, et al., 2018). However, to note, BBIQ alkaloids carry two coclaurine units which can be joined head-to-head (e.g. tetrandrine) or head-to-tail (e.g. tubocurarine), those (including tetrandrine and fangchinoline) have a clear impact on the translocation of MERS pseudovirus are "head-to-head" formed BBIQ alkaloids. While the "head to tail" formed BBIQ failed to impair the translocation. Interestingly, cepharanthine also belongs to the "head-to-head" BBIQ alkaloids group (Bailly, 2019). Given the above, BBIQ alkaloids might block TPC depending on their chemical structures. Analysis of structure-activity relationship therefore is needed for better understanding the effects of BBIQ alkaloids on TPCs.

Although potent, tetrandrine is not selective for TPCs as it also targets multiple Cav channel isoforms (King et al., 1988; Liu et al., 1991; Sakurai et al., 2015). In fact, few of TPC blockers are selective to the channel. In addition, some of the blockers might

have an indirect effect on TPCs, such as Ned-19 and PPADS that are known to affect NAADP binding (Billington & Genazzani, 2007; Rosen et al., 2009). Also, there are no approved drugs that target TPCs. To address these shortcomings, our lab therefore searched for novel TPC blockers (Penny et al., 2019). The strategy was to combine data from TPC2 pore structure-based screen with data from Ebola screens (Johansen et al., 2015; Kouznetsova et al., 2014). It has been reported that TPC activity is required for Ebola infection (Sakurai et al., 2015), the use of Ebola screens therefore is based on the deduction that anti-Ebola drugs may be TPC inhibitors. Such a strategy enabled a number of FDA-approved drugs targeting estrogen or dopamine receptors to be highlighted, for their high ranking and potent anti-Ebola activity. These drugs selectively blocked NAADP-induced Ca^{2+} signals in sea urchin egg homogenate. They also blocked NAADP and PI(3,5)P_2-induced channel activity of human TPC2 (Penny et al., 2019). Moreover, single channel analyses revealed that they are likely pore blockers (Penny et al., 2019). I therefore used these novel pharmacological tools to validate A1. Besides, such tests could inform the action of these novel tools on human TPC2 in intact cells, which remains to be characterized. At 10 μM, after a 5 minute incubation, the SERMs raloxifene, clomifene and tamoxifen fully inhibited A1 induced Ca^{2+} signals (Fig.3.3.7), although notably clomifene and tamoxifen were only tested once or twice. Under the same settings, the dopamine receptor antagonists (antipsychotics) fluphenazine and pimozide largely reduced A1-induced Ca^{2+} signals (Fig.3.3.8). Collectively, the idea that A1 is a TPC2 activator is further evidenced. Also, these data confirm the tested drugs are likely TPC2 blockers in intact cells.

Ebola entry is a complex process (Sakurai et al., 2015). After binding to certain cell surface proteins (Alvarez et al., 2002; Kondratowicz et al., 2011), the virus is internalized through macropinocytosis, followed by trafficking through the endolysosomal system where the fusion occurs between the virus and membrane. The genome released into the cells is then replicated. TPCs are proposed to play roles in the late stage of Ebola entry (Sakurai et al., 2015). Based on this, TPC blockers must be anti-Ebola drugs, while some anti-Ebola drugs may act through a TPC-independent mechanism. Of relevant, Ned-19, tetrandrine and catharanthine all can inhibit Ebola infection (Kouznetsova et al., 2014; Sakurai et al., 2015). Therefore, for those drugs that ranked highly in TPC2 screen but ineffective in blocking Ebola infection, they are highly likely false positives that have no effect on TPC2. In this case, I reasoned that

such drugs could serve be negative controls for the study on A1. Statins rank high in the virtual screen but had little effect on Ebola infection (Fig.3.3.9A and (Penny et al., 2019)). I therefore tested simvastatin, cerivastatin and lovastatin on A1 action in cells expressing PM TPC2, and none of them at 10 μM altered A1 signals (Fig.3.3.9B-F). Statins therefore could be false positives, and this indirectly confirms that A1 acts through TPC2. It is important to note, however, here, statins were only tested at one concentration. Higher concentrations should be examined in future. Nevertheless, these data together with those showing the effects of TPC inhibitors (i.e. SERMs and dopamine receptor modulators) on A1 signalling indicate the positive correlation between TPC inhibition and anti-Ebola activity, proving the effectiveness and usefulness of Ebola screens in identifying hits for TPCs.

Tetrandrine is known to be a Cav channel blocker (King et al., 1988; Liu et al., 1991). Like tetrandrine, the novel TPC blockers, including SERMs (raloxifene and tamoxifen) and dopamine receptor antagonists (fluphenazine and pimozide) have been reported to target at Cav channel (Borg et al., 2002; Sah & Bean, 1994; Wang et al., 2011). This could reflect that Cav are evolutionally linked to TPCs and to share a common pharmacological binding site (Rahman et al., 2014). Given this, maybe it is unavoidable that drugs that affect TPC also additionally affect Cav. However, given tetrandrine, raloxifene and fluphenazine at 10 μM after a 5 minute incubation did not inhibit ML-SA1-induced Ca^{2+} signals in cells expressing PM TRPML1 as they did inhibit A1 responses in cells expressing PM TPC2 (Fig.3.3.10), these drugs do appear to be selective for TPC2, at least, over TRPML1. To note, all the drugs were tested on TPC2 outside its native environment. At the PM, TPC2 is uncoupled from the ER (Brailoiu, Rahman, et al., 2010), so any effects would reflect a direct effect on the channel itself. Nonetheless, the drugs should also be tested on TPC2 localized to its native environment. To do so, future work could assay A1 in cells expressing TPC2 GCaMP6s or on A1's endogenous signals, which is thought to be TPC2 dependent.

In summary, I demonstrate that A1 and H07 are novel cell-permeable and selective TPC2 agonists. They activate TPC2 to induce pore-dependent Ca^{2+} signals, confirming the Ca^{2+} permeability of TPC2, an area of contention. A1 and H07 have differential effects on mobilizing Ca^{2+} but the reason behind this requires further investigations. A1 but not H07 coupled to the ER for signalling via activating lysosomal TPC2.

Moreover, I confirmed that a number of SERMs and dopamine receptor antagonists are TPC2 blockers, and that they are selective to TPC2 over TRPML1. Given these new TPC2 activators and blockers, the pharmacology of TPC2 has been largely expanded.

Chapter 4: TPC2 activators differentially activate TPC2 - addressing debate over channel characteristics.

4.1 Introduction

Compared to other voltage-gated ion channels, our current understanding of TPCs is just the tip of the iceberg. Even, the basic attributes of TPCs remain to be elucidated. For example, although being recognized as NAADP-gated Ca^{2+}-permeable channels (Brailoiu et al., 2009; Brailoiu, Rahman, et al., 2010; Calcraft et al., 2009; Pitt et al., 2010; Schieder et al., 2010; Zong et al., 2009), this idea has not been confirmed in all studies. In some studies, TPCs are insensitive to NAADP, instead being activated by $PI(3,5)P_2$ (Boccaccio et al., 2014; Cang et al., 2013, 2014; Guo et al., 2017; Wang et al., 2012). There are also studies that found TPCs can be activated by both NAADP and $PI(3,5)P_2$ (Grimm et al., 2014; Jha et al., 2014; Ogunbayo et al., 2018; Ruas et al., 2015), proposing a co-regulation model for channel activation by the two stimuli (reviewed in Patel, 2015). This may in part reconcile the conflicting data on activating ligands of TPC2 but few studies to date have fully addressed the NAADP/$PI(3,5)P_2$ controversy. Additionally, NAADP appears to have a more complicated mechanism of action than $PI(3,5)P_2$. Photo-affinity labelling studies have revealed an indirect action of NAADP on TPCs requiring binding to putative small accessory binding proteins (Lin-Moshier et al., 2012; Walseth et al., 2012). The identity of such proteins is under active investigations. In contrast, structural insights into MmuTPC1 and HsaTPC2 have uncovered that $PI(3,5)P_2$ activates the channel via direct binding to residues seated in the IS4-IS5 linker (She et al., 2018, 2019). To confuse matters further, TPC is non-selective and Ca^{2+}-permeable in some cases (Grimm et al., 2014; Jha et al., 2014; Ruas et al., 2015), while highly Na^+ selective (little Ca^{2+} permeability) in others (Guo et al., 2017; She et al., 2018; Wang et al., 2012). The ion selectivity of TPC thus is a major conundrum. Finally, as TPCs are localized to acidic organelles, TPCs are likely to be regulated by luminal pH. Indeed, this has been noted in a number of studies, but the exact effect is equivocal (see Table 4.1). Also, there is case where pH seems to have no effect on TPCs (Wang et al., 2012). Taken together, the gating

mechanism, ion selectivity and pH regulation of TPCs are debated and remain to be resolved.

Table 4.1 Summary of pH regulation of TPCs

Paper	**Channel**	**Activator**	**Method (Patch-clamp technique)**	**Regulation**
Pitt et al., 2010	TPC2	NAADP	Purified channel incorporated into lipid bilayers	Acidic pH (4.8) reduced channel open probability
Schieder et al., 2010	TPC2	NAADP	Enlarged lysosomes transfected with channel	Inhibited at neutral luminal pH (7.4)
Brailoiu, Rahman, et al., 2010	TPC2	NAADP	Redirected channel to the plasma membrane	Active at neutral "luminal" pH (7.4)
Rybalchenko et al., 2012	TPC1	NAADP	Purified channel incorporated into lipid bilayers	Inhibited at neutral luminal pH (7.4)
Wang et al., 2012	TPC1 and TPC2	$PI(3,5)P_2$	i) Enlarged lysosomes transfected with channel ii) Redirected channel to the plasma membrane	Both TPC1 and TPC2 are activate at neutral and acidic pH
Cang et al., 2014	TPC1	$PI(3,5)P_2$	Enlarged lysosomes transfected with channel	Slightly reduced at acidic pH 4.6, but activated at pH 5.6

Jha et al., 2014	TPC2	$PI(3,5)P_2$	Enlarged lysosomes transfected with channel	Luminal pH change from neutral (7.4) to acidic (6.5) had no effect on TPC2 current (note: in the absence of luminal Mg^{2+})

In chapter 3, A1 and H07 were identified as novel cell-permeable TPC2 activators. My findings confirm the Ca^{2+} permeability of TPC2, an area of contention as mentioned above. But their differential effects on elevating Ca^{2+} raise the intriguing possibility that the ion selectivity of TPC2 is not fixed but malleable depending on its activating ligand. If the hypothesis is validated, there is reason to suspect that other properties of TPC2 (e.g. gating mechanism and pH regulation) could be agonist-specific as well. In other words, "different" agonists confer TPC2 with different properties thereby resolving controversy. Therefore, in this chapter, I further characterized A1 and H07 with the aim to address conflicting reports on ion selectivity, activation mechanism and pH regulation of TPC2.

4.2 Methods

4.2.1 Cell culture

HeLa cells and HEK293 cells stably expressing $TPC2^{LL/AA}$ were cultured and plated for imaging as described in chapter 3.

4.2.2 Transfection

HeLa cell transfection was performed as described in chapter 3.

Plasmids used are listed below

Table 4.2 Plasmids

Name	**Tag**	**Reference**
PM TPC2 ($TPC2^{LL/AA}$)	mRFP or GFP	(Brailoiu, Rahman, et al., 2010)
TPC2 WT	GCaMP6s	(Gerndt et al., 2020)

PM TRPML1 ($TRPML1^{\Delta NC}$)	GFP	(Yamaguchi et al., 2011)
TRPML1 WT	GCaMP6s	(Gerndt et al., 2020)
K203A PM TPC2 ($TPC2^{LL/AA, K203A}$)	GFP	(She et al., 2019)
K204A PM TPC2 ($TPC2^{LL/AA, K204A}$)	GFP	(She et al., 2019)
K207A PM TPC2 ($TPC2^{LL/AA, K207A}$)	GFP	(She et al., 2019)
K204A TPC2 ($TPC2^{K204A}$)	GCaMP6s	(Gerndt et al., 2020) (see 4.2.3)
H527A PM TPC2 ($TPC2^{LL/AA, H527A}$)	GFP	Unpublished (see 4.2.3)

4.2.3 Site-directed mutagenesis

$TPC2^{K204A}$ GCaMP6s and $TPC2^{LL/AA, H527A}$ GFP were generated by site-directed mutagenesis (SDM) from TPC2 GCaMP6s and $TPC2^{LL/AA}$ GFP), respectively. Mutagenic primers were designed using NEB base changer (http://nebasechanger.neb.com/#).

Mutagenic primers		
$TPC2^{K204A}$ GCaMP6s	Forward Primer	5' -TATGATGAAGGCGACCTTGAAATGCATCCG- 3'
	Reverse Primer	5' -GAGGAGTTCTGCAGCAGG- 3'
$TPC2^{LL/AA, H527A}$ GFP	Forward Primer	5' -CCGATTGCCAGCCCCAGGCTGGA- 3'
	Reverse Primer	5' -TACACAGCCAGAGTTGAG- 3'

SDM was carried out using the Q5 Site-Directed Mutagenesis Kit (E0552S), according to the manufacturer's instructions. The generated PCR product was treated with Dpnl to remove the parental plasmids, and followed by transformation into XL10 gold competent cells. Plasmids were isolated using the Monarch Plasmid DNA miniprep

Kit (NEB #T1010), according to the manufacturer's instructions. Plasmids were sequenced in both directions to confirm the mutations.

4.2.4 Media for imaging

HEPES-buffered saline (HBS) was used in live-cell imaging experiments as described in chapter 2. For some experiments, modified HBS or MES-buffered saline (MBS) was used as detailed below.

Media	HBS	Ca^{2+}- free HBS	Na^{+}-free HBS	MBS
Composition (mM)	HEPES (10), KH_2PO_4 (1.25), $MgSO_4$ (2), KCl (3), NaCl (156), Glucose (10), $CaCl_2$ (2) pH = 7.4 by HCl (as described in chapter 2)	HEPES (10), KH_2PO_4 (1.25), $MgSO_4$ (2), KCl (3), NaCl (156), Glucose (10), pH = 7.4 by HCl (as described in chapter 2)	HEPES (10), KH_2PO_4 (1.25), $MgSO_4$ (2), KCl (3), N-methyl-D-glucamine (NMDG) (156), Glucose (10), $CaCl_2$ (2) pH = 7.4 by HCl	MES (10), KH_2PO_4 (1.25), $MgSO_4$ (2), KCl (3), NaCl (156), Glucose (10), $CaCl_2$ (2) pH = 5.5 by NaOH

4.2.5 Epifluorescence microscopy

4.2.5.1 Ca^{2+} measurements

Cytosolic Ca^{2+} was measured by Fura-2 or GCaMP6s and analysed as described in chapter 2 and 3. All GCaMP6s experiments were performed in Ca^{2+}-free HBS. Certain Fura-2 experiments were performed in Na^{+}-free HBS or MBS as indicated in figures. Cells were stimulated with A1 (10 µM and 30 µM), H07 (30 µM and 60 µM), ML-SA1 (20 µM), Ned-19 (10 µM and 100 µM) and ionomycin (2 µM). All compounds were prepared in DMSO.

4.2.5.2 Na^+ measurements

For measurement of cytosolic Na^+, cells were incubated with 5 μM SBFI-AM (Santa Cruz Biotechnology) and 0.005% pluronic acid in HBS for 1 hour at room temperature (Invitrogen). SBFI was excited at 340 nm/380 nm and emitted fluorescence was captured with 440 nm long pass filter every 3s with 20x objective. Where indicated, Na^+-free HBS was used in certain SBFI experiments.

SBFI ratio was calculated using TILLvisION software and averaged over a 90 second period to obtain a basal ratio before stimulus addition. If experiments were conducted in Na^+-free medium, the basal ratio was acquired after cells were washed into Na^+-free HBS. The change of the SBFI ratio between the basal ratio and the peak ratio (ΔNa^+) was calculated to quantify the magnitude of response.

4.2.6 Recurrent methods

Cell fixation and confocal microscopy were performed as described in chapter 3. Data presentation is as described in chapter 3. Statistical analysis was performed using Prism 9 as described in chapter 3. $P<0.05$ was regarded as statistically significant.

4.3 Results

4.3.1 A1 and H07 mediate Na^+ influx in cells stably expressing plasma membrane targeted TPC2

Electrophysiology studies have uncovered that TPC2 is permeable to Na^+ although it is unclear as to whether it is selective for Na^+ or not. I therefore examined whether A1 and H07 can activate TPC2 to induce Na^+ signals. To do this, I used cells stably expressing plasma membrane targeted TPC2 ($TPC2^{LL/AA}$) and loaded with SBFI, a ratio-metric Na^+ indicator. Cells were stimulated with 30 μM of the agonists that induce robust Ca^{2+} signals (Chapter 3). As shown in Fig.4.3.1A and B, both A1 and H07 induced an increase albeit modest in cytosolic Na^+ level in cells expressing $TPC2^{LL/AA}$. A1- and H07-induced Na^+ signals were abolished upon removal of extracellular Na^+ (Fig.4.3.1C and D), suggesting the source is extracellular. This is consistent with the PM localization of TPC2. These data were quantified in Fig.4.3.1E where I calculated the magnitudes of Na^+ signals by A1 or H07. Collectively, these data indicate that A1 and H07 can activate $TPC2^{LL/AA}$ to induce Na^+ influx.

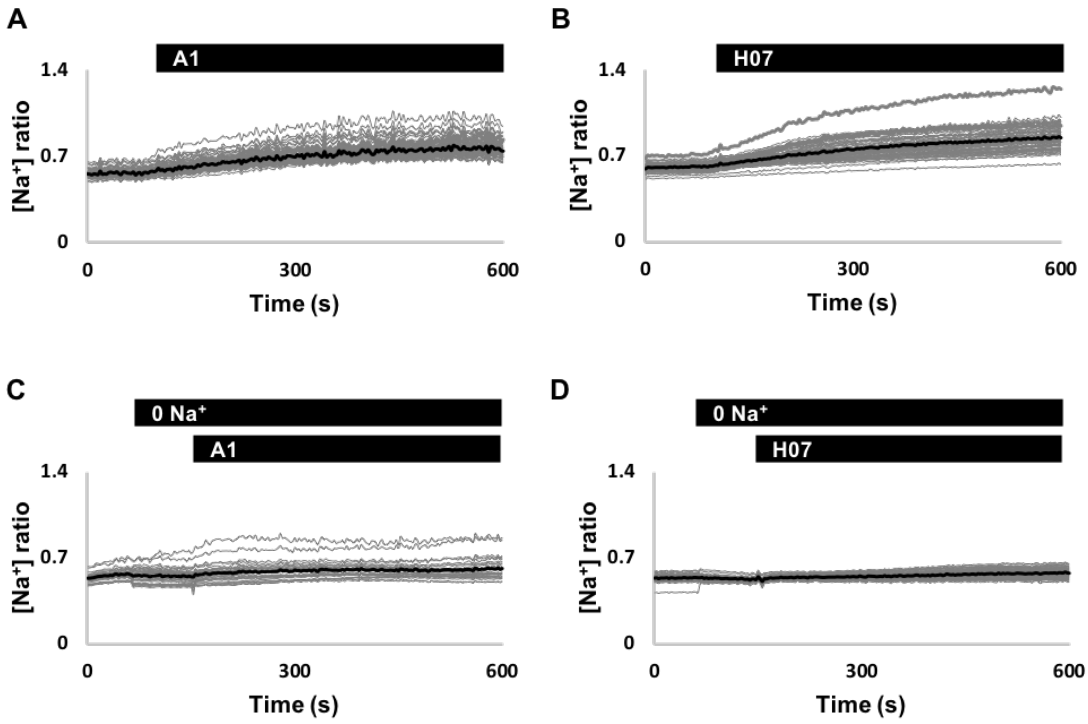

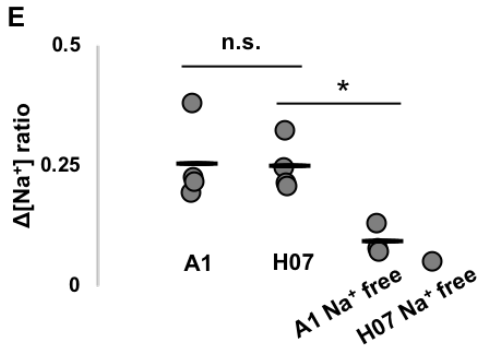

Figure 4.3.1 A1 and H07 mediate Na^+ influx in cells stably expressing plasma membrane targeted TPC2

(A and B) Cytosolic Na^+ responses to A1 (30 μM) (A) or H07 (30 μM) (B) in individual HEK293 cells stably expressing $TPC2^{LL/AA}$. The bars above graphs indicate the time of addition of the compound, which was at 90s. Gray traces represent recordings of all individual cells and black traces represent the population average.

(C and D) Similar to A and B except experiments were conducted in the absence of extracellular Na^+. Cells were immersed into Na^+-free HBS at 60s and were stimulated with A1 or H07 at 150s as indicated by the bar.

(E) Pooled data quantifying magnitude of the Na^+ signals in response to A1 and H07 with and without extracellular Na^+. Each plot point represents one experiment (n=1-4); n.s. not statistically significant * $P<0.05$ were determined by one-way ANOVA.

4.3.2 A1 and H07 have dissimilar effects on Ca^{2+} and Na^+ influx

So far, my results uncover that A1 and H07 can activate TPC2 to induce both Ca^{2+} and Na^+ signals. Fig. 4.3.2A-F compares Ca^{2+} and Na^+ influx using the same concentration of agonist. A1-induced Ca^{2+} signals were significantly greater in magnitude than those induced by H07 (Fig.4.3.2A and B) and there was a marked delay in H07 but not A1-induced Ca^{2+} influx (Fig.4.3.2A). The delay was quantified by measuring the rate of increase over the first 2 minutes in the presence of A1 or H07 (Fig.4.3.2C). Using the same quantification analyses, I characterized the effects of A1 and H07 on cytosolic Na^+. As shown in Fig.4.3.2D and E, in cells stably expressing $TPC2^{LL/AA}$, A1-induced Na^+ signals were similar in magnitude to those induced by H07. Of note, there was no delay in H07-induced Na^+ signals (Fig.4.3.2D and F). A direct comparison of the agonist-induced Ca^{2+} signals with Na^+ signals is presented in Fig.4.3.2G and H.

Collectively, these data indicate that A1 and H07 have distinct effects on Ca^{2+} signals but similar effects on Na^{+} signals.

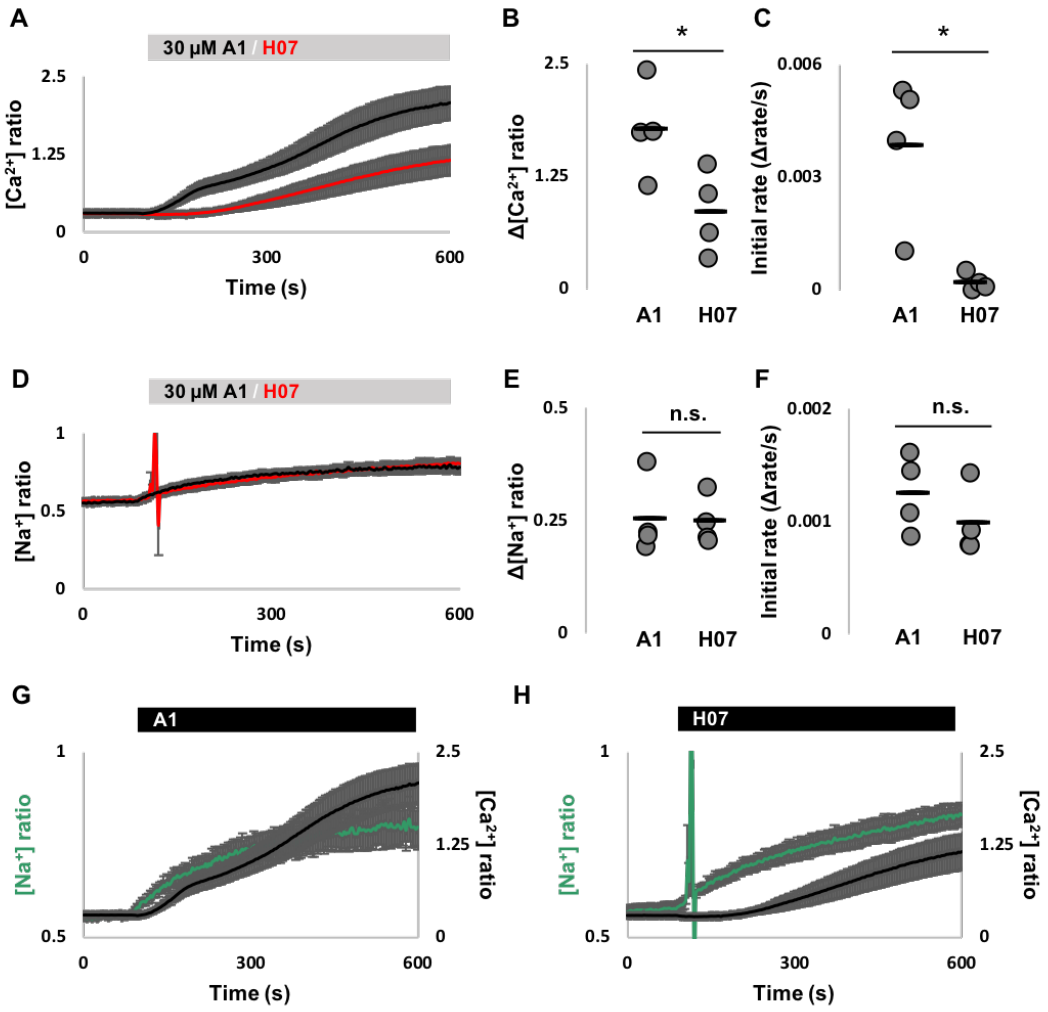

Figure 4.3.2 A1 and H07 have dissimilar effects on Ca^{2+} and Na^{+} influx

(A) Average cytosolic Ca^{2+} responses to A1 (30 µM) or H07 (30 µM) (mean ± S.E.M, 4 independent experiments) in HEK293 cells stably expressing $TPC2^{LL/AA}$. The bar above graph indicates the time of addition of the compound, which was at 90s.

(B) Pooled data quantifying magnitude of Ca^{2+} responses to A1 or H07 in A. * $P<0.05$ was determined by independent-samples t-tests.

(C) Pooled data quantifying the initial rate of Ca^{2+} rise over the first 2 minutes by A1 or H07 in A. * $P<0.05$ was determined by independent-samples t-tests.

(D-F) Similar to A-C except cytosolic Na^{+} responses were characterized using the Na^{+} indicator (SBFI-AM) (mean ± S.E.M, 4 independent experiments). n.s. not statistically significant was determined by independent-samples t-tests.

(G-H) Comparison of Ca^{2+} responses with Na^{+} responses by A1 (30 μM) (G) or H07 (30 μM) (H).

4.3.3 Removal of extracellular Na^{+} profoundly potentiates H07- but not A1-mediated Ca^{2+} signals

The above data reveal that there is a delay in H07-induced Ca^{2+} signals but not Na^{+} signals. This raises the possibility that Ca^{2+} and Na^{+} may compete for entering the cytoplasm via TPC2. To test this, in cells stably expressing $TPC2^{LL/AA}$, I examined the effects of A1 and H07 on cytosolic Ca^{2+} in the absence of extracellular Na^{+}. I used concentrations of A1 and H07 that induced relatively similar Ca^{2+} signals in the presence of extracellular Ca^{2+} (Chapter 3). As shown in Fig.4.3.3A-C, the magnitude of A1-induced Ca^{2+} signals were unaffected by removing extracellular Na^{+}, although the Ca^{2+} increase rate was modestly accelerated. In comparison, H07-induced Ca^{2+} signals were remarkably potentiated in both the magnitude and the rate of Ca^{2+} increase (Fig.4.3.3D-F) was such that the delay was essentially eliminated. Taken together, extracellular (luminal) Na^{+} has a profound impact on H07 but not A1 action.

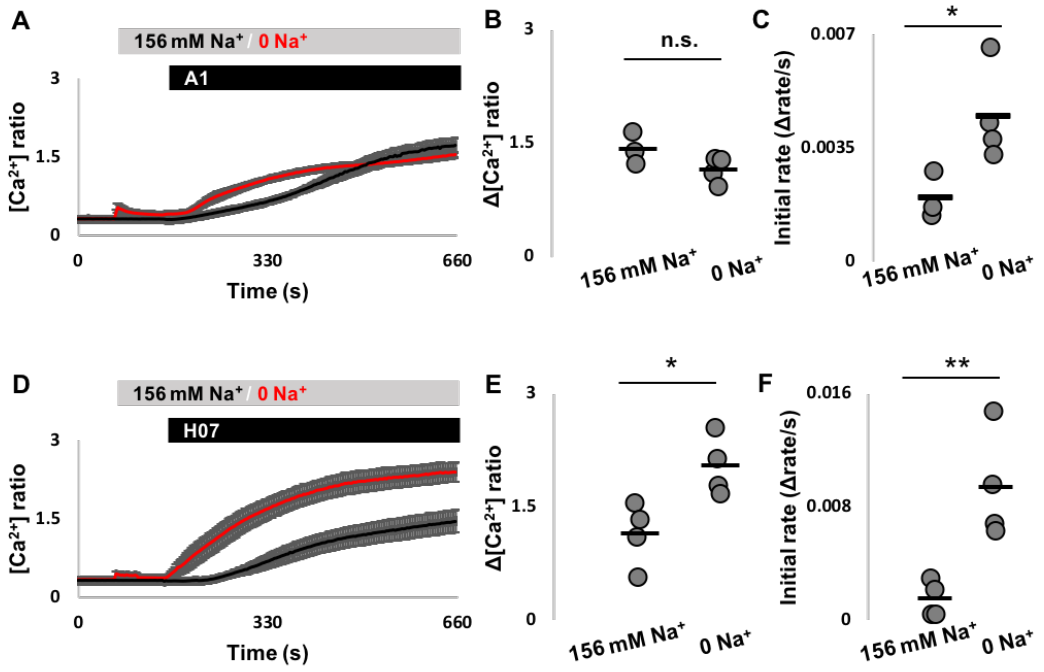

Figure 4.3.3 Removal of extracellular Na^{+} profoundly potentiates H07- but not A1-mediated Ca^{2+} signals

(A) Average cytosolic Ca^{2+} responses to A1 (30 μM) with and without extracellular Na^{+} (mean ± S.E.M, 4 independent experiments) in HEK293 cells stably expressing $TPC2^{LL/AA}$. Cells were immersed into Na^{+}-free HBS at 60s and were stimulated with A1 or H07 at 150s as indicated by the bar.
(B) Pooled data quantifying magnitude of Ca^{2+}responses to A1 in A. n.s. not statistically significant was determined by independent-samples t-tests.
(C) Pooled data quantifying rate of Ca^{2+} rise by A1 in A. * $P<0.05$ was determined by independent-samples t-tests.
(D-F) Similar to A-C except cells were stimulated with H07 (60 μM) (mean ± S.E.M, 4 independent experiments). * $P<0.05$ ** $P<0.01$ were determined by independent-samples t-tests.

4.3.4 Ned-19 appears to have differential effects on agonist-induced Ca^{2+} influx and Ca^{2+} release.

It has been suggested that NAADP activates TPCs indirectly via initial interactions with an accessory small binding protein that remains to be identified (Lin-Moshier et al., 2012; Walseth et al., 2012). To investigate the mechanism underlying A1 and H07's action on TPC2, I examined the effects of Ned-19 on A1- and H07-induced Ca^{2+} signals. Ned-19 is a potent NAADP antagonist identified in a ligand-based virtual screen (Naylor et al., 2009) and has been used widely for exploring NAADP signalling.

In chapter 3, in cells transiently expressing $TPC2^{LL/AA}$, I show that pre-treatment with 10 μM tetrandrine or other putative TPC2 blockers (e.g. raloxifene and fluphenazine) for 5 minutes effectively blocked A1-induced Ca^{2+} influx. Thus, to start, I adopted the same testing assay. As shown in Fig.4.3.4A, after a 5-minute treatment, 10 μM Ned-19 had no effect on A1-induced Ca^{2+} influx. I therefore prolonged the treatment time to 1hr. As shown in Fig.4.3.4B and C, following such treatment, Ned-19 appeared to potentiate A1-induced Ca^{2+} influx, but it had little effect on H07-induced Ca^{2+} influx. The effects of 10 μM Ned-19 were quantified in Fig.4.3.4D by calculating the magnitude of the responses to A1 or H07 following DMSO or Ned-19.

To further examine the effects of Ned-19, I used a higher concentration (100 μM). As shown in Fig.4.3.4E, in cells expressing $TPC2^{LL/AA}$, following DMSO, A1 induced

clear Ca^{2+} influx, while following 100 μM Ned-19 (5 minutes), such responses were partially reduced. Similar results were obtained with H07 (Fig.4.3.4F). Ned-19 therefore has inhibitory effects on A1 and H07-induced Ca^{2+} influx but requires a high concentration. The effect of 100 μM Ned-19 on ML-SA1 induced Ca^{2+} signals was examined as well. As shown in Fig. 4.3.4G, in cells expressing $TRPML1^{\Delta NC}$ (the PM version of TRPML1), ML-SA1-induced Ca^{2+} signals were maintained upon a 5-minute treatment with 100 μM Ned-19. The effect of 100 μM Ned-19 on A1-, H07- and ML-SA1-induced Ca^{2+} signals were quantified in Fig.4.3.4H.

Ned-19 was also tested in cells transiently expressing TPC2 GCaMP6s. In these experiments, cells were pre-treated with DMSO or 10 μM Ned-19 for 1hr prior to stimulation with A1. As shown in Fig.4.3.4I, Ned-19 tended to reduce the magnitude of A1-induced Ca^{2+} release, but it did not reach statistical significance (P-value= 0.07) as in one experiment there was no effect of Ned-19 on A1 responses (Fig.4.3.4J). I also studied the effect of Ned-19 on ML-SA1-induced Ca^{2+} release in cells expressing TRPML1 GCaMP6s. As shown in Fig.4.3.4K and L, interestingly, Ned-19 appeared to block ML-SA1-induced Ca^{2+} release as reflected by a trend for the magnitude of the responses to be reduced compared to the DMSO control.

Collectively, Ned-19 tended to cause differential effects on A1- and ML-SA1-induced Ca^{2+} influx and Ca^{2+} release.

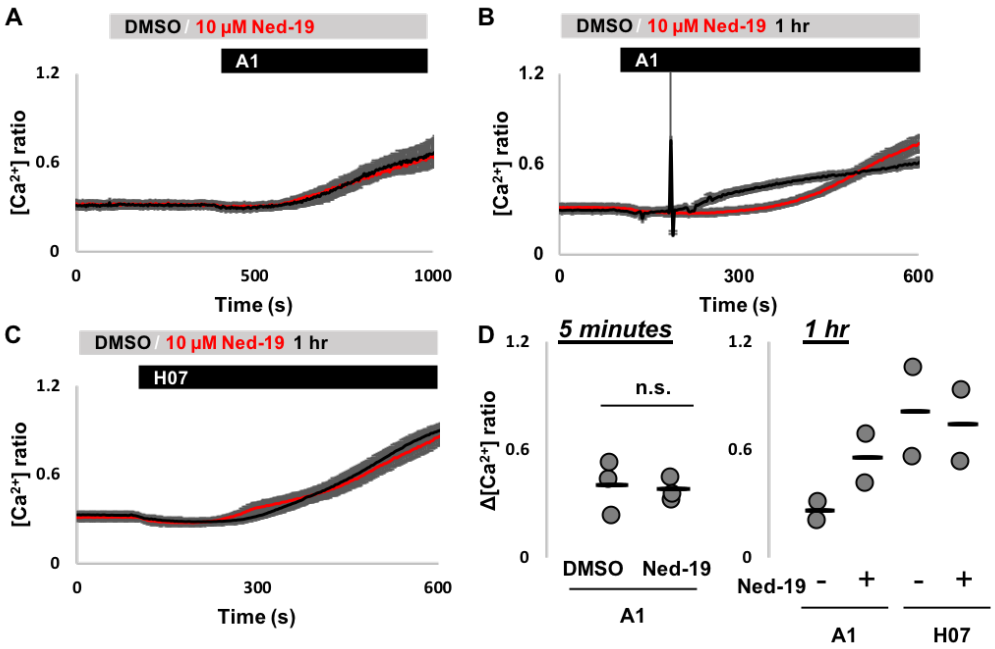

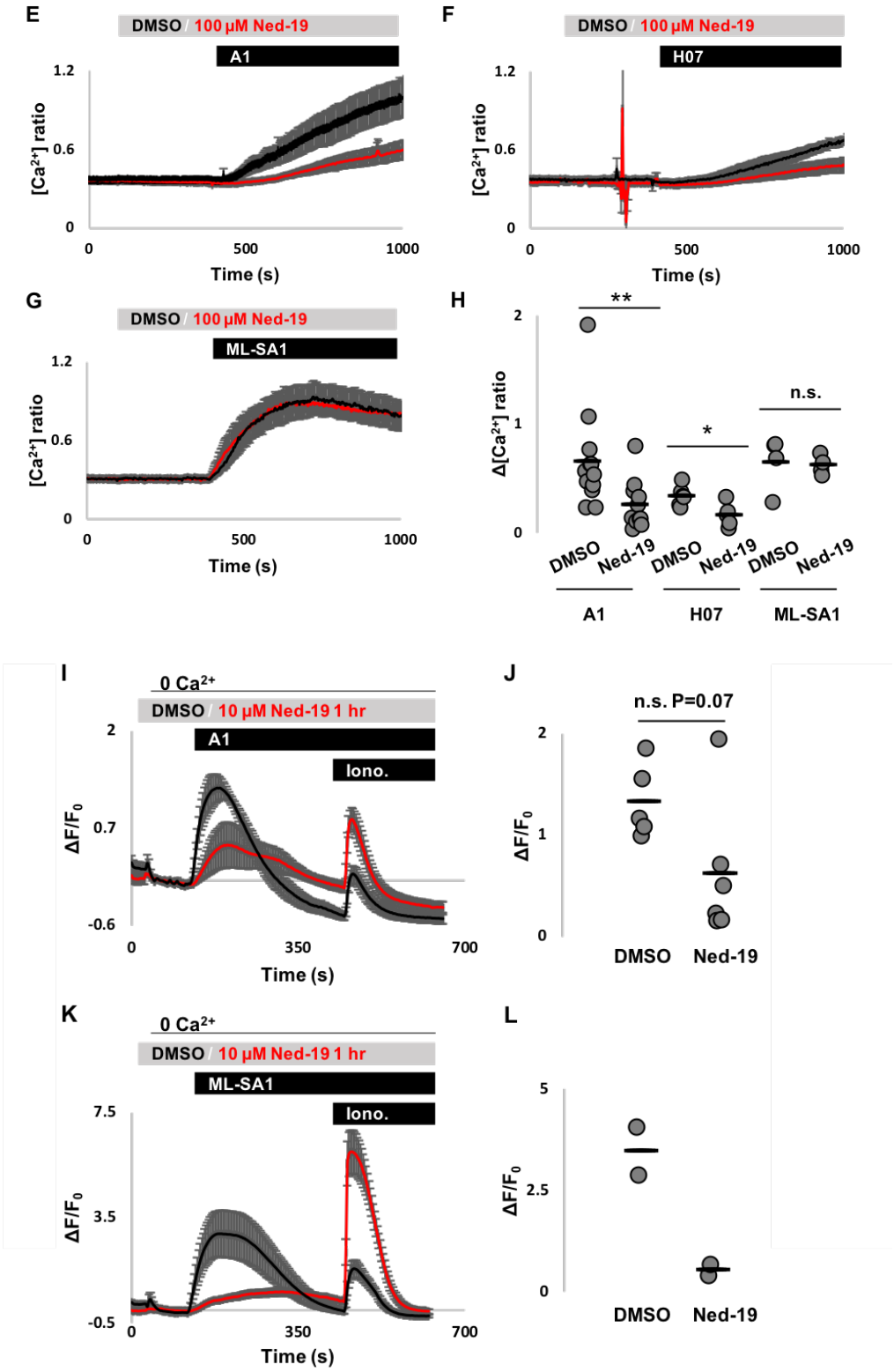

Figure 4.3.4 Ned-19 appears to have differential effects on agonist-induced Ca^{2+} influx and Ca^{2+} release

(A) Average cytosolic Ca^{2+} responses to A1 (10 µM) following DMSO or Ned-19 (10 µM) treatment for 5 minutes (mean ± S.E.M, 3 independent experiments) in HeLa cells transiently

expressing $TPC2^{LL/AA}$. The bar above graph indicates the time of addition of the compound, DMSO or Ned-19 was added at 90s, A1 was added at 390s.

(B and C) Average cytosolic Ca^{2+} responses to A1 (10 μM) (B) or H07 (30 μM) (C) following DMSO or Ned-19 (10 μM) treatment for 1 hr (mean from one independent experiment, S.E.M based on the number of cells from the experiment) in HEK293 cells stably expressing $TPC2^{LL/AA}$. A1 or H07 was added at 90s as indicated by the bar.

(D) Left panel: pooled data quantifying magnitude of A1 Ca^{2+} responses in A (n=3); n.s. not statistically significant was determined by independent-samples t-tests. Right panel: pooled data quantifying Ca^{2+} responses to A1 and H07 following 1 hr DMSO or Ned-19; each point plot represents one experiment (n=2).

(E and F) Average cytosolic Ca^{2+} responses to A1 (10 μM) (E) or H07 (10 μM) (F) following DMSO or Ned-19 (100 μM) treatment for 5 minutes (mean ± S.E.M, 5-11 independent experiments) in HeLa cells transiently expressing $TPC2^{LL/AA}$. DMSO or Ned-19 was added at 90s and A1 was added at 390s as indicated by the bar.

(G) Average cytosolic Ca^{2+} responses to ML-SA1 (3.16 μM) following DMSO or Ned-19 (100 μM) treatment for 5 minutes (mean ± S.E.M, 3 independent experiments) in HeLa cells transiently expressing $TRPML1^{\Delta NC}$.

(H) Pooled data quantifying magnitude of A1, H07 and ML-SA1 Ca^{2+} responses in E-G. n.s. not statistically significant * $P<0.05$ ** $P<0.01$ were determined by independent-samples t-tests or Mann-Whitney U test.

(I) Average cytosolic Ca^{2+} responses to A1 (30 μM), and then to ionomycin (Iono. 2 μM) following DMSO or Ned-19 (10 μM) treatment for 1 hr (mean ± S.E.M, 5-6 independent experiments) in HeLa cells transiently expressing TPC2 GCaMP6s. Experiments were performed in the absence of extracellular Ca^{2+}. Cells were immersed into Ca^{2+}-free HBS at 30s and were stimulated with A1 at 120s and Iono. at 450s. GCaMP6s fluorescence value has been normalized to basal fluorescence (i.e. $\Delta F/F_0$).

(J) Pooled data quantifying magnitude of A1 Ca^{2+} responses in I; n.s. not statistically significant was determined by Mann-Whitney U test.

(K) Average cytosolic Ca^{2+} responses to ML-SA1 (3.16 μM), and then to Iono. (2 μM) following DMSO or Ned-19 (10 μM) treatment for 1 hr (mean from one independent experiment, S.E.M based on the number of cells from the experiment) in HeLa cells transiently expressing TRPML1 GCaMP6s.

(L) Pooled data quantifying Ca^{2+} responses to ML-SA1 following 1hr DMSO or Ned-19; each point plot represents one experiment (n=2).

4.3.5 Mutation of a lysine residue reduces H07- but not A1-mediated Ca^{2+} signals in cells transiently expressing plasma membrane targeted TPC2

In contrast to NAADP, $PI(3,5)P_2$ is known to activate TPCs directly. A recent study on HsaTPC2 revealed that a number of lysine residues within the IS4-S5 linker (K203, K204 and K207) form the $PI(3,5)P_2$ binding site and are necessary for activation of the channel by $PI(3,5)P_2$ (She et al., 2019). I therefore examined the effects of mutating these residues on A1- and H07-induced Ca^{2+} signals. To do this, I used Fura-2 labelled cells transiently expressing $TPC2^{LL/AA}$ (the PM version of TPC2) with and without mutated lysine residues. Confocal imaging revealed that $TPC2^{LL/AA}$ with the K203A, K204A or K207A mutation were all expressed at the PM (Fig.4.3.5A-C). Functionally, as shown in Fig.4.3.5D, F and L, A1-induced Ca^{2+} signals appeared slightly potentiated in cells expressing $TPC2^{LL/AA}$ with the K203A mutation compared to that without K203A mutation. However, the magnitude of the signals by A1 in the presence of the mutation was not statistically different compared to the control (Fig.4.3.5N). H07-induced Ca^{2+} signals were unchanged in magnitude by K203A mutation (Fig.4.3.5E, G, M and N). I next assessed the impact of K204A mutation, as shown in Fig.4.3.5D, H and O, A1-induced Ca^{2+} signals were comparable in cells expressing $TPC2^{LL/AA}$ with and without K204A mutation. In contrast, H07-induced Ca^{2+} signals were reduced by half (Fig.4.3.5E, I and P). The magnitude of the responses to A1 or H07 in the presence or the absence of K204A mutation were quantified in Fig.4.3.5Q. Finally, I examined the effect of the K207A mutation. Both A1- and H07-induced Ca^{2+} signals were maintained in magnitude in the mutant-expressed cells (Fig.4.3.5D, E, J, K and R-T). Taken together, these data indicate that K203 and K207 have no major role on A1 or H07 action, while K204 is selectively required for H07 but not A1-induced Ca^{2+} signals.

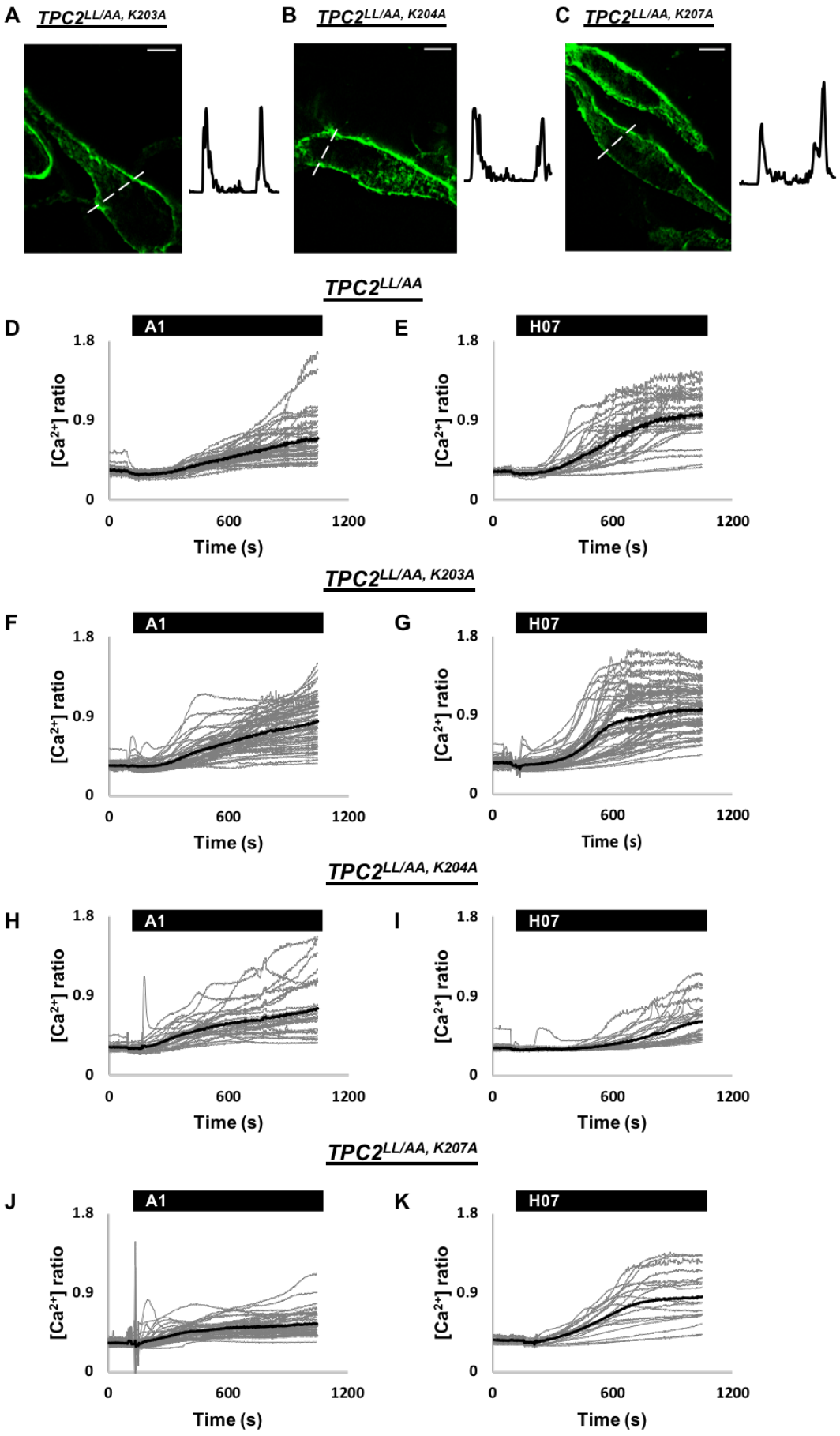
A
TPC2LL/AA, K203A
B
TPC2LL/AA, K204A
C
TPC2LL/AA, K207A
TPC2LL/AA
D
A1
E
H07
TPC2LL/AA, K203A
F
A1
G
H07
TPC2LL/AA, K204A
H
A1
I
H07
TPC2LL/AA, K207A
J
A1
K
H07
[Ca2+] ratio
1.8
0.9
0
0
600
1200
Time (s)

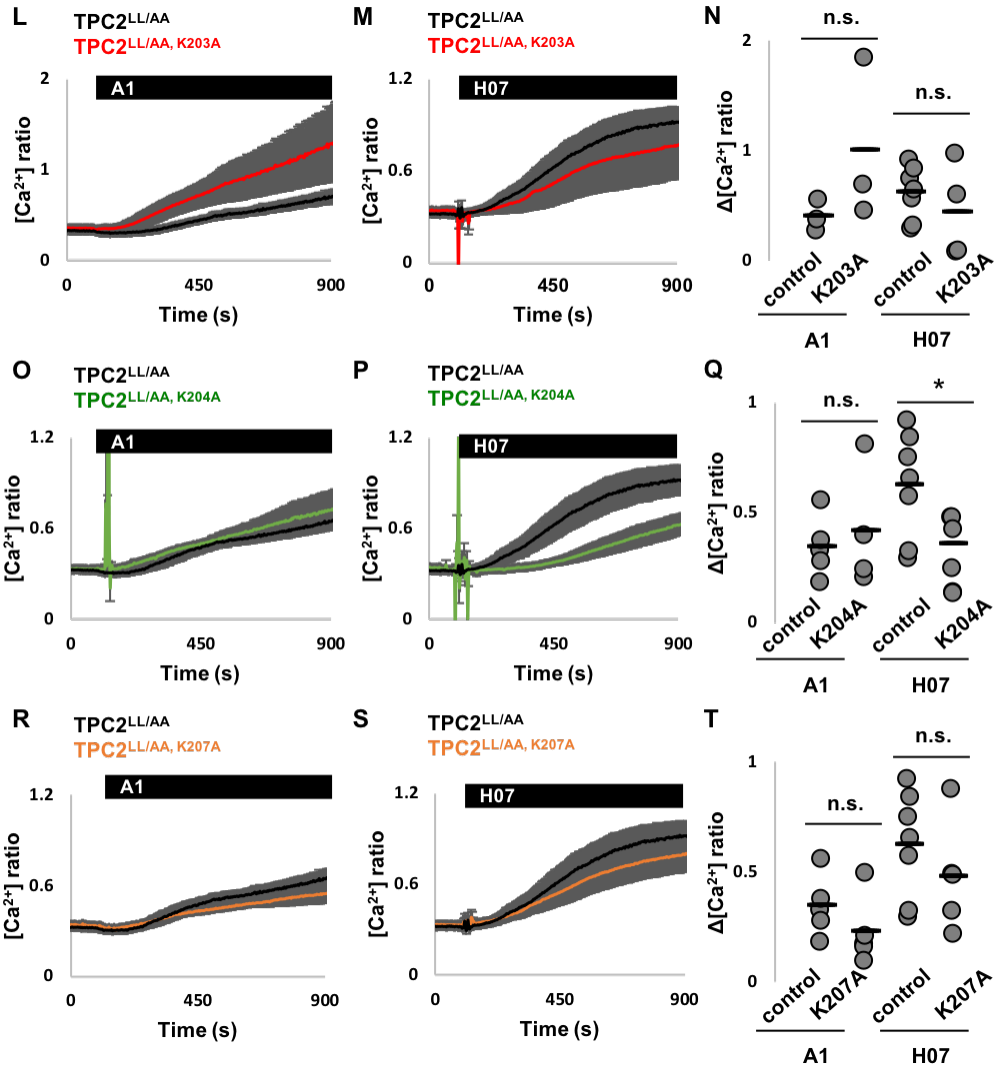

Figure 4.3.5 Mutation of a lysine residue reduces H07- but not A1-mediated Ca^{2+} signals in cells transiently expressing plasma membrane targeted TPC2

(A-C) Representative confocal images of HeLa cells transiently expressing $TPC2^{LL/AA, K203A}$ (A), $TPC2^{LL/AA, K204A}$ (B) or $TPC2^{LL/AA, K207A}$ (C). Scale bar = 10 µm. The fluorescence intensity plot on the right hand corresponds to the dashed line.

(D, F, H and J) Cytosolic Ca^{2+} responses to A1 (10 µM) in individual HeLa cells transiently expressing $TPC2^{LL/AA}$ (D), $TPC2^{LL/AA, K203A}$ (F), $TPC2^{LL/AA, K204A}$ (H) or $TPC2^{LL/AA, K207A}$ (J). The bars above graphs indicate the time of addition of the compound, which was at 90s. Gray traces represent recordings of all individual cells and black traces represent the population average.

(E, G, I and K) Cytosolic Ca^{2+} responses to H07 (30 µM) in individual HeLa cells transiently expressing $TPC2^{LL/AA}$ (E), $TPC2^{LL/AA, K203A}$ (G), $TPC2^{LL/AA, K204A}$ (I) or $TPC2^{LL/AA, K207A}$ (K)

(L and M) Average cytosolic Ca^{2+} responses to A1 (10 μM) (L) or H07 (30 μM) (M) in HeLa cells transiently expressing $TPC2^{LL/AA}$ or $TPC2^{LL/AA, K203A}$ (mean ± S.E.M, 3-7 independent experiments).

(N) Pooled data quantifying magnitude of Ca^{2+} responses to A1 or H07 in L and M. n,s, not statistically significant was determined by independent-samples t-tests.

(O-Q) Similar to L-N except cells were transiently transfected with $TPC2^{LL/AA, K204A}$ rather than $TPC2^{LL/AA, K203A}$ (mean ± S.E.M, 4-7 independent experiments). n,s, not statistically significant * $P<0.05$ were determined by independent-samples t-tests.

(R-T) Similar to L-N except cells were transiently transfected with $TPC2^{LL/AA, K207A}$ rather than $TPC2^{LL/AA, K203A}$ (mean ± S.E.M, 4-7 independent experiments). n,s, not statistically significant was determined by independent-samples t-tests.

4.3.6 Mutation of a lysine residue reduces H07- but not A1-mediated Ca^{2+} release in cells transiently expressing lysosomal TPC2

The findings that K204 is required for activation of TPC2 by H07 but not A1 was further investigated in the lysosome environment, by using cells transiently expressing TPC2 GCaMP6s with and without the K204A mutation. When examined by confocal microscopy, TPC2 GCaMP6s with the K204A mutation had a punctate distribution as well as a reticular appearance (Fig.4.3.6A). As shown in Fig.4.3.6B and C, A1-induced Ca^{2+} release was similar in magnitude in cells expressing TPC2 GCaMP6s with and without the K204A mutation. In contrast, the K204A mutation significantly reduced the magnitude of H07-induced Ca^{2+} release (Fig.4.3.6D and E). Thus, similar to the results obtained with PM TPC2, lysosomal TPC2 shows a selective requirement of K204 when activated by H07.

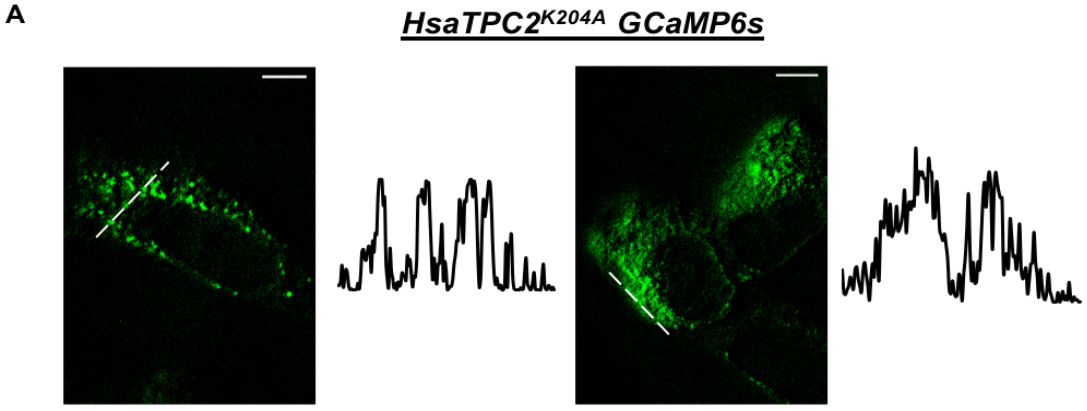

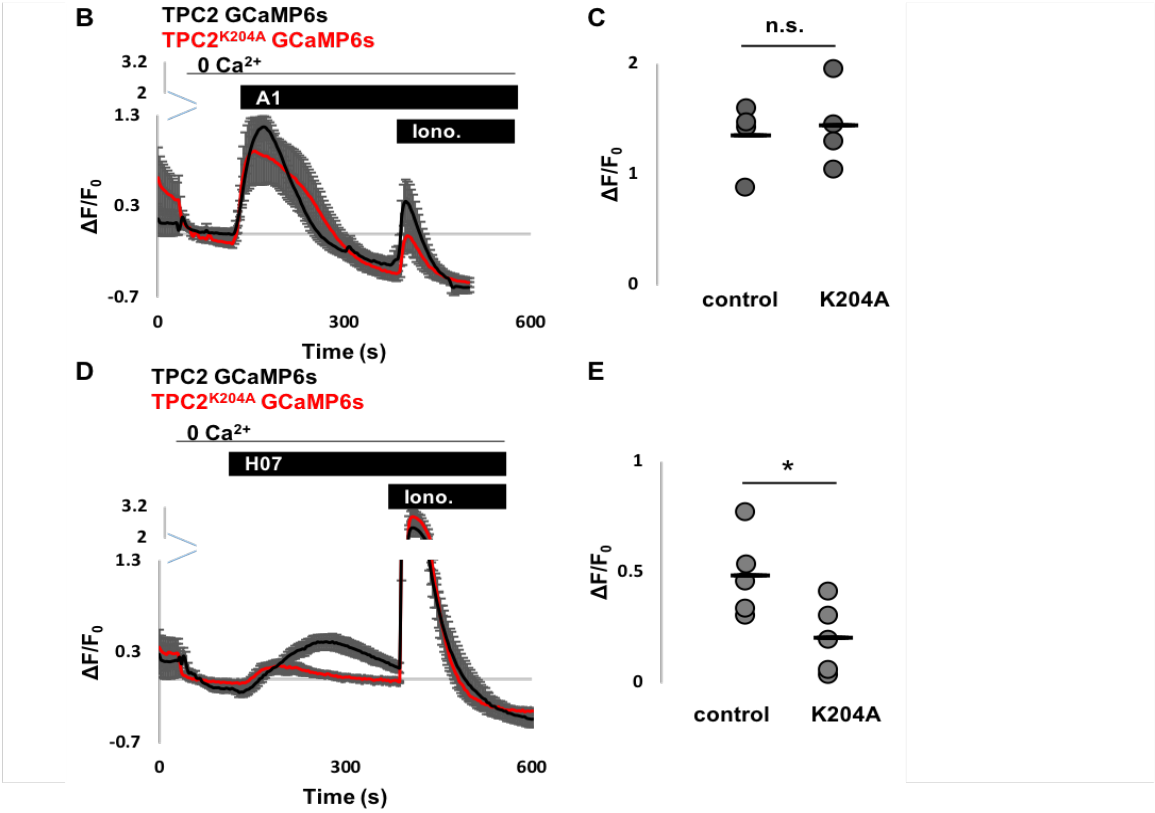

Figure 4.3.6 Mutation of a lysine residue reduces H07- but not A1-mediated Ca^{2+} release in cells transiently expressing lysosomal TPC2

(A) Confocal images of HeLa cells transiently expressing $TPC2^{K204A}$ GCaMP6s. Scale bar = 10 μm. The fluorescence intensity plot on the right hand corresponds to the dashed line.

(B) Average cytosolic Ca^{2+} responses to A1 (30 μM), and then to ionomycin (Iono.) (2 μM) in cells transiently expressing TPC2 GCaMP6s or $TPC2^{K204A}$ GCaMP6s (mean ± S.E.M, 4 independent experiments). Experiments were performed in the absence of extracellular Ca^{2+}. Cells were immersed into Ca^{2+}-free HBS at 30s and were stimulated with A1 or H07 at 120s and Iono. at 390s.

(C) Pooled data quantifying magnitude of Ca^{2+} responses to A1 in B; n.s. not statistically significant was determined by independent-samples t-tests.

(D and E) Similar to B and C except cells were stimulated with H07 (60 μM) (mean ± S.E.M, 5 independent experiments). *P<0.05 was determined by independent-samples t-tests.

4.3.7 Extracellular acidic pH profoundly inhibits H07- but not A1-mediated Ca^{2+} signals in cells stably expressing plasma membrane targeted TPC2

Thus far, the effect of lysosomal luminal pH on TPCs is ambiguous. I therefore examined the effects of acidifying the extracellular (luminal) medium on A1 and H07-induced Ca^{2+} signals in cells stably expressing $TPC2^{LL/AA}$ (the PM version of TPC2). I reduced the pH from 7.4 to 5.5. As shown in Fig.4.3.7A and B, A1-induced Ca^{2+} signals were similar in magnitude at pH 7.4 and pH 5.5, although the rate of rise at pH 5.5 appeared to be slightly quicker than that at pH 7.4. In sharp contrast, H07-induced Ca^{2+} signals were abolished upon such a reduction in the pH (Fig.4.3.7C and D). At pH 5.5, ionomycin was added after H07 and was capable of inducing Ca^{2+} signals (Fig.4.3.7C). Taken together, these data indicate that acidic luminal pH has an inhibitory effect on H07- but not A1-mediated Ca^{2+} signals.

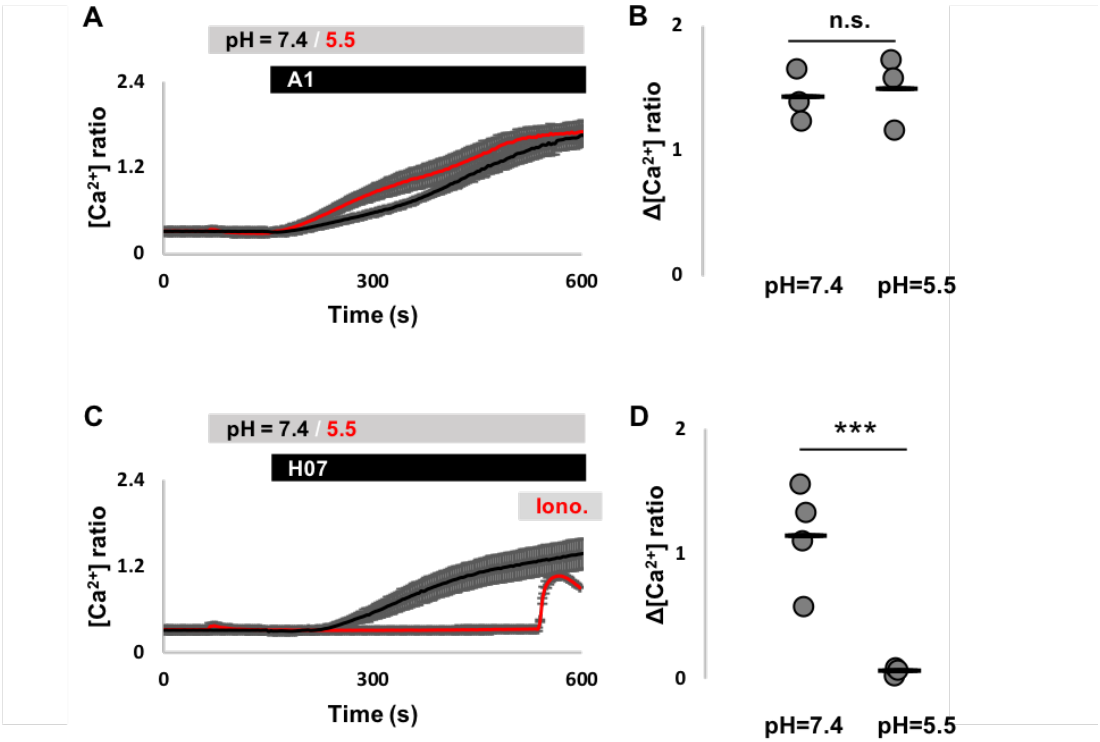

Figure.4.3.7 Extracellular acidic pH profoundly inhibits H07- but not A1-mediated Ca^{2+} signals in cells stably expressing plasma membrane targeted TPC2

(A) Average cytosolic Ca^{2+} responses to A1 (30 μM) at extracellular (luminal) pH of 7.4 or 5.5 in HEK293 cells stably expressing $TPC2^{LL/AA}$ (mean ± S.E.M, 3 independent experiments).

Cells were immersed into MBS (pH=5.5) at 60s and were stimulated with A1 or H07 at 150s as indicated by the bar.

(B) Pooled data quantifying magnitude of Ca^{2+} responses to A1 in A; n.s. not statistically significant was determined by independent-samples t-tests.

(C and D) Similar to A and B except cells were stimulated with H07 (60 μM) (mean ± S.E.M, 3-4 independent experiments). At pH 5.5, ionomycin (Iono.) (2 μM) were added after H07 at 540s. *** P<0.001 was determined by independent-samples t-tests.

4.3.8 Mutation of a histidine residue appears to have a pH-specific effect on A1- but not H07-induced Ca^{2+} signals in cells transiently expressing plasma membrane targeted TPC2

Histidine residues (pKa of 6) are known to mediate pH sensitivity of ion channels (Chanchevalap et al., 2000; Kim et al., 2008; Li & Hong, 2011; Sandoz et al., 2009). There are two luminal histidine residues within S3-S4 of domain I (H181) and domain II (H527) (Fig.4.3.8A). In comparison, H527 is more conserved among TPC2 across different species than H181. H527 might represent a functional pH sensor for TPC2. I therefore mutated H527 and examined its effects on A1- and H07-induced Ca^{2+} signals. I used cells transiently expressing $TPC2^{LL/AA}$ (the PM version of TPC2) with and without the H527A mutation. Confocal imaging revealed that $TPC2^{LL/AA}$ with H527A mutation had PM localization (Fig.4.3.8B). As shown in Fig.4.3.8C and E, In cells expressing $TPC2^{LL/AA}$, H07-induced Ca^{2+} signals appeared to be abolished upon a reduction in pH from 7.4 to 5.5, reproducing the results shown in Fig.4.3.7C and D. Essentially similar results were obtained upon H527A mutation (Fig.4.3.8D and E). Thus, H527 appears not to mediate the effect of acidic pH on H07-induced Ca^{2+} signals.

I also studied the effects of the mutation on A1-induced Ca^{2+} signals. As shown in Fig.4.3.8F, in cells expressing $TPC2^{LL/AA}$, A1-induced Ca^{2+} signals appeared similar at pH 7.4 and pH 5.5, reproducing the results shown in Fig.4.3.7A and B. Upon H527A mutation, however, A1-induced Ca^{2+} signals tended to be larger at pH 7.4 than that at pH 5.5 (Fig.4.3.8G). The magnitude of responses to A1 under different conditions were quantified in Fig.4.3.8H. Thus, H527A mutation seems to potentiate A1-induced Ca^{2+} signals in a pH-dependent manner.

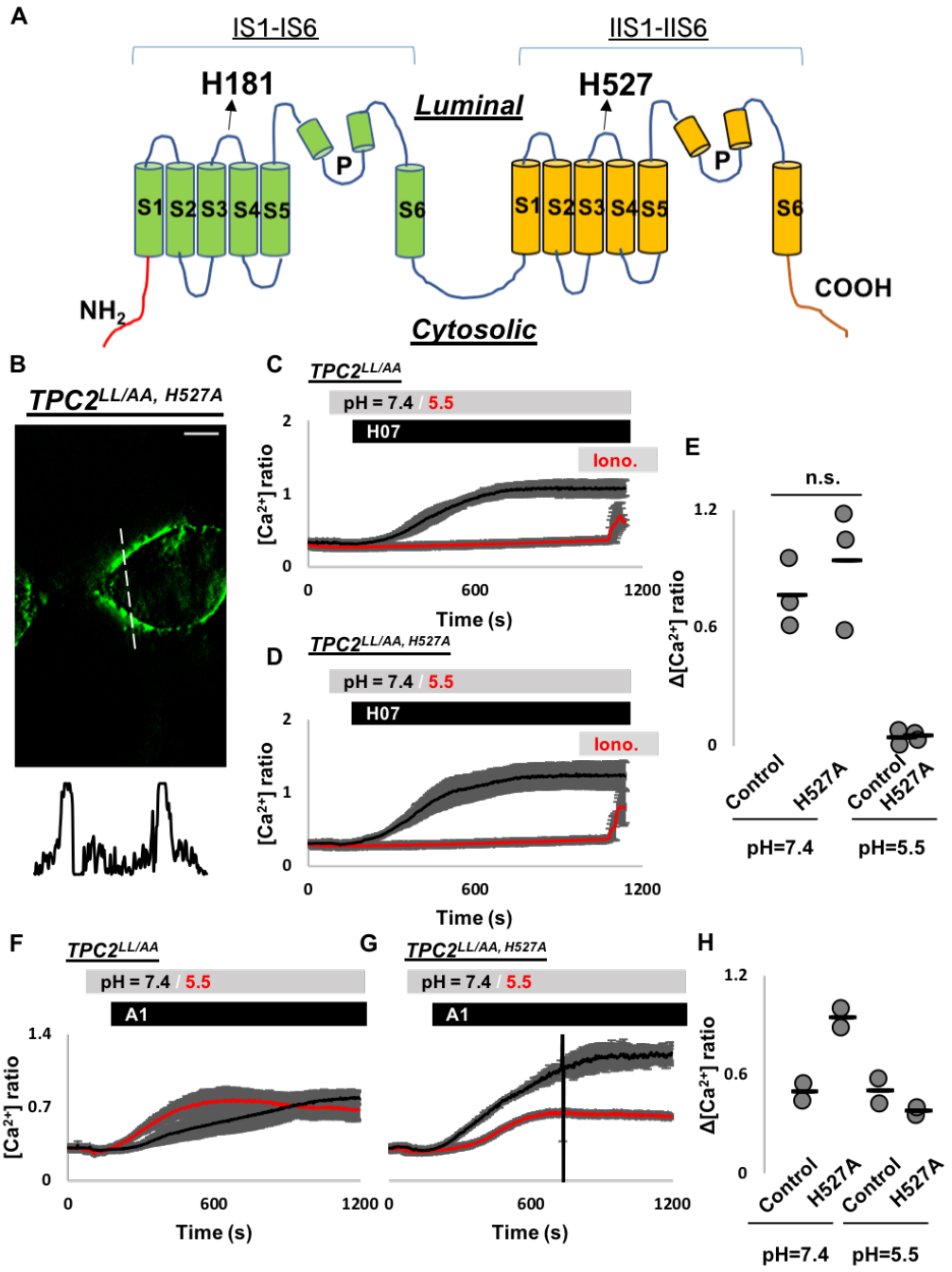

Figure.4.3.8. Mutation of a histidine residue appears to have a pH-specific effect on A1 but not H07-induced Ca^{2+} signals in cells transiently expressing plasma membrane targeted TPC2

(A) Topology of an HsaTPC2 subunit, containing two domains each with six membrane-spanning regions. H181 and H527 are within the luminal S3-S4 linkers of TPC2 (arrows).

(B) Representative confocal image of HeLa cells transiently expressing $TPC2^{LL/AA, H527A}$. Scale bar = 10 μm. The fluorescence intensity plot below corresponds to the dashed line.

(C and D) Average cytosolic Ca^{2+} responses to H07 (30 μM) at extracellular (luminal) pH of 7.4 or 5.5 in HeLa cells transiently expressing $TPC2^{LL/AA}$ (C) or $TPC2^{LL/AA,\ H527A}$ (D) (mean from a representative experiment, S.E.M. based on all cells in the experiment). Cells were immersed into MBS (pH=5.5) at 60s and were stimulated with A1 or H07 at 150s as indicated by the bar.

(E) Pooled data quantifying magnitude of Ca^{2+} responses to H07 under the indicated conditions. Each plot point represents one experiment (n=2-3), n.s. not statistically significant was determined by independent-samples t-tests.

(F-H) Similar to C-E except cells were stimulated with A1 (10 μM) (n=2).

4.4 Discussion

As ion channels associated with health and disease, fundamental properties of TPCs are still debated (e.g. activation mechanism and ion selectivity). In addition, although being localized to acidic stores, the role of acidic pH on TPC2 activity is also equivocal. In chapter 3, I used two novel cell-permeable TPC2 activators to establish the Ca^{2+} permeability of TPC2, a property lacking consistent support from electrophysiological measurements (Grimm et al., 2014; Guo et al., 2017; Jha et al., 2014; She et al., 2019; Wang et al., 2012). Here, I further characterized A1 and H07 to address controversial aspects of TPCs, and through which I uncover that TPC2 operates in an agonist-specific manner.

On the one hand, TPC2 was characterised as a non-selective (i.e. calcium-permeable) channel (Brailoiu, Rahman, et al., 2010; Grimm et al., 2014; Jha et al., 2014), while on the other hand, it emerged as a highly Na^+-selective channel (Boccaccio et al., 2014; Guo et al., 2017; Wang et al., 2012). In chapter 3, I demonstrated that TPC2 is permeable to Ca^{2+} in a cellular environment. In this chapter I examined the permeability of TPC2 to Na^+. Compared to well-established Ca^{2+} imaging methods, the development of Na^+ imaging is lagging behind. Among a limited number of commercially available Na^+ indicators, SBFI is the only one that can function in a ratio-metric mode (Minta & Tsien, 1989) and it has been widely used to record intracellular Na^+ alterations (Donoso et al., 1992; Harootunian et al., 1989; Iamshanova et al., 2016; Lasser-Ross & Ross, 1992; C.R. Rose et al., 1999; Christine R. Rose, 2012). I therefore utilized SBFI to record Na^+ changes in response to A1 and

H07. In cells expressing plasma membrane targeted TPC2, 30 μM A1 and H07 induced robust Ca^{2+} entry (chapter 3). Hence, I used the same concentrations and observed an increase in cytosolic Na^+ level by A1 and H07 (Fig.4.3.1), reaffirming the Na^+ permeability of TPC2. Consistent with my Na^+ imaging results, Gerndt et al., 2020 found that A1 and H07 are capable of mediating Na^+ currents using the patch-clamp method to directly record from enlarged endo-lysosomes expressing TPC2 (Gerndt et al., 2020). In the Na^+ imaging study (here), A1 and H07 have similar effects on Na^+ entry. However, the electrophysiological analyses revealed larger Na^+ currents for H07 compared to A1 (Gerndt et al., 2020). The discrepant results might be a result of saturation of SBFI with Na^+. Aside from SBFI, the other current available indicators are ANG, Sodium Green and CoroNa Green. Compared to the others, SBFI has the highest Na^+ binding affinity (Despa et al., 2000; Iamshanova et al., 2016), implying it could become saturated. In addition, SBFI has a small fluorescence change upon Na^+ binding (Minta & Tsien, 1989), which may have masked the differences in Na^+ signals by A1 and H07. To test for saturation, gramicidin (Meier et al., 2006), a Na^+ ionophore, could be added after A1 and H07 during the Na^+ recording. Alternatively, I could replace SBFI with ANG that has a lower Na^+ binding affinity (i.e. a higher Kd value) and a bigger fluorescence change in response to Na^+ increases, (Iamshanova et al., 2016; Lamy & Chatton, 2011). Although ANG is a single wavelength dye, like SBFI, it is able to record changes in intracellular Na^+ level within 0-50 mM range. This is the usual Na^+ change observed during physiological responses (Lamy & Chatton, 2011; Meier et al., 2006; Ona-Jodar et al., 2017).

Although only studied with PM TPC2, the ability of A1 and H07 to induce Na^+ signals is clear. In chapter 3, I revealed that A1 was a stronger Ca^{2+} agonist than H07. In line with this, here, at 30 μM, A1 induced significantly larger and faster Ca^{2+} signals than H07 in cells expressing PM TPC2 (Fig.4.3.2A-C). In contrast, A1 and H07 had similar effects on Na^+ entry (Fig.4.3.1 and 4.3.2D-F), and electrophysiology studies revealed a larger Na^+ currents by H07 than by A1 (Gerndt et al., 2020). A1 and H07's effects on Na^+ therefore did not "follow" their effects on Ca^{2+}. As A1 mediates stronger Ca^{2+} signals and H07 mediates stronger Na^+ currents, this raises an intriguing possibility that the selectivity of TPC2 to Ca^{2+} and Na^+ might agonist dependent.

I compared the kinetics of the agonist-evoked Ca^{2+} and Na^{+} signals in cells expressing PM TPC2. For A1, the Ca^{2+} and Na^{+} signals tended to occur simultaneously, immediately after addition, and at a similar rate (Fig.4.3.2G). While for H07, its Ca^{2+} signals occurred a few minutes after the onset of its Na^{+} signals (Fig.4.3.2H). This is perplexing. One possibility to explain this is that Na^{+} and Ca^{2+} compete for entry when TPC2 is activated by H07. Consistent with this, I found that removing extracellular (luminal) Na^{+} profoundly increased H07 but not A1-induced Ca^{2+} signals (Fig.4.3.3). To note, in the absence of extracellular Na^{+}, NCX which is expressed in non-excitable cells (including HEK293 cell line) might be activated (Eder et al., 2007; Markova et al., 2014) in reverse mode (Ca^{2+} entry-Na^{+} extrusion) (Blaustein & Lederer, 1999; Iwamoto, 2005; Verkhratsky et al., 2018). However, given that removing extracellular Na^{+} potentiated H07-induced Ca^{2+} signals whereas only modestly increased the rate of the Ca^{2+} rise by A1, NCX is unlikely to be the major reason for the potentiation on Ca^{2+} signals upon removal of Na^{+}. To confirm this, I could test NCX inhibitors that are known to block the reverse mode of NCX (Iwamoto, 2007; Iwamoto et al., 2004; Iwamoto & Kita, 2006). The implication from the above imaging results is that Na^{+} is the predominant ion that passes through H07- but not A1-activated TPC2. In support of this, the delay in the onset of H07-induced Ca^{2+} signals was eliminated in the absence of Na^{+} (Fig.4.3.3D). In addition, Jha et al., 2014 shows that $PI(3,5)P_2$-induced Ca^{2+} influx through PM TPC2 was potentiated when lowering "luminal" Na^{+} (Jha et al., 2014). H07-activated TPC2 therefore might be a Na^{+}-selective channel like in the presence of $PI(3,5)P_2$. Conversely, given 1) the simultaneous onset of A1's Ca^{2+} and Na^{+} signals; 2) that the removal of "luminal" Na^{+} only slightly altered the rate of the Ca^{2+} rise by A1, A1-activated TPC2 might be non-selective like in the presence of NAADP. To further test this, future experiments should examine the agonists' Na^{+} signals in the absence of extracellular (luminal) Ca^{2+}. Collectively, my imaging results suggest that A1 and H07 may confer TPC2 with different ion selectivity.

Gerndt and colleagues directly measured the Ca^{2+} and Na^{+} permeability ratio (PCa/PNa) of A1- and H07-induced currents. In concert with my imaging results, the ratio for H07 is 0.04 ± 0.01, thus Na^{+} selective, whereas, the ratio for A1 is 0.65 ± 0.13, thus non-selective (Gerndt et al., 2020). In parallel studies, Gerndt and colleagues examined P_{Ca}/P_{Na} in response to NAADP and $PI(3,5)P_2$. Strikingly, they found the ratio for A1 is similar to that for NAADP (0.73 ± 0.14), and the ratio for H07 is similar

to that for $PI(3,5)P_2$ (0.08 ± 0.01) (Gerndt et al., 2020). Such observations thus indicate TPC2 is a non-selective Ca^{2+} permeable channel when activated by A1 or NAADP, while a Na^+ selective channel when activated by H07 or $PI(3,5)P_2$. The ion selectivity of TPC2 therefore is agonist-dependent. Such findings could resolve the long-held controversary surrounding the gating and selectivity of TPC2.

Ion selectivity is thought to be an intrinsic and immutable property of ion channels. Here, the agonist-specific ion selectivity of TPC2 indicates that this is not always the case. Aside from TPC2, there are other channels that have been shown to have malleable ion selectivity. For example, the CRAC channel can alter its Ca^{2+} selectivity depending on the levels of its cellular partner, STIM1 (McNally et al., 2012). The mitochondrial uniporter can change from Mn^{2+}-impermeable to permeable in the presence of its regulatory subunit, MICU1 (Kamer et al., 2018). TRPV1 and TRPV2 have dual activation gates with one at the selectivity filter (SF). The SF possesses conformational plasticity, and thus, conferring the channel with tunable ion selectivity (Cao et al., 2013; Zubcevic et al., 2018). Moreover, TEME16F increased its permeability to Cl- with increased intracellular Ca^{2+} level (Ye et al., 2019). Finally, P2X channels have been shown to increase their permeability to large cations upon sustained activation (Khakh & Lester, 1999; Virginio et al., 1999) although controversially (Li et al., 2015). However, it is important to note that TPC2 is unique compared to the others. To the best of my knowledge, TPC2 is the first ion channel that switch ion selectivity by endogenous ligands, while the other channels, as aforementioned, relies on accessory proteins or ions to alter ion selectivity.

As A1 and H07 appear to mimic NAADP and $PI(3,5)P_2$ in terms of the ion selectivity, whether they also share a similar mechanism of action with the endogenous cues was then examined. NAADP is thought to activate TPCs indirectly via putative NAADP binding proteins (Lin-Moshier et al., 2012; Marchant et al., 2012; Walseth et al., 2012), although the identity of the proteins is, as yet, unclear. The most widely used NAADP antagonist is Ned-19, which was identified by Naylor et.al in 2009 via a NAADP-ligand based screen (Naylor et al., 2009). As an antagonistic analogue of NAADP, Ned-19 therefore can offer a route to examine the possibility that A1 and H07 utilize a similar mechanism as NAADP to activate TPC2. In contrast to tetrandrine and other direct TPC2 blockers (chapter 3), in cells expressing PM TPC2, Ned-19 at 10 μM was

unable to alter A1- and H07-induced Ca^{2+} signals. Prolonging the Ned-19 treatment from 5 minutes to 1hr also appeared to have no inhibitory effect (Fig.4.3.4A-D). I therefore increased the concentration to 100 μM, which is a high concentration but has been used previously for probing NAADP signalling (Ali et al., 2016; Avdonin et al., 2017; Davis et al., 2020; Sakurai et al., 2015; Suárez-Cortés et al., 2017). Under these conditions, I observed an inhibitory effect of Ned-19 on A1 and H07-induced Ca^{2+} influx (Fig.4.3.4E, F and H). To note, 100 μM Ned-19 left ML-SA1-induced Ca^{2+} signals in cells expressing PM TRPML1 intact (Fig.4.3.4G and H), attesting to specificity. The use of PM TPC2 therefore indicates Ned-19 can block both A1 and H07 Ca^{2+} signalling but requiring high concentration. This low affinity is consistent with the results of Gunaratne and colleagues who recently found the IC_{50} for Ned-19 against NAADP-induced Ca^{2+} release in sea urchin egg homogenate was about 150 μM (Gunaratne, Johns, et al., 2018) and not in the nanomolar range as originally reported (Naylor et al., 2009; Rosen et al., 2009). In addition, in mammalian cells, they observed that 10 μM Ned-19 left NAADP Ca^{2+} signals intact (Gunaratne, Johns, et al., 2018). Therefore, it might be unavoidable that a high concentration of Ned-19 is needed for blocking Ca^{2+} signalling through TPC. I also tested Ned-19 against A1 in the lysosome environment. Different from its effects on A1-induced Ca^{2+} signals via PM TPC2, an hour treatment with 10 μM Ned-19 tended to reduce A1-induced Ca^{2+} release in cells expressing TPC2 GCaMP6s but this was not statistically significant (Fig.4.3.4I and J). The Inhibitory effect was observed 5 times. But in one experiment, Ned-19 had no effect, which could be an outlier. Interestingly, Ned-19 also appeared to inhibit ML-SA1-induced Ca^{2+} release in cells expressing TRPML1 GCaMP6s (Fig.4.3.4K and L). Therefore, compared to the PM, at lysosomes, Ned-19 tends to be more potent in blocking A1 action and non-selective. One consideration for such disparate results at the PM and the lysosomes is that Ned-19 might be a lysosomotropic compound, which accumulates at high concentrations inside lysosomes, and thus alkalizing lysosomal pH and disrupting lysosome function (Villamil Giraldo et al., 2014; Walls et al., 2010). However, in an early study by Naylor and colleagues, bafilomycin A1 treatment eliminated LTR staining but had no effect on the punctate and organellar localizations of Ned-19. Naylor and colleagues' observations therefore indicate that Ned-19 is not acid-trapped inside lysosomes but likely labelled NAADP receptors (Naylor et al., 2009).

It may not be easy to explain the differential activity of Ned-19 at the PM and the lysosomes. In fact, so far, our understanding of how Ned-19 functions in mammalian system is lacking. Its mechanism of action remains unclear. It has been reported that there are two binding sites for NAADP on its receptors, one is of high-affinity and one is of low-affinity. In the sea urchin system, Ned-19 has been proposed to block NAADP action via binding to one of the two sites, thus having an indirect action on TPC2 (Rosen et al., 2009). However, given that NAADP-induced Ca^{2+} release shows strong kinetic differences in sea urchin and mammals (Berg et al., 2000; Cancela et al., 1999; Churamani et al., 2006; Genazzani et al., 1996; Masgrau et al., 2003), the mechanism for Ned-19 in the sea urchin might not be applicable in the mammals. In our lab's recently published paper, we found that unlike raloxifene and fluphenazine, Ned-19 did not reduce the open time of human TPC2 (Penny et al., 2019). Ned-19 was therefore suggested to work at a distal site from the pore. But whether this is on the channel or an accessory protein is unclear. Given the lack of information as to how exactly Ned-19 behaves and here, Ned-19's non-selective action on lysosomal TPC, Ned-19 may not be the best tool to examine any similarity in the mechanisms underlying A1, H07 and NAADP action. BZ194, a N-alkylated nicotinic acid derivative (Dammermann et al., 2009), and PPADS are known to compete with NAADP in binding assays (Billington & Genazzani, 2007). These two compounds could be used in the future to replace Ned-19 to study the relationship between NAADP, A1 and H07.

Compared to NAADP, the mechanism by which $PI(3,5)P_2$ activates TPCs appears to be simpler. Structural studies indicate that it acts in a direct manner by binding to residues within the IS4-IS5 linker within domain I of the channel (She et al., 2018; Wang et al., 2012). Recently, a study on human TPC2 identified K203, K204 and K207 as critical (She et al., 2019). Mutation of any of them disrupted $PI(3,5)P_2$ activation. Here, I show that all three mutations seem to have no major impact on A1-induced Ca^{2+} influx, although it should be noted that the A1 responses in the presence of the mutations varied somewhat. Such variability "led to" a slight (statistically insignificant) potentiation in A1 responses in the presence of the K203A mutation (Fg.4.3.5L and N). Thus, it would be preferable to have more data for making a firmer conclusion regarding the effects of the mutations on the A1 responses. For H07, the K203A and K207A mutation displayed little effect on its Ca^{2+} signals. However, the K204A

mutation reduced H07-induced Ca^{2+} signals by half, which is in stark contrast to its effect on A1 action (Fig.4.3.5). K204 therefore was prioritised and studied in the lysosome environment. Consistent with the PM data, at lysosomes, again, the K204A mutation significantly reduced H07- but not A1-induced Ca^{2+} release (Fig.4.3.6O-Q). Collectively, H07 but not A1 requires K204 for action. This thus hints at a similar mechanism of action could be shared by H07 and $PI(3,5)P_2$. Interestingly, H07 also mimics $PI(3,5)P_2$ in rendering TPC2 Na^+ selective (Gerndt et al., 2020), as mentioned above. Thus, H07 might be a $PI(3,5)P_2$-like agonist. However, $PI(3,5)P_2$ is known to activate TPC1 and TRPML1 via binding to residues within IS4-IS5 linker of TPC1 (She et al., 2018) and the N-terminus of TRPML1 (Chen et al., 2017; Dong et al., 2010). In comparison, although it was clear that H07 is selective for TPC2 as H07 of 60 μM cannot activate TPC1 or TRPML1 to induce Ca^{2+} signals (chapter 3), it was less clear as to whether TPC1/TRPML1 are targets for H07 as higher concentrations (e.g. 100 μM) have not been tested. Nevertheless, H07 and $PI(3,5)P_2$ binding sites are likely overlapping but also different given the lack of effect of the K203A and K207A on H07 action. Returning to the differential effect of K204A mutation on A1 and H07-induced Ca^{2+} signals, it is clear that A1 and H07 activate TPC2 via different mechanisms. In addition, given the mechanism and ion selectivity similarity between H07 and $PI(3,5)P_2$, but not between A1 and $PI(3,5)P_2$, there could be a causal link between the gating mechanism (at the molecular level) and channel ion permeation, that is, K204 binding is associated with Na^+ selection in some way.

In contrast to A1 and H07 which alter TPC2 ion selectivity in an agonist-dependent manner, TCAs and riluzole (the other novel identified activators)-activated TPC2 are selective to Na^+ and have low Ca^{2+} permeability. However, unlike $PI(3,5)P_2$ and H07, TCAs and riluzole do not require K204 for action. This further reveals the agonist-specific gating mechanism of TPC2. Besides, this argues against K204 as the sole determinant for mediating Na^+ selectivity. Also, this highlights the importance of further investigating the molecular basis for activation by $PI(3,5)P_2$, H07, TCAs and riluzole and how this contributes to the Na^+ selectivity of the channel. Similar investigations should also be performed for A1 and NAADP that render TPC2 non-selective. Moreover, Zhang and colleagues found that TCAs-induced TPC2 currents exhibited strong inward rectification and voltage-dependence. In contrast, currents by riluzole was linear and voltage-independent resembling those induced by $PI(3,5)P_2$. It

is therefore concluded that there is agonist-specific voltage-gating mechanism of TPC2. Information for TPC2 activators has been summarised in Table 4.3.

Table 4.3 Characteristics of TPC2 activators

Name	**NAADP**	**PI(3,5)P_2**	**A1 (TPC2-A1-N)**	**H07 (TPC2-AI-P)**	**TCAs (LyNa-VAs)**	**Riluzole (Ly-NA1)**
Action on TPC1	Activator	Activator	No action at 30 μM	No action at 60 μM	Activator/ Inhibitor	Inhibitor
Action on TRPML1	Debated	Activator	No action at 30 μM	No action at 60 μM	No action	No action
Ionic selectivity	Ca^{2+}/Na^{+}= 0.7x	Ca^{2+}/Na^{+}= 0.08x	Ca^{2+}/Na^{+}= 0.7x	Ca^{2+}/Na^{+}= 0.05x	Na^{+} >> Ca^{2+}	Na^{+} >> Ca^{2+}
Voltage-dependent	no	no	no	no	yes	no
K204-dependent	_	yes	no	yes	no	no

As lysosomal ion channels, it has been reported that acidic pH regulates TPC2 channel activity. For example, in one study, acidic pH appeared to reduce the open probability of NAADP-activated TPC2 (Pitt et al., 2010), while in the other study, acidic pH potentiated TPC2-induced currents in the presence of NAADP (Schieder et al., 2010). To note, in Schieder et al. study, there was no TPC2 activity at pH 7.2 at all, which is not in agreement with data shown here and in other studies (Brailoiu, Rahman, et al., 2010; Gerndt et al., 2020; Wang et al., 2012; Zhang et al., 2019). Besides, there are also cases where TPCs seem to be pH-insensitive, and are active at both acidic and luminal pH (Wang et al., 2012). Through use of PM TPC2 which allows easy modification of the extracellular (luminal) pH, I observed that acidic pH left A1-induced Ca^{2+} signals intact, but blocked H07-induced Ca^{2+} signals (Fig.4.3.7). At lysosomes but not the PM, 30 μM A1 induced dramatic larger Ca^{2+} responses than 60 μM H07. In chapter 3, I reasoned that the cause for that was that A1 but not H07 coupled to the ER. And now, acidic pH's inhibitory effect on H07 but not A1 might be another reason. Regarding the inhibitory effect of acidic pH on H07 Ca^{2+} responses, there are a number of possibilities. First, H07 may be acid-trapped extracellularly and

thus unable to activate TPC2 given it requires K204 that is on the cytosolic side. However, if H07 is a lysosomotropic agent, one would expect a change in lysosomal pH by H07. In Gerndt et al., 2020, H07 cannot affect the pH. Second, protons may compete with Ca^{2+} to enter the cells via H07-activated TPC2. But there is no proton permeability for H07-activated TPC2 (Gerndt et al., 2020). Rather, A1 renders TPC2 proton-permeable. A final possibility is that the ion selectivity of H07-activated TPC2 is pH-sensitive. In other words, at acidic pH, H07-gated TPC2 becomes highly Na^{+} selective and therefore less Ca^{2+} permeable. If this is the case, then there should be a functional pH sensor within TPC2. Among the amino acids, histidine has a pKa of about 6 and is therefore protonated at acidic pH (Li & Hong, 2011). For this reason, histidine residues can render channels pH sensitive. For example, TREK1 lost its sensitivity to acidic pH upon H126 mutation (Sandoz et al., 2009). For TRPML3, regulation by luminal pH is mediated by a string of histidine residues on the luminal side of the channel (Kim et al., 2008). And there is a histidine residue-dependent pH regulation of ROMK channels (Chanchevalap et al., 2000). In TPC2, there are two histidine residues localized on the luminal side within the S3-S4 linkers on domain, H181 and H527. In comparison, H527 is more conserved than H181 across species, so I hypothesized that it function as a pH sensor for TPC2. H07 was tested upon H527A mutation. And I found that acidic pH still appeared to block H07-induced Ca^{2+} signals regardless of the presence of H527A mutation (Fig.4.3.8C, D and E). This implies that H527 is unlikely to be a pH sensor. Thus, future mutational studies are required which may identify the pH sensor. Interestingly, while testing A1 in the presence of H527 mutation as a control, its Ca^{2+} signals seemed to be potentiated compared to the WT channel but only at neutral pH (Fig.4.3.8F, G and H). The reason behind this is unclear, but worth further investigation. Collectively, the pH test revealed that A1- and H07-induced Ca^{2+} signals via TPC2 are differentially regulated by acidic pH and likely H527 as well.

A1 and H07 are different activators for TPC2 in terms of ion selectivity, K204 binding and acidic pH regulation, it is therefore of great interest to study the physiological consequence of activation of TPC2 by the agonists. Gerndt et al., 2020 examined the effects of A1 and H07 on certain key lysosomal functions. For example, Gerndt et al., 2020 revealed that A1 but not H07 increases lysosomal pH. Interestingly, previous studies have revealed increases in lysosomal pH upon NAADP stimulation (Cosker et

al., 2010; Morgan et al., 2013; Morgan & Galione, 2007). A1 therefore not only mimics NAADP in terms of ion selectivity but also physiological function. A1- but not H07-activated TPC2 is permeable to protons, this may explain why A1 but not H07 alters lysosomal pH. In addition, Gerndt et al., 2020, found that H07 but not A1 induces lysosomal exocytosis. Lysosomal exocytosis is a Ca^{2+}-sensitive process, which can be driven by local calcium released through TRPML1 (Dong et al., 2009; Samie et al., 2013; Tsunemi et al., 2019; Xu & Ren, 2015). There is also a study linking NAADP-activated TPCs to exocytosis stimulation (Davis et al., 2012). It is therefore surprising that H07 but not A1 has been linked to exocytosis given A1 is of high Ca^{2+} permeability but H07 is of low Ca^{2+} permeability. A1 but not H07 blocked lysosome motility (Gerndt et al., 2020). Perhaps, this is the reason that A1 cannot induce the exocytosis like NAADP pointing to subtle differences in their action. Collectively, A1 and H07 activate TPC2 differently, and in turn mediate distinct physiological activities. Thus, TPC2 can "switch" its physiological role depending on how it activated. As a final point, previous work has shown that NAADP-induced Ca^{2+} release was largely reduced by inhibiting $PI(3,5)P_2$ synthesis, while it is potentiated upon an increase in lysosomal $PI(3,5)P_2$ by expression of PIKfyve (a kinase that facilitates synthesis of $PI(3,5)P_2$ from PI(3)P) (Jha et al., 2014). $PI(3,5)P_2$ therefore has a permissive effect on NAADP action. In the real world, perhaps, the endogenous cues modulate TPC2 "collaboratively". Driven by this, it is necessary to explore whether A1 and H07 work in similar ways, and if they do, then how this affects the ion selectivity of TPC2 and downstream physiological effects.

To summarise, A1-activated TPC2 is non-selective for Ca^{2+} and Na^{+}, while H07-activated TPC2 is selective for Na^{+} over Ca^{2+}. A1 does not require the lysine residue K204 to activate the channel, while H07 does resembling $PI(3,5)P_2$. A1-induced Ca^{2+} signals via TPC2 are not affected by acidic pH, while H07-induced Ca^{2+} signals are inhibited by acidic pH. A1 and H07 therefore differentially activate TPC2 in terms of the ion selectivity, activation mechanism and pH regulation. These findings indicate that TPC2 signals in an agonist-specific manner, offering explanations for conflicting reports on TPC2 properties.

Chapter 5: Revealing a role for TPC2 in agonist-evoked global Ca^{2+} signalling

5.1 Introduction

A diverse range of cellular processes are co-ordinated by changes in cytosolic Ca^{2+}. Ca^{2+} signals can function locally, or the local signals propagate over long distances to function globally. TPCs induce local Ca^{2+} release from acidic compartments when activated by NAADP. Also, the local release by NAADP can generate global Ca^{2+} signals via initiating CICR through IP_3Rs and RyRs on the ER, which is ascribed to the MCSs formed between acidic stores and the ER (Kilpatrick et al., 2013, 2017; Penny et al., 2014)

Local Ca^{2+} release from endo-lysosomal organelles has long been appreciated for its role in vesicular fusion (or fission) (Luzio et al., 2007). In accord, TPCs participate in the regulation of endo-lysosomal trafficking, including trafficking of viruses (Sakurai et al., 2015) and cholesterol (Grimm et al., 2014). Additionally, TPCs regulate endo-lysosomal morphology (Hockey et al., 2015; Kilpatrick et al., 2017; Lin-Moshier et al., 2014; Ruas et al., 2010). As TPCs are required for global NAADP-induced Ca^{2+} signals, TPCs would not be limited to the "local" functions. However, although use of GPN, bafilomycin A1, Ned-19 and/or self-inactivating concentrations of NAADP, has shown that lysosomes and NAADP are important for a number of physiological agonist-induced global Ca^{2+} signals (e.g. carbachol, glucose, insulin and histamine) (summarised in Yates, 2017), there is very little direct evidence that TPCs are implicated in such cell-wide events. In other words, the functional requirement for TPCs during physiological Ca^{2+} signalling requires investigation.

The focus of this chapter therefore is to study whether TPCs are required for global Ca^{2+} signals evoked by extracellular stimuli. To do so, I used GPN (characterised in Chapter 2), novel identified TPC inhibitors (from chapter 3) and TPC knockdown.

5.2 Methods

5.2.1 Cell culture

Human dermal fibroblasts were cultured and were plated for imaging as described in chapter 2.

5.2.2 siRNA transfection

Fibroblasts were plated at 100,000 cells/ml (in 24 well-plate (on coverslips, 0.4 ml/well) for imaging or in 6 well-plate (2 ml/well) for quantitative PCR) and transfected with siRNA (15 nM) using lipofectamine RNAiMAX (Invitrogen) for 24 hours. After initial 24-hour treatment, fibroblasts were re-transfected with siRNA for another 24 hours and cultured for a final 24 hours in siRNA free media prior to imaging/qPCR. Details of siRNA used are listed below:

Name	**Brand**	**Product name**	**Target exon**	**Target sequence**
TPC1 siRNA	Thermo Fisher	s28727	22	GGCTACTATTATCTCAATA
TPC2 siRNA	Thermo Fisher	s47773	3	CGGTATTACTCGAACGTAT
Control siRNA	Qiagen	AllStars Negative Control siRNA		

The above TPC siRNAs have been confirmed to effectively knock down TPCs in fibroblasts (Kilpatrick et al., 2017).

5.2.3 Quantitative PCR

siRNA-transfected fibroblasts in 6 well plates were collected by scraping into RNA/DNA free tubes. Cells were then centrifuged for 5 minutes at 300xg. Supernatants were removed and pellets were stored at -80^{O}C. After thawing, RNA was extracted using the RNeasy Mini Kit and RNase-free DNase Set (both Qiagen) according to the manufacturer's procedures. cDNA was synthesized from RNA, using superscript III reverse transcriptase (Invitrogen). cDNA was then used as the template for the qPCR which was carried out using Bio-Rad CFX PCR detection system. cDNA

was amplified using SYBR Green JumpStart^{TM} Taq ReadyMix^{TM} (Sigma) and primers for human TPC1, TPC2 and UBC which is a housekeeping gene (Brailoiu et al., 2009). The following PCR conditions were used: 2 minutes at 94^{O}C, followed by 39 cycles of 15s at 94^{O}C (denaturation), 30s at 60^{O}C (annealing) and 30s at 72^{O}C (extension). TPC1 and TPC2 expression was normalized to UBC expression. Details of primers are shown as follows:

Gene	**Forward Primer (5'-3')**	**Reverse Primer (5'-3')**
TPC1	TTCTGTGTTTTGCTTTAGGG	ATTCCGCTTCCATTAGATCC
TPC2	GTTTGACATGGAGAGAACCTTGAC	GATGAAAATAACTGGCAATCAGAACC
UBC	GAAGATGGACGCACCCTGTC	CCTTGTCTTGGATCTTTGCCTT

5.2.4 Recurrent methods

Cytosolic Ca^{2+} was measured by Fura-2 and analysed as described in chapter 2. Cells were stimulated with histamine (3.16 μM and 316 μM) (Sigma), bradykinin (10 nM and 316 nM) (Sigma), GPN (200 μM), thapsigargin (1 μM), tetrandrine (10 μM), raloxifene (1 μM and 10 μM) and fluphenazine (1 μM and 10 μM). All compounds were prepared in DMSO, except histamine and bradykinin which were prepared in H_2O. For some Fura-2 measurements, Ca^{2+} was removed from HBS. This has been indicated in figures.

Data presentation is as described in chapter 2. Statistical analysis was performed using Prism 9 as described in chapter 2 and 3. $P<0.05$ was regarded as statistically significant.

5.3 Results

5.3.1 Histamine but not bradykinin profoundly inhibits GPN-mediated Ca^{2+} signals

Histamine and bradykinin were chosen to investigate the relevance of TPCs to physiological global Ca^{2+} signalling in fibroblasts. Both of them are known to work through the ER store by stimulating IP_3 production (Ataei et al., 2013; Hill et al., 1997; Montero et al., 2003; Willets et al., 2008). Histamine has also been reported to induce NAADP synthesis (Soares et al., 2007). To start, I examined the role of lysosomes on agonist-induced Ca^{2+} signals. To achieve this, I employed GPN, which has been shown to deplete lysosomal Ca^{2+} (chapter 2). In fibroblasts, GPN-induced Ca^{2+} release is complex and long-lasting (Fig.5.3.1A; Kilpatrick et al., 2013; chapter 2). This would complicate examination of the subsequent Ca^{2+} responses induced by the physiological stimuli. For this reason, instead of adding GPN before histamine or bradykinin, the experiment was conducted in a reverse mode (stimulation with histamine / bradykinin prior to GPN). Also, the experiment was conducted in the absence of extracellular Ca^{2+} to ensure recording of Ca^{2+} release only. And I used a maximal agonist concentration to fully discharge the target Ca^{2+} stores. As shown in Fig.5.3.1A, B and C, compared to the H_2O control, following histamine, GPN-induced Ca^{2+} signals were largely abolished. Following bradykinin, however, the GPN Ca^{2+} signals appeared to be only modestly reduced (Fig.5.3.1A, D and E). These data were quantified by calculating both the magnitude of the GPN response (the initial phase) and the area under the GPN Ca^{2+} traces (AUC) (the later phase). Both the magnitude and the AUC were significantly reduced by histamine. Bradykinin tended to reduce the AUC (but not in a statistically significant way) and left the magnitude unchanged (Fig.5.3.1F and G). Histamine but not bradykinin therefore profoundly inhibited GPN-induced Ca^{2+} signals.

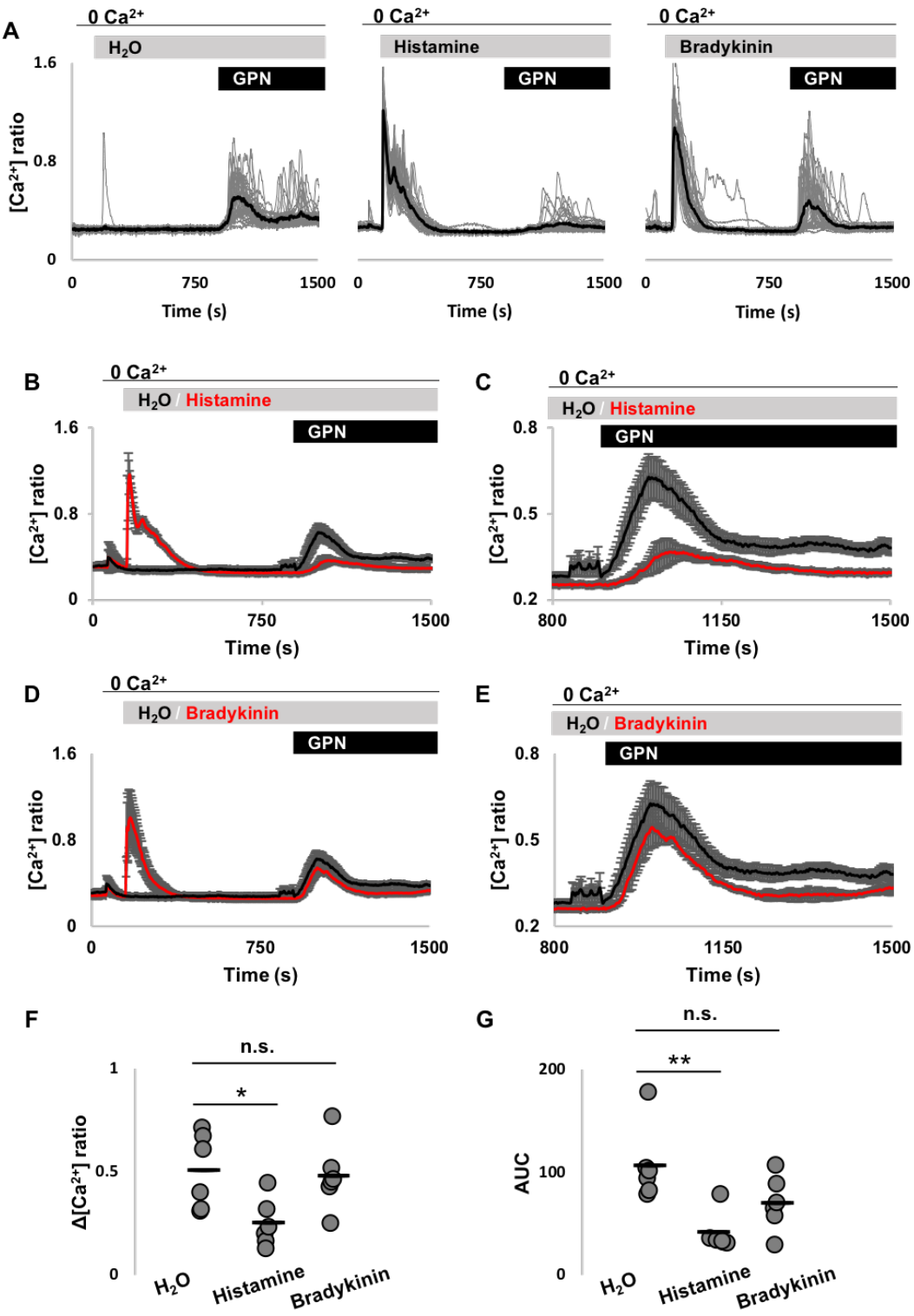

Figure 5.3.1 Histamine but not bradykinin profoundly inhibits GPN-mediated Ca^{2+} signals

(A) Cytosolic Ca^{2+} responses to GPN (200 µM) following H_2O or histamine (316 µM) or bradykinin (316 nM) in individual fibroblasts in the absence of extracellular Ca^{2+}. Cells were immersed into Ca^{2+}-free HBS at 60s and were stimulated with H_2O or histamine or bradykinin

at 150s and GPN at 900s as indicated by the bar. Gray traces represent recordings of all individual cells and black traces represent the population average.

(B) Average cytosolic Ca^{2+} responses (mean ± S.E.M, from 6 independent experiments) to GPN (200 μM) following H_2O or histamine (316 μM) in fibroblasts in the absence of extracellular Ca^{2+}.

(C) The same dataset as B but with expanded x- and y-axes to show GPN responses.

(D) Average cytosolic Ca^{2+} responses (mean ± S.E.M, from 6 independent experiments) to GPN (200 μM) following H_2O or bradykinin (316 nM) in fibroblasts in the absence of extracellular Ca^{2+}.

(E) The same dataset as D but with expanded x- and y-axes to show GPN responses.

(F and G) Data quantifying magnitudes and area under the Ca^{2+} curve (AUC) of GPN responses in B-E (n=6); n.s. not statistically significant *P<0.05 ** P<0.01were determined by one-way ANOVA or Kruskal-Wallis H test.

5.3.2 Histamine but not bradykinin modestly inhibits thapsigargin-mediated Ca^{2+} signals

Histamine and bradykinin are well established in inducing ER Ca^{2+} release through IP_3 signalling. To assess the contribution of the ER to their Ca^{2+} signals in fibroblasts, I utilized thapsigargin and adopted the same testing assay as that for lysosomes. That is, stimulating the fibroblasts first with histamine or bradykinin, and then examining the subsequent thapsigargin-induced Ca^{2+} signals. As shown in Fig.5.3.2A, B and C, in the presence of histamine, thapsigargin-induced Ca^{2+} signals were modestly reduced. To be precise, the magnitude was unaltered, but the return to basal Ca^{2+} appeared to be accelerated as reflected by a reduction in the AUC (Fig.5.3.2C, F and G). In contrast, in the presence of bradykinin, thapsigargin-induced Ca^{2+} signals were not inhibited (Fig. 5.3.2A and D-G). Histamine but not bradykinin therefore modestly reduced thapsigargin-induced Ca^{2+} signals.

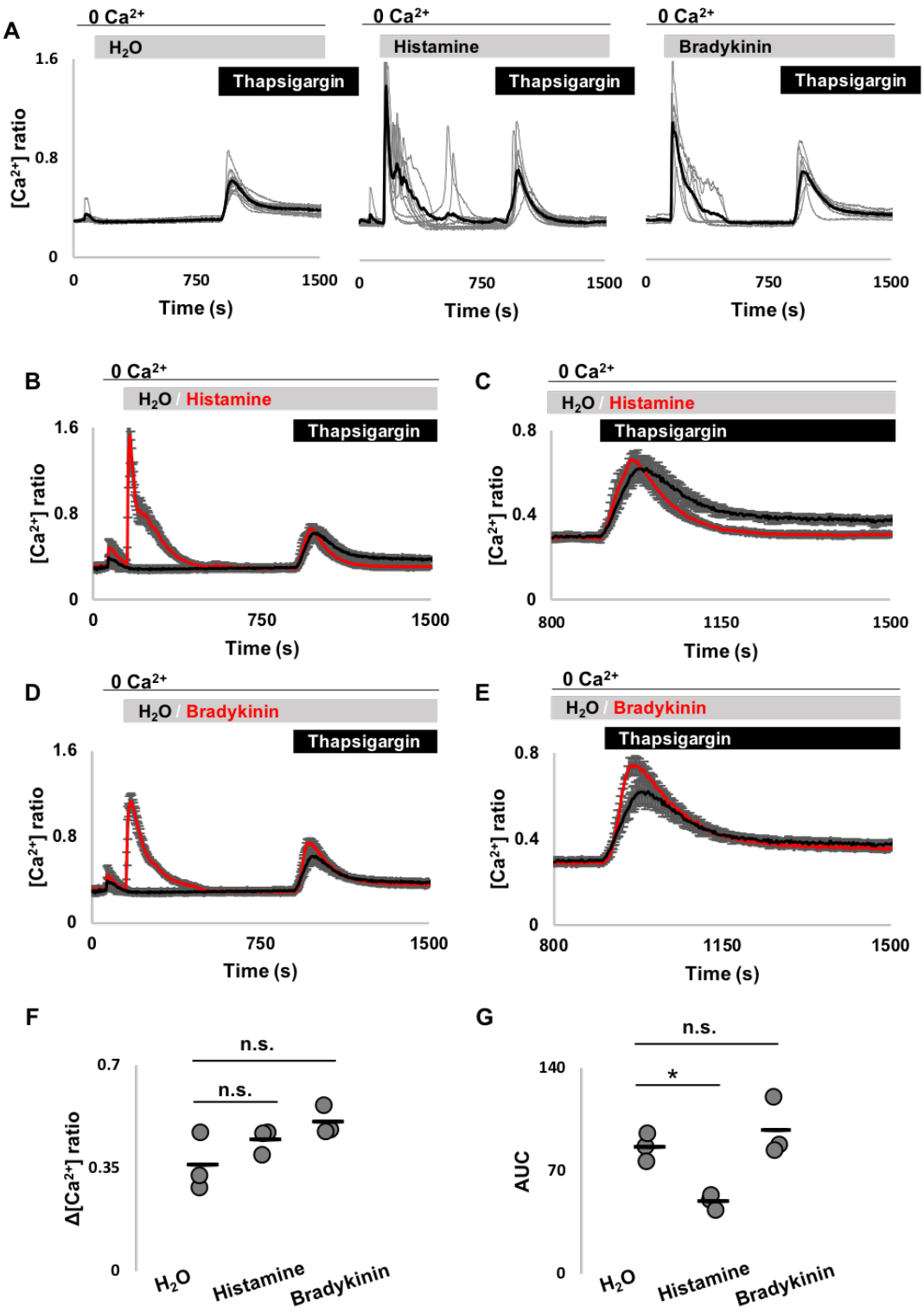

Figure 5.3.2 Histamine but not bradykinin modestly inhibits thapsigargin-mediated Ca^{2+} signals

(A) Cytosolic Ca^{2+} responses to thapsigargin (1 μM) following H_2O or histamine (316 μM) or bradykinin (316 nM) in individual fibroblasts in the absence of extracellular Ca^{2+}. Cells were immersed into Ca^{2+}-free HBS at 60s and were stimulated with H_2O or histamine or bradykinin

at 150s and thapsigargin at 900s as indicated by the bar. Gray traces represent recordings of all individual cells and black traces represent the population average.
(B) Average cytosolic Ca^{2+} responses (mean ± S.E.M, from 3 independent experiments) to thapsigargin (1 μM) following H_2O or histamine (316 μM) in fibroblasts in the absence of extracellular Ca^{2+}.
(C) The same dataset as B but with expanded x- and y-axes to show thapsigargin responses
(D) Average cytosolic Ca^{2+} responses (mean ± S.E.M, from 3 independent experiments) to thapsigargin (1 μM) following H_2O or bradykinin (316 nM) in fibroblasts in the absence of extracellular Ca^{2+}.
(E) The same dataset as D but with expanded X- and y-axes to show thapsigargin responses
(F and G) Data quantifying magnitudes and AUC of thapsigargin responses in B-E (n=3);
n.s. not statistically significant *P<0.05 were determined by one-way ANOVA.

5.3.3 Histamine- and bradykinin-mediated Ca^{2+} signals are reduced by tetrandrine to different degrees

Having observed that histamine is better coupled to lysosomes than bradykinin, I went onto examine whether TPCs are implicated in histamine and bradykinin-induced Ca^{2+} signals. For these tests, I utilized the EC_{50} concentration of histamine (3.16 μM) and bradykinin (10 nM) (established in Yates, 2017). As shown in Fig.5.3.3A and B, histamine produces a biphasic response, a peak followed by a phase with complex Ca^{2+} fluctuations, whereas bradykinin-induced response is just a single peak. I first applied a pharmacological approach. Tetrandrine is known to reduce Ebola infection by inhibiting TPCs (Sakurai et al., 2015). And In chapter 3, tetrandrine blocked the TPC2 agonist A1-induced Ca^{2+} signals. Thus, tetrandrine was used to examine the role of TPCs on histamine and bradykinin-induced Ca^{2+} signals. During recordings, 10 μM tetrandrine was added to fibroblasts 15 minutes before the physiological stimuli. As shown in Fig.5.3.3C-F and quantified in Fig.5.3.3K, compared to the DMSO control, tetrandrine reduced histamine-induced Ca^{2+} signals by 40-50% in both the magnitude and the AUC. In contrast, for bradykinin, the magnitude of its Ca^{2+} signals were unchanged, but the Ca^{2+} signals exhibited a relatively quick decay (Fig.5.3.3G-J and L). Accordingly, the AUC was reduced by tetrandrine (Fig.5.3.3L). Histamine and bradykinin-induced Ca^{2+} signals therefore are differentially reduced by tetrandrine.

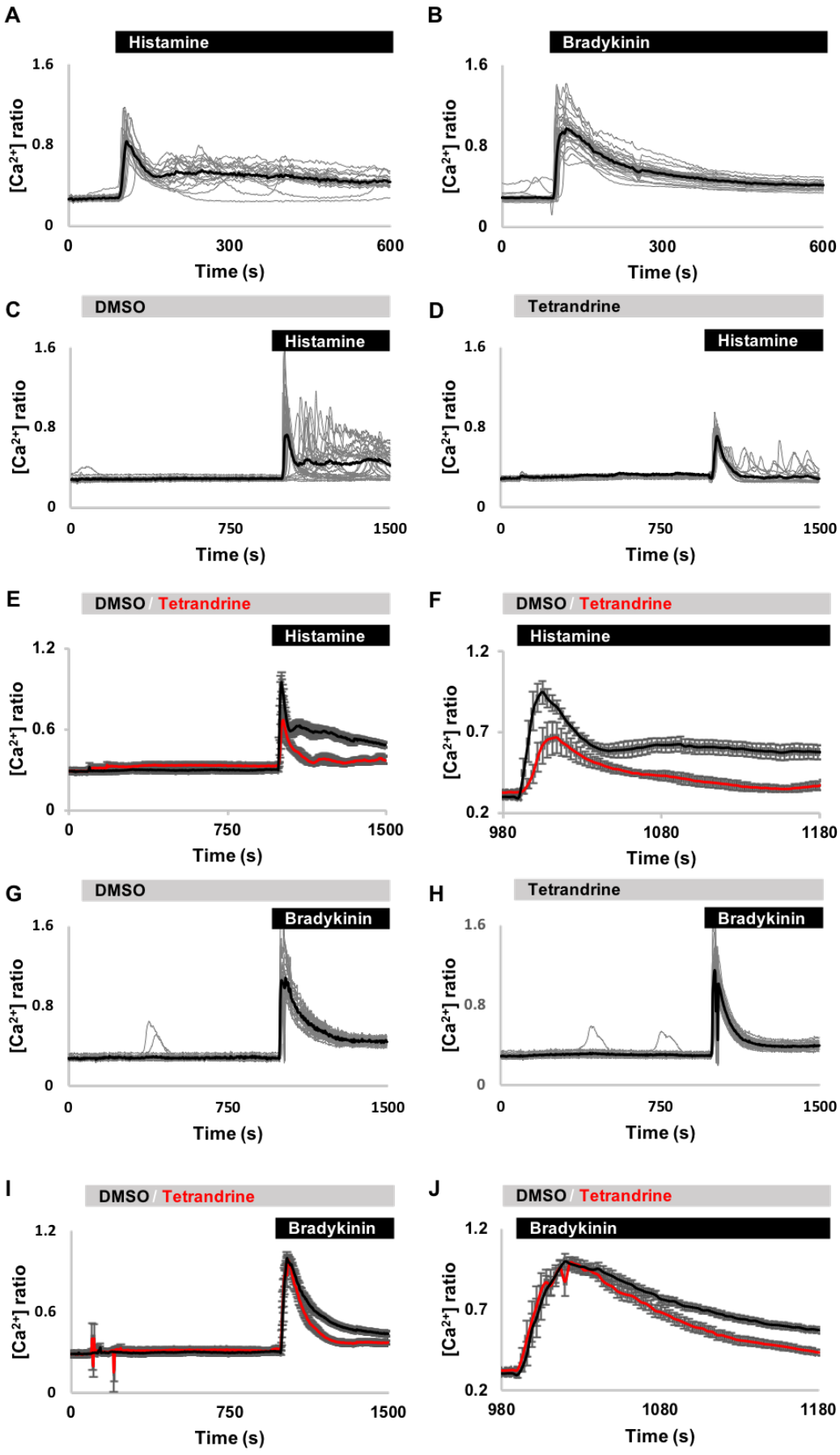
A
Histamine
1.6
0.8
0
[Ca2+] ratio
0
300
600
Time (s)
B
Bradykinin
1.6
0.8
0
[Ca2+] ratio
0
300
600
Time (s)
C
DMSO
Histamine
1.6
0.8
0
[Ca2+] ratio
0
750
1500
Time (s)
D
Tetrandrine
Histamine
1.6
0.8
0
[Ca2+] ratio
0
750
1500
Time (s)
E
DMSO / Tetrandrine
Histamine
1.2
0.6
0
[Ca2+] ratio
0
750
1500
Time (s)
F
DMSO / Tetrandrine
Histamine
1.2
0.7
0.2
[Ca2+] ratio
980
1080
1180
Time (s)
G
DMSO
Bradykinin
1.6
0.8
0
[Ca2+] ratio
0
750
1500
Time (s)
H
Tetrandrine
Bradykinin
1.6
0.8
0
[Ca2+] ratio
0
750
1500
Time (s)
I
DMSO / Tetrandrine
Bradykinin
1.2
0.6
0
[Ca2+] ratio
0
750
1500
Time (s)
J
DMSO / Tetrandrine
Bradykinin
1.2
0.7
0.2
[Ca2+] ratio
980
1080
1180
Time (s)

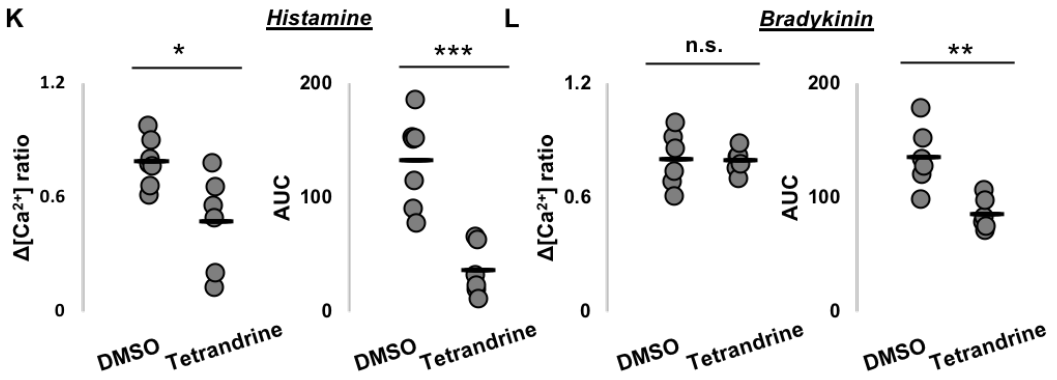

Figure 5.3.3 Histamine- and bradykinin-mediated Ca^{2+} signals are reduced by tetrandrine to different degrees

(A and B) Representative cytosolic Ca^{2+} responses to histamine (3.16 μM) (A) and to bradykinin (10 nM) in individual fibroblasts. The bars above graphs indicate the time of addition of the compound, which was at 90s. Gray traces represent recordings of all individual cells and black traces represent the population average.

(C and D) Cytosolic Ca^{2+} responses to histamine (3.16 μM) following DMSO (C) or tetrandrine (10 μM) (D) in individual fibroblasts. The bars above graphs indicate the time of addition of the compound, DMSO or tetrandrine was added at 90s, histamine was added at 990s.

(E) Average cytosolic Ca^{2+} responses (mean ± S.E.M, from 6-7 independent experiments) to histamine (3.16 μM) following DMSO or tetrandrine (10 μM) in fibroblasts.

(F) The same dataset as E but with expanded x- and y-axes.

(G and H) Cytosolic Ca^{2+} responses to bradykinin (10 nM) following DMSO (G) or tetrandrine (10 μM) (H) in individual fibroblasts. Cells were stimulated with DMSO or tetrandrine at 90s and bradykinin at 990s as indicated by the bars.

(I) Average cytosolic Ca^{2+} responses (mean ± S.E.M, from 6 independent experiments) to bradykinin (10 nM) following DMSO or tetrandrine (10 μM) in fibroblasts.

(J) The same dataset as I but with expanded x- and y-axes.

(K) Data quantifying magnitudes and AUC of histamine responses in E and F (n=6-7).

* $P<0.05$ *** $P<0.001$ were determined by independent-samples t-tests.

(L) Data quantifying magnitudes and AUC of bradykinin responses in I and J (n=6). n.s. not statistically significant ** $P<0.01$ were determined by independent-samples t-tests.

5.3.4 Raloxifene and fluphenazine induce Ca^{2+} signals

Raloxifene and fluphenazine are novel TPC pore blockers recently identified by our lab and characterised in chapter 3. In fibroblasts, as shown in Fig.5.3.4A-C, compared to the DMSO control, 10 μM raloxifene induced robust Ca^{2+} signals. Likewise, 10 μM fluphenazine induced robust Ca^{2+} signals as well. These data were quantified by calculating the magnitudes of responses to DMSO, raloxifene or fluphenazine (Fig.5.3.4D).

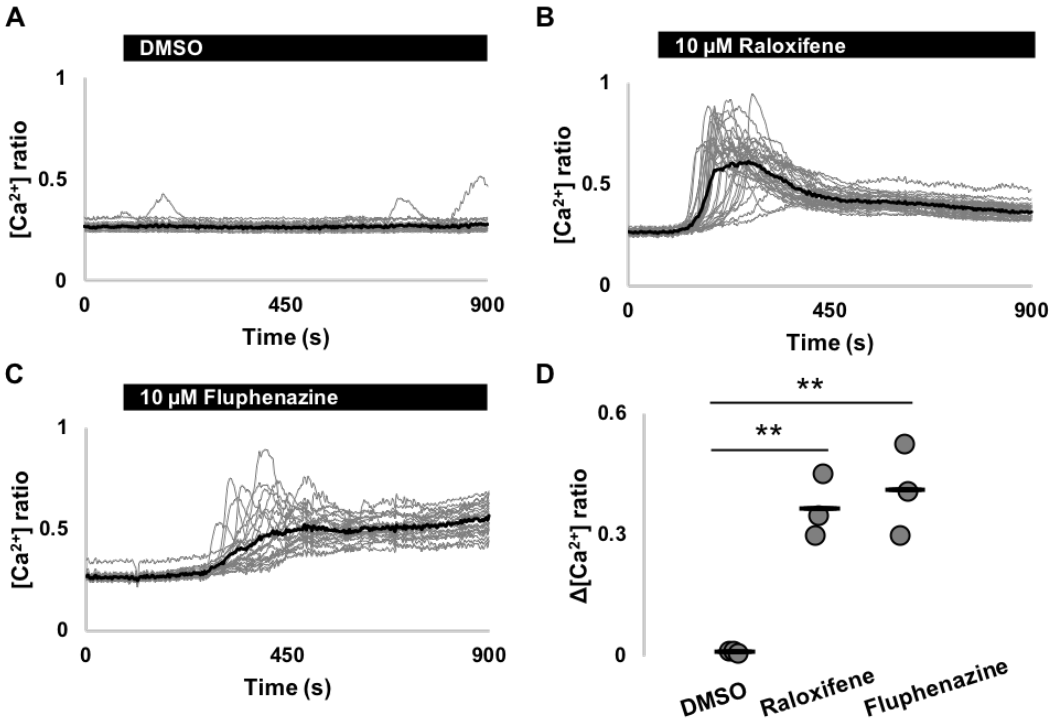

Figure 5.3.4 Raloxifene and fluphenazine induce Ca^{2+} signals

(A-C) Cytosolic Ca^{2+} responses to DMSO (A), to raloxifene (10 μM) (B) and to fluphenazine (10 μM) in individual fibroblasts. The bars above graphs indicate the time of addition of the compound, which was at 90s. Gray traces represent recordings of all individual cells and black traces represent the population average.

(D) Pooled data quantifying magnitudes of responses by DMSO, raloxifene and fluphenazine. Each plot points represents one experiment (n=3); ** $P<0.01$ was determined by one-way ANOVA.

5.3.5 Histamine- and bradykinin-mediated Ca^{2+} signals are reduced by raloxifene to different degrees

The Ca^{2+} signals evoked by raloxifene and fluphenzine (as shown in Fig. 5.3.4) would complicate the analysis of the relation of TPCs to the physiological stimuli Ca^{2+} signalling. I therefore used lower drug concentrations (1 μM) to reduce their Ca^{2+} responses. Compared to 10 μM, raloxifene of 1 μM was associated with a smaller increase in cytosolic Ca^{2+} (Fig.5.3.5A and B). As shown in Fig.5.3.5C-F and quantified in Fig.5.3.5K, following raloxifene, histamine-induced Ca^{2+} signals were significantly reduced in both the magnitude and the AUC. In comparison, raloxifene left the magnitude of bradykinin-induced Ca^{2+} signals unaltered, but there was an acceleration on the decay phase of the Ca^{2+} signals (a reduction in the AUC) (Fig.5.3.5G-J and L). To obtain the "correct" magnitude of histamine/bradykinin responses following 1 μM raloxifene, the basal ratio was acquired by averaging fluorescence from a 90 second recording before addition of histamine/bradykinin. Thus, the increased Ca^{2+} signals by raloxifene were taken into account. Collectively, histamine and bradykinin-induced Ca^{2+} signals are differentially reduced by raloxifene.

5.3.6 Fluphenazine inhibits histamine- but not bradykinin-mediated Ca^{2+} signals

The effect of fluphenazine on histamine- and bradykinin-induced Ca^{2+} signals was examined in the same manner as that for raloxifene at 1 μM to minimise its intrinsic Ca^{2+} responses. As shown in Fig.5.3.6A-D and quantified in Fig.5.3.6I, fluphenazine completely blocked histamine-induced Ca^{2+} signals. In stark contrast, bradykinin-induced Ca^{2+} signals were maintained in the presence of fluphenazine (neither the magnitude nor the AUC was altered) (Fig.5.3.6E-H and J). Fluphenazine therefore blocks histamine- but not bradykinin-induced Ca^{2+} signals.

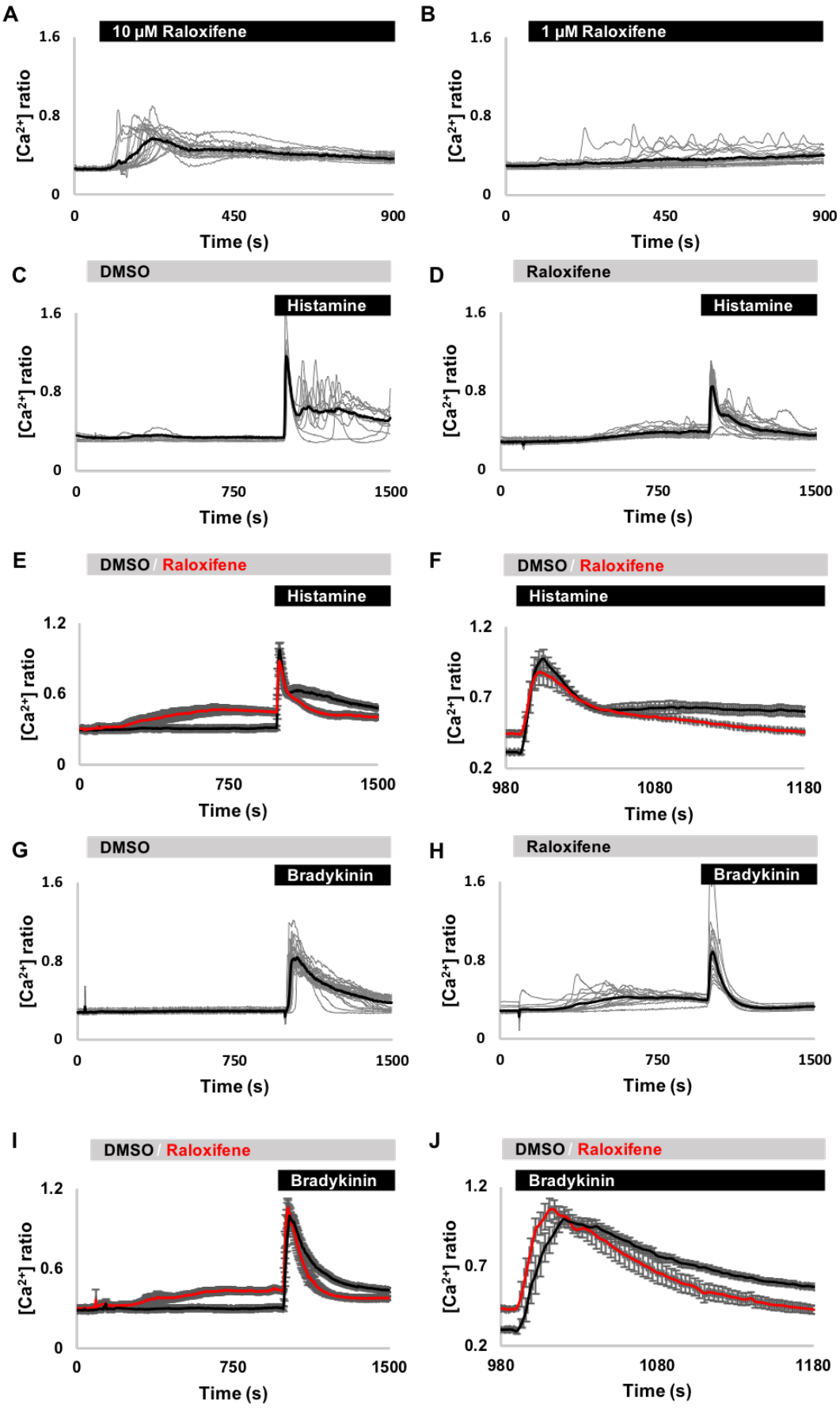
A
10 μM Raloxifene
B
1 μM Raloxifene
[Ca2+] ratio
Time (s)
C
DMSO
Histamine
D
Raloxifene
Histamine
E
DMSO / Raloxifene
Histamine
F
DMSO / Raloxifene
Histamine
G
DMSO
Bradykinin
H
Raloxifene
Bradykinin
I
DMSO / Raloxifene
Bradykinin
J
DMSO / Raloxifene
Bradykinin

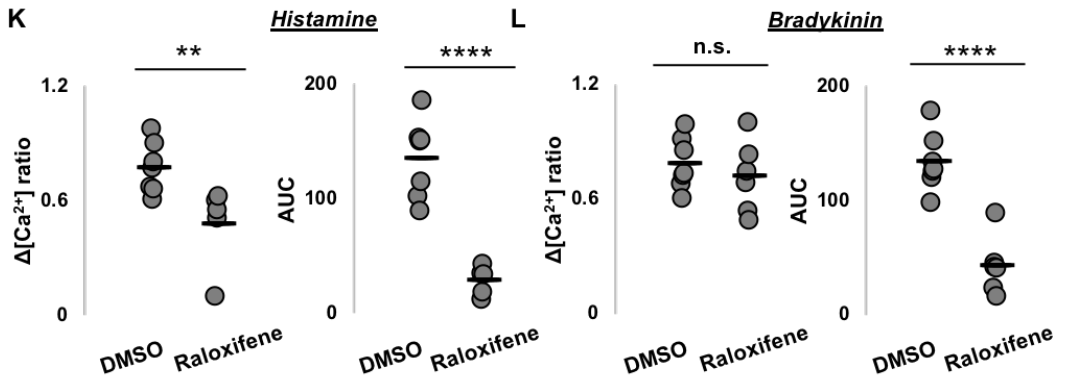

Figure 5.3.5 Histamine- and bradykinin-mediated Ca^{2+} signals are reduced by raloxifene to different degrees

(A and B) Cytosolic Ca^{2+} responses to raloxifene of 10 μM (A) or 1 μM (B) in individual fibroblasts.

(C and D) Cytosolic Ca^{2+} responses to histamine (3.16 μM) following DMSO (C) or raloxifene (1 μM) (D) in individual fibroblasts. The bars above graphs indicate the time of addition of the compound, DMSO or raloxifene was added at 90s, histamine was added at 990s. Gray traces represent recordings of all individual cells and black traces represent the population average.

(E) Average cytosolic Ca^{2+} responses (mean ± S.E.M, from 5-7 independent experiments) to histamine (3.16 μM) following DMSO or raloxifene (1 μM) in fibroblasts.

(F) The same dataset as E but with expanded x- and y-axes.

(G and H) Cytosolic Ca^{2+} responses to bradykinin (10 nM) following DMSO (G) or raloxifene (1 μM) (H) in individual fibroblasts. Cells were stimulated with DMSO or raloxifene at 90s and bradykinin at 990s as indicated by the bars.

(I) Average cytosolic Ca^{2+} responses (mean ± S.E.M, from 6-7 independent experiments) to bradykinin (10 nM) following DMSO or raloxifene (1 μM) in fibroblasts.

(J) The same dataset as I but with expanded x- and y-axes.

(K) Data quantifying magnitudes and AUC of histamine responses in E and F (n=5-7).

** P<0.01 **** P<0.0001 were determined by independent-samples t-tests or Mann Whitney U test.

(L) Data quantifying magnitudes and AUC of bradykinin responses in I and J (n=6-7). n.s. not statistically significant **** P<0.0001 were determined by independent-samples t-tests.

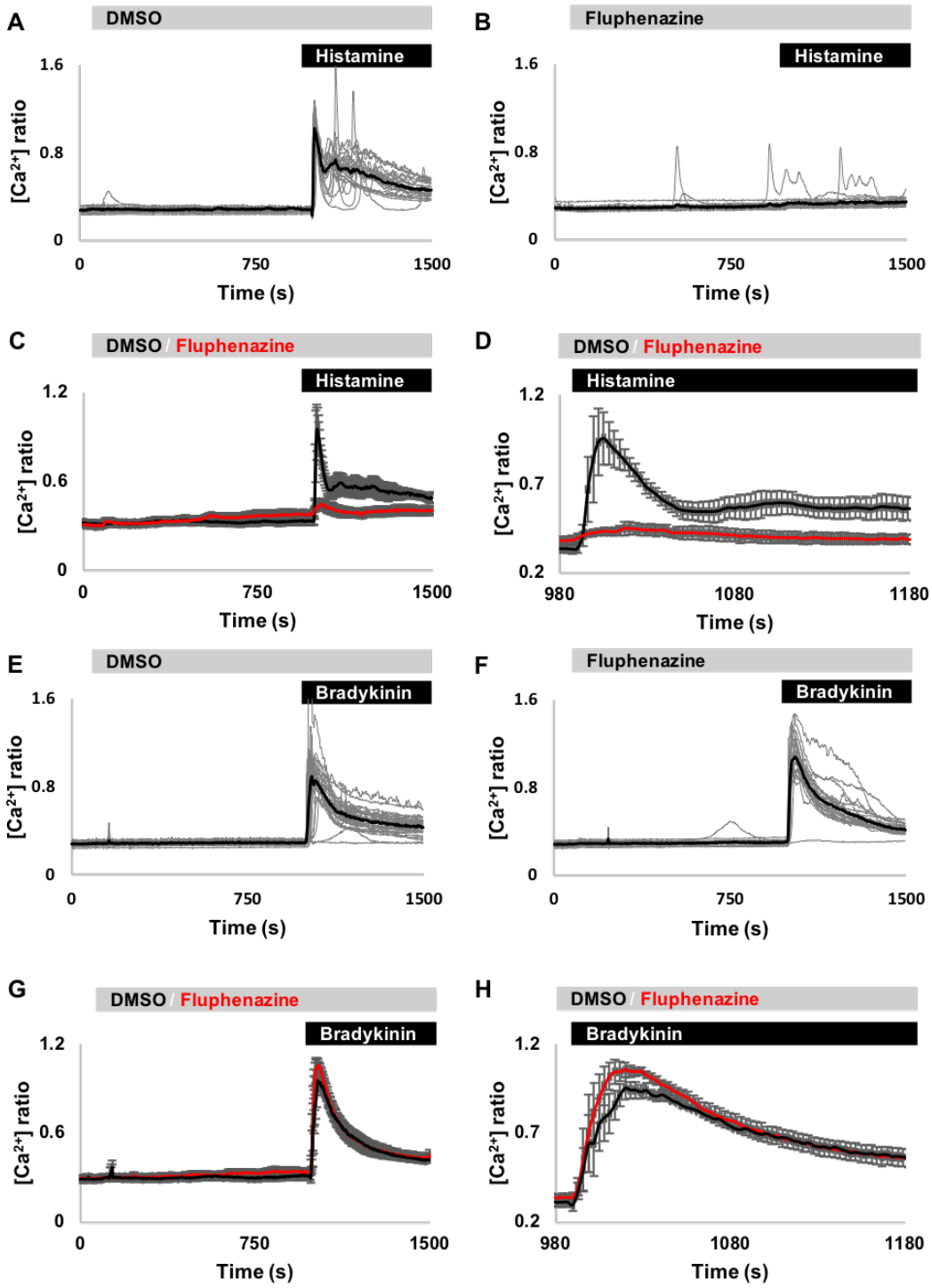
A
DMSO
Histamine
1.6
0.8
0
[Ca2+] ratio
0
750
1500
Time (s)
B
Fluphenazine
Histamine
1.6
0.8
0
[Ca2+] ratio
0
750
1500
Time (s)
C
DMSO / Fluphenazine
Histamine
1.2
0.6
0
[Ca2+] ratio
0
750
1500
Time (s)
D
DMSO / Fluphenazine
Histamine
1.2
0.7
0.2
[Ca2+] ratio
980
1080
1180
Time (s)
E
DMSO
Bradykinin
1.6
0.8
0
[Ca2+] ratio
0
750
1500
Time (s)
F
Fluphenazine
Bradykinin
1.6
0.8
0
[Ca2+] ratio
0
750
1500
Time (s)
G
DMSO / Fluphenazine
Bradykinin
1.2
0.6
0
[Ca2+] ratio
0
750
1500
Time (s)
H
DMSO / Fluphenazine
Bradykinin
1.2
0.7
0.2
[Ca2+] ratio
980
1080
1180
Time (s)

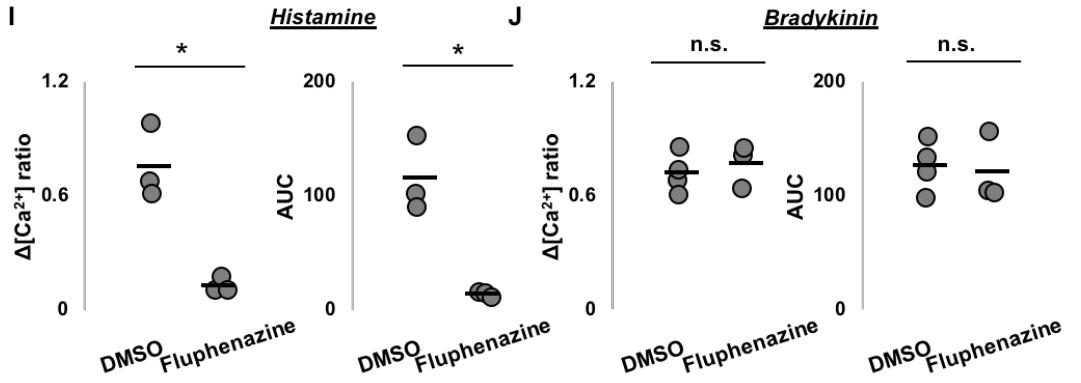

Figure 5.3.6 Fluphenazine inhibits histamine- but not bradykinin-mediated Ca^{2+} signals

(A and B) Cytosolic Ca^{2+} responses to histamine (3.16 μM) following DMSO (A) or fluphenazine (1 μM) (B) in individual fibroblasts. The bars above graphs indicate the time of addition of the compound, DMSO or fluphenazine was added at 90s, histamine was added at 990s. Gray traces represent recordings of all individual cells and black traces represent the population average.

(C) Average cytosolic Ca^{2+} responses (mean ± S.E.M, from 3 independent experiments) to histamine (3.16 μM) following DMSO or fluphenazine (1 μM) in fibroblasts.

(D) The same dataset as C but with expanded x- and y-axes.

(E and F) Cytosolic Ca^{2+} responses to bradykinin (10 nM) following DMSO (E) or fluphenazine (1 μM) (F) in individual fibroblasts. Cells were stimulated with DMSO or fluphenazine at 90s and bradykinin at 990s as indicated by the bars.

(G) Average cytosolic Ca^{2+} responses (mean ± S.E.M, from 3 independent experiments) to bradykinin (10 nM) following DMSO or fluphenazine (1 μM) in fibroblasts.

(H) The same dataset as G but with expanded x- and y-axes.

(I) Data quantifying magnitudes and AUC of histamine responses in C and D (n=3); * $P<0.01$ was determined by independent-samples t-tests.

(J) Data quantifying magnitudes and AUC of bradykinin responses in G and H (n=3-4); n.s. not statistically significant was determined by independent-samples t-tests.

5.3.7 Validation of TPC knockdown in fibroblasts by quantitative PCR

In addition to pharmacologically reducing TPC activity, I also applied siRNA-mediated TPC knockdown to investigate the role of TPCs on histamine and bradykinin-induced Ca^{2+} signals. I used quantitative PCR (qPCR) to measure the mRNA levels of TPCs from cells transfected with TPC1 siRNA and/or TPC2 siRNA. TPC transcript levels were normalized to the house-keeping gene ubiquitin C (UBC) and are presented in Fig.5.3.7A and C. Notably, native TPC1 levels were far higher than TPC2. As shown in Fig.5.3.7A and B, in cells co-transfected with siRNAs targeted to TPC1 and TPC2, TPC1 and TPC2 levels were reduced by about 85% and 65%, respectively. I also performed single knockdowns. In cells treated with TPC1 siRNA only, the TPC1 level was largely reduced. Similarly, in cells treated with TPC2 siRNA only, the TPC2 level was largely reduced (Fig.5.3.7C and D). Therefore, qPCR confirmed knockdown of TPC1 and TPC2 by siRNAs in fibroblasts.

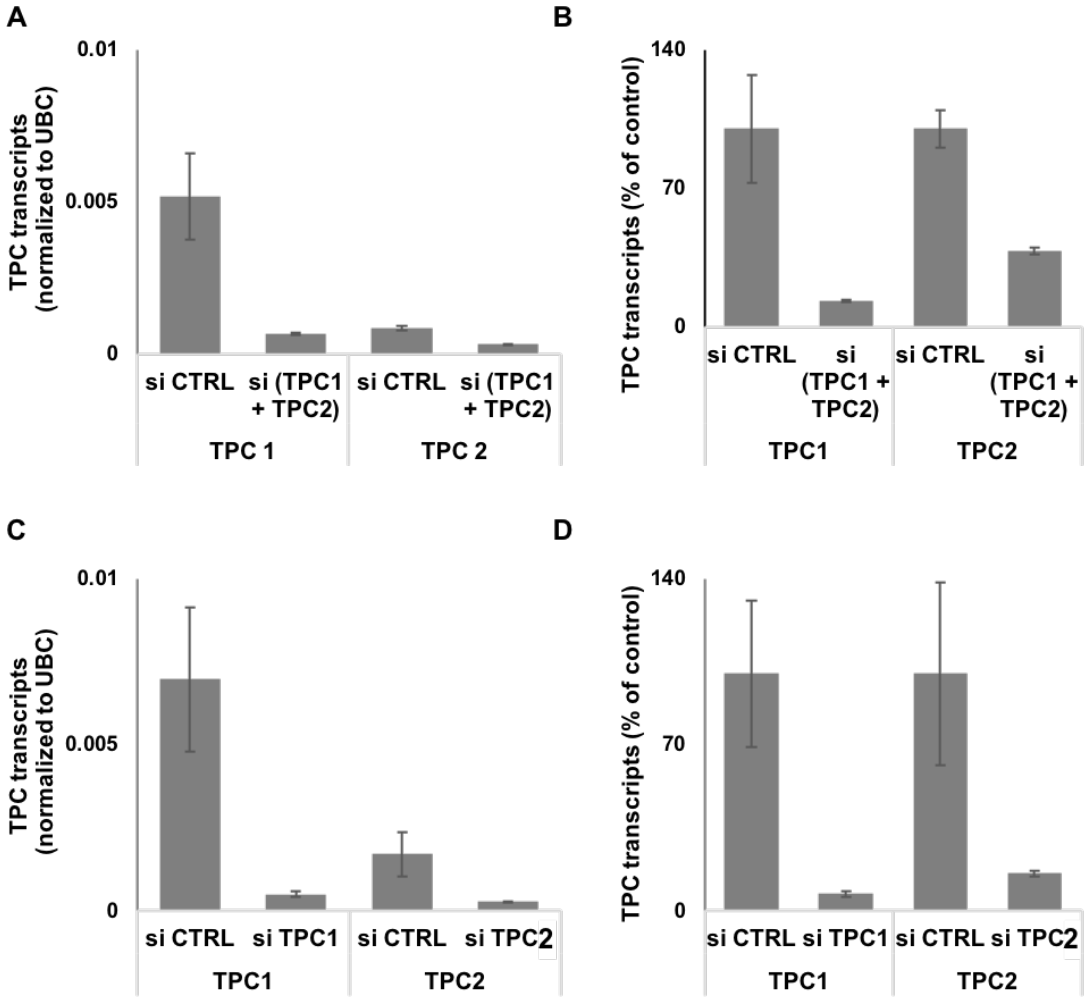

Figure 5.3.7 Validation of TPC knockdown in fibroblasts by quantitative PCR

(A-D) Data quantifying TPC transcripts after normalized to housekeeping gene UBC (A and C) and presented as percentage of the TPC levels in cells transfected with control siRNA (B and D) The mean ± S.E.M of three replicates from one experiment is displayed.

5.3.8 TPC knockdown modestly inhibits histamine- but not bradykinin-mediated Ca^{2+} signals

As TPC KD can be successfully achieved in fibroblasts, I first examined histamine- and bradykinin-induced Ca^{2+} signals in cells co-transfected with TPC1 siRNA and TPC2 siRNA. In these cells, histamine-induced Ca^{2+} signals were reduced compared to cells treated with control siRNA (Fig.5.3.8A-D). To note, the reduction was modest - about 25% in the magnitude and the AUC (Fig.5.3.8I). Bradykinin-induced Ca^{2+} signals, however, were similar in cells treated with control siRNA and those with TPC1 siRNA and TPC2 siRNA (Fig.5.3.8E-H and J). These data therefore suggest that TPC double knockdown reduces histamine but not bradykinin-induced Ca^{2+} signals albeit modestly.

5.3.9 TPC2 but not TPC1 knockdown modestly inhibits histamine-mediated Ca^{2+} signals

Having observed histamine-induced Ca^{2+} signals were reduced in cells co-transfected with TPC1 siRNA and TPC2 siRNA, I went on to examine the contribution of each isoform on histamine mediated Ca^{2+} signalling. As shown in Fig.5.3.9A-C and quantified in Fig.5.3.9F and G, in cells transfected with TPC1 siRNA, there was no significant reduction in either the magnitude or the AUC of histamine-induced Ca^{2+} signals, although more cells seemed to exhibit oscillatory responses (Fig.5.3.9A). In contrast, in cells treated with TPC2 siRNA, histamine-induced Ca^{2+} signals were visibly reduced (Fig.5.3.9A, D and E) although modestly. That is, the peak was maintained but the phase with complex Ca^{2+} fluctuations was reduced (a reduction in the AUC) (Fig.5.3.9F and G). Collectively, these data suggest that there could be an isoform-selective role for TPC in histamine-induced Ca^{2+} signalling.

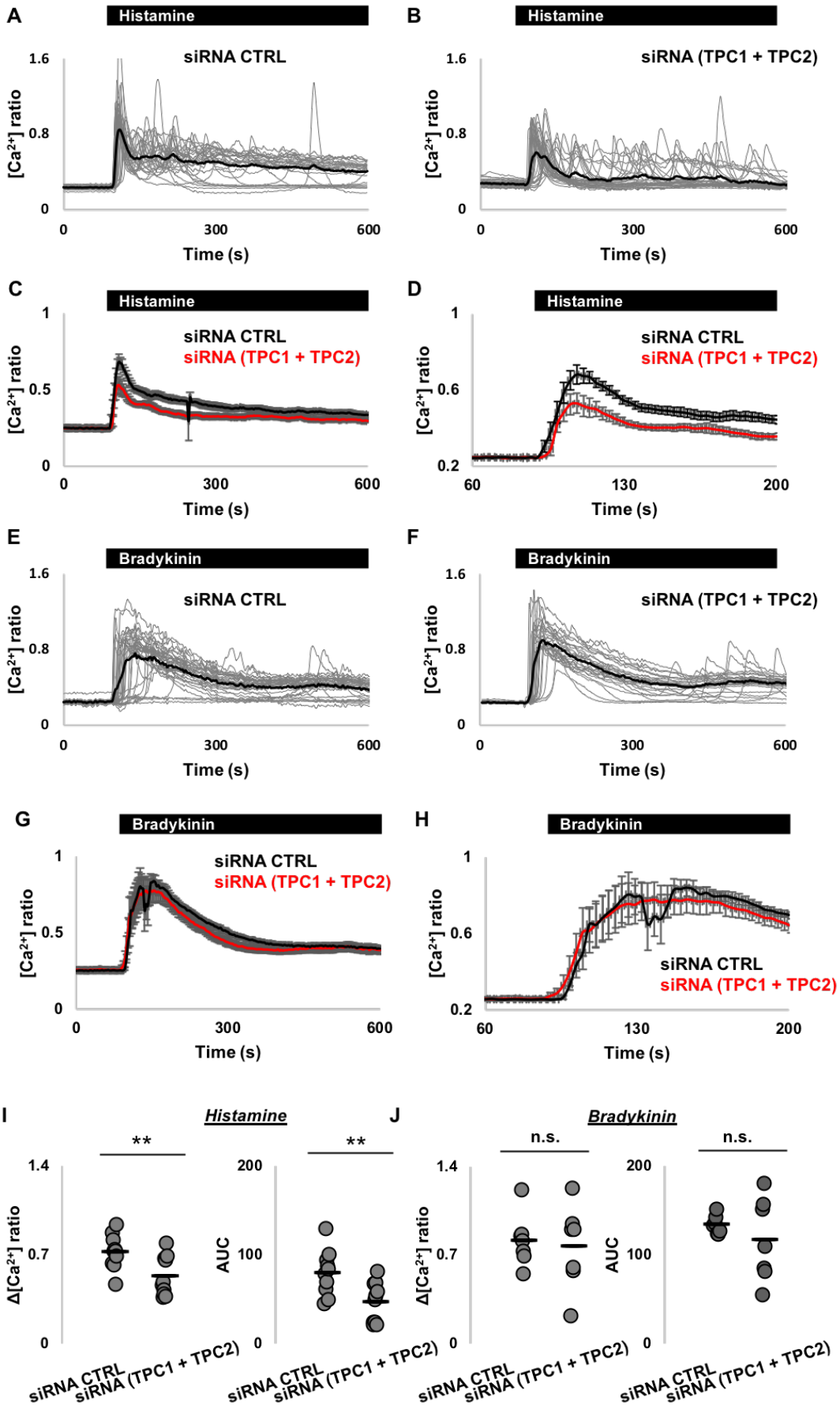
A
Histamine
siRNA CTRL
[Ca2+] ratio
Time (s)
B
Histamine
siRNA (TPC1 + TPC2)
C
Histamine
siRNA CTRL
siRNA (TPC1 + TPC2)
D
Histamine
E
Bradykinin
siRNA CTRL
F
Bradykinin
siRNA (TPC1 + TPC2)
G
Bradykinin
H
Bradykinin
I
Histamine
J
Bradykinin
Δ[Ca2+] ratio
AUC
**
n.s.
siRNA CTRL
siRNA (TPC1 + TPC2)

Figure 5.3.8. TPC knockdown modestly inhibits histamine- but not bradykinin-mediated Ca^{2+} signals

(A and B) Cytosolic Ca^{2+} responses to histamine (3.16 μM) in individual fibroblasts transfected with control siRNA (A) or co-transfected with TPC1 siRNA and TPC2 siRNA (B). The bars above graphs indicate the time of addition of the compound, which was at 90s. Gray traces represent recordings of all individual cells and black traces represent the population average.

(C) Average cytosolic Ca^{2+} responses (mean ± S.E.M, from 10 independent experiments) to histamine (3.16 μM) in fibroblasts transfected with control siRNA or co-transfected with TPC1 siRNA and TPC2 siRNA.

(D) The same dataset as C but with expanded x- and y-axes.

(E and F) Cytosolic Ca^{2+} responses to bradykinin (10 nM) in individual fibroblasts transfected with control siRNA (E) or co-transfected with TPC1 siRNA and TPC2 siRNA (F). The bars above graphs indicate the time of addition of the compound, which was at 90s.

(G) Average cytosolic Ca^{2+} responses (mean ± S.E.M, from 7 independent experiments) to bradykinin (10 nM) in fibroblasts transfected with control siRNA or co-transfected with TPC1 siRNA and TPC2 siRNA.

(H) The same dataset as G but with expanded x- and y-axes.

(I) Data quantifying magnitudes and AUC of histamine responses in C and D (n=10).

** $P<0.01$ was determined by independent-samples t-tests.

(J) Data quantifying magnitudes and AUC of bradykinin responses in G and H (n=7).

n.s. not statistically significant was determined by independent-samples t-tests.

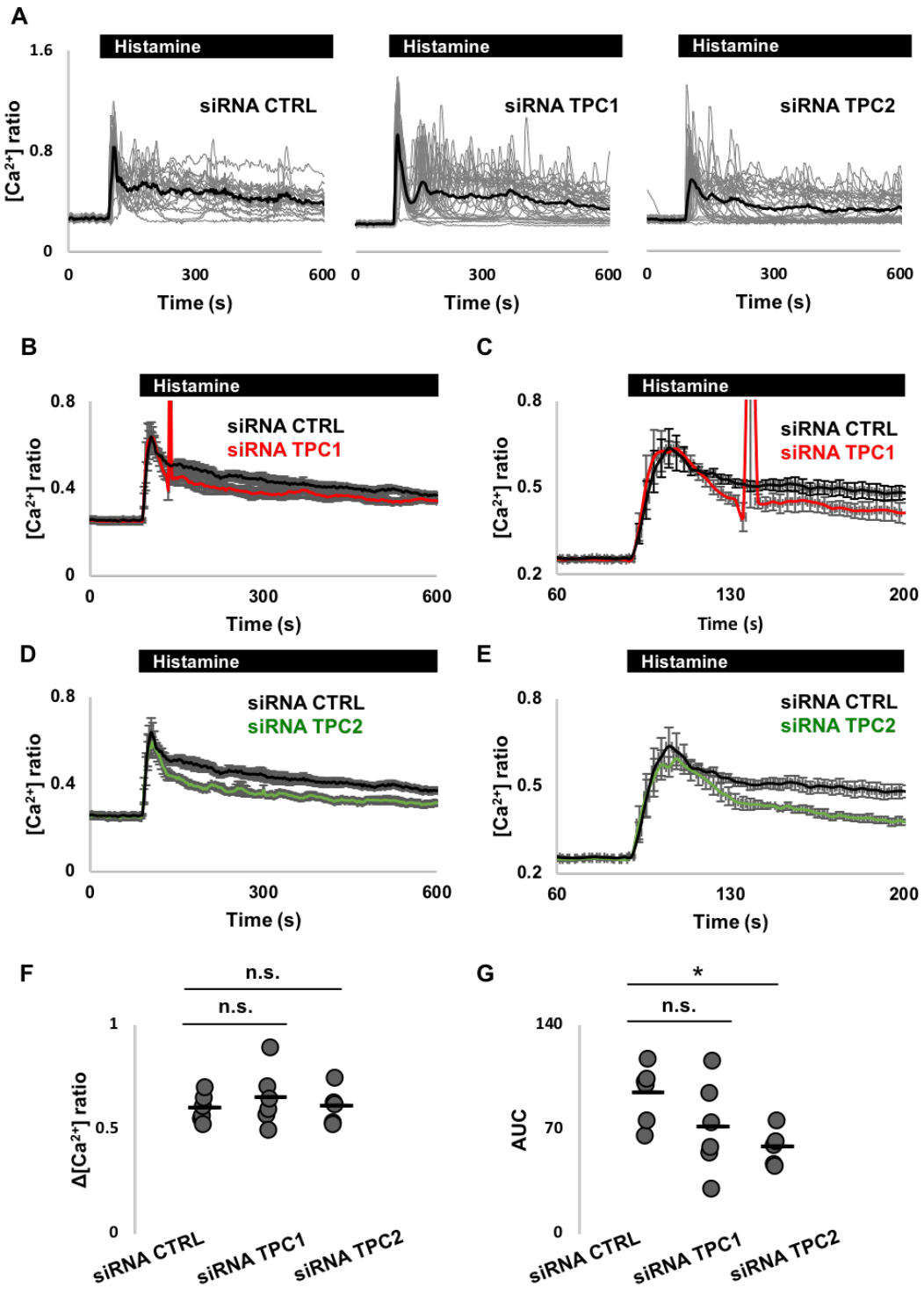

Figure 5.3.9. TPC2 but not TPC1 knockdown modestly inhibits histamine-mediated Ca^{2+} signals

(A) Cytosolic Ca^{2+} responses to histamine (3.16 μM) in individual fibroblasts transfected with control siRNA or TPC1 siRNA or TPC2 siRNA. The bars above graphs indicate the time of addition of the compound, which was at 90s. Gray traces represent recordings of all individual cells and black traces represent the population average.

(B) Average cytosolic Ca^{2+} responses (mean ± S.E.M, from 6 independent experiments) to histamine (3.16 μM) in fibroblasts transfected with control siRNA or TPC1 siRNA.
(C) The same dataset as B but with expanded x- and y-axes.
(D) Average cytosolic Ca^{2+} responses (mean ± S.E.M, from 5-6 independent experiments) to histamine (3.16 μM) in fibroblasts transfected with control siRNA or TPC2 siRNA.
(E) The same dataset as D but with expanded x- and y-axes.
(F and G) Data quantifying magnitudes and AUC of histamine responses in B-E (n=5-6). n.s. not statistically significant * $P < 0.05$ were determined by one-way ANOVA.

5.4 Discussion

Ca^{2+} signals can function in both "local" and "global" mode. TPCs regulate endo-lysosomal trafficking through elevation of local Ca^{2+} (Hockey et al., 2015; Kilpatrick et al., 2017; Lin-Moshier et al., 2014; Ruas et al., 2010). TPCs are also required for NAADP-induced global Ca^{2+} signals (Brailoiu et al., 2009; Calcraft et al., 2009; Pereira et al., 2014). However, there is very little information about the relevance of TPCs to physiological global Ca^{2+} signals evoked by extracellular stimuli. In this chapter, I examined the role of TPCs in histamine- and bradykinin-induced Ca^{2+} signals in fibroblasts using both pharmacological and molecular approaches. My results indicate that TPCs are implicated in physiological global Ca^{2+} signals, possibly in an agonist- and isoform-specific manner.

To investigate whether TPCs are required for physiological global Ca^{2+} signals, I employed histamine and bradykinin. Histamine is an essential inflammatory mediator involved in the immune response. It has been reported to induce IP_3 and cADPR production (Hill et al., 1997; Kip et al., 2006; Montero et al., 2003; Willets et al., 2008). Besides, it has also been shown to cause NAADP production (Soares et al., 2007). Bradykinin is a naturally synthesized vasodilator that can induce IP3 and cADPR production (Ataei et al., 2013; Kip et al., 2006; Lambert et al., 1986). However, there is no study suggests that bradykinin causes NAADP production. I found that in fibroblasts, both histamine and bradykinin induced robust Ca^{2+} signals but with different kinetics. I observed that histamine elicited a two-phase response, a peak and then a phase with complex Ca^{2+} fluctuations. In comparison, the bradykinin response was a simple, single peak, in accordance with that observed previously (Kilpatrick et

al., 2013). The differential Ca^{2+} responses by histamine and bradykinin have also been reported in tracheal epithelial cell lines (Harris & Hanrahan, 1993).

As an initial step to examine whether TPCs are required for histamine and bradykinin Ca^{2+} signalling, I studied whether lysosomes contribute to their Ca^{2+} signals. GPN is a widely used and classical tool for probing lysosomal Ca^{2+} signalling, as it permeabilizes lysosomal membranes inducing leakage of luminal content (e.g. Ca^{2+}) (Haller et al., 1996; Jadot et al., 1984). A recent study, however, has questioned the action of GPN on lysosomes. Instead it was suggested that GPN induces Ca^{2+} release from the ER via its cytosolic alkalizing effect (Atakpa et al., 2019). In chapter 2, I re-affirmed that lysosomes are primary targets for GPN in fibroblast. Further supporting this, in chapter 3, I found that GPN works differently from thapsigargin and it completely inhibited Ca^{2+} release by the TPC2 agonists A1 and H07. In fibroblasts, GPN-induced Ca^{2+} signals are complex and long-lasting, even in the absence of extracellular Ca^{2+} (chapter 2, Kilpatrick et al. 2013). This could cause complication to subsequent analysis of other Ca^{2+} signals. To avoid this, instead of testing the effects of GPN pretreatment on histamine and bradykinin Ca^{2+} signals, I performed the experiment in the reverse mode, that is, testing the effects of histamine and bradykinin pretreatment on GPN-induced Ca^{2+} signals. For experiments carried out in this way, a saturating concentration of histamine and bradykinin was used to maximally deplete intracellular Ca^{2+} stores. Also, the experiments were carried out in the absence of extracellular Ca^{2+}. This was to allow detection of Ca^{2+} release only. Following histamine, GPN-induced Ca^{2+} signals were largely but not completely abolished (Fig5.3.1B, C, F and G). This could suggest that lysosomes are implicated in histamine-induced Ca^{2+} signals. But on the other hand, given that GPN also mobilizes ER Ca^{2+} likely via MCSs in fibroblasts (Kilpatrick et al., 2013; Penny et al., 2014) and histamine signals through inducing ER Ca^{2+} release (Hill et al., 1997; Kip et al., 2006; Montero et al., 2003; Pinheiro, Paramos-De-carvalho, et al., 2013; Willets et al., 2008), the reduced GPN responses after histamine could be due to reduced ER Ca^{2+}. Two lines of evidence argue against this. First, I found that in contrast to histamine's strong inhibitory effect on GPN Ca^{2+} signals, bradykinin only appeared to modestly reduce GPN Ca^{2+} signals (not statistically significant, Fig5.3.1D-G) even though it is also known to function through the ER (Ataei et al., 2013; Lambert et al., 1986; Pinheiro, Paramos-De-Carvalho, et al., 2013). My results are consistent with Kilpatrick et al.,

2013 where bradykinin turns GPN Ca^{2+} signals from oscillatory to monotonic (Fig.5.3.1A). Second were the results of experiments where I tested the effects of histamine and bradykinin on thapsigargin-induced Ca^{2+} release. Thapsigargin is a SERCA inhibitor that can deplete ER Ca^{2+} (i.e. indirect "monitoring" ER Ca^{2+} level) (Sehgal et al., 2017; Treiman et al., 1998). Surprisingly, I observed that following histamine, thapsigargin Ca^{2+} signals were largely maintained, and following bradykinin, thapsigargin Ca^{2+} signals were not affected at all (Fig.5.3.2). This suggests that the ER store is refilled after agonist stimulation, which is unexpected as experiments were performed without extracellular Ca^{2+}. The mechanism behind such refilling requires investigation. Nevertheless, this indirectly indicates that the reduced GPN signals after histamine is due to reduced lysosomal Ca^{2+}. Moreover, the facts that after histamine, GPN but not thapsigargin Ca^{2+} signals were largely reduced could indicate that the ER but not lysosomes are refilled with Ca^{2+} after agonist stimulation, or perhaps, lysosomes are less effective than the ER in taking up Ca^{2+}. In fact, as discussed in chapter 2, the mechanism for lysosomal Ca^{2+} uptake remains elusive.

I next examined whether TPCs are implicated in histamine and bradykinin Ca^{2+} signals. I first utilized a pharmacological approach. Ned-19 is a selective NAADP antagonist (Naylor et al., 2009). Using Ned-19, NAADP has been associated with a number of extracellular stimuli-induced Ca^{2+} signals, including carbachol, glucose and histamine (Aley et al., 2013; Esposito et al., 2011; Naylor et al., 2009). But Ned-19 is not the top choice for probing TPC involvement for several reasons. First, NAADP is known to activate TPCs indirectly under regulation of multiple factors (Jha et al., 2014; Lin-Moshier et al., 2012; Walseth et al., 2012), it is therefore likely that Ned-19 blocks TPCs indirectly as well. Importantly, in chapter 3, I found that Ned-19 is more potent in blocking A1-induced TPC2-dependent Ca^{2+} signals when environment changed from the near-neutral extracellular space to the acidic lysosomes. Second, Ned-19 has been shown to activate TPC2 activity at nanomolar concentration (Pitt et al., 2010). Third, Ned-19 and NAADP may not be entirely selective for TPCs. It has been reported that NAADP can activate TRPML1 and Ned-19 can block TRPML1 Ca^{2+} signals induced by ML-SA1 (Lee et al., 2015; Zhang et al., 2009). In line with this, in chapter 3, I observed that Ned-19 tended to inhibit TRPML1-evoked Ca^{2+} release. Besides, an action of NAADP on RyRs has also been reported (Hohenegger et al., 2002; Langhorst et al., 2004; Dammermann and Guse, 2005) although controversially

(Copello et al., 2001; Wagner et al., 2014). NAADP antagonism (using Ned-19) therefore offers a relatively complicated route to inhibit TPC activity, and possibly accompanied with off-target or undesired effects.

I therefore took advantage of the developing TPC pharmacology. The most potent TPC blocker is tetrandrine which was identified in 2015 (Sakurai et al., 2015). Consistent with its TPC blocking identity, in chapter 3, I show that tetrandrine blocked Ca^{2+} signals by the TPC2 agonist, A1. Also, tetrandrine is likely to bind to the pore of TPCs to elicit action. This is because tetrandrine is a Cav blocker (King et al., 1988; Liu et al., 1992; Sakurai et al., 2015), and docking analysis reveal Cav blockers targeted at the pore region of TPCs as they did on evolutionarily-linked Cav (Rahman et al., 2014). Tetrandrine therefore was utilized to investigate whether TPCs are required for histamine- and bradykinin-induced Ca^{2+} signals. For these experiments, I used half-maximal concentrations of histamine and bradykinin, which have been established by a previous lab member (Yates, 2017). I observed that tetrandrine reduced histamine-induced Ca^{2+} signals by two-fold whereas it only modestly reduced bradykinin-induced Ca^{2+} signals (Fig.5.3.3). Tetrandrine therefore affects both agonists, with a stronger inhibitory effect on histamine signals than that on bradykinin signals. The experiments were conducted with extracellular Ca^{2+}, therefore, one consideration is that the inhibition by tetrandrine could be via blocking Ca^{2+} entry. Tetrandrine is known to inhibit L-type and T-type Cav (King et al., 1988; Liu et al., 1992), and the latter was shown to be required for histamine-induced Ca^{2+} influx in a neuroendocrine tumour cell line (Pfanzagl et al., 2019). However, in non-excitable fibroblasts, if Cavs are present, they would not be expected to be functional. Cavs are therefore unlikely to contribute on the signal inhibition by tetrandrine. In non-excitable cells, store-operated Ca^{2+} channels (SOCCs) offer the major route for Ca^{2+} entry, which is activated upon ER store depletion (Baumann, 2012; Jardin et al., 2018). In an early study, tetrandrine has been shown to block thapsigargin-induced Ca^{2+} influx in NIH/3T3 fibroblasts (Takemura et al., 1996), indicating that tetrandrine may block SOCE. However, to note, tetrandrine has a stronger inhibitory effect on histamine Ca^{2+} signals than bradykinin Ca^{2+} signals. Given the "extra" effect of tetrandrine on histamine, the reduced histamine signals is unlikely to be solely due to an action of tetrandrine on Ca^{2+} entry. Similarly, this 'extra' block is unlikely to be due to an effect on ER Ca^{2+} release. Never-the-less testing tetrandrine against histamine and

bradykinin in the absence of extracellular Ca^{2+} could be informative. Rather my findings that histamine Ca^{2+} signals are more tetrandrine-sensitive echoes the findings that histamine Ca^{2+} signals are lysosome-dependent. Taken together, histamine possibly induces TPC-dependent Ca^{2+} signals.

In 2018, through a drug screening approach, a number of novel TPC pore blockers have come to light (Penny et al., 2019), including those targeting estrogen receptors (e.g. raloxifene) and dopamine receptors (e.g. fluphenazine). In chapter 3, these drugs blocked Ca^{2+} signals by the TPC2 agonist, A1, confirming their identity as TPC blockers. Therefore, in addition to tetrandrine, I also applied these novel blockers to study the TPC involvement in histamine and bradykinin-evoked Ca^{2+} signals. Interestingly, in fibroblasts, 10 μM raloxifene and fluphenazine induced robust Ca^{2+} signals (Fig.5.3.4). This effect was not seen in HeLa cells (in chapter 3). The mechanism for their Ca^{2+} responses is unclear. For fluphenazine, perhaps, this could be explained by its reported ability to inhibit SERCA and the subsequent Ca^{2+} efflux from the ER (Michelangeli & East, 2011). However, considering the lack of Ca^{2+} signals in HeLa cells, such SERCA inhibition may not be the reason. Or perhaps, the SERCA inhibition is a cell-type specific behaviour of fluphenazine. Regardless of how raloxifene and fluphenazine induce Ca^{2+} signals (still requiring investigations), their Ca^{2+} signals would complicate the subsequent analysis of histamine- and bradykinin-induced Ca^{2+} signals. To minimise the Ca^{2+} responses, I used lower concentrations of raloxifene and fluphenazine. Raloxifene of 1 μM reduced both histamine and bradykinin Ca^{2+} signals (Fig.5.3.5). Encouragingly, similar to tetrandrine, raloxifene's effect on histamine signals was stronger than that on bradykinin signals. The "extra" effect on histamine signals therefore could be due to an inhibitory effect of raloxifene on a pathway that is not required by bradykinin for generating Ca^{2+} signals. To reasonably extrapolate, compared to bradykinin, the "extra" inhibition of the histamine response by raloxifene might be caused by raloxifene's inhibitory effect on TPCs, further echoing the role of lysosomes on histamine signals.

Fluphenazine at 1 μM fully blocked histamine Ca^{2+} signals but left bradykinin-induced Ca^{2+} signals intact (Fig.5.3.6). However, notably, Fluphenazine has been reported to be a potent histamine receptor antagonist (Yonemura & Miyanaga, 1998). In contrast, there is no literature suggests an action of tetrandrine and raloxifene on histamine

receptors. Therefore, fluphenazine is not ideal to study the relation of TPCs to histamine Ca^{2+} signalling. But fluphenazine does reveal that Ca^{2+} signals by bradykinin are unlikely to be TPC dependent.

From the above results, I propose that histamine utilizes TPCs for Ca^{2+} signalling but bradykinin does not. Strengthening the pharmacological evidence that histamine Ca^{2+} signalling might be TPC-dependent, in 2017, naringenin was shown to block histamine Ca^{2+} signalling, and this effect was ascribed to inhibited TPC activity (Pafumi et al., 2017). In addition to TPCs, TRPML1 has also been shown to induce global signals by functionally coupling to ER Ca^{2+} release and stimulating Ca^{2+} influx from the extracellular space (Kilpatrick, Yates, et al., 2016). It is reassuring that TPC blockers (tetrandrine, raloxifene or fluphenazine) are selective to TPCs over TRPML (chapter 3). Additionally, although TRPML1 can induce global Ca^{2+} signalling upon activation by its synthetic activator ML-SA1 (Kilpatrick, Yates, et al., 2016), there is very little information about whether TRPML1 is important for physiological agonists-induced global Ca^{2+} signals. $PI(3,5)P_2$ can activate endogenous TRPML1 currents (Dong et al., 2010), but whether it induce TRPML1-mediated Ca^{2+} signals is unknown.

Although reduced histamine signals by tetrandrine and raloxifene have been interpreted as a direct inhibition on TPC activity by the drugs, being prudent, it is necessary to consider another possibility, which is lysosomal "trapping". It has been known for decades that lipophilic weak bases can accumulate inside lysosomes upon protonation (De Duve et al., 1974; Nadanaciva et al., 2011). This lysosomotropism can raise lysosomal pH (Lemieux et al., 2004). As lysosomal Ca^{2+} uptake is thought to require the lysosomal pH gradient (Morgan et al., 2011; Patel & Docampo, 2010), lysosomotropism therefore may reduce lysosomal Ca^{2+}. Accordingly, if a compound is a lysosomotropic agent (i.e. causing lysosomotropism), it would be expected to reduce lysosomal Ca^{2+} signals, regardless of whether it can directly block TPCs. Whether a compound has propensity to be trapped inside the lysosomes is dictated by two physiochemical properties, an acid dissociation constant (pKa) > 7 and a lipophilicity (logP) > 2 (Nadanaciva et al., 2011). Raloxifene has a pKa value of 8.89 and a logP value of 5.69 as shown by ChemAxon; https://go.drugbank.com/drugs/DB00481. Similarly, the pKa and logP for tetrandrine has been reported to be 8.3 and 5.6, respectively (Xiao et al., 2017). Tetrandrine and

raloxifene therefore have the potential to be lysosomotropic agents. Testing tetrandrine and raloxifene on lysosomal pH under my conditions could be informative. This could be done indirectly with LTR (Chapter 2) which is in fact a fluorophore that relies on acid-trapping to target lysosomes (Kilpatrick et al., 2015). However, it is important to note, even if tetrandrine and raloxifene are lysosomotropic agents, their rates of trapping (i.e. the rate of lysosomal pH increase) could be slow (as NH_4Cl from chapter 2). Also, in chapter 2, I have pointed out that the Ca^{2+} leak upon increased lysosomal pH could also be slow. In light of the above, there is a possibility that tetrandrine and raloxifene may require a sustained incubation time to have a clear impact on lysosomal Ca^{2+} by lysosomotropism. Therefore, even if tetrandrine and raloxifene may become trapped inside the lysosomes, the reduced histamine signals observed after 15-minute treatment may be independent of this. Favouring this, within the 15-minute period, tetrandrine did not cause Ca^{2+} signals upon acute treatment. Although raloxifene at 1 μM did induce a rise in cytosolic Ca^{2+}, the rise was modest and the source for the Ca^{2+} rise is unclear, requiring further investigation. Regarding the lysosomotropism issue, two other experiments could be considered: 1) searching for compounds that cannot block TPCs but can cause similar degree of lysosomotropism as tetrandrine or raloxifene, and then testing the compounds against histamine action (may serve as a negative control); 2) searching for compounds that can block TPCs and free from being "trapped" inside the lysosomes (Gunaratne, Johns, et al., 2018), and then testing the compounds against histamine action (may serve as a positive control).

Aside from using a pharmacological approach, I also examined the effects of TPC knockdown on histamine and bradykinin Ca^{2+} signals. I used TPC siRNAs which have been validated previously in fibroblasts (Kilpatrick et al., 2017). Using qPCR, I found that in fibroblasts, TPC1 transcripts are much higher than that of TPC2 (Fig.5.3.7A and C), as also found in other cell lines (Brailoiu et al., 2009; Faris et al., 2019; Nguyen et al., 2017; Trufanov et al., 2019). As expected, TPC1 and TPC2 transcripts were reduced by their respective siRNA. To be precise, TPC1 level was reduced by about 85%, and TPC2 level was reduced by about 65% (Fig.5.3.7B and D). Efficient TPC1 and TPC2 knockdown therefore can be achieved in fibroblasts, although the knockdown of TPC2 is less efficient than that of TPC1 which has also been reported in other studies (García-Rúa et al., 2016; Sakurai et al., 2015). In cells with reduced levels of both TPC1 and TPC2 (double knockdown), I found that histamine but not

bradykinin-induced Ca^{2+} signals were also reduced (Fig.5.3.8). This somewhat is in accord with the effect of the TPC blockers (tetrandrine and raloxifene) on the Ca^{2+} signals evoked by the two agonists. Notably, TPC knockdown only reduced histamine signals by 25%, less effective than the TPC blockers. Perhaps this is because that TPC blockers have off-target effects on other components required by histamine signals. Given that bradykinin signals were also modestly reduced by TPC blockers but not by TPC knockdown, the other components could be the ER store and SOCCs. Returning back to the effects of TPC knockdown on histamine signals, this could reflect that TPC has a small contribution on histamine signals. But on the other hand, given that qPCR can only inform on the mRNA level, the protein levels of TPC1 and TPC2 may still high. Western blot can determine protein level, but the lack of a good TPC antibody is the chief obstacle. It is worth trying other commercial TPC siRNAs. Also, rescue experiments (e.g. using siRNA-resistant construct (Kilpatrick et al., 2017)) should be considered in the future for assessing specificity.

As TPCs are required by histamine-induced Ca^{2+}signalling, I next examined the relative TPC1 and TPC2 involvement. I found that there was a significant reduction in histamine-induced Ca^{2+} signals upon TPC2 but not TPC1 knockdown (Fig.5.3.9). The implication could be that TPC2 but not TPC1 is implicated in histamine Ca^{2+} signalling. To note, TPC2 is predominantly localized to lysosomes (Calcraft et al., 2009). Although TPC1 has been reported to have a wider distribution within the endo-lysosomal system (Brailoiu et al., 2009), the endosomes appear to be its major site (Castonguay et al., 2017; Kilpatrick et al., 2017). The differential localization of TPC1 and TPC2 within the endo-lysosomal system therefore may explain why TPC2 (lysosomes) but not TPC1 (endosomes) are required by histamine for signalling. Or perhaps, histamine recruits endosomes for Ca^{2+} signalling but via other calcium channels rather than TPC1. Supporting the role of TPC2 on histamine Ca^{2+} signalling, previously, it has been shown that TPCs are required by histamine type 1 receptor-induced von Willebrand factor (VWF) secretion (Esposito et al., 2011) although they did not measure Ca^{2+} in TPC-depleted cells.

As the relevance of TPC2 to global Ca^{2+} signals has been revealed, the next step therefore should be to study the physiological and pathophysiological meaning of this. For example, in fibroblasts carrying TPC2 polymorphism M484L, there was a

significant increase in endogenous $PI(3,5)P_2$ currents compared to TPC2 WT fibroblasts (Chao et al., 2017). Such an increase may also apply to histamine Ca^{2+} signals, which should be tested. Notably, altered physiological Ca^{2+} signalling may impact human health under stress conditions. NAADP-induced Ca^{2+} signals are augmented in PD patient fibroblasts (Hockey et al., 2015), which could be translated as augmented TPC2-dependent histamine Ca^{2+} signalling. In other words, TPC2 may contribute to the development of diseases (e.g. PD) via a global Ca^{2+} route.

In summary, I used three different approaches to examine the relation of TPCs to physiological agonist-induced Ca^{2+} signals. First, I used GPN and I found Ca^{2+} signals by GPN were largely reduced after histamine but not bradykinin stimulation. Second, I used TPC blockers and I found that tetrandrine and raloxifene reduced histamine signals to a larger extent compared to their effects on bradykinin signals. Finally, I used TPC knockdown and I found that histamine but not bradykinin signals were reduced by the knockdown. More specifically, histamine signals were reduced by TPC2 but not TPC1 knockdown. Together, TPCs are implicated in physiological global Ca^{2+} signals, likely in an agonist- and isoform-specific manner.

Chapter 6: Conclusions and Future Directions

TPCs are one class of cation channels in the endolysosomal system. For the last decade, TPCs have been associated with various physiological and pathophysiological functions (Grimm et al., 2017; Patel & Kilpatrick, 2018). However, our current understanding on this channel remains limited. Abundant evidence exists to show that TPCs are NAADP-activated non-selective Ca^{2+}-permeable channels (Calcraft et al., 2009; Grimm et al., 2014; Penny et al., 2019; Ruas et al., 2015; Schieder et al., 2010), while other evidence indicates that TPCs are $PI(3,5)P_2$-activated Na^+-selective channels (Cang et al., 2013, 2014; Guo et al., 2017; She et al., 2018; Wang et al., 2012). The gating mechanism and ion selectivity of TPCs, thus, are disputed. In addition, TPC-mediated local Ca^{2+} signals have been found to regulate membrane trafficking (Grimm et al., 2014; Hockey et al., 2015; Lin-Moshier et al., 2014; Vassileva et al., 2020). The local signals can be converted into global signals by lysosome-ER Ca^{2+} coupling likely via MCSs (Kilpatrick et al., 2013; Penny et al., 2015). But it is less clear as to whether TPCs are required for physiological Ca^{2+} signalling evoked by extracellular stimuli. Above all, the pharmacology of TPCs is limited and there are no effective TPC modulators that can aid research and drug discovery. In this thesis, I have provided new insight into known modulators and developed new ones (Fig.6.1).

The lysosomotropic agent, GPN, has long been appreciated to evoke Ca^{2+} release from acidic organelles and thus to probe TPC function. GPN does so because it is cleaved by cathepsin C. The resultant products are thought to rupture lysosomal membranes by evoking an osmotic stress (Jadot et al., 1984). This longstanding view, however, has recently been challenged (Atakpa et al., 2019). The new study instead suggests that GPN induces Ca^{2+} release from the ER by increasing cytosolic pH. In chapter 2, the focus therefore was to re-examine GPN action. In human fibroblasts, I found that GPN increased cytosolic pH, but when compared to its effects on cytosolic Ca^{2+}, there was a kinetic discrepancy. Specifically, the change in pH occurred faster than the onset of Ca^{2+} responses. Further supporting such discrepancy, the weak base NH_4Cl induced a similar change in cytosolic pH as GPN but only very modest Ca^{2+} responses. The GPN Ca^{2+} response thus is unlikely to be a result of cytosolic pH alkalization. Moreover, to examine the role of acidic organelles on GPN action, I used bafilomycin A1, a V-type ATPase inhibitor that is thought to perturb acidic Ca^{2+} stores by

dissipating the luminal pH gradient. In fibroblasts, one notable observation was that bafilomycin A1 slowly increased luminal pH. When bafilomycin A1 had a modest effect on lysosomal pH (i.e. acute treatment), GPN- and thapsigargin-induced Ca^{2+} signals were both potentiated. In contrast, when bafilomycin A1 induced a dramatic change in the luminal pH (i.e. chronic treatment), GPN but not thapsigargin Ca^{2+} responses were inhibited. My data thus supported an action of GPN on acidic organelles. However, future work still requires exploring how this exactly happens. There is compelling evidence showing that GPN-induced Ca^{2+} signals are independent of cathepsin C (Atakpa et al., 2019). But this does not equate to a lack of effect of GPN on membrane integrity given that GPN isoform, D-GPN, a non-cathepsin C substrate, was shown previously to permeabilize lysosomal membranes (Jadot et al., 1990) and increase cytosolic Ca^{2+} (Atakpa et al., 2019). To study this, the effects of GPN on endocytosed fluorophores could be assayed in the future.

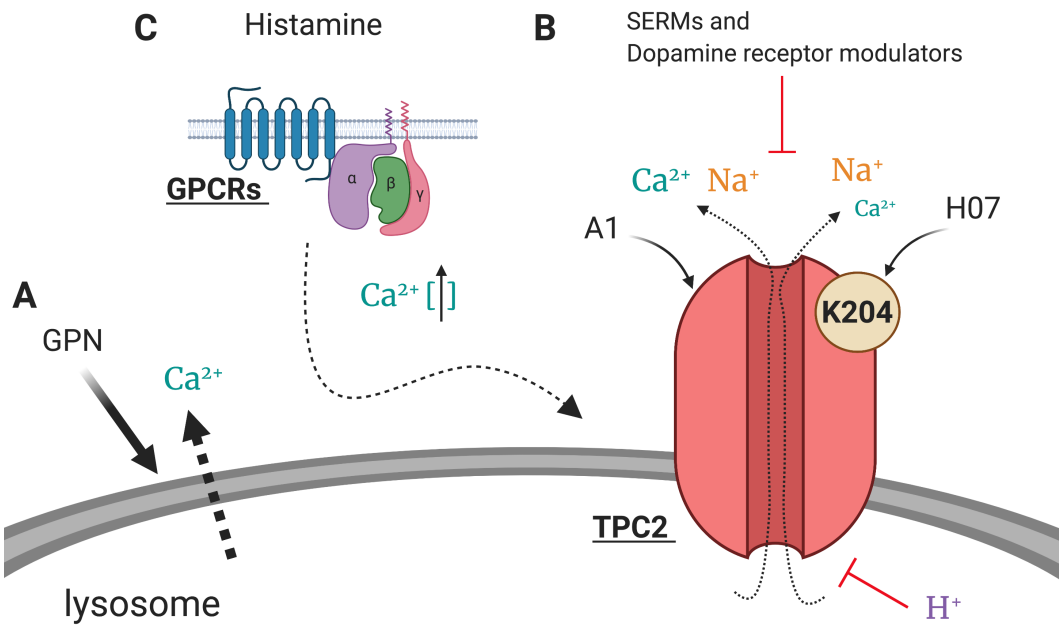

Figure 6.1 Overview of chemical tools for studying endolysosomal two-pore channels. Conclusions and future directions

(A) GPN induces Ca^{2+} signals by targeting acidic organelles such as lysosomes, but the underlying mechanism requires further investigation.

(B) A1 and H07 are cell-permeable and selective TPC2 activators. They activate TPC2 to induce pore-dependent Ca^{2+} signals, confirming the Ca^{2+} permeability of TPC2, They also induce Na^{+} signals, consistent with the Na^{+} permeability of the channel. In comparison, A1 induces larger Ca^{2+} signals but similar Na^{+} signals as H07 (left). H07 but not A1 requires K204

for action resembling $PI(3,5)P_2$ (right). H07- but not A1-induced Ca^{2+} signals are regulated by acidic luminal pH. Together, TPC2 activity is regulated in an activity dependent manner. Some SERMs and dopamine receptor modulators are novel TPC2 inhibitors. Future work should further characterize these novel TPC modulators provided in this thesis.
(C) Lysosomes and TPCs are required for physiological global Ca^{2+} signals induced by extracellular stimuli (e.g. histamine), likely in an isoform-specific manner. Future work should examine the physiological and pathophysiological meaning of this.

The association of TPCs with diseases has highlighted the significance of having direct TPC modulators as they can be used for research and drug discovery. In chapter 3, I introduced and characterized novel TPC modulators given the extant chemical tools are limited (Table 1.1 and 1.2). I identified A1 and H07 as structurally different cell-permeable TPC2 activators. I showed that they can activate recombinant TPC2 to induce pore-dependent Ca^{2+} signals. Importantly, A1 also induced endogenous Ca^{2+} responses. Such endogenous responses are likely to be TPC2 dependent as the responses to A1 were largely reduced in cells expressing dominant-negative TPC2. Future works should also examine A1 and H07 in TPC2 KO cells (Grimm et al., 2014; Ruas et al., 2015) or in cells treated with TPC2 siRNA (Hockey et al., 2015; Kilpatrick et al., 2017) for making a firmer conclusion. Moreover, I showed that A1 and H07 are selective to TPC2 as they cannot activate TRPML1 or TPC1 at concentrations that induced TPC2-dependent Ca^{2+} responses. However, my results were less clear regarding whether TRPML1/TPC1 are targets for A1/H07 as much higher concentrations (e.g. 100 μM) were not examined. This could be established in the future. In the same chapter, I also confirmed that a number of drugs targeting dopamine and estrogen receptors are TPC2 inhibitors. These compounds were first identified from a drug re-purposing approach designed for pursuing novel TPC inhibitors (Penny et al., 2019). Here, these compounds and also tetrandrine (a TPC inhibitor identified in Sakurai et al., 2015) blocked A1-induced Ca^{2+} signals in cells expressing PM TPC2, further confirming the action of A1 on TPC2. Future structure-activity approaches are warranted.

One interesting finding from chapter 3 was that A1 and H07 activated TPC2 to differentially affect Ca^{2+}. Specifically, A1 induced larger Ca^{2+} signals than H07 in cells transfected with lysosomal TPC2 (i.e. TPC2 GCaMP6s). Depleting the ER and

lysosome stores indicated that A1 but not H07 resembled NAADP in coupling both stores for signalling. The larger signals thus can be explained. However, in cells expressing PM TPC2, that is functionally uncoupled to the ER, A1 also induced larger Ca^{2+} signals than H07 at certain concentrations. Strikingly, there was a visible delay in H07 but not A1-induced Ca^{2+} signals, which cannot be resolved by increasing the concentration of H07. Thus, in cells transfected with TPC2 GCaMP6s, part of the reason that A1 exhibits larger Ca^{2+} responses than H07 could be ER-coupling, and another reason could be that A1 releases more lysosomal Ca^{2+}. Future work could use GECO of lower Ca^{2+} affinity and manipulators of membrane contact sites to disentangle 'trigger' and 'amplification' signals (Davis et al., 2020).

In chapter 4, I further characterized A1 and H07. It remains to be determined whether TPCs are NAADP-gated non-selective Ca^{2+}-permeable channels or $PI(3,5)P_2$-gated Na^+-selective channels. I showed that TPC2 is permeable to both Ca^{2+} and Na^+ as both A1 and H07 can activate the channel to induce Ca^{2+} and also Na^+ signals. Notably, however, when comparing their responses, I found that A1 induced larger Ca^{2+} signals (also as indicated in chapter 3) but similar Na^+ signals as H07. One intriguing hypothesis is that the ion selectivity of TPC2 is agonist-dependent. Indeed, I found that kinetically, for A1, there was no apparent difference between its Ca^{2+} responses and Na^+ responses. In contrast, for H07, its Na^+ signals occurred a few minutes prior to the onset of its Ca^{2+} signals. Importantly, removing Na^+ had a remarkable potentiating effect on H07 but not A1-induced Ca^{2+} signals. Therefore, the implication could be that when activated by A1, TPC2 might be non-selective like in the presence of NAADP, while when activated by H07, TPC2 might be Na^+-selective like in the presence of $PI(3,5)P_2$. This has been confirmed by electrophysiology studies where PCa/PNa ratios for their respective currents were examined (Gerndt et al., 2020); the ratio for A1 and NAADP (0.65 ± 0.13 versus 0.73 ± 0.14) and the ratio for H07 and $PI(3,5)P_2$ (0.04 ± 0.01 versus 0.08 ± 0.0) were similar. The ion selectivity of TPC2 thus appears to be agonist-specific. This finding is of major significance as this could resolve the long-held debate over the gating and selectivity of TPC2. However, it is uncertain whether TPC1 also possesses a similar property. Identification of TPC1 activators would be most useful to the community.

I also showed that H07- but not A1-induced Ca^{2+} responses were inhibited by mutation in K204, a residue mapped to the IS4-IS5 linker and required for activation by $PI(3,5)P_2$ (She et al., 2019). Considering both H07 and $PI(3,5)P_2$ render TPC2 Na^+ selective and require K204 for action, I reasoned that how the channel is activated molecularly might determine its ion selectivity. In other words, K204 binding might be associated with Na^+ selectivity. However, tricyclic anti-depressants (TCAs) and riluzole, the other cell-permeable TPC2 activators identified by Zhang et al., 2019, do not require K204 for action but they also induce Na^+-selective cation currents. This could mean that K204 is not the sole determinant. Thus, in the future, the molecular basis for TPC2 activation by the agonist should be further investigated, as this may inform how the ion selectivity of the channel is conferred at a molecular level. In particular, we know nothing of the molecular determinants concerning A1 activation. Finally, I found that H07- but not A1-induced Ca^{2+} responses were inhibited by "luminal" acidic pH. In this chapter, I therefore showed that A1 and H07 differentially activate TPC2 in terms of ion selectivity, K204 binding and pH regulation. Interestingly, in Gerndt et al., 2020, A1 and H07 have been linked to distinct lysosomal functions, further pointing to TPC2 as a unique channel that signals in an agonist-dependent manner through different ions. More work is required to understand how Na^+ signals regulate cellular processes. However, what would be interesting to me is to know how TPC signals in the presence of both A1 and H07 as this would be similar to the situation in cells where both NAADP and $PI(3,5P)_2$ coexist.

TPCs regulate membrane trafficking likely by mediating local lysosomal Ca^{2+} signals (Marchant & Patel, 2015; Vassileva et al., 2020). TPCs are also involved in global Ca^{2+} signalling (Calcraft et al., 2009; Jha et al., 2014; Ogunbayo et al., 2011). What remains unclear, however, is that whether TPCs are implicated in extracellular stimuli-induced physiological global Ca^{2+} signalling. In the final chapter, this was investigated. First, in fibroblasts, I found that histamine but not bradykinin largely reduced GPN-induced Ca^{2+} signals. Given that in chapter 2, GPN was shown to work through acidic organelles, these data thus suggested that lysosomes are important for histamine but not bradykinin Ca^{2+} signals. Second, when cells were challenged with TPC inhibitors (those characterized in chapter 3), histamine-induced Ca^{2+} signals were reduced by a larger extent than bradykinin Ca^{2+} signals. The "extra" reduction in histamine signals therefore is likely due to an action of the inhibitors on a pathway that is irrelevant to

bradykinin stimulation, which could be TPCs given the involvement of lysosomes in histamine signalling. However, one should also be cautious that those TPC inhibitors may simply be acid-trapped inside lysosomes to inhibit histamine-induced Ca^{2+} signals. Finally, when cells were subjected to TPC knockdown, histamine but not bradykinin-induced Ca^{2+} signals were reduced albeit modestly, again suggesting that TPCs are required for histamine but not bradykinin action. TPC siRNA used here can cause efficient TPC knockdown in fibroblasts, which has been validated previously by qPCR (Kilpatrick et al., 2017) and confirmed here. Even so, it is still worth trying other commercial TPC siRNAs. In addition, future work should also consider rescue experiments using, for instance, siRNA-resistant construct (Kilpatrick et al., 2017), to assess specificity. The relative involvement of TPC1 and TPC2 in histamine Ca^{2+} responses were subsequently examined via similar siRNA knockdown approach, and TPC2 but not TPC1 was found to be important. The relevance of TPCs to global Ca^{2+} signalling by stimuli therefore has been established. Future work should examine TPC knockout cells to confirm this. Also, the pathophysiological meaning of this requirement should be pursued given exaggerated NAADP-induced global Ca^{2+} signals were observed in cells from patients with Parkinson's disease (PD) (Hockey et al., 2015). In other words, dysfunction in TPC2 may alter global signals evoked by physiological agonists (e.g. histamine) to contribute to pathologies.

In summary (Fig. 6.1), I showed that GPN targets acidic organelles to evoke Ca^{2+} signals, although it remains a mystery in regard to how this occurs. Importantly, I identified cell-permeable and selective TPC2 activators, with which TPCs can now be easily studied in more detail. Characterizations on the novel activators unveiled that agonist-specific TPC2 activation and regulation. This resolves the long-held debate over the gating and selectivity of TPCs. That is, TPCs are NAADP-gated non-selective Ca^{2+}-permeable channels and also $PI(3,5)P_2$-gated Na^+-selective channels. In addition, I confirmed a number of estrogen and dopamine receptor modulators as TPC2 inhibitors. Future research should further characterize these novel TPC2 modulators. Finally, I demonstrated that TPCs are required for global Ca^{2+} signals induced by extracellular stimuli, likely in an isoform-specific manner. This sets up future work to study how TPCs are implicated in diseases where global Ca^{2+} signals are altered.

Published papers associated with this thesis

Morgan, A. J., **Yuan, Y.**, Patel, S., & Galione, A. (2020). Does lysosomal rupture evoke Ca2+ release? A question of pores and stores. *Cell Calcium*, *86*, 102139.

Gerndt, S., Chen, C.-C., Chao, Y.-K., **Yuan, Y**., Burgstaller, S., Rosato, A. S, Krogsaeter, E., Urban, N., Jacob, K., Nguyen, O. N. P., Miller, M. T., Keller, M., Vollmar, A. M., Gudermann, T., Zierler, S., Schredelseker, J., Schaefer, M., Biel, M., Malli, R., … Grimm, C. (2020). Agonist-mediated switching of ion selectivity in TPC2 differentially promotes lysosomal function. *Elife*, *9,* e*54716.* (**First co-autthor**)

Penny, C. J., Vassileva, K., Jha, A., **Yuan, Y**., Chee, X., Yates, E., Mazzon, M., Kilpatrick, B.S., Muallem, S., Marsh, M., Rahman, T., & Patel, S. (2019). Mining of Ebola virus entry inhibitors identifies approved drugs as two-pore channel pore blockers. *Biochimica et Biophysica Acta (BBA)-Molecular Cell Research*, *1866*(7), *1151-1161.*

References

Aarhus, R., Dickey, D. M., Graeff, R. M., Gee, K. R., Walseth, T. F., & Lee, H. C. (1996). Activation and Inactivation of Ca Release by NAADP. *Journal of Biological Chemistry*, *271*(15), 8513–8516.

Aarhus, R., Graeff, R. M., Dickey, D. M., Walseth, T. F., & Lee, H. C. (1995). ADP-ribosyl cyclase and CD38 catalyze the synthesis of a calcium-mobilizing metabolite from NADP. *The Journal of Biological Chemistry*, *270*(51), 30327–30333.

Aley, P. K., Mikolajczyk, A. M., Munz, B., Churchill, G. C., Galione, A., & Berger, F. (2010). Nicotinic acid adenine dinucleotide phosphate regulates skeletal muscle differentiation via action at two-pore channels. *Proceedings of the National Academy of Sciences*, *107*(46), 19927–19932.

Aley, P. K., Singh, N., Brailoiu, G. C., Brailoiu, E., & Churchill, G. C. (2013). Nicotinic Acid Adenine Dinucleotide Phosphate (NAADP) Is a Second Messenger in Muscarinic Receptor-induced Contraction of Guinea Pig Trachea. *Journal of Biological Chemistry*, *288*(16), 10986–10993.

Ali, R. A., Camick, C., Wiles, K., Walseth, T. F., Slama, J. T., Bhattacharya, S., Giovannucci, D. R., & Wall, K. A. (2016). Nicotinic Acid Adenine Dinucleotide Phosphate Plays a Critical Role in Naive and Effector Murine T Cells but Not Natural Regulatory T Cells. *Journal of Biological Chemistry*, *291*(9), 4503–4522.

Alpy, F., Rousseau, A., Schwab, Y., Legueux, F., Stoll, I., Wendling, C., Spiegelhalter, C., Kessler, P., Mathelin, C., Rio, M. C., Levine, T. P., & Tomasetto, C. (2013). STARD3 or STARD3NL and VAP form a novel molecular tether between late endosomes and the ER. *Journal of Cell Science*.

Alvarez, C. P., Lasala, F., Carrillo, J., Muñiz, O., Corbí, A. L., & Delgado, R. (2002). C-Type Lectins DC-SIGN and L-SIGN Mediate Cellular Entry by Ebola Virus in cis and in trans. *Journal of Virology*, *76*(13), 6841–6844.

Ambrosio, A. L., Boyle, J. A., Aradi, A. E., Christian, K. A., & Di Pietro, S. M. (2016). TPC2 controls pigmentation by regulating melanosome pH and size. *Proceedings of the National Academy of Sciences of the United States of America*, *113*(20), 5622–5627.

Arndt, L., Castonguay, J., Arlt, E., Meyer, D., Hassan, S., Borth, H., Zierler, S., Wennemuth, G., Breit, A., Biel, M., Wahl-Schott, C., Gudermann, T., Klugbauer, N., & Boekhoff, I. (2014). NAADP and the two-pore channel protein 1 participate in the acrosome reaction in mammalian spermatozoa. *Molecular Biology of the Cell*, *25*(6), 948–964.

Arredouani, A., Ruas, M., Collins, S. C., Parkesh, R., Clough, F., Pillinger, T., Coltart, G., Rietdorf, K., Royle, A., Johnson, P., Braun, M., Zhang, Q., Sones, W., Shimomura, K.,

Morgan, A. J., Lewis, A. M., Chuang, K.-T., Tunn, R., Gadea, J., … Galione, A. (2015). Nicotinic Acid Adenine Dinucleotide Phosphate (NAADP) and Endolysosomal Two-pore Channels Modulate Membrane Excitability and Stimulus-Secretion Coupling in Mouse Pancreatic β Cells. *The Journal of Biological Chemistry*, *290*(35), 21376–21392.

Ataei, F., Torkzadeh-Mahani, M., & Hosseinkhani, S. (2013). A novel luminescent biosensor for rapid monitoring of IP3 by split-luciferase complementary assay. *Biosensors and Bioelectronics*, *41*, 642–648.

Atakpa, P., Thillaiappan, N. B., Mataragka, S., Prole, D. L., & Taylor, C. W. (2018). IP3 Receptors Preferentially Associate with ER-Lysosome Contact Sites and Selectively Deliver Ca2+ to Lysosomes. *Cell Reports*, *25*(11), 3180-3193.e7.

Atakpa, P., van Marrewijk, L. M., Apta-Smith, M., Chakraborty, S., & Taylor, C. W. (2019). GPN does not release lysosomal Ca2+ but evokes Ca2+ release from the ER by increasing the cytosolic pH independently of cathepsin C. *Journal of Cell Science*, *132*(3).

Atlas, D. (2014). Voltage-gated calcium channels function as Ca2+-activated signaling receptors. *Trends in Biochemical Sciences*, *39*(2), 45–52.

Austin, S., Tavakoli, M., Pfeiffer, C., Seifert, J., Mattarei, A., De Stefani, D., Zoratti, M., & Nowikovsky, K. (2017). LETM1-Mediated K+ and Na+ Homeostasis Regulates Mitochondrial Ca2+ Efflux. *Frontiers in Physiology*, *8*.

Avdonin, P. V., Nadeev, A. D., Tsitrin, E. B., Tsitrina, A. A., Avdonin, P. P., Mironova, G. Y., Zharkikh, I. L., & Goncharov, N. V. (2017). Involvement of two-pore channels in hydrogen peroxide-induced increase in the level of calcium ions in the cytoplasm of human umbilical vein endothelial cells. *Doklady Biochemistry and Biophysics*, *474*(1), 209–212.

Bailly, C. (2019). Cepharanthine: An update of its mode of action, pharmacological properties and medical applications. *Phytomedicine*, *62*(May), 152956.

Baize, S., Pannetier, D., Oestereich, L., Rieger, T., Koivogui, L., Magassouba, N., Soropogui, B., Sow, M. S., Keïta, S., De Clerck, H., Tiffany, A., Dominguez, G., Loua, M., Traoré, A., Kolié, M., Malano, E. R., Heleze, E., Bocquin, A., Mély, S., … Günther, S. (2014). Emergence of Zaire Ebola Virus Disease in Guinea. *New England Journal of Medicine*, *371*(15), 1418–1425.

Bandyopadhyay, D., Cyphersmith, A., Zapata, J. A., Kim, Y. J., & Payne, C. K. (2014). Lysosome Transport as a Function of Lysosome Diameter. *PLoS ONE*, *9*(1), e86847.

Barsukova, A., Komarov, A., Hajnóczky, G., Bernardi, P., Bourdette, D., & Forte, M. (2011). Activation of the mitochondrial permeability transition pore modulates Ca2+ responses to physiological stimuli in adult neurons. *The European Journal of*

Neuroscience, *33*(5), 831–842.

Báthori, G., Csordás, G., Garcia-Perez, C., Davies, E., & Hajnóczky, G. (2006). Ca2+-dependent control of the permeability properties of the mitochondrial outer membrane and voltage-dependent anion-selective channel (VDAC). *The Journal of Biological Chemistry*, *281*(25), 17347–17358.

Baughman, J. M., Perocchi, F., Girgis, H. S., Plovanich, M., Belcher-Timme, C. A., Sancak, Y., Bao, X. R., Strittmatter, L., Goldberger, O., Bogorad, R. L., Koteliansky, V., & Mootha, V. K. (2011). Integrative genomics identifies MCU as an essential component of the mitochondrial calcium uniporter. *Nature*, *476*(7360), 341–345.

Baumann, K. (2012). Signalling: Stop refilling (Ca 2+stores). *Nature Reviews Molecular Cell Biology*, *13*(5), 277.

Baylor, S. M., & Hollingworth, S. (1988). Fura-2 calcium transients in frog skeletal muscle fibres. *The Journal of Physiology*, *403*, 151–192.

Beck, A., Kolisek, M., Bagley, L. A., Fleig, A., & Penner, R. (2006). Nicotinic acid adenine dinucleotide phosphate and cyclic ADP-ribose regulate TRPM2 channels in T lymphocytes. *FASEB Journal : Official Publication of the Federation of American Societies for Experimental Biology*, *20*(7), 962–964.

Behne, M. J., Tu, C.-L., Aronchik, I., Epstein, E., Bench, G., Bikle, D. D., Pozzan, T., & Mauro, T. M. (2003). Human keratinocyte ATP2C1 localizes to the Golgi and controls Golgi Ca2+ stores. *The Journal of Investigative Dermatology*, *121*(4), 688–694.

Bellono, N. W., Escobar, I. E., & Oancea, E. (2016). A melanosomal two-pore sodium channel regulates pigmentation. *Scientific Reports*, *6*(1), 26570.

Benkerrou, D., Minicozzi, V., Gradogna, A., Milenkovic, S., Bodrenko, I. V., Festa, M., Lagostena, L., Cornara, L., D'Amore, A., Ceccarelli, M., Filippini, A., & Carpaneto, A. (2019). A perspective on the modulation of plant and animal two pore channels (TPCs) by the flavonoid naringenin. *Biophysical Chemistry*, *254*, 106246.

Berg, I., Potter, B. V. L., Mayr, G. W., & Guse, A. H. (2000). Nicotinic Acid Adenine Dinucleotide Phosphate (Naadp+) Is an Essential Regulator of T-Lymphocyte Ca2+-Signaling. *Journal of Cell Biology*, *150*(3), 581–588.

Bernardi, P., & von Stockum, S. (2012). The permeability transition pore as a Ca(2+) release channel: new answers to an old question. *Cell Calcium*, *52*(1), 22–27.

Berridge, M. J. (2002). The endoplasmic reticulum: a multifunctional signaling organelle. *Cell Calcium*, *32*(5–6), 235–249.

Berridge, M. J., Bootman, M. D., & Roderick, H. L. (2003). Calcium signalling: dynamics, homeostasis and remodelling. *Nature Reviews Molecular Cell Biology*, *4*(7), 517–529.

Berridge, M. J., Lipp, P., & Bootman, M. D. (2000). The versatility and universality of calcium signalling. *Nature Reviews. Molecular Cell Biology*, *1*(1), 11–21.

Bezprozvanny, I., Watras, J., & Ehrlich, B. E. (1991). Bell-shaped calcium-response curves of Ins(1,4,5)P3- and calcium-gated channels from endoplasmic reticulum of cerebellum. *Nature*, *351*(6329), 751–754.

Bhagya, N., & Chandrashekar, K. R. (2016). Tetrandrine – A molecule of wide bioactivity. *Phytochemistry*, *125*, 5–13.

Billington, R. A., & Genazzani, A. A. (2007). PPADS is a reversible competitive antagonist of the NAADP receptor. *Cell Calcium*, *41*(6), 505–511.

Blaustein, M. P., & Lederer, W. J. (1999). Sodium/Calcium Exchange: Its Physiological Implications. *Physiological Reviews*, *79*(3), 763–854.

Boccaccio, A., Scholz-Starke, J., Hamamoto, S., Larisch, N., Festa, M., Gutla, P. V. K., Costa, A., Dietrich, P., Uozumi, N., & Carpaneto, A. (2014). The phosphoinositide PI(3,5)P2 mediates activation of mammalian but not plant TPC proteins: functional expression of endolysosomal channels in yeast and plant cells. *Cellular and Molecular Life Sciences*, *71*(21), 4275–4283.

Boittin, F.-X., Galione, A., & Evans, A. M. (2002). Nicotinic Acid Adenine Dinucleotide Phosphate Mediates Ca 2+ Signals and Contraction in Arterial Smooth Muscle via a Two-Pool Mechanism. *Circulation Research*, *91*(12), 1168–1175.

Borg, J. J., Yuill, K. H., Hancox, J. C., Spencer, I. C., & Kozlowski, R. Z. (2002). Inhibitory Effects of the Antiestrogen Agent Clomiphene on Cardiac Sarcolemmal Anionic and Cationic Currents. *Journal of Pharmacology and Experimental Therapeutics*, *303*(1), 282–292.

Brailoiu, E., Churamani, D., Cai, X., Schrlau, M. G., Brailoiu, G. C., Gao, X., Hooper, R., Boulware, M. J., Dun, N. J., Marchant, J. S., & Patel, S. (2009a). Essential requirement for two-pore channel 1 in NAADP-mediated calcium signaling. *Journal of Cell Biology*, *186*(2), 201–209.

Brailoiu, E., Churamani, D., Cai, X., Schrlau, M. G., Brailoiu, G. C., Gao, X., Hooper, R., Boulware, M. J., Dun, N. J., Marchant, J. S., & Patel, S. (2009b). Essential requirement for two-pore channel 1 in NAADP-mediated calcium signaling. *The Journal of Cell Biology*, *186*(2), 201–209.

Brailoiu, E., Hoard, J. L., Filipeanu, C. M., Brailoiu, G. C., Dun, S. L., Patel, S., & Dun, N. J. (2005). Nicotinic Acid Adenine Dinucleotide Phosphate Potentiates Neurite Outgrowth. *Journal of Biological Chemistry*, *280*(7), 5646–5650.

Brailoiu, E., Hooper, R., Cai, X., Brailoiu, G. C., Keebler, M. V., Dun, N. J., Marchant, J. S., & Patel, S. (2010). An Ancestral Deuterostome Family of Two-pore Channels Mediates Nicotinic Acid Adenine Dinucleotide Phosphate-dependent Calcium Release from Acidic Organelles. *Journal of Biological Chemistry*, *285*(5), 2897–2901.

Brailoiu, E., Rahman, T., Churamani, D., Prole, D. L., Brailoiu, G. C., Hooper, R., Taylor,

C. W., & Patel, S. (2010). An NAADP-gated Two-pore Channel Targeted to the Plasma Membrane Uncouples Triggering from Amplifying Ca 2+ Signals. *Journal of Biological Chemistry*, *285*(49), 38511–38516.

Brailoiu, G. C., Gurzu, B., Gao, X., Parkesh, R., Aley, P. K., Trifa, D. I., Galione, A., Dun, N. J., Madesh, M., Patel, S., Churchill, G. C., & Brailoiu, E. (2010). Acidic NAADP-sensitive calcium stores in the endothelium: agonist-specific recruitment and role in regulating blood pressure. *The Journal of Biological Chemistry*, *285*(48), 37133–37137.

Bright, N. A., Davis, L. J., & Luzio, J. P. (2016). Endolysosomes Are the Principal Intracellular Sites of Acid Hydrolase Activity. *Current Biology*, *26*(17), 2233–2245.

Brini, M., & Carafoli, E. (2011). The plasma membrane Ca^2+ ATPase and the plasma membrane sodium calcium exchanger cooperate in the regulation of cell calcium. *Cold Spring Harbor Perspectives in Biology*, *3*(2).

Burgoyne, T., Patel, S., & Eden, E. R. (2015). Calcium signaling at ER membrane contact sites. *Biochimica et Biophysica Acta - Molecular Cell Research*, *1853*(9), 2012–2017.

Calcraft, P. J., Ruas, M., Pan, Z., Cheng, X., Arredouani, A., Hao, X., Tang, J., Rietdorf, K., Teboul, L., Chuang, K.-T., Lin, P., Xiao, R., Wang, C., Zhu, Y., Lin, Y., Wyatt, C. N., Parrington, J., Ma, J., Evans, A. M., … Zhu, M. X. (2009). NAADP mobilizes calcium from acidic organelles through two-pore channels. *Nature*, *459*(7246), 596–600.

Camello, C., Lomax, R., Petersen, O. ., & Tepikin, A. . (2002). Calcium leak from intracellular stores—the enigma of calcium signalling. *Cell Calcium*, *32*(5–6), 355–361.

Cancela, J. M., Churchill, G. C., & Galione, A. (1999). Coordination of agonist-induced Ca2+-signalling patterns by NAADP in pancreatic acinar cells. *Nature*, *398*(6722), 74–76.

Cang, C., Bekele, B., & Ren, D. (2014). The voltage-gated sodium channel TPC1 confers endolysosomal excitability. *Nature Chemical Biology*, *10*(6), 463–469.

Cang, C., Zhou, Y., Navarro, B., Seo, Y., Aranda, K., Shi, L., Battaglia-Hsu, S., Nissim, I., Clapham, D. E., & Ren, D. (2013). mTOR Regulates Lysosomal ATP-Sensitive Two-Pore Na+ Channels to Adapt to Metabolic State. *Cell*, *152*(4), 778–790.

Cao, E., Liao, M., Cheng, Y., & Julius, D. (2013). TRPV1 structures in distinct conformations reveal activation mechanisms. *Nature*, *504*(7478), 113–118.

Cao, Q., Yang, Y., Zhong, X. Z., & Dong, X. P. (2017). The lysosomal Ca2+ release channel TRPML1 regulates lysosome size by activating calmodulin. *Journal of Biological Chemistry*, *292*(20), 8424–8435.

Capel, R. A., Bolton, E. L., Lin, W. K., Aston, D., Wang, Y., Liu, W., Wang, X., Burton, R.-A. B., Bloor-Young, D., Shade, K.-T., Ruas, M., Parrington, J., Churchill, G. C., Lei,

M., Galione, A., & Terrar, D. A. (2015). Two-pore Channels (TPC2s) and Nicotinic Acid Adenine Dinucleotide Phosphate (NAADP) at Lysosomal-Sarcoplasmic Reticular Junctions Contribute to Acute and Chronic β-Adrenoceptor Signaling in the Heart. *Journal of Biological Chemistry*, *290*(50), 30087–30098.

Carette, J. E., Raaben, M., Wong, A. C., Herbert, A. S., Obernosterer, G., Mulherkar, N., Kuehne, A. I., Kranzusch, P. J., Griffin, A. M., Ruthel, G., Dal Cin, P., Dye, J. M., Whelan, S. P., Chandran, K., & Brummelkamp, T. R. (2011). Ebola virus entry requires the cholesterol transporter Niemann-Pick C1. *Nature*, *477*(7364), 340–343.

Castonguay, J., Orth, J. H. C., Müller, T., Sleman, F., Grimm, C., Wahl-Schott, C., Biel, M., Mallmann, R. T., Bildl, W., Schulte, U., & Klugbauer, N. (2017). The two-pore channel TPC1 is required for efficient protein processing through early and recycling endosomes. *Scientific Reports*, *7*(1), 10038.

Chanchevalap, S., Yang, Z., Cui, N., Qu, Z., Zhu, G., Liu, C., Giwa, L. R., Abdulkadir, L., & Jiang, C. (2000). Involvement of histidine residues in proton sensing of ROMK1 channel. *Journal of Biological Chemistry*, *275*(11), 7811–7817.

Chang, C.-L., Chen, Y.-J., & Liou, J. (2017). ER-plasma membrane junctions: Why and how do we study them? *Biochimica et Biophysica Acta (BBA) - Molecular Cell Research*, *1864*(9), 1494–1506.

Chao, Y.-K., Schludi, V., Chen, C.-C., Butz, E., Nguyen, O. N. P., Müller, M., Krüger, J., Kammerbauer, C., Ben-Johny, M., Vollmar, A. M., Berking, C., Biel, M., Wahl-Schott, C. A., & Grimm, C. (2017). TPC2 polymorphisms associated with a hair pigmentation phenotype in humans result in gain of channel function by independent mechanisms. *Proceedings of the National Academy of Sciences*, *114*(41), E8595–E8602.

Chen, C.-C., Keller, M., Hess, M., Schiffmann, R., Urban, N., Wolfgardt, A., Schaefer, M., Bracher, F., Biel, M., Wahl-Schott, C., & Grimm, C. (2014). A small molecule restores function to TRPML1 mutant isoforms responsible for mucolipidosis type IV. *Nature Communications*, *5*(May), 4681.

Chen, Q., She, J., Zeng, W., Guo, J., Xu, H., Bai, X., & Jiang, Y. (2017). Structure of mammalian endolysosomal TRPML1 channel in nanodiscs. *Nature*, *550*(7676), 415–418.

Chen, T.-W., Wardill, T. J., Sun, Y., Pulver, S. R., Renninger, S. L., Baohan, A., Schreiter, E. R., Kerr, R. A., Orger, M. B., Jayaraman, V., Looger, L. L., Svoboda, K., & Kim, D. S. (2013). Ultrasensitive fluorescent proteins for imaging neuronal activity. *Nature*, *499*(7458), 295–300.

Chini, E. N., & Dousa, T. P. (1996). Nicotinate-adenine dinucleotide phosphate-induced Ca(2+)-release does not behave as a Ca(2+)-induced Ca(2+)-release system. *The Biochemical Journal*, *316 (Pt 3*(3), 709–711.

Chow, C. Y., Landers, J. E., Bergren, S. K., Sapp, P. C., Grant, A. E., Jones, J. M., Everett, L., Lenk, G. M., McKenna-Yasek, D. M., Weisman, L. S., Figlewicz, D., Brown, R. H., & Meisler, M. H. (2009). Deleterious Variants of FIG4, a Phosphoinositide Phosphatase, in Patients with ALS. *The American Journal of Human Genetics*, *84*(1), 85–88.

Chow, C. Y., Zhang, Y., Dowling, J. J., Jin, N., Adamska, M., Shiga, K., Szigeti, K., Shy, M. E., Li, J., Zhang, X., Lupski, J. R., Weisman, L. S., & Meisler, M. H. (2007). Mutation of FIG4 causes neurodegeneration in the pale tremor mouse and patients with CMT4J. *Nature*, *448*(7149), 68–72.

Christensen, K. A., Myers, J. T., & Swanson, J. A. (2002). pH-dependent regulation of lysosomal calcium in macrophages. *Journal of Cell Science*, *115*(Pt 3), 599–607.

Churamani, D., Dickinson, G. D., Ziegler, M., & Patel, S. (2006). Time sensing by NAADP receptors. *The Biochemical Journal*, *397*(2), 313–320.

Churamani, D., Hooper, R., Rahman, T., Brailoiu, E., & Patel, S. (2013). The N-terminal region of two-pore channel 1 regulates trafficking and activation by NAADP. *Biochemical Journal*, *453*(1), 147–151.

Churchill, G. C., & Galione, A. (2000). Spatial control of Ca2+ signaling by nicotinic acid adenine dinucleotide phosphate diffusion and gradients. *The Journal of Biological Chemistry*, *275*(49), 38687–38692.

Churchill, G. C., Okada, Y., Thomas, J. M., Genazzani, A. A., Patel, S., & Galione, A. (2002). NAADP Mobilizes Ca2+ from Reserve Granules, Lysosome-Related Organelles, in Sea Urchin Eggs. *Cell*, *111*(5), 703–708.

Churchill, & Galione, A. (2001). NAADP induces Ca2+ oscillations via a two-pool mechanism by priming IP3- and cADPR-sensitive Ca2+ stores. *The EMBO Journal*, *20*(11), 2666–2671.

Churchill, Grant C., O'Neill, J. S., Masgrau, R., Patel, S., Thomas, J. M., Genazzani, A. A., & Galione, A. (2003). Sperm Deliver a New Second Messenger. *Current Biology*, *13*(2), 125–128.

Clapham, D. E. (2007). Calcium signaling. *Cell*, *131*(6), 1047–1058.

Coen, K., Flannagan, R. S., Baron, S., Carraro-Lacroix, L. R., Wang, D., Vermeire, W., Michiels, C., Munck, S., Baert, V., Sugita, S., Wuytack, F., Hiesinger, P. R., Grinstein, S., & Annaert, W. (2012). Lysosomal calcium homeostasis defects, not proton pump defects, cause endo-lysosomal dysfunction in PSEN-deficient cells. *The Journal of Cell Biology*, *198*(1), 23–35.

Collin, T., Chat, M., Lucas, M. G., Moreno, H., Racay, P., Schwaller, B., Marty, A., & Llano, I. (2005). Developmental changes in parvalbumin regulate presynaptic Ca2+ signaling. *The Journal of Neuroscience : The Official Journal of the Society for*

Neuroscience, *25*(1), 96–107.

Copello, J. A., Qi, Y., Jeyakumar, L. H., Ogunbunmi, E., & Fleischer, S. (2001). Lack of effect of cADP-ribose and NAADP on the activity of skeletal muscle and heart ryanodine receptors. *Cell Calcium*, *30*(4), 269–284.

Cosker, F., Cheviron, N., Yamasaki, M., Menteyne, A., Lund, F. E., Moutin, M.-J., Galione, A., & Cancela, J.-M. (2010). The Ecto-enzyme CD38 Is a Nicotinic Acid Adenine Dinucleotide Phosphate (NAADP) Synthase That Couples Receptor Activation to Ca 2+ Mobilization from Lysosomes in Pancreatic Acinar Cells. *Journal of Biological Chemistry*, *285*(49), 38251–38259.

Cruzblanca, H., Koh, D.-S., & Hille, B. (1998). Bradykinin inhibits M current via phospholipase C and Ca2+ release from IP3-sensitive Ca2+ stores in rat sympathetic neurons. *Proceedings of the National Academy of Sciences*, *95*(12), 7151–7156.

Csordás, G., Renken, C., Várnai, P., Walter, L., Weaver, D., Buttle, K. F., Balla, T., Mannella, C. A., & Hajnóczky, G. (2006). Structural and functional features and significance of the physical linkage between ER and mitochondria. *Journal of Cell Biology*, *174*(7), 915–921.

Dammermann, W., & Guse, A. H. (2005). Functional ryanodine receptor expression is required for NAADP-mediated local Ca2+ signaling in T-lymphocytes. *The Journal of Biological Chemistry*, *280*(22), 21394–21399.

Dammermann, W., Zhang, B., Nebel, M., Cordiglieri, C., Odoardi, F., Kirchberger, T., Kawakami, N., Dowden, J., Schmid, F., Dornmair, K., Hohenegger, M., Flugel, A., Guse, A. H., & Potter, B. V. L. (2009). NAADP-mediated Ca2+ signaling via type 1 ryanodine receptor in T cells revealed by a synthetic NAADP antagonist. *Proceedings of the National Academy of Sciences*, *106*(26), 10678–10683.

Danthuluri, N. R., Kim, D., & Brock, T. A. (1990). Intracellular alkalinization leads to Ca2+ mobilization from agonist-sensitive pools in bovine aortic endothelial cells. *The Journal of Biological Chemistry*, *265*(31), 19071–19076.

Davidson, S. M., Foote, K., Kunuthur, S., Gosain, R., Tan, N., Tyser, R., Zhao, Y. J., Graeff, R., Ganesan, A., Duchen, M. R., Patel, S., & Yellon, D. M. (2015). Inhibition of NAADP signalling on reperfusion protects the heart by preventing lethal calcium oscillations via two-pore channel 1 and opening of the mitochondrial permeability transition pore. *Cardiovascular Research*, *108*(3), 357–366.

Davis, L. C., Morgan, A. J., Chen, J.-L., Snead, C. M., Bloor-Young, D., Shenderov, E., Stanton-Humphreys, M. N., Conway, S. J., Churchill, G. C., Parrington, J., Cerundolo, V., & Galione, A. (2012). NAADP Activates Two-Pore Channels on T Cell Cytolytic Granules to Stimulate Exocytosis and Killing. *Current Biology*, *22*(24), 2331–2337.

Davis, L. C., Morgan, A. J., & Galione, A. (2020). <scp>NAADP</scp> -regulated two-pore

channels drive phagocytosis through endo-lysosomal Ca $^{2+}$ nanodomains, calcineurin and dynamin. *The EMBO Journal*, *39*(14).

De Duve, C., De Barsy, T., Poole, B., Trouet, A., Tulkens, P., & Van Hoof, F. (1974). Lysosomotropic agents. *Biochemical Pharmacology*, *23*(18), 2495–2531.

De Vos, K. J., Mórotz, G. M., Stoica, R., Tudor, E. L., Lau, K.-F., Ackerley, S., Warley, A., Shaw, C. E., & Miller, C. C. J. (2012). VAPB interacts with the mitochondrial protein PTPIP51 to regulate calcium homeostasis. *Human Molecular Genetics*, *21*(6), 1299–1311.

DeLuca, H. F., & Engstrom, G. W. (1961). Calcium uptake by rat kidney mitochondria. *Proceedings of the National Academy of Sciences*, *47*(11), 1744–1750.

Despa, S., Vecer, J., Steels, P., & Ameloot, M. (2000). Fluorescence Lifetime Microscopy of the Na+ Indicator Sodium Green in HeLa Cells. *Analytical Biochemistry*, *281*(2), 159–175.

Dickson, E. J., Duman, J. G., Moody, M. W., Chen, L., & Hille, B. (2012). Orai-STIM-mediated Ca2+ release from secretory granules revealed by a targeted Ca2+ and pH probe. *Proceedings of the National Academy of Sciences of the United States of America*, *109*(51), E3539-48.

Dong, Xian-ping, Shen, D., Wang, X., Dawson, T., Li, X., Zhang, Q., Cheng, X., Zhang, Y., Weisman, L. S., Delling, M., & Xu, H. (2010). PI(3,5)P(2) controls membrane trafficking by direct activation of mucolipin Ca(2+) release channels in the endolysosome. *Nature Communications*, *1*, 38.

Dong, Xian-ping, Wang, X., Shen, D., Chen, S., Liu, M., Wang, Y., Mills, E., Cheng, X., Delling, M., & Xu, H. (2009). Activating Mutations of the TRPML1 Channel Revealed by Proline-scanning Mutagenesis. *Journal of Biological Chemistry*, *284*(46), 32040–32052.

Dong, Xianping, Cheng, X., Mills, E., Delling, M., Wang, F., Kurz, T., & Xu, H. (2008). The type IV mucolipidosis-associated protein TRPML1 is an endolysosomal iron release channel. *Nature*, *455*(7215), 992–996.

Donoso, P., Mill, J. G., O'Neill, S. C., & Eisner, D. A. (1992). Fluorescence measurements of cytoplasmic and mitochondrial sodium concentration in rat ventricular myocytes. *The Journal of Physiology*, *448*(1), 493–509.

Dove, S. K., Dong, K., Kobayashi, T., Williams, F. K., & Michell, R. H. (2009). Phosphatidylinositol 3,5-bisphosphate and Fab1p/PIKfyve underPPIn endo-lysosome function. *Biochemical Journal*, *419*(1), 1–13.

Eden, E. R., Huang, F., Sorkin, A., & Futter, C. E. (2012). The Role of EGF Receptor Ubiquitination in Regulating Its Intracellular Traffic. *Traffic*, *13*(2), 329–337.

Eden, E. R., Sanchez-Heras, E., Tsapara, A., Sobota, A., Levine, T. P., & Futter, C. E.

(2016). Annexin A1 Tethers Membrane Contact Sites that Mediate ER to Endosome Cholesterol Transport. *Developmental Cell*, *37*(5), 473–483.

Eden, E. R., White, I. J., Tsapara, A., & Futter, C. E. (2010). Membrane contacts between endosomes and ER provide sites for PTP1B-epidermal growth factor receptor interaction. *Nature Cell Biology*, *12*(3), 267–272.

Eder, P., Probst, D., Rosker, C., Poteser, M., Wolinski, H., Kohlwein, S. D., Romanin, C., & Groschner, K. (2007). Phospholipase C-dependent control of cardiac calcium homeostasis involves a TRPC3-NCX1 signaling complex. *Cardiovascular Research*, *73*(1), 111–119.

Esposito, B., Gambara, G., Lewis, A. M., Palombi, F., D'Alessio, A., Taylor, L. X., Genazzani, A. A., Ziparo, E., Galione, A., Churchill, G. C., & Filippini, A. (2011). NAADP links histamine H1 receptors to secretion of von Willebrand factor in human endothelial cells. *Blood*, *117*(18), 4968–4977.

Falardeau, J. L., Kennedy, J. C., Acierno, J. S., Sun, M., Stahl, S., Goldin, E., & Slaugenhaupt, S. A. (2002). Cloning and characterization of the mouse Mcoln1 gene reveals an alternatively spliced transcript not seen in humans. *BMC Genomics*, *3*(1), 3.

Falcón-Pérez, J. M., Nazarian, R., Sabatti, C., & Dell'Angelica, E. C. (2005). Distribution and dynamics of Lamp1-containing endocytic organelles in fibroblasts deficient in BLOC-3. *Journal of Cell Science*, *118*(Pt 22), 5243–5255.

Fameli, N., Ogunbayo, O. A., van Breemen, C., & Evans, A. M. (2014). Cytoplasmic nanojunctions between lysosomes and sarcoplasmic reticulum are required for specific calcium signaling. *F1000Research*, *3*, 93.

Faouzi, M., & Penner, R. (2014). TRPM2. *Handbook of Experimental Pharmacology*, *222*, 403–426.

Faris, P., Pellavio, G., Ferulli, F., Di Nezza, F., Shekha, M., Lim, D., Maestri, M., Guerra, G., Ambrosone, L., Pedrazzoli, P., Laforenza, U., Montagna, D., & Moccia, F. (2019). Nicotinic acid adenine dinucleotide phosphate (NAADP) induces intracellular Ca2+ release through the two-pore channel tpc1 in metastatic colorectal cancer cells. *Cancers*, *11*(4), 1–19.

Fasolato, C., Zottini, M., Clementi, E., Zacchetti, D., Meldolesi, J., & Pozzan, T. (1991). Intracellular Ca2+ pools in PC12 cells. Three intracellular pools are distinguished by their turnover and mechanisms of Ca2+ accumulation, storage, and release. *The Journal of Biological Chemistry*, *266*(30), 20159–20167.

Favia, A., Desideri, M., Gambara, G., D'Alessio, A., Ruas, M., Esposito, B., Del Bufalo, D., Parrington, J., Ziparo, E., Palombi, F., Galione, A., & Filippini, A. (2014). VEGF-induced neoangiogenesis is mediated by NAADP and two-pore channel-2-dependent Ca2+ signaling. *Proceedings of the National Academy of Sciences of the United States*

of America, *111*(44), E4706-15.

Foskett, J. K., White, C., Cheung, K.-H., & Mak, D.-O. D. (2007). Inositol trisphosphate receptor Ca2+ release channels. *Physiological Reviews*, *87*(2), 593–658.

Franzini-Armstrong, C., Protasi, F., & Ramesh, V. (1999). Shape, Size, and Distribution of Ca2+ Release Units and Couplons in Skeletal and Cardiac Muscles. *Biophysical Journal*, *77*(3), 1528–1539.

Furuichi, T., Cunningham, K. W., & Muto, S. (2001). A Putative Two Pore Channel AtTPC1 Mediates Ca2+ Flux in Arabidopsis Leaf Cells. *Plant and Cell Physiology*, *42*(9), 900–905.

Galione, A., & Churchill, G. C. (2000). Cyclic ADP Ribose as a Calcium-Mobilizing Messenger. *Science Signaling*, *2000*(41), pe1–pe1.

Galione, Antony. (2011). NAADP receptors. *Cold Spring Harbor Perspectives in Biology*, *3*(1), a004036.

Galione, Antony, Chuang, K.-T., Funnell, T. M., Davis, L. C., Morgan, A. J., Ruas, M., Parrington, J., & Churchill, G. C. (2014). Synthesis of NAADP-AM as a Membrane-Permeant NAADP Analog. *Cold Spring Harbor Protocols*, *2014*(10), pdb.prot076927-pdb.prot076927.

García-Rúa, V., Feijóo-Bandín, S., Rodríguez-Penas, D., Mosquera-Leal, A., Abu-Assi, E., Beiras, A., María Seoane, L., Lear, P., Parrington, J., Portolés, M., Roselló-Lletí, E., Rivera, M., Gualillo, O., Parra, V., Hill, J. A., Rothermel, B., González-Juanatey, J. R., & Lago, F. (2016). Endolysosomal two-pore channels regulate autophagy in cardiomyocytes. *The Journal of Physiology*, *594*(11), 3061–3077.

Garrity, A. G., Wang, W., Collier, C. M. D., Levey, S. A., Gao, Q., & Xu, H. (2016). The endoplasmic reticulum, not the pH gradient, drives calcium refilling of lysosomes. *ELife*, *5*, e15887.

Genazzani, A. A., Empson, R. M., & Galione, A. (1996). Unique Inactivation Properties of NAADP-sensitive Ca Release. *Journal of Biological Chemistry*, *271*(20), 11599–11602.

Genazzani, A. A., Mezna, M., Dickey, D. M., Michelangeli, F., Walseth, T. F., & Galione, A. (1997). Pharmacological properties of the Ca2+-release mechanism sensitive to NAADP in the sea urchin egg. *British Journal of Pharmacology*, *121*(7), 1489–1495.

Gerndt, S., Chen, C.-C., Chao, Y.-K., Yuan, Y., Burgstaller, S., Scotto Rosato, A., Krogsaeter, E., Urban, N., Jacob, K., Nguyen, O. N. P., Miller, M. T., Keller, M., Vollmar, A. M., Gudermann, T., Zierler, S., Schredelseker, J., Schaefer, M., Biel, M., Malli, R., … Grimm, C. (2020). Agonist-mediated switching of ion selectivity in TPC2 differentially promotes lysosomal function. *ELife*, *9*, e54716.

Gómez-Suaga, P., Luzón-Toro, B., Churamani, D., Zhang, L., Bloor-Young, D., Patel, S.,

Woodman, P. G., Churchill, G. C., & Hilfiker, S. (2012). Leucine-rich repeat kinase 2 regulates autophagy through a calcium-dependent pathway involving NAADP. *Human Molecular Genetics*, *21*(3), 511–525.

Gomez-Suaga, P., Paillusson, S., Stoica, R., Noble, W., Hanger, D. P., & Miller, C. C. J. (2017). The ER-Mitochondria Tethering Complex VAPB-PTPIP51 Regulates Autophagy. *Current Biology*, *27*(3), 371–385.

Gómez-Suaga, P., Rivero-Ríos, P., Fdez, E., Blanca Ramírez, M., Ferrer, I., Aiastui, A., López De Munain, A., & Hilfiker, S. (2014). LRRK2 delays degradative receptor trafficking by impeding late endosomal budding through decreasing Rab7 activity. *Human Molecular Genetics*, *23*(25), 6779–6796.

Grimm, C., Chen, C.-C., Wahl-Schott, C., & Biel, M. (2017). Two-Pore Channels: Catalyzers of Endolysosomal Transport and Function. *Frontiers in Pharmacology*, *08*.

Grimm, C., Holdt, L. M., Chen, C.-C., Hassan, S., Müller, C., Jörs, S., Cuny, H., Kissing, S., Schröder, B., Butz, E., Northoff, B., Castonguay, J., Luber, C. A., Moser, M., Spahn, S., Lüllmann-Rauch, R., Fendel, C., Klugbauer, N., Griesbeck, O., … Wahl-Schott, C. (2014). High susceptibility to fatty liver disease in two-pore channel 2-deficient mice. *Nature Communications*, *5*(1), 4699.

Grynkiewicz, G., Poenie, M., & Tsien, R. Y. (1985). A new generation of Ca2+ indicators with greatly improved fluorescence properties. *The Journal of Biological Chemistry*, *260*(6), 3440–3450.

Gunaratne, G. S., Johns, M. E., Hintz, H. M., Walseth, T. F., & Marchant, J. S. (2018). A screening campaign in sea urchin egg homogenate as a platform for discovering modulators of NAADP-dependent Ca2+ signaling in human cells. *Cell Calcium*, *75*, 42–52.

Gunaratne, G. S., Yang, Y., Li, F., Walseth, T. F., & Marchant, J. S. (2018). NAADP-dependent Ca2+ signaling regulates Middle East respiratory syndrome-coronavirus pseudovirus translocation through the endolysosomal system. *Cell Calcium*, *75*, 30–41.

Guo, J., Zeng, W., Chen, Q., Lee, C., Chen, L., Yang, Y., Cang, C., Ren, D., & Jiang, Y. (2016). Structure of the voltage-gated two-pore channel TPC1 from Arabidopsis thaliana. *Nature*, *531*(7593), 196–201.

Guo, J., Zeng, W., & Jiang, Y. (2017). Tuning the ion selectivity of two-pore channels. *Proceedings of the National Academy of Sciences*, *114*(5), 1009–1014.

Haller, T., Dietl, P., Deetjen, P., & Völkl, H. (1996). The lysosomal compartment as intracellular calcium store in MDCK cells: a possible involvement in InsP3-mediated Ca2+ release. *Cell Calcium*, *19*(2), 157–165.

Hansen, K. B., Yi, F., Perszyk, R. E., Furukawa, H., Wollmuth, L. P., Gibb, A. J., & Traynelis, S. F. (2018). Structure, function, and allosteric modulation of NMDA

receptors. *The Journal of General Physiology*, *150*(8), 1081–1105.

Harootunian, A. T., Kao, J. P. Y., Eckert, B. K., & Tsien, R. Y. (1989). Fluorescence ratio imaging of cytosolic free Na+ in individual fibroblasts and lymphocytes. *Journal of Biological Chemistry*, *264*(32), 19458–19467.

Harris, R. A., & Hanrahan, J. W. (1993). Histamine stimulates a biphasic calcium response in the human tracheal epithelial cell line CF/T43. *The American Journal of Physiology*, *265*(3 Pt 1).

Harteneck, C., & Gollasch, M. (2011). Pharmacological Modulation of Diacylglycerol-Sensitive TRPC3/6/7 Channels. *Current Pharmaceutical Biotechnology*, *12*(1), 35–41.

Hasegawa, J., Strunk, B. S., & Weisman, L. S. (2017). PI5P and PI(3,5)P2: Minor, but Essential Phosphoinositides. *Cell Structure and Function*, *42*(1), 49–60.

Hill, S. J., Ganellin, C. R., Timmerman, H., Schwartz, J. C., Shankley, N. P., Young, J. M., Schunack, W., Levi, R., & Haas, H. L. (1997). International Union of Pharmacology. XIII. Classification of histamine receptors. *Pharmacological Reviews*, *49*(3), 253–278.

Hockerman, G. H., Peterson, B. Z., Johnson, B. D., & Catterall, W. A. (1997). Molecular determinants of drug binding and action on L-type calcium channels. *Annual Review of Pharmacology and Toxicology*, *37*, 361–396.

Hockey, L. N., Kilpatrick, B. S., Eden, E. R., Lin-Moshier, Y., Brailoiu, G. C., Brailoiu, E., Futter, C. E., Schapira, A. H., Marchant, J. S., & Patel, S. (2015). Dysregulation of lysosomal morphology by pathogenic LRRK2 is corrected by TPC2 inhibition. *Journal of Cell Science*, *128*(2), 232–238.

Hofmann, T., Obukhov, A. G., Schaefer, M., Harteneck, C., Gudermann, T., & Schultz, G. (1999). Direct activation of human TRPC6 and TRPC3 channels by diacylglycerol. *Nature*, *397*(6716), 259–263.

Hogan, P. G., & Rao, A. (2015). Store-operated calcium entry: Mechanisms and modulation. *Biochemical and Biophysical Research Communications*, *460*(1), 40–49.

Höglinger, D., Haberkant, P., Aguilera-Romero, A., Riezman, H., Porter, F. D., Platt, F. M., Galione, A., & Schultz, C. (2015). Intracellular sphingosine releases calcium from lysosomes. *ELife*, *4*, e10616.

Hohenegger, M., Suko, J., Gscheidlinger, R., Drobny, H., & Zidar, A. (2002). Nicotinic acid-adenine dinucleotide phosphate activates the skeletal muscle ryanodine receptor. *The Biochemical Journal*, *367*(Pt 2), 423–431.

Hooper, R., Churamani, D., Brailoiu, E., Taylor, C. W., & Patel, S. (2011). Membrane Topology of NAADP-sensitive Two-pore Channels and Their Regulation by N-linked Glycosylation. *Journal of Biological Chemistry*, *286*(11), 9141–9149.

Huang, P., Zou, Y., Zhong, X. Z., Cao, Q., Zhao, K., Zhu, M. X., Murrell-Lagnado, R., & Dong, X.-P. (2014). P2X4 forms functional ATP-activated cation channels on

lysosomal membranes regulated by luminal pH. *The Journal of Biological Chemistry*, *289*(25), 17658–17667.

Huang, X., Godfrey, T. E., Gooding, W. E., McCarty, K. S., & Gollin, S. M. (2006). Comprehensive genome and transcriptome analysis of the 11q13 amplicon in human oral cancer and synteny to the 7F5 amplicon in murine oral carcinoma. *Genes, Chromosomes & Cancer*, *45*(11), 1058–1069.

Iacobucci, G. J., & Popescu, G. K. (2017). NMDA receptors: linking physiological output to biophysical operation. *Nature Reviews. Neuroscience*, *18*(4), 236–249.

Iamshanova, O., Mariot, P., Lehen'kyi, V., & Prevarskaya, N. (2016). Comparison of fluorescence probes for intracellular sodium imaging in prostate cancer cell lines. *European Biophysics Journal*, *45*(7), 765–777.

Islas, L. D. (2017). Molecular Mechanisms of Temperature Gating in TRP Channels. In *Neurobiology of TRP Channels* (pp. 11–25). CRC Press.

Iwai, M., Michikawa, T., Bosanac, I., Ikura, M., & Mikoshiba, K. (2007). Molecular Basis of the Isoform-specific Ligand-binding Affinity of Inositol 1,4,5-Trisphosphate Receptors. *Journal of Biological Chemistry*, *282*(17), 12755–12764.

Iwamoto, T. (2005). Sodium–calcium exchange inhibitors: therapeutic potential in cardiovascular diseases. *Future Cardiology*, *1*(4), 519–529.

Iwamoto, T. (2007). Na+/Ca2+ exchange as a drug target--insights from molecular pharmacology and genetic engineering. *Annals of the New York Academy of Sciences*, *1099*(1), 516–528.

Iwamoto, T., & Kita, S. (2006). YM-244769, a Novel Na + /Ca 2+ Exchange Inhibitor That Preferentially Inhibits NCX3, Efficiently Protects against Hypoxia/Reoxygenation-Induced SH-SY5Y Neuronal Cell Damage. *Molecular Pharmacology*, *70*(6), 2075–2083.

Iwamoto, T., Kita, S., Uehara, A., Imanaga, I., Matsuda, T., Baba, A., & Katsuragi, T. (2004). Molecular Determinants of Na + /Ca 2+ Exchange (NCX1) Inhibition by SEA0400. *Journal of Biological Chemistry*, *279*(9), 7544–7553.

Jadot, M., Colmant, C., Wattiaux-De Coninck, S., & Wattiaux, R. (1984). Intralysosomal hydrolysis of glycyl-l-phenylalanine 2-naphthylamide. *Biochemical Journal*, *219*(3), 965–970.

Jadot, Michel, Biélande, V., Beauloye, V., Wattiaux-De Coninck, S., & Wattiaux, R. (1990). Cytotoxicity and effect of glycyl-D-phenylalanine-2-naphthylamide on lysosomes. *Biochimica et Biophysica Acta*, *1027*(2), 205–209.

Jahidin, A. H., Stewart, T. A., Thompson, E. W., Roberts-Thomson, S. J., & Monteith, G. R. (2016). Differential effects of two-pore channel protein 1 and 2 silencing in MDA-MB-468 breast cancer cells. *Biochemical and Biophysical Research Communications*,

477(4), 731–736.

James-Kracke, M. R., Sloane, B. F., Shuman, H., & Somlyo, A. P. (1979). Lysosomal composition in cultured vascular smooth muscle cells: electron probe analysis. *Proceedings of the National Academy of Sciences*, *76*(12), 6461–6465.

Jardin, I., Lopez, J. J., Salido, G. M., & Rosado, J. A. (2018). Store-operated Ca 2+ entry in breast cancer cells: Remodeling and functional role. *International Journal of Molecular Sciences*, *19*(12), 1–14.

Jha, A., Ahuja, M., Patel, S., Brailoiu, E., & Muallem, S. (2014). Convergent regulation of the lysosomal two-pore channel-2 by Mg2+, NAADP, PI(3,5)P2 and multiple protein kinases. *The EMBO Journal*, *33*(5), 501–511.

Jiang, D., Zhao, L., & Clapham, D. E. (2009). Genome-wide RNAi screen identifies Letm1 as a mitochondrial Ca2+/H+ antiporter. *Science (New York, N.Y.)*, *326*(5949), 144–147.

Johansen, L. M., DeWald, L. E., Shoemaker, C. J., Hoffstrom, B. G., Lear-Rooney, C. M., Stossel, A., Nelson, E., Delos, S. E., Simmons, J. A., Grenier, J. M., Pierce, L. T., Pajouhesh, H., Lehár, J., Hensley, L. E., Glass, P. J., White, J. M., & Olinger, G. G. (2015). A screen of approved drugs and molecular probes identifies therapeutics with anti–Ebola virus activity. *Science Translational Medicine*, *7*(290), 290ra89-290ra89.

Johnson, C. L., Johnson, C. G., Bazan, E., Garver, D., Gruenstein, E., & Ahluwalia, M. (1990). Histamine receptors in human fibroblasts: inositol phosphates, Ca2+, and cell growth. *American Journal of Physiology-Cell Physiology*, *258*(3), C533–C543.

Johnson, D. E., Ostrowski, P., Jaumouillé, V., & Grinstein, S. (2016). The position of lysosomes within the cell determines their luminal pH. *Journal of Cell Biology*, *212*(6), 677–692.

Jongsma, M. L. M., Berlin, I., Wijdeven, R. H. M., Janssen, L., Janssen, G. M. C., Garstka, M. A., Janssen, H., Mensink, M., van Veelen, P. A., Spaapen, R. M., & Neefjes, J. (2016). An ER-Associated Pathway Defines Endosomal Architecture for Controlled Cargo Transport. *Cell*, *166*(1), 152–166.

Jouaville, L. S., Ichas, F., Holmuhamedov, E. L., Camacho, P., & Lechleiter, J. D. (1995). Synchronization of calcium waves by mitochondrial substrates in Xenopus laevis oocytes. *Nature*, *377*(6548), 438–441.

Kamer, K. J., Sancak, Y., Fomina, Y., Meisel, J. D., Chaudhuri, D., Grabarek, Z., & Mootha, V. K. (2018). MICU1 imparts the mitochondrial uniporter with the ability to discriminate between Ca 2+ and Mn 2+. *Proceedings of the National Academy of Sciences*, *115*(34), E7960–E7969.

Karlstad, J., Sun, Y., & Singh, B. B. (2012). Ca(2+) signaling: an outlook on the characterization of Ca(2+) channels and their importance in cellular functions. *Advances in Experimental Medicine and Biology*, *740*, 143–157.

Kelu, J. J., Webb, S. E., Galione, A., & Miller, A. L. (2019). Characterization of ADP-ribosyl cyclase 1-like (ARC1-like) activity and NAADP signaling during slow muscle cell development in zebrafish embryos. *Developmental Biology*, *445*(2), 211–225.

Khakh, B. S., & Lester, H. A. (1999). Dynamic Selectivity Filters in Ion Channels. *Neuron*, *23*(4), 653–658.

Khakh, B. S., & North, R. A. (2012). Neuromodulation by extracellular ATP and P2X receptors in the CNS. *Neuron*, *76*(1), 51–69.

Khan, N., Halcrow, P. W., Lakpa, K. L., Afghah, Z., Miller, N. M., Dowdy, S. F., Geiger, J. D., & Chen, X. (2020). Two-pore channels regulate Tat endolysosome escape and Tat-mediated HIV-1 LTR transactivation. *The FASEB Journal*, *34*(3), 4147–4162.

Kilpatrick, B. S., Eden, E. R., Hockey, L. N., Futter, C. E., & Patel, S. (2015). Methods for monitoring lysosomal morphology. In *Methods in cell biology* (Vol. 126, pp. 1–19).

Kilpatrick, B. S., Eden, E. R., Hockey, L. N., Yates, E., Futter, C. E., & Patel, S. (2017). An Endosomal NAADP-Sensitive Two-Pore Ca 2+ Channel Regulates ER-Endosome Membrane Contact Sites to Control Growth Factor Signaling. *Cell Reports*, *18*(7), 1636–1645.

Kilpatrick, B. S., Eden, E. R., Schapira, A. H., Futter, C. E., & Patel, S. (2013). Direct mobilisation of lysosomal Ca2+ triggers complex Ca2+ signals. *Journal of Cell Science*, *126*(Pt 1), 60–66.

Kilpatrick, B. S., Magalhaes, J., Beavan, M. S., McNeill, A., Gegg, M. E., Cleeter, M. W. J., Bloor-Young, D., Churchill, G. C., Duchen, M. R., Schapira, A. H., & Patel, S. (2016). Endoplasmic reticulum and lysosomal Ca2+ stores are remodelled in GBA1-linked Parkinson disease patient fibroblasts. *Cell Calcium*, *59*(1), 12–20.

Kilpatrick, B. S., Yates, E., Grimm, C., Schapira, A. H., & Patel, S. (2016). Endo-lysosomal TRP mucolipin-1 channels trigger global ER Ca 2+ release and Ca 2+ influx. *Journal of Cell Science*, *129*(20), 3859–3867.

Kim, H. J., Li, Q., Tjon-Kon-Sang, S., So, I., Kiselyov, K., & Muallem, S. (2007). Gain-of-function mutation in TRPML3 causes the mouse Varitint-Waddler phenotype. *The Journal of Biological Chemistry*, *282*(50), 36138–36142.

Kim, H. J., Li, Q., Tjon-Kon-Sang, S., So, I., Kiselyov, K., Soyombo, A. A., & Muallem, S. (2008). A novel mode of TRPML3 regulation by extracytosolic pH absent in the varitint-waddler phenotype. *EMBO Journal*, *27*(8), 1197–1205.

Kim, H. J., Soyombo, A. A., Tjon-Kon-Sang, S., So, I., & Muallem, S. (2009). The Ca(2+) channel TRPML3 regulates membrane trafficking and autophagy. *Traffic (Copenhagen, Denmark)*, *10*(8), 1157–1167.

Kim, S.-Y., Cho, B. H., & Kim, U.-H. (2010). CD38-mediated Ca2+ signaling contributes to angiotensin II-induced activation of hepatic stellate cells: attenuation of hepatic fibrosis

by CD38 ablation. *The Journal of Biological Chemistry*, *285*(1), 576–582.

King, V., Garcia, M., & Himmel, D. (1988). Interaction of tetrandrine with slowly inactivating calcium channels. Characterization of calcium channel modulation by an alkaloid of Chinese medicinal herb origin. *Journal of Ethnopharmacology*, *23*(2–3), 343.

Kinnear, N. P., Boittin, F.-X., Thomas, J. M., Galione, A., & Evans, A. M. (2004). Lysosome-Sarcoplasmic Reticulum Junctions. *Journal of Biological Chemistry*, *279*(52), 54319–54326.

Kintzer, A. F., & Stroud, R. M. (2016). Structure, inhibition, and regulatory sites of TPC1 from Arabidopsis thaliana. *Nature*, *531*(7593), 258–262.

Kip, S. N., Smelter, M., Iyanoye, A., Chini, E. N., Prakash, Y. S., Pabelick, C. M., & Sieck, G. C. (2006). Agonist-induced cyclic ADP ribose production in airway smooth muscle. *Archives of Biochemistry and Biophysics*, *452*(2), 102–107.

Kirichok, Y., Krapivinsky, G., & Clapham, D. E. (2004). The mitochondrial calcium uniporter is a highly selective ion channel. *Nature*, *427*(6972), 360–364.

Kiselyov, K., Chen, J., Rbaibi, Y., Oberdick, D., Tjon-Kon-Sang, S., Shcheynikov, N., Muallem, S., & Soyombo, A. (2005). TRP-ML1 is a lysosomal monovalent cation channel that undergoes proteolytic cleavage. *The Journal of Biological Chemistry*, *280*(52), 43218–43223.

Kolisek, M., Beck, A., Fleig, A., & Penner, R. (2005). Cyclic ADP-ribose and hydrogen peroxide synergize with ADP-ribose in the activation of TRPM2 channels. *Molecular Cell*, *18*(1), 61–69.

Kondratowicz, A. S., Lennemann, N. J., Sinn, P. L., Davey, R. A., Hunt, C. L., Moller-Tank, S., Meyerholz, D. K., Rennert, P., Mullins, R. F., Brindley, M., Sandersfeld, L. M., Quinn, K., Weller, M., McCray, P. B., Chiorini, J., & Maury, W. (2011). T-cell immunoglobulin and mucin domain 1 (TIM-1) is a receptor for Zaire Ebolavirus and Lake Victoria Marburgvirus. *Proceedings of the National Academy of Sciences*, *108*(20), 8426–8431.

Kouznetsova, J., Sun, W., Martínez-Romero, C., Tawa, G., Shinn, P., Chen, C. Z., Schimmer, A., Sanderson, P., McKew, J. C., Zheng, W., & García-Sastre, A. (2014). Identification of 53 compounds that block Ebola virus-like particle entry via a repurposing screen of approved drugs. *Emerging Microbes & Infections*, *3*(1), 1–7.

Lambert, T. L., Kent, R. S., & Whorton, A. R. (1986). Bradykinin stimulation of inositol polyphosphate production in porcine aortic endothelial cells. *The Journal of Biological Chemistry*, *261*(32), 15288–15293.

Lamy, C. M., & Chatton, J.-Y. (2011). Optical probing of sodium dynamics in neurons and astrocytes. *NeuroImage*, *58*(2), 572–578.

Lange, I., Yamamoto, S., Partida-Sanchez, S., Mori, Y., Fleig, A., & Penner, R. (2009). TRPM2 functions as a lysosomal Ca2+-release channel in beta cells. *Science Signaling*, *2*(71), ra23.

Langhorst, M. F., Schwarzmann, N., & Guse, A. H. (2004). Ca2+ release via ryanodine receptors and Ca2+ entry: major mechanisms in NAADP-mediated Ca2+ signaling in T-lymphocytes. *Cellular Signalling*, *16*(11), 1283–1289.

Lasser-Ross, N., & Ross, W. N. (1992). Imaging voltage and synaptically activated sodium transients in cerebellar Purkinje cells. *Proceedings. Biological Sciences*, *247*(1318), 35–39.

Lear, P. V., González-Touceda, D., Porteiro Couto, B., Viaño, P., Guymer, V., Remzova, E., Tunn, R., Chalasani, A., García-Caballero, T., Hargreaves, I. P., Tynan, P. W., Christian, H. C., Nogueiras, R., Parrington, J., & Diéguez, C. (2015). Absence of Intracellular Ion Channels TPC1 and TPC2 Leads to Mature-Onset Obesity in Male Mice, Due to Impaired Lipid Availability for Thermogenesis in Brown Adipose Tissue. *Endocrinology*, *156*(3), 975–986.

Lee, C. S.-K., Tong, B. C.-K., Cheng, C. W.-H., Hung, H. C.-H., & Cheung, K.-H. (2016). Characterization of Two-Pore Channel 2 by Nuclear Membrane Electrophysiology. *Scientific Reports*, *6*(1), 20282.

Lee, H.C. (2000). Enzymatic Functions and Structures of CD38 and Homologs. In *Human CD38 and Related Molecules* (pp. 39–59). KARGER.

Lee, Hon Cheung, & Aarhus, R. (1995). A derivative of NADP mobilizes calcium stores insensitive to inositol trisphosphate and cyclic ADP-ribose. *The Journal of Biological Chemistry*, *270*(5), 2152–2157.

Lee, Hon Cheung, Aarhus, R., Graeff, R., Gurnack, M. E., & Walseth, T. F. (1994). Cyclic ADP ribose activation of the ryanodine receptor is mediated by calmodulin. *Nature*, *370*(6487), 307–309.

Lee, Hon Cheung, & Zhao, Y. J. (2019). Resolving the topological enigma in Ca2+ signaling by cyclic ADP-ribose and NAADP. *Journal of Biological Chemistry*, *294*(52), 19831–19843.

Lee, J. H., McBrayer, M. K., Wolfe, D. M., Haslett, L. J., Kumar, A., Sato, Y., Lie, P. P. Y., Mohan, P., Coffey, E. E., Kompella, U., Mitchell, C. H., Lloyd-Evans, E., & Nixon, R. A. (2015). Presenilin 1 Maintains Lysosomal Ca2+ Homeostasis via TRPML1 by Regulating vATPase-Mediated Lysosome Acidification. *Cell Reports*, *12*(9), 1430–1444.

Lee, S. H., Schwaller, B., & Neher, E. (2000). Kinetics of Ca2+ binding to parvalbumin in bovine chromaffin cells: implications for [Ca2+] transients of neuronal dendrites. *The Journal of Physiology*, *525 Pt 2*, 419–432.

LeFurgey, A., Spencer, A. J., Jacobs, W. R., Ingram, P., & Mandel, L. J. (1991). Elemental microanalysis of organelles in proximal tubules. I. Alterations in transport and metabolism. *Journal of the American Society of Nephrology : JASN*, *1*(12), 1305–1320.

Lemieux, B., Percival, M. D., & Falgueyret, J.-P. (2004). Quantitation of the lysosomotropic character of cationic amphiphilic drugs using the fluorescent basic amine Red DND-99. *Analytical Biochemistry*, *327*(2), 247–251.

Li, L.-H., Tian, X.-R., Jiang, Z., Zeng, L.-W., He, W.-F., & Hu, Z.-P. (2013). The Golgi Apparatus: Panel Point of Cytosolic Ca(2+) Regulation. *Neuro-Signals*, *21*(3–4), 272–284.

Li, M., Toombes, G. E. S., Silberberg, S. D., & Swartz, K. J. (2015). Physical basis of apparent pore dilation of ATP-activated P2X receptor channels. *Nature Neuroscience*, *18*(11), 1577–1583.

Li, S., & Hong, M. (2011). Protonation, Tautomerization, and Rotameric Structure of Histidine: A Comprehensive Study by Magic-Angle-Spinning Solid-State NMR. *Journal of the American Chemical Society*, *133*(5), 1534–1544.

Lin-Moshier, Y., Keebler, M. V., Hooper, R., Boulware, M. J., Liu, X., Churamani, D., Abood, M. E., Walseth, T. F., Brailoiu, E., Patel, S., & Marchant, J. S. (2014). The Two-pore channel (TPC) interactome unmasks isoform-specific roles for TPCs in endolysosomal morphology and cell pigmentation. *Proceedings of the National Academy of Sciences of the United States of America*, *111*(36), 13087–13092.

Lin-Moshier, Y., Walseth, T. F., Churamani, D., Davidson, S. M., Slama, J. T., Hooper, R., Brailoiu, E., Patel, S., & Marchant, J. S. (2012). Photoaffinity Labeling of Nicotinic Acid Adenine Dinucleotide Phosphate (NAADP) Targets in Mammalian Cells. *Journal of Biological Chemistry*, *287*(4), 2296–2307.

Lin, P.-H., Duann, P., Komazaki, S., Park, K. H., Li, H., Sun, M., Sermersheim, M., Gumpper, K., Parrington, J., Galione, A., Evans, A. M., Zhu, M. X., & Ma, J. (2015). Lysosomal Two-pore Channel Subtype 2 (TPC2) Regulates Skeletal Muscle Autophagic Signaling. *Journal of Biological Chemistry*, *290*(6), 3377–3389.

Lissandron, V., Podini, P., Pizzo, P., & Pozzan, T. (2010). Unique characteristics of Ca2+ homeostasis of the trans-Golgi compartment. *Proceedings of the National Academy of Sciences of the United States of America*, *107*(20), 9198–9203.

Liu, B., Cao, W., Li, J., & Liu, J. (2018). Lysosomal exocytosis of ATP is coupled to P2Y2 receptor in marginal cells in the stria vascular in neonatal rats. *Cell Calcium*, *76*(July), 62–71.

Liu, J., & Wang, L.-N. (2018). The efficacy and safety of riluzole for neurodegenerative movement disorders: a systematic review with meta-analysis. *Drug Delivery*, *25*(1), 43–48.

Liu, Q.-Y., Karpinski, E., Rao, M.-R., & Pang, P. K. T. (1991). Tetrandrine: A novel calcium channel antagonist inhibits type I calcium channels in neuroblastoma cells. *Neuropharmacology*, *30*(12), 1325–1331.

Liu, Qin-Yue, Karpinski, E., & Pang, P. K. T. (1992). Tetrandrine Inhibits Both T and L Calcium Channel Currents in Ventricular Cells. *Journal of Cardiovascular Pharmacology*, *20*(4), 513–519.

Lloyd-Evans, E., Morgan, A. J., He, X., Smith, D. A., Elliot-Smith, E., Sillence, D. J., Churchill, G. C., Schuchman, E. H., Galione, A., & Platt, F. M. (2008). Niemann-Pick disease type C1 is a sphingosine storage disease that causes deregulation of lysosomal calcium. *Nature Medicine*, *14*(11), 1247–1255.

Lloyd-Evans, E., Waller-Evans, H., Peterneva, K., Francis, L., & Walker, M. (2014). Uncovering the role of lysosomal Ca2+ signalling in two neurodegenerative lysosomal disorders, Niemann-Pick disease type C and mucolipidosis type IV. *Molecular Genetics and Metabolism*, *111*(2), S70.

Lock, J. T., Parker, I., & Smith, I. F. (2015). A comparison of fluorescent Ca2+ indicators for imaging local Ca2+ signals in cultured cells. *Cell Calcium*, *58*(6), 638–648.

López-Sanjurjo, C. I., Tovey, S. C., Prole, D. L., & Taylor, C. W. (2013). Lysosomes shape Ins(1,4,5) P 3 -evoked Ca 2+ signals by selectively sequestering Ca 2+ released from the endoplasmic reticulum. *Journal of Cell Science*, *126*(1), 289–300.

López, J. J., Camello-Almaraz, C., Pariente, J. A., Salido, G. M., & Rosado, J. A. (2005). Ca2+ accumulation into acidic organelles mediated by Ca2+- and vacuolar H+-ATPases in human platelets. *Biochemical Journal*, *390*(1), 243–252.

Lopez, J. J., Jardin, I., Sanchez-Collado, J., Salido, G. M., Smani, T., & Rosado, J. A. (2020). TRPC Channels in the SOCE Scenario. *Cells*, *9*(1), 126.

Luzio, J. P., Pryor, P. R., & Bright, N. A. (2007). Lysosomes: fusion and function. *Nature Reviews. Molecular Cell Biology*, *8*(8), 622–632.

Macgregor, A., Yamasaki, M., Rakovic, S., Sanders, L., Parkesh, R., Churchill, G. C., Galione, A., & Terrar, D. A. (2007). NAADP controls cross-talk between distinct Ca2+ stores in the heart. *The Journal of Biological Chemistry*, *282*(20), 15302–15311.

Mackrill, J. J., Challiss, R. A., O'connell, D. A., Lai, F. A., & Nahorski, S. R. (1997). Differential expression and regulation of ryanodine receptor and myo-inositol 1,4,5-trisphosphate receptor Ca2+ release channels in mammalian tissues and cell lines. *The Biochemical Journal*, *327 (Pt 1*(1), 251–258.

Manford, A. G., Stefan, C. J., Yuan, H. L., MacGurn, J. A., & Emr, S. D. (2012). ER-to-Plasma Membrane Tethering Proteins Regulate Cell Signaling and ER Morphology. *Developmental Cell*, *23*(6), 1129–1140.

Manzoni, C. (2017). The LRRK2-macroautophagy axis and its relevance to Parkinson's

disease. *Biochemical Society Transactions*, *45*(1), 155–162.

Manzoni, C., Mamais, A., Dihanich, S., Abeti, R., Soutar, M. P. M., Plun-Favreau, H., Giunti, P., Tooze, S. A., Bandopadhyay, R., & Lewis, P. A. (2013). Inhibition of LRRK2 kinase activity stimulates macroautophagy. *Biochimica et Biophysica Acta (BBA) - Molecular Cell Research*, *1833*(12), 2900–2910.

Marchant, J. S., Lin-Moshier, Y., Walseth, T. F., & Patel, S. (2012). The Molecular Basis for Ca2+ Signalling by NAADP: Two-Pore Channels in a Complex? *Messenger (Los Angeles, Calif. : Print)*, *1*(1), 63–76.

Marchant, J. S., & Patel, S. (2015). Two-pore channels at the intersection of endolysosomal membrane traffic. *Biochemical Society Transactions*.

Marchant, J. S., & Taylor, C. W. (1997). Cooperative activation of IP3 receptors by sequential binding of IP3 and Ca2+ safeguards against spontaneous activity. *Current Biology*, *7*(7), 510–518.

Markova, J., Hudecova, S., Soltysova, A., Sirova, M., Csaderova, L., Lencesova, L., Ondrias, K., & Krizanova, O. (2014). Sodium/calcium exchanger is upregulated by sulfide signaling, forms complex with the β1 and β3 but not β2 adrenergic receptors, and induces apoptosis. *Pflügers Archiv - European Journal of Physiology*, *466*(7), 1329–1342.

Martin, I., Kim, J. W., Dawson, V. L., & Dawson, T. M. (2014). LRRK2 pathobiology in Parkinson's disease. *Journal of Neurochemistry*, *131*(5), 554–565.

Martina, J. A., Chen, Y., Gucek, M., & Puertollano, R. (2012). MTORC1 functions as a transcriptional regulator of autophagy by preventing nuclear transport of TFEB. *Autophagy*, *8*(6), 903–914.

Masgrau, R., Churchill, G. C., Morgan, A. J., Ashcroft, S. J. H., & Galione, A. (2003). NAADP: a new second messenger for glucose-induced Ca2+ responses in clonal pancreatic beta cells. *Current Biology : CB*, *13*(3), 247–251.

Matheson, A. J., & Noble, S. (2000). Racecadotril. *Drugs*, *59*(4), 829–835; discussion 836-7.

McCartney, A. J., Zolov, S. N., Kauffman, E. J., Zhang, Y., Strunk, B. S., Weisman, L. S., & Sutton, M. A. (2014). Activity-dependent PI(3,5)P2 synthesis controls AMPA receptor trafficking during synaptic depression. *Proceedings of the National Academy of Sciences of the United States of America*, *111*(45), E4896-905.

McNally, B. A., Somasundaram, A., Yamashita, M., & Prakriya, M. (2012). Gated regulation of CRAC channel ion selectivity by STIM1. *Nature*, *482*(7384), 241–245.

Meier, S. D., Kovalchuk, Y., & Rose, C. R. (2006). Properties of the new fluorescent Na+ indicator CoroNa Green: Comparison with SBFI and confocal Na+ imaging. *Journal of Neuroscience Methods*, *155*(2), 251–259.

Mekahli, D., Bultynck, G., Parys, J. B., De Smedt, H., & Missiaen, L. (2011). Endoplasmic-

reticulum calcium depletion and disease. *Cold Spring Harbor Perspectives in Biology*, *3*(6).

Melchionda, M., Pittman, J. K., Mayor, R., & Patel, S. (2016). Ca2+/H+ exchange by acidic organelles regulates cell migration in vivo. *The Journal of Cell Biology*, *212*(7), 803–813.

Michelangeli, F., & East, J. M. (2011). A diversity of SERCA Ca2+ pump inhibitors. *Biochemical Society Transactions*, *39*(3), 789–797.

Minta, A., & Tsien, R. Y. (1989). Fluorescent indicators for cytosolic sodium. *The Journal of Biological Chemistry*, *264*(32), 19449–19457.

Moccia, F., Lim, D., Kyozuka, K., & Santella, L. (2004). NAADP triggers the fertilization potential in starfish oocytes. *Cell Calcium*, *36*(6), 515–524.

Montero, M., Lobatón, C. D., Gutierrez-Fernández, S., Moreno, A., & Alvarez, J. (2003). Modulation of histamine-induced Ca2+ release by protein kinase C: Effects on cytosolic and mitochondrial [Ca2+] PEAKS. *Journal of Biological Chemistry*, *278*(50), 49972–49979.

Morgan, A. J. (2016). Ca2+ dialogue between acidic vesicles and ER. *Biochemical Society Transactions*, *44*(2), 546–553.

Morgan, A. J., Davis, L. C., & Galione, A. (2015). Imaging approaches to measuring lysosomal calcium. *Methods in Cell Biology*, *126*, 159–195.

Morgan, A. J., Davis, L. C., Wagner, S. K. T. Y., Lewis, A. M., Parrington, J., Churchill, G. C., & Galione, A. (2013). Bidirectional Ca^{2+} signaling occurs between the endoplasmic reticulum and acidic organelles. *The Journal of Cell Biology*, *200*(6), 789–805.

Morgan, A. J., & Galione, A. (2007). Fertilization and Nicotinic Acid Adenine Dinucleotide Phosphate Induce pH Changes in Acidic Ca 2+ Stores in Sea Urchin Eggs. *Journal of Biological Chemistry*, *282*(52), 37730–37737.

Morgan, A. J., Platt, F. M., Lloyd-Evans, E., & Galione, A. (2011). Molecular mechanisms of endolysosomal Ca2+ signalling in health and disease. *Biochemical Journal*, *439*(3), 349–378.

Morgan, A. J., Yuan, Y., Patel, S., & Galione, A. (2020). Does lysosomal rupture evoke Ca2+ release? A question of pores and stores. *Cell Calcium*, *86*, 102139.

Murrell-Lagnado, R. D., & Frick, M. (2019). P2X4 and lysosome fusion. *Current Opinion in Pharmacology*, *47*, 126–132.

Nadanaciva, S., Lu, S., Gebhard, D. F., Jessen, B. A., Pennie, W. D., & Will, Y. (2011). A high content screening assay for identifying lysosomotropic compounds. *Toxicology in Vitro*, *25*(3), 715–723.

Nägerl, U. V., Novo, D., Mody, I., & Vergara, J. L. (2000). Binding kinetics of calbindin-D(28k) determined by flash photolysis of caged Ca(2+). *Biophysical Journal*, *79*(6),

3009–3018.

Naylor, E., Arredouani, A., Vasudevan, S. R., Lewis, A. M., Parkesh, R., Mizote, A., Rosen, D., Thomas, J. M., Izumi, M., Ganesan, A., Galione, A., & Churchill, G. C. (2009). Identification of a chemical probe for NAADP by virtual screening. *Nature Chemical Biology*, *5*(4), 220–226.

Neely Kayala, K. M., Dickinson, G. D., Minassian, A., Walls, K. C., Green, K. N., & Laferla, F. M. (2012). Presenilin-null cells have altered two-pore calcium channel expression and lysosomal calcium: implications for lysosomal function. *Brain Research*, *1489*, 8–16.

Nguyen, O. N. P., Grimm, C., Schneider, L. S., Chao, Y. K., Atzberger, C., Bartel, K., Watermann, A., Ulrich, M., Mayr, D., Wahl-Schott, C., Biel, M., & Vollmar, A. M. (2017). Two-pore channel function is crucial for the migration of invasive cancer cells. *Cancer Research*, *77*(6), 1427–1438.

Notomi, T., Kuno, M., Hiyama, A., Nozaki, T., Ohura, K., Ezura, Y., & Noda, M. (2017). Role of lysosomal channel protein TPC2 in osteoclast differentiation and bone remodeling under normal and low-magnesium conditions. *The Journal of Biological Chemistry*, *292*(51), 20998–21010.

Ogunbayo, O. A., Duan, J., Xiong, J., Wang, Q., Feng, X., Ma, J., Zhu, M. X., & Evans, A. M. (2018). mTORC1 controls lysosomal Ca2+ release through the two-pore channel TPC2. *Science Signaling*, *11*(525), eaao5775.

Ogunbayo, O. A., Zhu, Y., Rossi, D., Sorrentino, V., Ma, J., Zhu, M. X., & Evans, A. M. (2011). Cyclic Adenosine Diphosphate Ribose Activates Ryanodine Receptors, whereas NAADP Activates Two-pore Domain Channels. *Journal of Biological Chemistry*, *286*(11), 9136–9140.

Ona-Jodar, T., Gerkau, N. J., Aghvami, S. S., Rose, C. R., & Egger, V. (2017). Stwo-photon Na+ imaging reports somatically evoked action potentials in rat olfactory bulb mitral and granule cell neurites. *Frontiers in Cellular Neuroscience*, *11*(February), 1–12.

Orrenius, S., Zhivotovsky, B., & Nicotera, P. (2003). Regulation of cell death: the calcium-apoptosis link. *Nature Reviews. Molecular Cell Biology*, *4*(7), 552–565.

Padamsey, Z., McGuinness, L., Bardo, S. J., Reinhart, M., Tong, R., Hedegaard, A., Hart, M. L., & Emptage, N. J. (2017). Activity-Dependent Exocytosis of Lysosomes Regulates the Structural Plasticity of Dendritic Spines. *Neuron*, *93*(1), 132–146.

Pafumi, I., Festa, M., Papacci, F., Lagostena, L., Giunta, C., Gutla, V., Cornara, L., Favia, A., Palombi, F., Gambale, F., Filippini, A., & Carpaneto, A. (2017). Naringenin Impairs Two-Pore Channel 2 Activity And Inhibits VEGF-Induced Angiogenesis. *Scientific Reports*, *7*(1), 5121.

Palty, R., Silverman, W. F., Hershfinkel, M., Caporale, T., Sensi, S. L., Parnis, J., Nolte, C.,

Fishman, D., Shoshan-Barmatz, V., Herrmann, S., Khananshvili, D., & Sekler, I. (2010). NCLX is an essential component of mitochondrial Na+/Ca2+ exchange. *Proceedings of the National Academy of Sciences of the United States of America*, *107*(1), 436–441.

Pandey, V., Chuang, C.-C., Lewis, A. M., Aley, P. K., Brailoiu, E., Dun, N. J., Churchill, G. C., & Patel, S. (2009). Recruitment of NAADP-sensitive acidic Ca2+ stores by glutamate. *The Biochemical Journal*, *422*(3), 503–512.

Parkesh, R., Lewis, A. M., Aley, P. K., Arredouani, A., Rossi, S., Tavares, R., Vasudevan, S. R., Rosen, D., Galione, A., Dowden, J., & Churchill, G. C. (2008). Cell-permeant NAADP: a novel chemical tool enabling the study of Ca2+ signalling in intact cells. *Cell Calcium*, *43*(6), 531–538.

Parzych, K. R., & Klionsky, D. J. (2014). An overview of autophagy: morphology, mechanism, and regulation. *Antioxidants & Redox Signaling*, *20*(3), 460–473.

Patel, S. (2015). Function and dysfunction of two-pore channels. *Science Signaling*, *8*(384), re7–re7.

Patel, S., & Brailoiu, E. (2012). Triggering of Ca2+ signals by NAADP-gated two-pore channels: a role for membrane contact sites? *Biochemical Society Transactions*, *40*(1), 153–157.

Patel, S., & Cai, X. (2015). Evolution of acidic Ca2+ stores and their resident Ca2+-permeable channels. *Cell Calcium*, *57*(3), 222–230.

Patel, S., Churamani, D., & Brailoiu, E. (2017). NAADP-evoked Ca 2+ signals through two-pore channel-1 require arginine residues in the first S4-S5 linker. *Cell Calcium*, *68*, 1–4.

Patel, S., Churchill, G. C., & Galione, A. (2001). Coordination of Ca2+ signalling by NAADP. *Trends in Biochemical Sciences*, *26*(8), 482–489.

Patel, S., & Docampo, R. (2010). Acidic calcium stores open for business: expanding the potential for intracellular Ca2+ signaling. *Trends in Cell Biology*, *20*(5), 277–286.

Patel, S., & Kilpatrick, B. S. (2018). Two-pore channels and disease. *Biochimica et Biophysica Acta - Molecular Cell Research*, *1865*(11), 1678–1686.

Patel, S., & Muallem, S. (2011). Acidic Ca2+ stores come to the fore. *Cell Calcium*, *50*(2), 109–112.

Peiter, E., Maathuis, F. J. M., Mills, L. N., Knight, H., Pelloux, J., Hetherington, A. M., & Sanders, D. (2005). The vacuolar Ca2+-activated channel TPC1 regulates germination and stomatal movement. *Nature*, *434*(7031), 404–408.

Penny, C. J., Kilpatrick, B. S., Eden, E. R., & Patel, S. (2015). Coupling acidic organelles with the ER through Ca2+ microdomains at membrane contact sites. *Cell Calcium*, *58*(4), 387–396.

Penny, C. J., Kilpatrick, B. S., Han, J. M., Sneyd, J., & Patel, S. (2014). A computational model of lysosome-ER Ca2+ microdomains. *Journal of Cell Science*, *127*(13), 2934–2943.

Penny, C. J., & Patel, S. (2015). Poring Over Two-Pore Channel Pore Mutants. *Messenger*, *4*(1), 46–52.

Penny, C. J., Vassileva, K., Jha, A., Yuan, Y., Chee, X., Yates, E., Mazzon, M., Kilpatrick, B. S., Muallem, S., Marsh, M., Rahman, T., & Patel, S. (2019). Mining of Ebola virus entry inhibitors identifies approved drugs as two-pore channel pore blockers. *Biochimica et Biophysica Acta (BBA) - Molecular Cell Research*, *1866*(7), 1151–1161.

Pereira, G. J. S., Antonioli, M., Hirata, H., Ureshino, R. P., Nascimento, A. R., Bincoletto, C., Vescovo, T., Piacentini, M., Fimia, G. M., & Smaili, S. S. (2017). Glutamate induces autophagy via the two-pore channels in neural cells. *Oncotarget*, *8*(8), 12730–12740.

Pereira, G. J. S., Hirata, H., do Carmo, L. G., Stilhano, R. S., Ureshino, R. P., Medaglia, N. C., Han, S. W., Churchill, G., Bincoletto, C., Patel, S., & Smaili, S. S. (2014). NAADP-sensitive two-pore channels are present and functional in gastric smooth muscle cells. *Cell Calcium*, *56*(2), 51–58.

Pereira, G. J. S., Hirata, H., Fimia, G. M., do Carmo, L. G., Bincoletto, C., Han, S. W., Stilhano, R. S., Ureshino, R. P., Bloor-Young, D., Churchill, G., Piacentini, M., Patel, S., & Smaili, S. S. (2011). Nicotinic acid adenine dinucleotide phosphate (NAADP) regulates autophagy in cultured astrocytes. *The Journal of Biological Chemistry*, *286*(32), 27875–27881.

Perocchi, F., Gohil, V. M., Girgis, H. S., Bao, X. R., McCombs, J. E., Palmer, A. E., & Mootha, V. K. (2010). MICU1 encodes a mitochondrial EF hand protein required for Ca(2+) uptake. *Nature*, *467*(7313), 291–296.

Petronilli, V., Penzo, D., Scorrano, L., Bernardi, P., & Di Lisa, F. (2001). The mitochondrial permeability transition, release of cytochrome c and cell death. Correlation with the duration of pore openings in situ. *The Journal of Biological Chemistry*, *276*(15), 12030–12034.

Pfanzagl, B., Zevallos, V. F., Schuppan, D., Pfragner, R., & Jensen-Jarolim, E. (2019). Histamine causes influx via T-type voltage-gated calcium channels in an enterochromaffin tumor cell line: potential therapeutic target in adverse food reactions. *American Journal of Physiology-Gastrointestinal and Liver Physiology*, *316*(2), G291–G303.

Pinheiro, A. R., Paramos-De-Carvalho, D., Certal, M., Costa, C., Magalhães-Cardoso, M. T., Ferreirinha, F., Costa, M. A., & Correia-De-Sá, P. (2013). Bradykinin-induced Ca2+ signaling in human subcutaneous fibroblasts involves ATP release via hemichannels

leading to P2Y12 receptors activation. *Cell Communication and Signaling*, *11*(1), 1–17.

Pinheiro, A. R., Paramos-De-carvalho, D., Certal, M., Costa, M. A., Costa, C., Magalhães-Cardoso, M. T., Ferreirinha, F., Sévigny, J., & Correia-De-Sá, P. (2013). Histamine induces ATP release from human subcutaneous fibroblasts, via pannexin-1 hemichannels, leading to Ca2+ mobilization and cell proliferation. *Journal of Biological Chemistry*, *288*(38), 27571–27583.

Pinton, P., Pozzan, T., & Rizzuto, R. (1998). The Golgi apparatus is an inositol 1,4,5-trisphosphate-sensitive Ca2+ store, with functional properties distinct from those of the endoplasmic reticulum. *The EMBO Journal*, *17*(18), 5298–5308.

Pitt, S. J., Funnell, T. M., Sitsapesan, M., Venturi, E., Rietdorf, K., Ruas, M., Ganesan, A., Gosain, R., Churchill, G. C., Zhu, M. X., Parrington, J., Galione, A., & Sitsapesan, R. (2010). TPC2 Is a Novel NAADP-sensitive Ca 2+ Release Channel, Operating as a Dual Sensor of Luminal pH and Ca 2+. *Journal of Biological Chemistry*, *285*(45), 35039–35046.

Pitt, S. J., Lam, A. K. M., Rietdorf, K., Galione, A., & Sitsapesan, R. (2014). Reconstituted Human TPC1 Is a Proton-Permeable Ion Channel and Is Activated by NAADP or Ca2+. *Science Signaling*, *7*(326), ra46–ra46.

Plowey, E. D., Cherra, S. J., Liu, Y.-J., & Chu, C. T. (2008). Role of autophagy in G2019S-LRRK2-associated neurite shortening in differentiated SH-SY5Y cells. *Journal of Neurochemistry*, *105*(3), 1048–1056.

Popugaeva, E., & Bezprozvanny, I. (2013). Role of endoplasmic reticulum Ca2+ signaling in the pathogenesis of Alzheimer disease. *Frontiers in Molecular Neuroscience*, *6*, 29.

Prinz, W. A. (2014). Bridging the gap: membrane contact sites in signaling, metabolism, and organelle dynamics. *The Journal of Cell Biology*, *205*(6), 759–769.

Prinz, W. A., Toulmay, A., & Balla, T. (2020). The functional universe of membrane contact sites. *Nature Reviews Molecular Cell Biology*, *21*(1), 7–24.

Pu, J., Guardia, C. M., Keren-Kaplan, T., & Bonifacino, J. S. (2016). Mechanisms and functions of lysosome positioning. *Journal of Cell Science*, *129*(23), 4329–4339.

Putney, J. W. (2005). Capacitative calcium entry: sensing the calcium stores. *The Journal of Cell Biology*, *169*(3), 381–382.

Qureshi, O. S., Paramasivam, A., Yu, J. C. H., & Murrell-Lagnado, R. D. (2007). Regulation of P2X4 receptors by lysosomal targeting, glycan protection and exocytosis. *Journal of Cell Science*, *120*(Pt 21), 3838–3849.

Rah, S., Lee, Y., & Kim, U. (2017). NAADP-mediated Ca 2+ signaling promotes autophagy and protects against LPS-induced liver injury. *The FASEB Journal*, *31*(7), 3126–3137.

Rahman, T., Cai, X., Brailoiu, G. C., Abood, M. E., Brailoiu, E., & Patel, S. (2014). Two-

pore channels provide insight into the evolution of voltage-gated Ca2+ and Na+ channels. *Science Signaling*, *7*(352), ra109–ra109.

Rasola, A., & Bernardi, P. (2011). Mitochondrial permeability transition in Ca2+-dependent apoptosis and necrosis. *Cell Calcium*, *50*(3), 222–233.

Repnik, U., Borg Distefano, M., Speth, M. T., Ng, M. Y. W., Progida, C., Hoflack, B., Gruenberg, J., & Griffiths, G. (2017). L-leucyl-L-leucine methyl ester does not release cysteine cathepsins to the cytosol but inactivates them in transiently permeabilized lysosomes. *Journal of Cell Science*, *130*(18), 3124–3140.

Riccio, A., Mattei, C., Kelsell, R. E., Medhurst, A. D., Calver, A. R., Randall, A. D., Davis, J. B., Benham, C. D., & Pangalos, M. N. (2002). Cloning and functional expression of human short TRP7, a candidate protein for store-operated Ca2+ influx. *The Journal of Biological Chemistry*, *277*(14), 12302–12309.

Rietdorf, K., Funnell, T. M., Ruas, M., Heinemann, J., Parrington, J., & Galione, A. (2011). Two-pore Channels Form Homo- and Heterodimers. *Journal of Biological Chemistry*, *286*(43), 37058–37062.

Rizzuto, R. (1998). Close Contacts with the Endoplasmic Reticulum as Determinants of Mitochondrial Ca2+ Responses. *Science*, *280*(5370), 1763–1766.

Rizzuto, R., De Stefani, D., Raffaello, A., & Mammucari, C. (2012). Mitochondria as sensors and regulators of calcium signalling. *Nature Reviews. Molecular Cell Biology*, *13*(9), 566–578.

Rocha, N., Kuijl, C., van der Kant, R., Janssen, L., Houben, D., Janssen, H., Zwart, W., & Neefjes, J. (2009). Cholesterol sensor ORP1L contacts the ER protein VAP to control Rab7–RILP–p150Glued and late endosome positioning. *Journal of Cell Biology*, *185*(7), 1209–1225.

Rose, C.R., Kovalchuk, Y., Eilers, J., & Konnerth, A. (1999). Two-photon Na + imaging in spines and fine dendrites of central neurons. *Pflugers Archiv European Journal of Physiology*, *439*(1–2), 201–207.

Rose, Christine R. (2012). Two-Photon Sodium Imaging in Dendritic Spines. *Cold Spring Harbor Protocols*, *2012*(11), pdb.prot072074-pdb.prot072074.

Rosen, D., Lewis, A. M., Mizote, A., Thomas, J. M., Aley, P. K., Vasudevan, S. R., Parkesh, R., Galione, A., Izumi, M., Ganesan, A., & Churchill, G. C. (2009). Analogues of the Nicotinic Acid Adenine Dinucleotide Phosphate (NAADP) Antagonist Ned-19 Indicate Two Binding Sites on the NAADP Receptor. *Journal of Biological Chemistry*, *284*(50), 34930–34934.

Rossi, A. M., & Taylor, C. W. (2018). IP3 receptors - lessons from analyses ex cellula. *Journal of Cell Science*, *132*(4).

Ruas, M., Chuang, K.-T., Davis, L. C., Al-Douri, A., Tynan, P. W., Tunn, R., Teboul, L.,

Galione, A., & Parrington, J. (2014). TPC1 has two variant isoforms, and their removal has different effects on endo-lysosomal functions compared to loss of TPC2. *Molecular and Cellular Biology*, *34*(21), 3981–3992.

Ruas, M., Davis, L. C., Chen, C., Morgan, A. J., Chuang, K., Walseth, T. F., Grimm, C., Garnham, C., Powell, T., Platt, N., Platt, F. M., Biel, M., Wahl-Schott, C., Parrington, J., & Galione, A. (2015). Expression of Ca 2+ -permeable two-pore channels rescues NAADP signalling in TPC -deficient cells. *The EMBO Journal*, *34*(13), 1743–1758.

Ruas, M., Rietdorf, K., Arredouani, A., Davis, L. C., Lloyd-Evans, E., Koegel, H., Funnell, T. M., Morgan, A. J., Ward, J. A., Watanabe, K., Cheng, X., Churchill, G. C., Zhu, M. X., Platt, F. M., Wessel, G. M., Parrington, J., & Galione, A. (2010). Purified TPC isoforms form NAADP receptors with distinct roles for Ca(2+) signaling and endolysosomal trafficking. *Current Biology : CB*, *20*(8), 703–709.

Rybalchenko, V., Ahuja, M., Coblentz, J., Churamani, D., Patel, S., Kiselyov, K., & Muallem, S. (2012). Membrane Potential Regulates Nicotinic Acid Adenine Dinucleotide Phosphate (NAADP) Dependence of the pH- and Ca 2+ -sensitive Organellar Two-pore Channel TPC1. *Journal of Biological Chemistry*, *287*(24), 20407–20416.

Sah, D. W. Y., & Bean, B. P. (1994). Inhibition of P-type and N-type calcium channels by dopamine receptor antagonists. *Molecular Pharmacology*, *45*(1), 84–92.

Sakurai, Y., Kolokoltsov, A. A., Chen, C.-C., Tidwell, M. W., Bauta, W. E., Klugbauer, N., Grimm, C., Wahl-Schott, C., Biel, M., & Davey, R. A. (2015). Two-pore channels control Ebola virus host cell entry and are drug targets for disease treatment. *Science*, *347*(6225), 995–998.

Salido, G. M., Sage, S. O., & Rosado, J. A. (2009). TRPC channels and store-operated Ca(2+) entry. *Biochimica et Biophysica Acta*, *1793*(2), 223–230.

Samie, M., Wang, X., Zhang, X., Goschka, A., Li, X., Cheng, X., Gregg, E., Azar, M., Zhuo, Y., Garrity, A. G., Gao, Q., Slaugenhaupt, S., Pickel, J., Zolov, S. N., Weisman, L. S., Lenk, G. M., Titus, S., Bryant-Genevier, M., Southall, N., … Xu, H. (2013). A TRP Channel in the Lysosome Regulates Large Particle Phagocytosis via Focal Exocytosis. *Developmental Cell*, *26*(5), 511–524.

Sandoz, G., Douguet, D., Chatelain, F., Lazdunski, M., & Lesage, F. (2009). Extracellular acidification exerts opposite actions on TREK1 and TREK2 potassium channels via a single conserved histidine residue. *Proceedings of the National Academy of Sciences*, *106*(34), 14628–14633.

Saponara, S., Testai, L., Iozzi, D., Martinotti, E., Martelli, A., Chericoni, S., Sgaragli, G., Fusi, F., & Calderone, V. (2006). (+/-)-Naringenin as large conductance Ca(2+)-activated K+ (BKCa) channel opener in vascular smooth muscle cells. *British Journal*

of Pharmacology, *149*(8), 1013–1021.

Sbrissa, D., Ikonomov, O. C., & Shisheva, A. (1999). PIKfyve, a Mammalian Ortholog of Yeast Fab1p Lipid Kinase, Synthesizes 5-Phosphoinositides. *Journal of Biological Chemistry*, *274*(31), 21589–21597.

Sbrissa, D., & Shisheva, A. (2005). Acquisition of Unprecedented Phosphatidylinositol 3,5-Bisphosphate Rise in Hyperosmotically Stressed 3T3-L1 Adipocytes, Mediated by ArPIKfyve-PIKfyve Pathway. *Journal of Biological Chemistry*, *280*(9), 7883–7889.

Schampel, A., & Kuerten, S. (2017). Danger: High Voltage-The Role of Voltage-Gated Calcium Channels in Central Nervous System Pathology. *Cells*, *6*(4).

Schieder, M., Rötzer, K., Brüggemann, A., Biel, M., & Wahl-Schott, C. A. (2010). Characterization of Two-pore Channel 2 (TPCN2)-mediated Ca 2+ Currents in Isolated Lysosomes. *Journal of Biological Chemistry*, *285*(28), 21219–21222.

Schmidt, H., Stiefel, K. M., Racay, P., Schwaller, B., & Eilers, J. (2003). Mutational analysis of dendritic Ca2+ kinetics in rodent Purkinje cells: role of parvalbumin and calbindin D28k. *The Journal of Physiology*, *551*(Pt 1), 13–32.

Schnute, M. E., McReynolds, M. D., Kasten, T., Yates, M., Jerome, G., Rains, J. W., Hall, T., Chrencik, J., Kraus, M., Cronin, C. N., Saabye, M., Highkin, M. K., Broadus, R., Ogawa, S., Cukyne, K., Zawadzke, L. E., Peterkin, V., Iyanar, K., Scholten, J. A., … Nagiec, M. M. (2012). Modulation of cellular S1P levels with a novel, potent and specific inhibitor of sphingosine kinase-1. *Biochemical Journal*, *444*(1), 79–88.

Schwaller, B. (2010). Cytosolic Ca2+ buffers. *Cold Spring Harbor Perspectives in Biology*, *2*(11), a004051.

Schwartz, J. C. (2000). Racecadotril: a new approach to the treatment of diarrhoea. *International Journal of Antimicrobial Agents*, *14*(1), 75–79.

Sehgal, P., Szalai, P., Olesen, C., Praetorius, H. A., Nissen, P., Christensen, S. B., Engedal, N., & Møller, J. V. (2017). Inhibition of the sarco/endoplasmic reticulum (ER) Ca 2+ -ATPase by thapsigargin analogs induces cell death via ER Ca 2+ depletion and the unfolded protein response. *Journal of Biological Chemistry*, *292*(48), 19656–19673.

She, J., Guo, J., Chen, Q., Zeng, W., Jiang, Y., & Bai, X. (2018). Structural insights into the voltage and phospholipid activation of the mammalian TPC1 channel. *Nature*, *556*(7699), 130–134.

She, J., Zeng, W., Guo, J., Chen, Q., Bai, X., & Jiang, Y. (2019). Structural mechanisms of phospholipid activation of the human TPC2 channel. *ELife*, *8*, e45222.

Shen, D., Wang, X., Li, X., Zhang, X., Yao, Z., Dibble, S., Dong, X., Yu, T., Lieberman, A. P., Showalter, H. D., & Xu, H. (2012). Lipid storage disorders block lysosomal trafficking by inhibiting a TRP channel and lysosomal calcium release. *Nature Communications*, *3*, 731.

Singaravelu, K., & Deitmer, J. W. (2006). Calcium mobilization by nicotinic acid adenine dinucleotide phosphate (NAADP) in rat astrocytes. *Cell Calcium*, *39*(2), 143–153.

Singh, A., Hildebrand, M., Garcia, E., & Snutch, T. (2010). The transient receptor potential channel antagonist SKF96365 is a potent blocker of low-voltage-activated T-type calcium channels. *British Journal of Pharmacology*, *160*(6), 1464–1475.

Sivaramakrishnan, V., Bidula, S., Campwala, H., Katikaneni, D., & Fountain, S. J. (2012). Constitutive lysosome exocytosis releases ATP and engages P2Y receptors in human monocytes. *Journal of Cell Science*, *125*(19), 4567–4575.

Skowyra, M. L., Schlesinger, P. H., Naismith, T. V., & Hanson, P. I. (2018). Triggered recruitment of ESCRT machinery promotes endolysosomal repair. *Science (New York, N.Y.)*, *360*(6384).

Soares, S., Thompson, M., White, T., Isbell, A., Yamasaki, M., Prakash, Y., Lund, F. E., Galione, A., & Chini, E. N. (2007). NAADP as a second messenger: neither CD38 nor base-exchange reaction are necessary for in vivo generation of NAADP in myometrial cells. *American Journal of Physiology-Cell Physiology*, *292*(1), C227–C239.

Srinivas, S. P., Ong, A., Goon, L., Goon, L., & Bonanno, J. A. (2002). Lysosomal Ca(2+) stores in bovine corneal endothelium. *Investigative Ophthalmology & Visual Science*, *43*(7), 2341–2350.

Steinberg, B. E., Huynh, K. K., Brodovitch, A., Jabs, S., Stauber, T., Jentsch, T. J., & Grinstein, S. (2010). A cation counterflux supports lysosomal acidification. *Journal of Cell Biology*, *189*(7), 1171–1186.

Straub, I., Mohr, F., Stab, J., Konrad, M., Philipp, S., Oberwinkler, J., & Schaefer, M. (2013). Citrus fruit and fabacea secondary metabolites potently and selectively block TRPM3. *British Journal of Pharmacology*, *168*(8), 1835–1850.

Streb, H., Irvine, R. F., Berridge, M. J., & Schulz, I. (1983). Release of Ca2+ from a nonmitochondrial intracellular store in pancreatic acinar cells by inositol-1,4,5-trisphosphate. *Nature*, *306*(5938), 67–69.

Suárez-Cortés, P., Gambara, G., Favia, A., Palombi, F., Alano, P., & Filippini, A. (2017). Ned-19 inhibition of parasite growth and multiplication suggests a role for NAADP mediated signalling in the asexual development of Plasmodium falciparum. *Malaria Journal*, *16*(1), 366.

Sulem, P., Gudbjartsson, D. F., Stacey, S. N., Helgason, A., Rafnar, T., Jakobsdottir, M., Steinberg, S., Gudjonsson, S. A., Palsson, A., Thorleifsson, G., Pálsson, S., Sigurgeirsson, B., Thorisdottir, K., Ragnarsson, R., Benediktsdottir, K. R., Aben, K. K., Vermeulen, S. H., Goldstein, A. M., Tucker, M. A., … Stefansson, K. (2008). Two newly identified genetic determinants of pigmentation in Europeans. *Nature Genetics*, *40*(7), 835–837.

Sumoza-Toledo, A., & Penner, R. (2011). TRPM2: a multifunctional ion channel for calcium signalling. *The Journal of Physiology*, *589*(Pt 7), 1515–1525.

Takemura, H., Imoto, K., Ohshika, H., & Kwan, C.-Y. (1996). TETRANDRINE AS A CALCIUM ANTAGONIST. *Clinical and Experimental Pharmacology and Physiology*, *23*(8), 751–753.

Tang, Y., & Zucker, R. S. (1997). Mitochondrial involvement in post-tetanic potentiation of synaptic transmission. *Neuron*, *18*(3), 483–491.

Tarasov, A. I., Griffiths, E. J., & Rutter, G. A. (2012). Regulation of ATP production by mitochondrial Ca(2+). *Cell Calcium*, *52*(1), 28–35.

Tedeschi, V., Petrozziello, T., Sisalli, M. J., Boscia, F., Canzoniero, L. M. T., & Secondo, A. (2019). The activation of Mucolipin TRP channel 1 (TRPML1) protects motor neurons from L-BMAA neurotoxicity by promoting autophagic clearance. *Scientific Reports*, *9*(1), 1–11.

Thastrup, O., Cullen, P. J., Drobak, B. K., Hanley, M. R., & Dawson, A. P. (1990). Thapsigargin, a tumor promoter, discharges intracellular Ca2+ stores by specific inhibition of the endoplasmic reticulum Ca2(+)-ATPase. *Proceedings of the National Academy of Sciences*, *87*(7), 2466–2470.

Thiele, D. L., & Lipsky, P. E. (1990). Mechanism of L-leucyl-L-leucine methyl ester-mediated killing of cytotoxic lymphocytes: dependence on a lysosomal thiol protease, dipeptidyl peptidase I, that is enriched in these cells. *Proceedings of the National Academy of Sciences*, *87*(1), 83–87.

Thillaiappan, N. B., Chakraborty, P., Hasan, G., & Taylor, C. W. (2019). IP3 receptors and Ca2+ entry. *Biochimica et Biophysica Acta. Molecular Cell Research*, *1866*(7), 1092–1100.

Tóth, B., Iordanov, I., & Csanády, L. (2015). Ruling out pyridine dinucleotides as true TRPM2 channel activators reveals novel direct agonist ADP-ribose-2'-phosphate. *The Journal of General Physiology*, *145*(5), 419–430.

Treiman, M., Caspersen, C., & Christensen, S. B. (1998). A tool coming of age: Thapsigargin as an inhibitor of sarco-endoplasmic reticulum Ca2+-ATPases. *Trends in Pharmacological Sciences*.

Trufanov, S. K., Rybakova, E. Y., Avdonin, P. P., Tsitrina, A. A., Zharkikh, I. L., Goncharov, N. V, Jenkins, R. O., & Avdonin, P. V. (2019). The Role of Two-Pore Channels in Norepinephrine-Induced [Ca2+]i Rise in Rat Aortic Smooth Muscle Cells and Aorta Contraction. *Cells*, *8*(10).

Tsunemi, T., Perez-Rosello, T., Ishiguro, Y., Yoroisaka, A., Jeon, S., Hamada, K., Rammonhan, M., Wong, Y. C., Xie, Z., Akamatsu, W., Mazzulli, J. R., Surmeier, D. J., Hattori, N., & Krainc, D. (2019). Increased Lysosomal Exocytosis Induced by

Lysosomal Ca 2+ Channel Agonists Protects Human Dopaminergic Neurons from α-Synuclein Toxicity. *The Journal of Neuroscience*, *39*(29), 5760–5772.

Tu, C.-L., Chang, W., & Bikle, D. D. (2007). The role of the calcium sensing receptor in regulating intracellular calcium handling in human epidermal keratinocytes. *The Journal of Investigative Dermatology*, *127*(5), 1074–1083.

Turlova, E., Feng, Z.-P., & Sun, H.-S. (2018). The role of TRPM2 channels in neurons, glial cells and the blood-brain barrier in cerebral ischemia and hypoxia. *Acta Pharmacologica Sinica*, *39*(5), 713–721.

Vais, H., Foskett, J. K., Ullah, G., Pearson, J. E., & Daniel Mak, D.-O. (2012). Permeant calcium ion feed-through regulation of single inositol 1,4,5-trisphosphate receptor channel gating. *Journal of General Physiology*, *140*(6), 697–716.

Van Baelen, K., Vanoevelen, J., Callewaert, G., Parys, J. B., De Smedt, H., Raeymaekers, L., Rizzuto, R., Missiaen, L., & Wuytack, F. (2003). The contribution of the SPCA1 Ca2+ pump to the Ca2+ accumulation in the Golgi apparatus of HeLa cells assessed via RNA-mediated interference. *Biochemical and Biophysical Research Communications*, *306*(2), 430–436.

Vanoevelen, J., Raeymaekers, L., Parys, J. B., De Smedt, H., Van Baelen, K., Callewaert, G., Wuytack, F., & Missiaen, L. (2004). Inositol trisphosphate producing agonists do not mobilize the thapsigargin-insensitive part of the endoplasmic-reticulum and Golgi Ca2+ store. *Cell Calcium*, *35*(2), 115–121.

Vassileva, K., Marsh, M., & Patel, S. (2020). Two-pore channels as master regulators of membrane trafficking and endocytic well-being. *Current Opinion in Physiology*, *17*, 163–168.

Venkatachalam, K., & Montell, C. (2007). TRP channels. *Annual Review of Biochemistry*, *76*, 387–417.

Vergarajauregui, S., & Puertollano, R. (2006). Two Di-Leucine Motifs Regulate Trafficking of Mucolipin-1 to Lysosomes. *Traffic*, *7*(3), 337–353.

Verkhratsky, A., Trebak, M., Perocchi, F., Khananshvili, D., & Sekler, I. (2018). Crosslink between calcium and sodium signalling. *Experimental Physiology*, *103*(2), 157–169.

Villamil Giraldo, A. M., Appelqvist, H., Ederth, T., & Öllinger, K. (2014). Lysosomotropic agents: impact on lysosomal membrane permeabilization and cell death. *Biochemical Society Transactions*, *42*(5), 1460–1464.

Virginio, C., MacKenzie, A., Rassendren, F. A., North, R. A., & Surprenant, A. (1999). Pore dilation of neuronal P2X receptor channels. *Nature Neuroscience*, *2*(4), 315–321.

Visentin, S., De Nuccio, C., Bernardo, A., Pepponi, R., Ferrante, A., Minghetti, L., & Popoli, P. (2013). The stimulation of adenosine A2A receptors ameliorates the pathological phenotype of fibroblasts from Niemann-Pick type C patients. *The Journal of*

Neuroscience : The Official Journal of the Society for Neuroscience, *33*(39), 15388–15393.

Wagner, L. E., Groom, L. A., Dirksen, R. T., & Yule, D. I. (2014). Characterization of ryanodine receptor type 1 single channel activity using “on-nucleus” patch clamp. *Cell Calcium*, *56*(2), 96–107.

Waheed, A., Ludtmann, M. H. R., Pakes, N., Robery, S., Kuspa, A., Dinh, C., Baines, D., Williams, R. S. B., & Carew, M. A. (2014). Naringenin inhibits the growth of Dictyostelium and MDCK-derived cysts in a TRPP2 (polycystin-2)-dependent manner. *British Journal of Pharmacology*, *171*(10), 2659–2670.

Walls, K. C., Ghosh, A. P., Franklin, A. V., Klocke, B. J., Ballestas, M., Shacka, J. J., Zhang, J., & Roth, K. A. (2010). Lysosome Dysfunction Triggers Atg7-dependent Neural Apoptosis. *Journal of Biological Chemistry*, *285*(14), 10497–10507.

Walseth, T. F., Aarhus, R., Kerr, J. A., & Lee, H. C. (1993). Identification of cyclic ADP-ribose-binding proteins by photoaffinity labeling. *The Journal of Biological Chemistry*, *268*(35), 26686–26691.

Walseth, Timothy F., Lin-Moshier, Y., Jain, P., Ruas, M., Parrington, J., Galione, A., Marchant, J. S., & Slama, J. T. (2012). Photoaffinity Labeling of High Affinity Nicotinic Acid Adenine Dinucleotide Phosphate (NAADP)-Binding Proteins in Sea Urchin Egg. *Journal of Biological Chemistry*, *287*(4), 2308–2315.

Wang, G., & Lemos, J. (1994). Tetrandrine: A new ligand to block voltage-dependent Ca2+ and Ca2+-activated K+ channels. *Life Sciences*, *56*(5), 295–306.

Wang, Q., Lu, L., Gao, X., Wang, C., Wang, J., Cheng, J., Gao, R., & Xiao, H. (2011). Effects of Raloxifene on Voltage- Dependent T-Type Ca^{2+} Channels in Mouse Spermatogenic Cells. *Pharmacology*, *87*(1–2), 70–80.

Wang, X., Zhang, X., Dong, X., Samie, M., Li, X., Cheng, X., Goschka, A., Shen, D., Zhou, Y., Harlow, J., Zhu, M. X., Clapham, D. E., Ren, D., & Xu, H. (2012). TPC proteins are phosphoinositide- activated sodium-selective ion channels in endosomes and lysosomes. *Cell*, *151*(2), 372–383.

Wilkerson, P. M., & Reis-Filho, J. S. (2013). the 11q13-q14 amplicon: Clinicopathological correlations and potential drivers. *Genes, Chromosomes and Cancer*, *52*(4), 333–355.

Willets, J. M., Taylor, A. H., Shaw, H., Konje, J. C., & Challiss, R. A. J. (2008). Selective regulation of H1 histamine receptor signaling by G protein-coupled receptor kinase 2 in uterine smooth muscle cells. *Molecular Endocrinology*, *22*(8), 1893–1907.

Xiao, J., Rijal, P., Schimanski, L., Tharkeshwar, A. K., Wright, E., Annaert, W., & Townsend, A. (2017). Characterization of an influenza virus pseudotyped with Ebolavirus glycoprotein. *Journal of Virology*, *December*, JVI.00941-17.

Xu, H., & Ren, D. (2015). Lysosomal Physiology. *Annual Review of Physiology*, *77*(1), 57–

80.

Yagodin, S., Pivovarova, N. B., Andrews, S. B., & Sattelle, D. B. (1999). Functional characterization of thapsigargin and agonist-insensitive acidic Ca2+stores in Drosophila melanogaster S2 cell lines. *Cell Calcium*, *25*(6), 429–438.

Yamaguchi, S., Jha, A., Li, Q., Soyombo, A. A., Dickinson, G. D., Churamani, D., Brailoiu, E., Patel, S., & Muallem, S. (2011). Transient Receptor Potential Mucolipin 1 (TRPML1) and Two-pore Channels Are Functionally Independent Organellar Ion Channels. *Journal of Biological Chemistry*, *286*(26), 22934–22942.

Yang, Z., Pan, A., Zuo, W., Guo, J., & Zhou, W. (2014). Relaxant effect of flavonoid naringenin on contractile activity of rat colonic smooth muscle. *Journal of Ethnopharmacology*, *155*(2), 1177–1183.

Yarov-Yarovoy, V., Brown, J., Sharp, E. M., Clare, J. J., Scheuer, T., & Catterall, W. A. (2001). Molecular determinants of voltage-dependent gating and binding of pore-blocking drugs in transmembrane segment IIIS6 of the Na(+) channel alpha subunit. *The Journal of Biological Chemistry*, *276*(1), 20–27.

Yates, E. (2017). Lysosomal Ca2+ Signalling and Neurodegeneration: A Global View. Doctoral thesis (Ph.D). UCL (University College London)

Ye, W., Han, T. W., He, M., Jan, Y. N., & Jan, L. Y. (2019). Dynamic change of electrostatic field in TMEM16F permeation pathway shifts its ion selectivity. *ELife*, *8*, e45187.

Yonemura, K., & Miyanaga, K. (1998). *Profiles Drugs of for the Affinity of Receptors Neurotransmitter Clinical and Their*. *48*.

Yu, F. H., Yarov-Yarovoy, V., Gutman, G. A., & Catterall, W. A. (2005). Overview of molecular relationships in the voltage-gated ion channel superfamily. *Pharmacological Reviews*, *57*(4), 387–395.

Yu, P., Liu, Z., Yu, X., Ye, P., Liu, H., Xue, X., Yang, L., Li, Z., Wu, Y., Fang, C., Zhao, Y. J., Yang, F., Luo, J. H., Jiang, L.-H., Zhang, L., Zhang, L., & Yang, W. (2019). Direct Gating of the TRPM2 Channel by cADPR via Specific Interactions with the ADPR Binding Pocket. *Cell Reports*, *27*(12), 3684-3695.e4.

Zamponi, G. W., Striessnig, J., Koschak, A., & Dolphin, A. C. (2015). The Physiology, Pathology, and Pharmacology of Voltage-Gated Calcium Channels and Their Future Therapeutic Potential. *Pharmacological Reviews*, *67*(4), 821–870.

Zeevi, D. A., Frumkin, A., Offen-Glasner, V., Kogot-Levin, A., & Bach, G. (2009). A potentially dynamic lysosomal role for the endogenous TRPML proteins. *The Journal of Pathology*, *219*(2), 153–162.

Zhang, F., Jin, S., Yi, F., & Li, P. L. (2009). TRP-ML1 functions as a lysosomal NAADP-sensitive Ca 2+ release channel in coronary arterial myocytes. *Journal of Cellular and*

Molecular Medicine, *13*(9 B), 3174–3185.

Zhang, F., Xu, M., Han, W.-Q., & Li, P.-L. (2011). Reconstitution of lysosomal NAADP-TRP-ML1 signaling pathway and its function in TRP-ML1 −/− cells. *American Journal of Physiology-Cell Physiology*, *301*(2), C421–C430.

Zhang, S. L., Yu, Y., Roos, J., Kozak, J. A., Deerinck, T. J., Ellisman, M. H., Stauderman, K. A., & Cahalan, M. D. (2005). STIM1 is a Ca2+ sensor that activates CRAC channels and migrates from the Ca2+ store to the plasma membrane. *Nature*, *437*(7060), 902–905.

Zhang, S., Li, N., Zeng, W., Gao, N., & Yang, M. (2017). Cryo-EM structures of the mammalian endo-lysosomal TRPML1 channel elucidate the combined regulation mechanism. *Protein & Cell*, *8*(11), 834–847.

Zhang, X., Chen, W., Li, P., Calvo, R., Southall, N., Hu, X., Bryant-Genevier, M., Feng, X., Geng, Q., Gao, C., Yang, M., Tang, K., Ferrer, M., Marugan, J. J., & Xu, H. (2019). Agonist-specific voltage-dependent gating of lysosomal two-pore Na+ channels. *ELife*, *8*, 1–18.

Zhang, X., Cheng, X., Yu, L., Yang, J., Calvo, R., Patnaik, S., Hu, X., Gao, Q., Yang, M., Lawas, M., Delling, M., Marugan, J., Ferrer, M., & Xu, H. (2016). MCOLN1 is a ROS sensor in lysosomes that regulates autophagy. *Nature Communications*, *7*(May), 12109.

Zhang, Yang, Xu, M., Xia, M., Li, X., Boini, K. M., Wang, M., Gulbins, E., Ratz, P. H., & Li, P.-L. (2014). Defective autophagosome trafficking contributes to impaired autophagic flux in coronary arterial myocytes lacking CD38 gene. *Cardiovascular Research*, *102*(1), 68–78.

Zhang, Yanling, Zolov, S. N., Chow, C. Y., Slutsky, S. G., Richardson, S. C., Piper, R. C., Yang, B., Nau, J. J., Westrick, R. J., Morrison, S. J., Meisler, M. H., & Weisman, L. S. (2007). Loss of Vac14, a regulator of the signaling lipid phosphatidylinositol 3,5-bisphosphate, results in neurodegeneration in mice. *Proceedings of the National Academy of Sciences*, *104*(44), 17518–17523.

Zhang, Z.-H., Lu, Y.-Y., & Yue, J. (2013). Two pore channel 2 differentially modulates neural differentiation of mouse embryonic stem cells. *PloS One*, *8*(6), e66077.

Zhao, L.-X., Li, D.-D., Hu, D.-D., Hu, G.-H., Yan, L., Wang, Y., & Jiang, Y.-Y. (2013). Effect of Tetrandrine against Candida albicans Biofilms. *PLoS ONE*, *8*(11), e79671.

Zhou, Y., Cai, S., Moutal, A., Yu, J., Gómez, K., Madura, C. L., Shan, Z., Pham, N. Y. N., Serafini, M. J., Dorame, A., Scott, D. D., François-Moutal, L., Perez-Miller, S., Patek, M., Khanna, M., & Khanna, R. (2019). The Natural Flavonoid Naringenin Elicits Analgesia through Inhibition of NaV1.8 Voltage-Gated Sodium Channels. *ACS Chemical Neuroscience*, *10*(12), 4834–4846.

Zhu, M. X., Ma, J., Parrington, J., Calcraft, P. J., Galione, A., & Evans, A. M. (2010).

Calcium signaling via two-pore channels: local or global, that is the question. *American Journal of Physiology-Cell Physiology*, *298*(3), C430–C441.

Zolov, S. N., Bridges, D., Zhang, Y., Lee, W.-W., Riehle, E., Verma, R., Lenk, G. M., Converso-Baran, K., Weide, T., Albin, R. L., Saltiel, A. R., Meisler, M. H., Russell, M. W., & Weisman, L. S. (2012). In vivo, Pikfyve generates PI(3,5)P2, which serves as both a signaling lipid and the major precursor for PI5P. *Proceedings of the National Academy of Sciences*, *109*(43), 17472–17477.

Zong, X., Schieder, M., Cuny, H., Fenske, S., Gruner, C., Rötzer, K., Griesbeck, O., Harz, H., Biel, M., & Wahl-Schott, C. (2009). The two-pore channel TPCN2 mediates NAADP-dependent Ca2+-release from lysosomal stores. *Pflügers Archiv - European Journal of Physiology*, *458*(5), 891–899.

Zubcevic, L., Le, S., Yang, H., & Lee, S.-Y. (2018). Conformational plasticity in the selectivity filter of the TRPV2 ion channel. *Nature Structural & Molecular Biology*, *25*(5), 405–415.

Zuccolo, E., Laforenza, U., Negri, S., Botta, L., Berra-Romani, R., Faris, P., Scarpellino, G., Forcaia, G., Pellavio, G., Sancini, G., & Moccia, F. (2019). Muscarinic M5 receptors trigger acetylcholine-induced Ca 2+ signals and nitric oxide release in human brain microvascular endothelial cells. *Journal of Cellular Physiology*, *234*(4), 4540–4562.